VILPPU TUOMINEN

Virtual Microscopy

Design and Implementation of Novel Software Applications for Diagnostic Pathology

ACADEMIC DISSERTATION
To be presented, with the permission of
the board of Institute of Biomedical Technology of the University of Tampere,
for public discussion in the Jarmo Visakorpi Auditorium,
of the Arvo Building, Lääkärinkatu 1, Tampere,
on May 4th, 2012, at 12 o'clock.

UNIVERSITY OF TAMPERE

UNIVERSITY
OF TAMPERE

ACADEMIC DISSERTATION
University of Tampere, Institute of Biomedical Technology
Tampere Graduate Program in Biomedicine and Biotechnology (TGPBB)
Finland

Supervised by
Professor Jorma Isola
University of Tampere
Finland

Reviewed by
Professor Martti Juhola
University of Tampere
Finland
Professor Tuomo Karttunen
University of Oulu
Finland

Distribution
Bookshop TAJU
P.O. Box 617
33014 University of Tampere
Finland

Tel. +358 40 190 9800
Fax +358 3 3551 7685
taju@uta.fi
www.uta.fi/taju
http://granum.uta.fi

Cover design by
Mikko Reinikka

Acta Universitatis Tamperensis 1720
ISBN 978-951-44-8773-6 (print)
ISSN-L 1455-1616
ISSN 1455-1616

Acta Electronica Universitatis Tamperensis 1190
ISBN 978-951-44-8774-3 (pdf)
ISSN 1456-954X
http://acta.uta.fi

Tampereen Yliopistopaino Oy – Juvenes Print
Tampere 2012

ABSTRACT

Accurate histopathological diagnosis is an essential part of clinical cancer patient treatment, and is used, for example, to determine the patient's eligibility for surgical and adjuvant therapies, such as chemotherapy. Pathologists reach the diagnosis by inspecting stained tumor section slides with a light microscope or, increasingly, by digitizing the specimens and inspecting them with a computer display. The digitization of an entire microscope specimen at a diagnostically adequate resolution and the subsequent data processing are collectively referred to as virtual microscopy. Similarly, the digitized specimen slides are referred to as virtual slides. Although currently available technology enables routine usage of virtual microscopy, the amount of data generated with high-throughput virtual slide scanning is enormous– up to hundreds of gigabytes of uncompressed data per slide. Processing the data requires specialized information technology methods, which differ considerably from other medical imaging disciplines. Automated specimen scanning, processing, image analysis, archival, linkage to clinical information systems, and distribution to the end-users all present their own unique challenges to the software and hardware development. The aim of the present thesis study is to identify these problems and solve them by designing and implementing an open and standards-based software platform, which will facilitate the large-scale usage of virtual microscopy in clinical pathology, research, and education.

The sample material of the study consisted primarily of histological tumor section slides and secondarily of radiological imagery. The slides were digitized using various commercial and in-house scanning systems, for which an automated slide acquisition controller (DirObserver) and a stitching software application (LargeMontage) were developed. The suitability of JPEG2000 image compression standard for virtual microscopy, its compression efficiency, performance, and the optimal code-stream parameterization were studied, and based on these results, two software packages were designed and implemented. The first package allows the utilization of JPEG2000 in virtual microscopy and consists of three applications: a virtual slide

viewer (JVSview), a slide server (JVSserv), and a slide converter (JVScomp). The second package provides proof-of-concept software for linking virtual slides with clinical information systems and Picture Archiving and Communication System (PACS) -based image databases, which follow the Digital Imaging and Communications in Medicine (DICOM) standard in image data exchange. The package consists of three applications: a DICOM PACS client (JVSdicom Workstation), a DICOM PACS server (JVSdicom Server), and a DICOM image converter (JVSdicom Compressor). For the automated image analysis of immunohistochemical (IHC) samples stained for the breast cancer biomarkers estrogen receptor (ER), progesterone receptor (PR), Ki-67, and Human Epidermal growth factor Receptor 2 (HER2), two web-based image analysis applications were developed (ImmunoRatio and ImmunoMembrane), which were calibrated to match the visual assessment of expert pathologists. The software development for the present study was done using various programming languages, libraries, frameworks, and development environments. All the executable binaries, web applications, and/or software source code have been released for free and public use on our research group website http://jvsmicroscope.uta.fi/.

The virtual microscopy software platform we have developed is currently being used in several academic and clinical institutions throughout Finland, and there has been significant interest from abroad as well. We have shown that JPEG2000 is a viable solution as the universal virtual slide format, readily linkable with clinical information systems. By using the image analysis software we have described, routine clinical diagnostics of ER, PR, Ki-67, and HER2 IHC can be made in shorter overall analysis time, while improving the reproducibility and repeatability of the analysis. We anticipate that virtual microscopy will continue to gain momentum in the clinical pathology diagnostics, research, and education in the near future.

TIIVISTELMÄ

Täsmällinen histopatologinen diagnoosi on olennainen osa syöpäpotilaiden kliinistä hoitoa. Diagnoosia hyödynnetään valittaessa potilaalle sopivia hoitomuotoja, kuten esimerkiksi solunsalpaajalääkitystä. Tavanomaisesti patologit muodostavat diagnoosin tutkimalla syöpäkudosta sisältäviä näytelaseja valomikroskoopin avulla, mutta nykyisin yhä enenevissä määrin myös digitoimalla näytemateriaalin ja tarkastelemalla sitä tietokonenäytöltä. Mikroskooppinäytteiden digitointia riittävän korkealla tarkkuudella ja muodostuvan informaation tietokoneperustaista käsittelyä kutsutaan virtuaalimikroskopiaksi. Vastaavasti fyysisen näytelasin digitaalista vastinetta kutsutaan virtuaalinäytelasiksi. Vaikka nykyiset kuvantamistekniikat ja tietojenkäsittelymenetelmät mahdollistavatkin virtuaalimikroskopian rutiinikäytön, näytelasien digitoimisesta muodostuva tietomäärä on valtava – jopa useita satoja gigatavuja pakkaamatonta tietoa per näytelasi. Näin suuren tietomäärän automaattinen käsittely vaatii teknisiä erityisratkaisuja, jotka poikkeavat huomattavasti muilla lääketieteellisen kuvantamisen alueilla käytettävistä menetelmistä. Automaattinen näyteskannaus, prosessointi, analysointi, arkistointi sekä jakelu loppukäyttäjille asettavat kaikki oman erityishaasteensa. Tämän väitöskirjatutkimuksen tavoitteena on tunnistaa nämä ongelmakohdat ja ratkaista ne kehittämällä kattava lääketieteellisten tietokoneohjelmistojen kokonaisuus, joka mahdollistaa virtuaalimikroskopian laajan käyttöönoton sekä patologian kliinisessä työssä että opetus- ja tutkimuskäytössä.

Tutkimuksessa käytettävä aineisto koostui pääosin histologisista syöpänäytteistä sekä radiologista kuvamateriaalista. Histologinen materiaali kuvannettiin usealla eri mikroskooppikameralla sekä automatisoiduilla skannauslaitteilla, joita varten kehitimme kuvantamisohjausohjelmiston (DirObserver) sekä näytelasien osittaiskuvantamiseen suunnatun sovelluksen (LargeMontage). Tutkimme JPEG2000-kuvanpakkausstandardin soveltuvuutta virtuaalimikroskopiaan, sen pakkaustehokkuutta, suorituskykyä ja optimaalista koodivirtaparametrisointia, joiden perusteella suunnittelimme ja toteutimme kaksi erillistä ohjelmistopakettia. Ensimmäinen ohjelmistopaketti mahdollistaa JPEG2000-standardin hyödyntämisen virtuaalimikro-

skopiassa ja se koostuu kolmesta sovelluksesta: katseluohjelmisto (JVSview), palvelinohjelmisto (JVSserv) ja konvertointiohjelmisto (JVScomp). Toinen ohjelmistopaketti mahdollistaa virtuaalinäytelasien integroinnin terveydenhuollon tietojärjestelmiin ja Picture Archiving and Communication System (PACS) -kuvatietokantoihin, joiden kuvatiedonsiirto perustuu Digital Imaging and Communications in Medicine (DICOM) -standardiin. Ohjelmistopaketti koostuu kolmesta sovelluksesta: DICOM-PACS-työasemaohjelmisto (JVSdicom Workstation), DICOM-PACS-palvelinohjelmisto (JVSdicom Server) ja DICOM-kuvakonversio-ohjelmisto (JVSdicom Compressor). Rintasyöpäbiomarkkereiden estrogeenireseptori (ER), progesteronireseptori (PR), Ki-67 sekä Human Epidermal growth factor Receptor 2 (HER2) automatisoitua immunohistokemiallista kuva-analyysia varten kehitimme kaksi web-pohjaista ohjelmistoa (ImmunoRatio ja ImmunoMembrane), jotka kalibroitiin vastaamaan ammattipatologien visuaalista arviointia ja tulkintaa. Tutkimuksen ohjelmistokehityksessä hyödynnettiin lukuisia eri ohjelmointikieliä, sovelluskirjastoja, ohjelmistokehyksiä ja -ympäristöjä. Kaikkien ohjelmistojen suorituskelpoiset binääritiedostot, web-ohjelmistot ja/tai lähdekoodi on asetettu vapaasti saataville tutkimusryhmämme web-sivuille http://jvsmicroscope.uta.fi/.

Julkaisemamme avoin virtuaalimikroskopiaohjelmistojen perhe on laajalti käytössä useissa suomalaisissa kliinisissä ja akateemisissa yksiköissä, jonka lisäksi olemme saaneet myös merkittävää ulkomaista huomiota. Olemme osoittaneet JPEG2000-standardin olevan hyvin soveltuva virtuaalinäytelasien universaaliksi kuvaformaatiksi, jonka avulla virtuaalimikroskopia voidaan integroida osaksi terveydenhuollon tietojärjestelmiä. Rintasyövän diagnosointiin kohdennetut kuva-analyysiohjelmistomme mahdollistavat näytetulkintojen tekemisen sekä nopeammin että paremmalla luotettavuudella ja toistettavuudella. Uskomme, että virtuaalimikroskopia tulee lähitulevaisuudessa saamaan merkittävää jalansijaa patologian kliinisessä diagnostiikassa, opetuksessa ja tutkimuksessa.

CONTENTS

LIST OF ORIGINAL COMMUNICATIONS

The thesis is based on the following original communications, which are referred to in the text by their Roman numerals.

I **Tuominen VJ**, Isola J. The application of JPEG2000 in virtual microscopy. J Digit Imaging. 2009 Jun;22(3):250–8. (IF: 1.42)

II **Tuominen VJ**, Isola J. Linking whole-slide microscope images with DICOM by using JPEG2000 Interactive Protocol. J Digit Imaging. 2010 Aug;23(4):454–62. (IF: 1.42)

III **Tuominen VJ**, Ruotoistenmäki S, Viitanen A, Jumppanen M, Isola J. ImmunoRatio: a publicly available web application for quantitative image analysis of estrogen receptor (ER), progesterone receptor (PR), and Ki-67. Breast Cancer Res. 2010;12(4):R56. (IF: 5.79)

IV **Tuominen VJ**, Tolonen TT, Isola J. ImmunoMembrane: a publicly available web application for digital image analysis of HER2 immunohistochemistry. Histopathol. 2012. In press. (IF: 3.57)

ABBREVIATIONS

ADC	analog-to-digital converter
AE	Application Entity
AIC	Advanced Image Coding
AMDD	Amended Medical Devices Directive
ANN	artificial neural network
ASCO	American Society of Clinical Oncology
ASE	approximate standard error
ATA	AT Attachment
BMP	bitmap
CAP	College of American Pathologists
CCD	charge-coupled device
CE	Conformité Européenne
CIELUV	CIE 1976 L*u*v color model
CISH	chromogenic *in situ* hybridization
CMOS	complementary metal-oxide-semiconductor
CMYK	cyan-magenta-yellow-black
CPRL	component-position-resolution-layer
CUDA	Compute Unified Device Architecture
DAB	diaminobenzidine
DICOM	Digital Imaging and Communications in Medicine
DWT	discrete wavelet transformation
EBCOT	Embedded Block Coding with Optimized Truncation
ECW	Enhanced Compression Wavelet
EDTA	ethylenediaminetetraacetic acid
ER	estrogen receptor
FIFO	first-in-first-out
FISH	fluorescence *in situ* hybridization
GNU	GNU's Not Unix!

GPL	General Public License
H&E	hematoxylin & eosin
HER2	Human Epidermal growth factor Receptor 2
HIS	hospital information system
HL7	Health Level Seven
HR	hazard ratio
HTTP	Hypertext Transfer Protocol
ICC	International Color Consortium
ICT	irreversible color transformation
IEC	International Electrotechnical Commission
IHC	immunohistochemistry
IHE	Integrating the Healthcare Enterprise
IOD	Information Object Definition
ISH	*in situ* hybridization
ISO	International Organization of Standardization
ITU	International Telecommunications Union
IVD	In Vitro Diagnostic
JAR	Java archive
JPEG	Joint Photographic Experts Group
JPIP	JPEG2000 Interactive Protocol
LCD	liquid crystal display
LIS	laboratory information system
LRCP	layer-resolution-component-position
LZW	Lempel-Ziv-Welch
MDD	Medical Devices Directive
MFC	Microsoft Foundation Classes
MIB-1	mindbomb homolog 1
MOS	mean opinion score
NA	numerical aperture
OD	optical density
PACS	Picture Archiving and Communication System
PBS	phosphate-buffered saline
PCRL	position-component-resolution-layer

PNG	Portable Network Graphics
PNM	Portable Anymap
PPM	Portable Pixmap
PR	progesterone receptor
PSNR	peak signal-to-noise-ratio
RAM	random access memory
RCT	reversible color transformation
RFC	Request for Comments
RGB	red-green-blue
RIS	radiology information system
RLCP	resolution-layer-component-position
RMSE	root mean squared error
ROI	region of interest
RPCL	resolution-position-component-layer
sCMOS	scientific CMOS
SCP	Service Class Provider
SCU	Service Class User
SDK	software development kit
SNR	signal-to-noise ratio
SOP	Service Object Pair
TCP	Transmission Control Protocol
TDI	time-delay-and-integration
TIFF	Tagged Image File Format
TMA	tissue microarray
UDP	User Datagram Protocol
URL	Uniform Resource Locator
VSLI	very large scale integration
W3C	World Wide Web Consortium
WG-26	DICOM Working Group for Pathology
XML	Extensible Markup Language
XSD	XML Schema Definition

1. INTRODUCTION

One of the central scientific instruments in life sciences is arguably the optical microscope. Optical microscopes are extensively used in clinical laboratory medicine, biomedical research, and education. The most common optical microscope variant is the light microscope, which is especially suitable for medical disciplines involving tissue morphology-based disease diagnosis, such as pathology. By studying histological tumor sections with a light microscope, pathologists can identify structural and molecular alterations in order to perform reliable disease diagnoses. Accurate and reliable histopathological diagnosis is pivotal in numerous disease treatments and is used to determine the patient's eligibility for surgical and adjuvant therapies (e.g., cancer chemotherapy).

Typical histological microscope specimens are thin tissue slices (1–10 µm) with sizes up to 20 × 30 mm, which are mounted on a transparent glass slide. For inspecting the specimens at cellular level, the light microscope is fitted with an optical lens system, which magnifies the image several hundredfold. When using magnifications this high, the microscope's field of view covers only a small area of the whole specimen, and conversely, when using low magnifications, the field of view captures larger areas, but with inadequate resolution. For this reason, the use of digital imaging methods in light microscopy has been limited to acquiring single snapshot micrographs from representative specimen areas. However, recent advancements in information technology and imaging equipment, such as the introduction of charge-coupled devices (CCD), have made it possible to digitize the entire microscope specimen area at high resolutions.

The process of imaging the entire microscope specimen at a diagnostically adequate resolution, and handling the digitized information, is collectively known as *virtual microscopy* (also as whole-slide imaging). The specimen digitization is performed automatically using a microscope scanner, which can be either a conventional light microscope with an attached motorized specimen stage and a robotic slide loader, or a dedicated laboratory instrument with an embedded slide loading

mechanism and stripped-down microscope functionality. The scanned image is a digital representation of the physical specimen slide and is referred to as a *virtual slide*. Owing to the large size of the virtual slides – up to hundreds of gigabytes of uncompressed data per slide – they have to be compressed in order to be distributed and archived efficiently. However, conventional image compression algorithms and file formats, such as JPEG, are not suitable for this, because of their various size restrictions in the standard specifications. Therefore, nearly all scanner manufacturers have developed their own proprietary, closed image formats, which are non-compatible with each other. Furthermore, there is no guarantee that the manufacturers keep supporting their current formats in the future. This presents a significant risk to long-term slide archives, which are accumulated over years or even decades. To ensure long-term compatibility and to facilitate the widespread adoption of virtual microscopy, a universally accepted and open virtual slide format is needed.

The significance of quantifying biomarkers in diagnostic pathology is increasing. Two commonly used biomarker detection techniques are *in situ* hybridization (ISH), which is used to quantify gene expressions within the cellular environment, and immunohistochemistry (IHC), which is used to localize proteins in tissue sections. Despite the advances in specimen processing techniques, such as standardized IHC staining kits, manual (or visual) biomarker quantification is often tedious and time-consuming. Pathology, in particular, has a long history in relying on the visual interpretation of the microscope specimen. As a consequence, the subjective assessment of a specimen by different pathologists may differ considerably (inter-observer variability) and even the diagnoses made by the same pathologist over time may vary (intra-observer variability). Moreover, since the human visual perception is context-dependent, distinguishing the intensity and structure of identical cellular objects in different surroundings might be inconsistent. Therefore, there is a significant need for objective image measurements. By applying digital image analysis techniques, the quantification can be made more accurately and with increased repeatability and reproducibility. In routine large-scale clinical diagnostics, the overall diagnosis time can be lowered and made more cost-efficient, thereby resulting in improved patient care.

Although currently available technology enables routine use of virtual microscopy, the amount of data generated with high-throughput virtual slide scanning is enormous. Processing the data requires specialized information technology methods,

which differ considerably from other medical imaging disciplines. Automated specimen scanning, processing, image analysis, archival, and distribution to the end-users all present their own unique challenges to the software and hardware development. Moreover, large-scale clinical adoption of virtual microscopy requires integration with hospital and laboratory clinical information systems. Most clinical information systems are based on a central Picture Archiving and Communication System (PACS), which is interfaced through the Digital Imaging and Communications in Medicine (DICOM) image exchange standard. Although a DICOM PACS generally supports multi-modal medical imagery, the large size of virtual slides prohibits their direct usage with existing server and workstation architectures.

The central aim of the present thesis study is to identify these problems and solve them by designing and implementing an open and standards-based software platform, which will facilitate the large-scale usage of virtual microscopy in clinical, research, and educational environments. The study consists of four original communications (I–IV) and is structured as follows. After the introduction, Chapter 2 of the document presents an in-depth review to the relevant methodology and literature. The specific aims of the study are presented in Chapter 3 and the sample material, methods, and empirical tests involved are described in Chapter 4. A summary of the results of the original communications is given in Chapter 5 and the implications of these results are discussed in Chapter 6. Finally, Chapter 7 contains a short summary and concluding remarks.

2. REVIEW OF THE METHODOLOGY

2.1 Theory of light microscopy

The origins of light microscopy reach back to the 16th and 17th century. Although no particular founding person can be traced, some of the most notable figures were Robert Hooke (1665) as the first person to view cells and Anton van Leeuwenhoek (1673) for the construction and distribution of light microscopes with robust components. Later, the work of Carl Zeiss and Ernst Abbe (1887) led to the production of first high-quality objective lenses, which were based on sound optical theory, and with the illumination technique developed by August Köhler (1893), full resolving potential of these lenses could be utilized. Modern light microscopy began to form in the late 1980s, when the industry largely shifted to using infinity-corrected optics and the market was introduced with first high-grade digitalization equipment (Walter & Berns 1986, Weiss *et al*. 1989).

2.1.1 Specimen magnification

The optical pathway of a light microscope consists of several lenses, of which the most significant are the objective lens and the substage condenser lens (Goldstein 1999). The condenser lens focuses light from the illuminator onto a small area of the specimen on the stage. The light passes through the light-absorbing specimen, partly scatters, and is collected by the objective lens, which produces the magnified image (Murphy 2001). Most lenses used in contemporary microscopes are compound lenses. Compound lenses are constructed from several refracting lens elements, which are sealed together to form a complex *thick lens*. The light ray paths of optical systems based on a thick lens are traceable, but impractical to illustrate. Howev-

er, the principles of a simple system based on a single *thin lens* provide a good approximation (Figure 1).

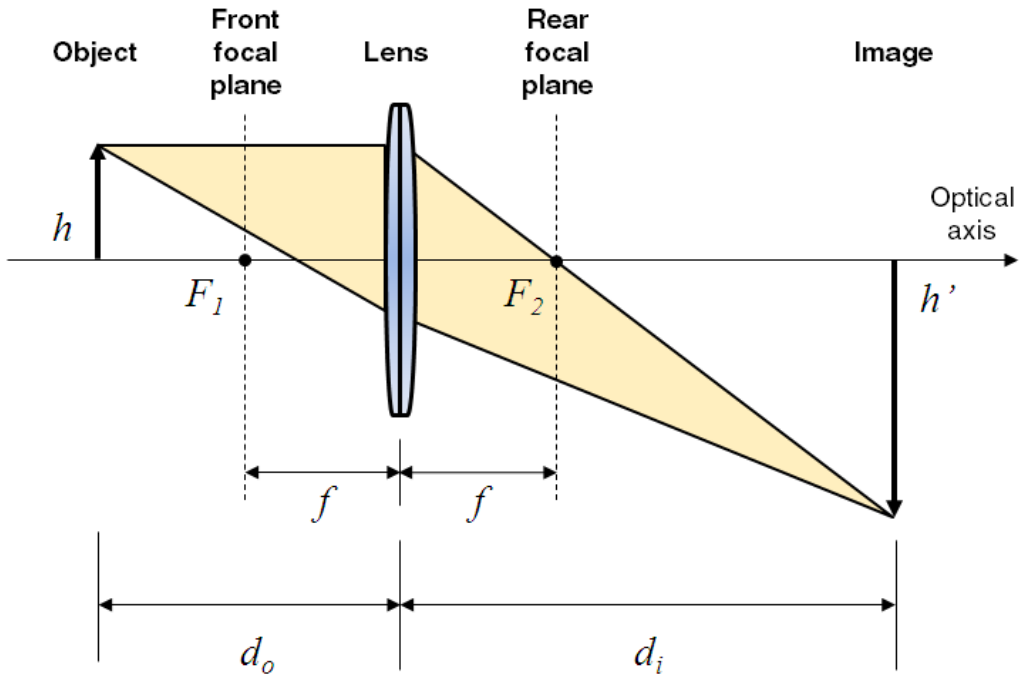

Figure 1. Magnification by a converging, double-convex thin lens with focal length f. An object with height h is at distance d_o from the lens, which projects a magnified (inverted) image with height h' at distance d_i. The lens refracts light rays that are parallel with the optical axis through the rear focal point F_2. Similarly, rays passing through the front focal point F_1 are bent in a direction parallel to the optical axis. Rays passing through the center of the lens are not deviated.

The refraction capabilities of a lens are characterized by its size and shape (Hecht 2002). In the simplest case, the double-convex surfaces of a thin lens must be spherical in order to converge the entering divergent light. Based on the curvature of the surfaces, we can derive the fundamental property of a lens, the focal length. The focal length is dependent on the radii of the surfaces and the refractive indices of the lens material (typically glass) and the surrounding medium (typically either air or immersion oil). For a thin lens, the focal length f is given by

$$\frac{1}{f} = \left(\frac{n_l}{n_m} - 1\right)\left(\frac{1}{R_1} + \frac{1}{R_2}\right), \quad (1)$$

where n_l is the refractive index of the lens (for glass, $n \approx 1.51$), n_m is the refractive index of the medium (for air, $n = 1.00$; for immersion oil, $n \approx 1.51$), R_1 is the radius of the front surface, and R_2 is the radius of the rear surface.

The focal length determines the distance at which two focal planes, front and rear, reside. The focal planes are parallel to the lens and perpendicular to the optical axis. Object located within the front focal plane at focal point F_1 will appear at an infinite distance on the rear side of the lens. Conversely, an object located at infinite distance (typically $> 30 * f$) on the front side of the lens will appear at focal point F_2 within the rear focal plane. In modern infinity-corrected microscope systems, the specimen is placed at the front focal plane, causing light rays to emerge from the objective lens parallel to the optical axis into infinity, which are then converged into an image using another lens called a tube lens (Bradbury & Bracegirdle 1998). This architecture allows the manufacturers to add various accessory modules within the "infinity space" between the two lenses. The accessories include fluorescence filter cubes, differential-interference-contrast prisms, and polarizers (Abramowitz 1987).

In order to achieve images that are in focus, optical systems must have precise inter-component distances (Smith 1992). Given the lens focal length f, the distance between the object and the lens (d_o), and the distance between the lens and the magnified image (d_i), a magnified in-focus image is produced if the following *lens equation* is satisfied:

$$\frac{1}{d_o} + \frac{1}{d_i} = \frac{1}{f}. \tag{2}$$

The inter-component distances are also responsible for the magnification M of the optical system, such that

$$M = \frac{d_i}{d_o}. \tag{3}$$

In contemporary light microscopes, d_i corresponds to the mechanical tube length, which is the distance between the lens mounting opening and the image plane, and is nominally set to 160 mm (Inoué & Spring 1997). Furthermore, the distance d_i is, in practice, always much greater than the distance d_o.

Although *M* is used to specify the magnifying power of an objective lens, in traditional microscope viewing the image is further magnified by another lens located in the ocular (or eyepiece), which conventionally has a 10× magnification power. Consequently, the total magnification of a light microscope is usually given as the product of the objective lens magnification and the ocular lens magnification. However, within the scope of the present study, we ignore the ocular and concentrate only on digital imaging detectors, such as CCD (reviewed in Section 2.2).

2.1.2 Optical lens aberrations

Lenses are prone to various optical distortions and faults called aberrations, which have to be corrected in order to obtain good image quality (Gage & Gage 1914). The most common aberration types are *spherical* and *chromatic* aberration (Figure 2). Spherical aberration occurs due to inadequate shape of the lens surface, which causes light rays parallel to the optical axis to refract differently depending on whether they enter the periphery or the center of the lens. Chromatic aberration is related to the refractive index of the lens material, causing light rays parallel to the optical axis to bend differently depending on their wavelength. Other aberration types include coma, astigmatism, field curvature, barrel distortion, and pincushion distortion (Murphy 2001). The effect of aberrations can be reduced or eliminated by using compound lens structures, which are widely used in contemporary microscope objectives.

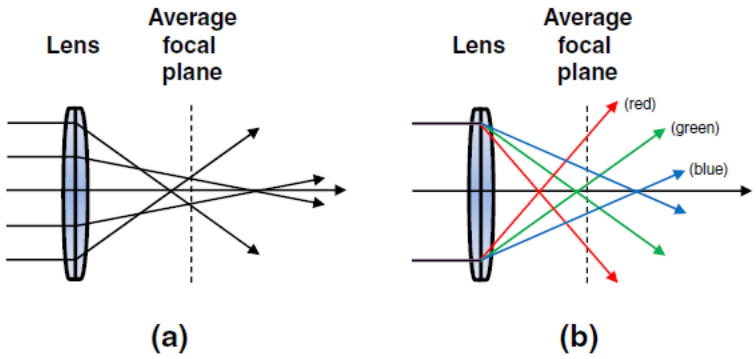

Figure 2. Common types of lens aberrations, which cause distortion in the image. Spherical aberration (a) occurs when parallel light rays entering the periphery of the lens refract more strongly than rays entering the lens center. Chromatic aberration (b) causes parallel light rays of different wavelength to refract non-uniformly.

2.1.3 Image formation by diffraction

Magnifying the specimen with a light microscope is alone insufficient for producing a meaningful image. To discern details and structures that exist in the specimen, the magnified image has to have adequately high *image contrast*, which in turn results from the wave optical phenomenon called *diffraction* (Pluta 1988, Hecht 2002). When light is transmitted through a microscope specimen, some of the light passes through and around undeviated and is referred to as direct light. Some light, however, passes through the small openings in the specimen causing the light to spread into a series of spherical wavefronts and is referred to as diffracted light (Figure 3). The objective lens collects both the direct and diffracted light and separates the rays into groups, which are referred to as diffraction orders (0 through *n*). The 0^{th} order represents the direct light, whereas the 1^{st}, 2^{nd}, 3^{rd}, …, n^{th} orders contain the diffracted rays based on their angle of entry. When using a periodic object, such as a stage micrometer or similar grating, the diffraction orders are distinguishable as spots in the rear focal plane of the lens (diffraction plane). From the diffraction plane, the light continues to propagate into the image plane (e.g., the surface of a digital camera detector).

Upon arrival at the image plane, the diffracted light causes *interference* with coincident direct light (Figure 4) (Born & Wolf 2000). If diffracted light has the same phase as the direct light, the light waves experience *constructive* interference, resulting in brighter local areas. Similarly, if the two coinciding light waves have shifted phase, the interference is *destructive*, resulting in darker local areas. If the relative phase shift is one-half the wavelength ($\lambda/2$) and both waves have the same amplitude, the waves eliminate each other. The contrast between the alternating patterns of dark and bright local areas is what we perceive as an image of the specimen and is the basis of image formation in light microscopy.

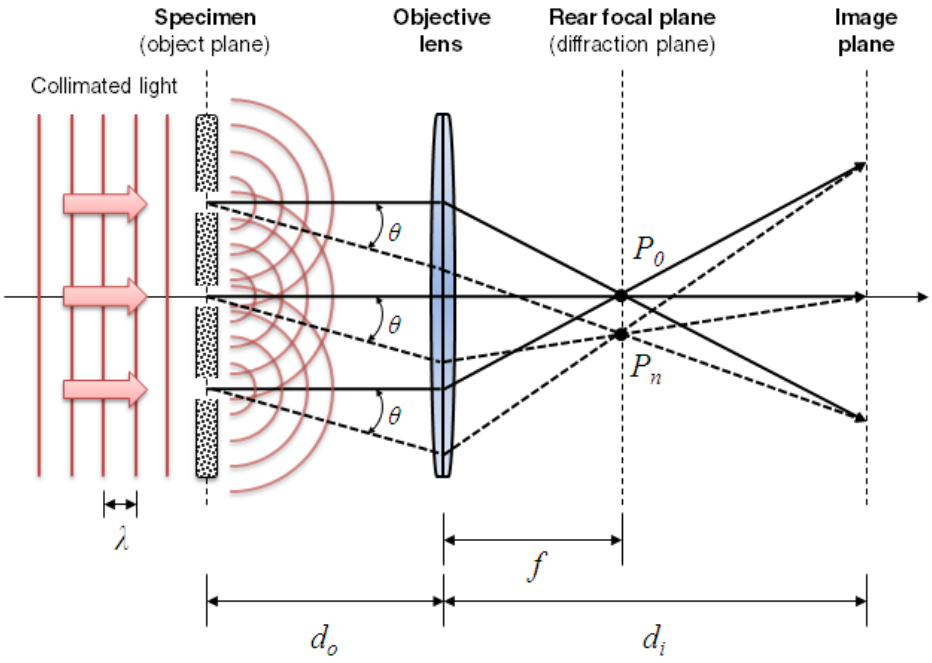

Figure 3. Diffraction-based image formation in a light microscope. A planar wavefront of light with wavelength λ passes through the specimen in focus, causing the light to diffract into a series of spherical wavefronts. The objective lens collects the wavefronts and projects a diffraction image on the rear focal plane of the lens, separating undeviated light rays (0^{th} order) and deviated rays (n^{th} order) into diffraction groups (P_0–P_n). The light rays are again combined in the image plane, where interference between 0^{th} and n^{th} order light rays generates image contrast.

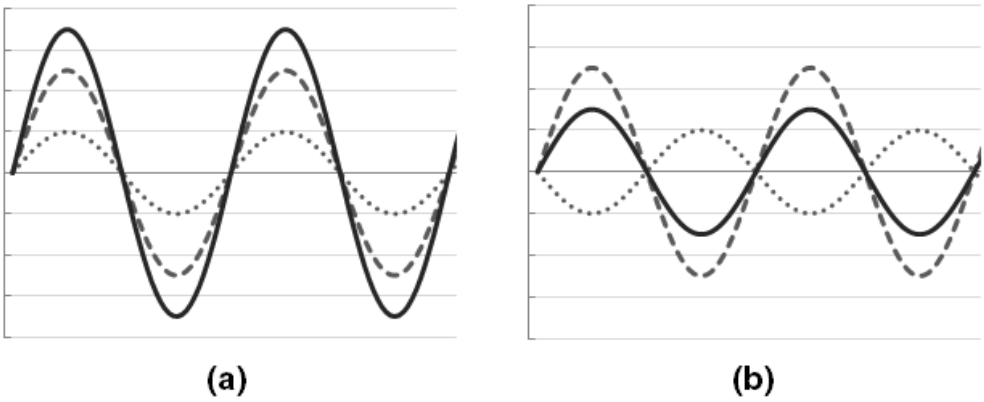

Figure 4. Interference of two coincident light waves (dotted and dashed lines) of same wavelength. Constructive interference (a) occurs when the two waves have the same phase, whereas destructive interference (b) occurs when the waves are out of phase with each other. The resulting wave (solid line) is the arithmetic sum of the amplitudes of the original waves.

2.1.4 Spatial resolution

The amount of detail that a microscope is able to resolve is defined using a characteristic called *spatial resolution* (Ash & Nicholls 1972). Formally, the spatial (or optical) resolution of a light microscope is defined as the minimum distance at which two object points are recognizable as separate. Using contemporary objective lenses, the theoretical resolution limit of a light microscope is approximately 0.2 µm (whereas the human eye is ~70 µm), but since resolution is dependent on several factors, such as the quality of the specimen and the illumination, the practical limit is always higher. In biomedical context, light microscopes are capable of resolving structures that exist in cellular and bacterial level, whereas smaller objects require instrumentation with higher resolution, such as transmission electron microscopes (Figure 5).

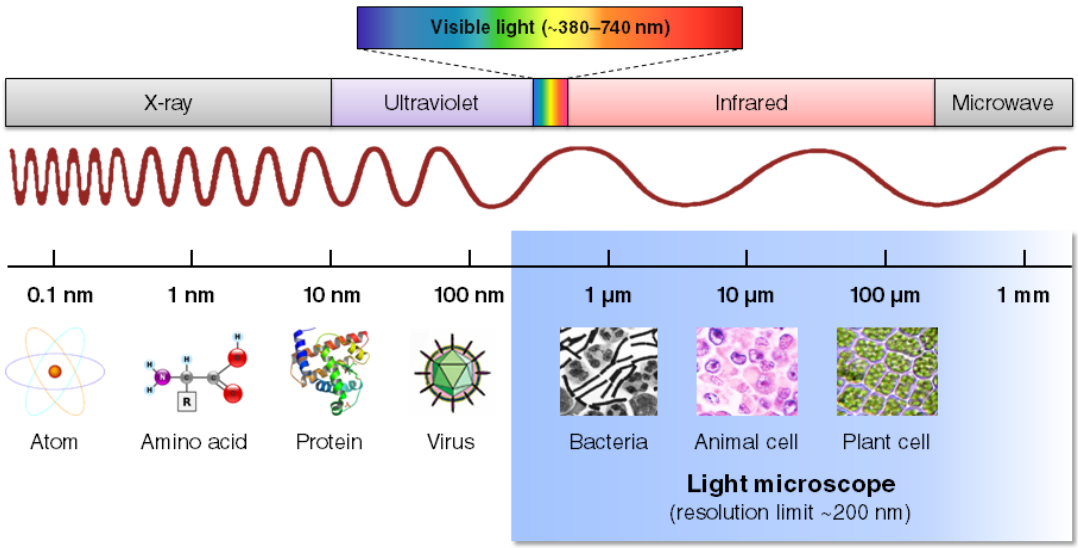

Figure 5. The resolving power of a light microscope and its relationship to the wavelength λ of electromagnetic radiation (logarithmic scale). The upper part depicts radiation types and their respective wavelength ranges, whereas the lower part exemplifies the relative sizes of common biological structures. Text modified from Murphy (2001); icon imagery public domain.

Spatial resolution is primarily governed by the angle at which the objective lens can collect the entering light. First of all, to produce any image details whatsoever, the lens must be able to capture at least two diffraction orders. By capturing only the 0^{th} order, there will be no interference in the image plane, and thus no image is

formed. Capturing additional higher orders will increase the image fidelity and resolution. Moreover, if the surrounding medium between the specimen and the lens has a higher refractive index than air (such as immersion oil), the objective lens is capable of capturing light with wider diffraction angle, thus increasing the resolution. Furthermore, since the diffraction angle increases as the wavelength of light increases, using monochromatic blue light results in narrower diffraction angle and thus the objective lens is capable of capturing higher number of diffraction orders. The acceptance angle of an objective lens is defined using a property called *numerical aperture* (NA), which is, along with magnification, the most important characteristics of an objective lens. The numerical aperture *NA* of an objective lens is given by

$$NA = n * sin\theta \, , \tag{4}$$

where n is the refractive index of the surrounding medium and θ is the half angle of the collected cone of light.

Before defining criteria for the minimum resolvable point distance, one has to take into consideration another manifestation of the diffraction phenomenon. When the objective lens projects light through the circular rear aperture of the lens, light waves experience bending around the edges of the aperture. As a consequence, a point in the object is never projected as a point onto the image plane, but rather a spot with circular diffraction rings with gradually decreasing intensity (Figure 6). The central spot is referred to as an *Airy disk* and its size is related to the wavelength of light and the numerical aperture of the objective lens (Airy 2007).

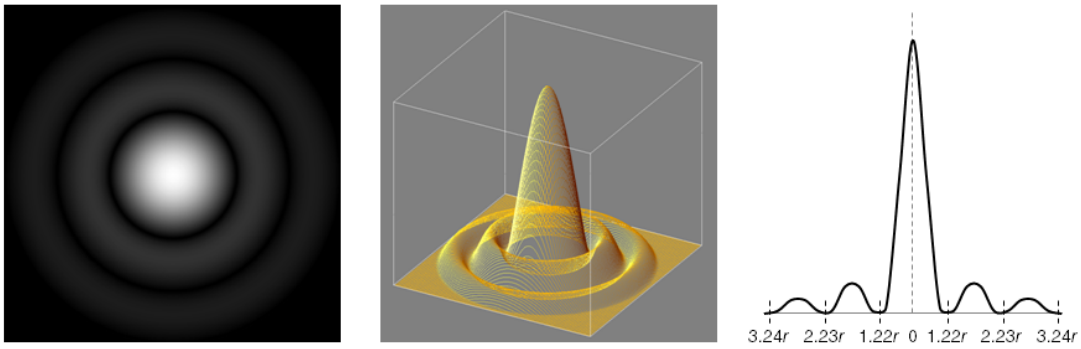

Figure 6. The image of a point source of light due to diffraction. The point is projected as a diffraction pattern (a) with a central spot called an Airy disk and surrounding diffraction rings. The pattern can also be modeled using a three dimensional representation (b) as a point spread function. The intensity profile (c) shows the radii of the diffraction rings and their relationship with the wavelength of light λ and the numerical aperture NA of the objective lens, such that $r = \lambda/2NA$.

Assuming the numerical aperture of the substage condenser lens equals or exceeds that of the objective lens NA, the radius r of the central Airy disk is given as

$$r = 1.22\frac{\lambda}{2NA} = 0.61\frac{\lambda}{NA}. \quad (5)$$

According to the *Rayleigh criterion of resolution*, two adjacent diffraction spots with a distance δ in between can be resolved as separate if $\delta \geq r$ (Rayleigh 1896). In practice, however, the maximum resolution can be achieved only if the microscope is properly calibrated by using, for example, the Köhler illumination technique, which ensures that all the optical components of the microscope are aligned correctly with respect to each other (Köhler 1893).

2.2 Specimen digitization

When using a light microscope with an attached digital camera, the objective lens projects the magnified specimen image directly onto the surface of the camera detector instead of an intermediate image plane, which is needed for ocular observation (Murphy 2001). The camera detector collects and stores the incoming light and the auxiliary electronics translates the amount of electrons captured into a discrete, digital signal that is suitable for computer-based processing. The digitization involves sampling and interpolation, hindered by aliasing and various types of noise, ultimately resulting in a digital image–a two-dimensional sequence of pixel samples with associated intensity values.

2.2.1 Solid-state camera hardware

There are a number of solid-state (i.e., without mechanical movement) detector types available on the market, two of the most common being the low-cost, high-noise complementary metal-oxide-semiconductor (CMOS), and the high-cost, low-noise charge-coupled device (CCD) (Nakamura 2005). An emerging derivative of the CMOS detector type, the so-called scientific CMOS (sCMOS), aims at combining low manufacturing costs, low noise rates, and fast frame speeds (Coates *et al.* 2009). For the purposes of the present study, CCD is the primary detector type of interest.

2.2.2 Grayscale image acquisition

CCD cameras have detectors that contain a rectangular array of sensor elements, photodiodes, which have a 1:1 correspondence with a pixel in the resulting digital image (Wayne 2009). The diodes function as light gathering wells with a fixed capacity, and the number of electrons stored is a direct linear measure of the light intensity. The diode sensitivity to light varies along the spectral range and is described using a property called *quantum efficiency*, which is the fraction of input photons converted to stored electrons. On a set interval, the accumulated electrons in the wells are transferred to an on-chip pre-amplifier, which forms an analog signal and

transmits it to an auxiliary analog-to-digital converter (ADC) for quantification to produce an integer value. The bit depth (2^n) of the ADC dictates the number of intensity steps available, which, for instance, in a 12-bit ADC is 4,096 (2^{12}). The end result is a grayscale image with pixels that have varying intensities.

2.2.3 Color image acquisition

The camera detectors, such as CCD, are not inherently capable of distinguishing color. In order to detect color information, cameras have to be fitted with special constructions, which separate the wavelength ranges of light corresponding to colors red, green, and blue (RGB). Several constructions have been developed, of which the most notable are: a three-CCD detector with a prism in the middle for splitting the light into RGB components and directing them onto their respective detectors (Wootton 2005); a single CCD detector with a mechanically rotating color filter wheel in front (Parulski *et al.* 1990); and, the most widely employed, a single CCD detector with a *Bayer filter* (Bayer 1976).

The Bayer filter is a mask that is overlaid on top of the CCD detector (Figure 7). The mask is composed of an alternating pattern of microlenses, which pass through light corresponding to the RGB colors. The passed light is registered in the detector grid as groups of four adjacent pixels (25% red, 50% green, 25% blue), from which the final RGB color image is formed by component-wise interpolation. As a consequence, the image resolution is reduced to some extent, depending on the wavelength of the light and the quality of the interpolation (Ramanath *et al.* 2002).

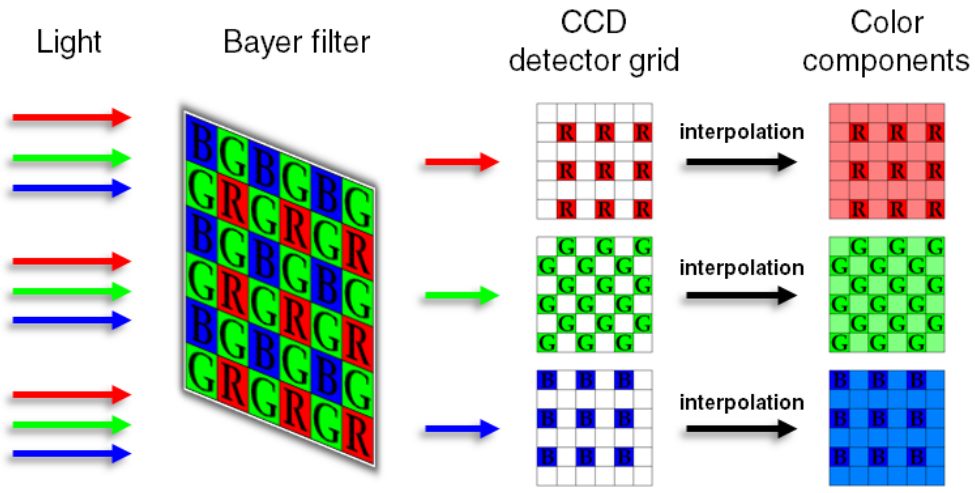

Figure 7. Color image acquisition using the Bayer filter. A filter mask is overlaid on top of the CCD detector, which selectively assigns the pixels of the detector grid to receive light with wavelength ranges corresponding to colors red, green, and blue. The final, full-resolution color components are formed via interpolation.

2.2.4 Sampling and aliasing

In order to create a faithful digital representation of the image, the optical image has to be sampled at adequate spacing. According to the *Shannon sampling theorem* (Shannon 1948), no information is lost if a continuous, band-limited function is sampled using spacing Δx such that

$$\Delta x \leq \frac{1}{2f_{max}}, \tag{6}$$

where f_{max} is the highest frequency content of the function. In other words, there must be at least two sample points per highest frequency content of the function; this is commonly known as the *Nyquist criterion*. Sampling at spacing $\Delta x < 1/2f_{max}$ is considered as *oversampling*, generating redundant data, whereas sampling at the specific spacing $\Delta x = 1/2f_{max}$ is referred to as *critical sampling*.

If the sample spacing $\Delta x > 1/2f_{max}$, the function will be *undersampled*, which results in loss of critical data and the function cannot be reconstructed without error (Jerri 1977). In the case of digital images, undersampling introduces a phenomenon called *aliasing*, which occurs when an image is sampled at a coarse spacing in relation to the size of the details present in the image (Legault 1973). The effects of ali-

asing become visible as reconstruction errors known as Moiré patterns in images or image areas, which contain repeating patterns of high-frequency details (Figure 8) (Jain *et al.* 2001).

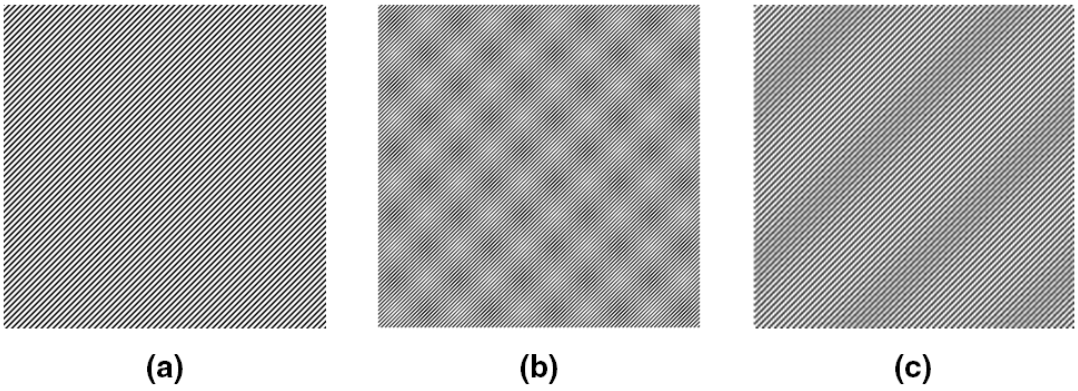

Figure 8. The aliasing phenomenon during image sampling. The original image contains black diagonal stripes, which are displayed correctly (a) when using a sample spacing that satisfies the Nyquist criterion. If the sample spacing is too coarse, reconstruction errors known as Moiré patterns begin to appear (b, c).

2.2.5 Camera noise

The specimen digitization process introduces unwanted image noise, which can be reduced either by camera hardware or by software image processing (Irie *et al.* 2008). The three primary sources of noise in a CCD camera are: *photon noise*, *dark noise*, and *readout noise*. Photon noise is due to the inherent statistical variation in the arrival rate of the photons, and cannot be reduced by camera design. Dark noise arises from the generation of thermal electrons due to CCD temperature, and can be reduced by using active cooling. Readout noise comprises all electronic noise sources of the camera components. Both the photon and the dark noise follow the Poisson distribution and are therefore equivalent to the square-root of the signal. The total performance of the CCD imaging system can be characterized using the *signal-to-noise ratio* (SNR), which combines all the three noise sources, such that

$$SNR = \frac{PQ_e t}{\sqrt{PQ_e t + Dt + N_r^2}}, \tag{7}$$

where P is the photon flux incident on the CCD (photons per pixel per second), Q_e is the quantum efficiency of the CCD, t is the integration time (in seconds), D is the dark noise current (electrons per pixel per second), and N_r^2 is the read noise. In practice, $SNR > 50$ is considered to provide sufficient image quality (Wayne 2009).

2.2.6 Detector resolution and pixel size

The optical image projected on to the camera detector surface consists of a myriad of adjacent and overlapping diffraction spots with a given Airy disk radius r. During image sampling, the Nyquist criterion is satisfied if at least two adjacent detector pixels cover the projected Airy disk radius (Table 1). Consequently, when using a high optical magnification (e.g., 40×), the diffraction spots are resolvable by the detector more easily, making the objective lens the primary component to affect the overall system resolution. On the other hand, when using a lower magnification (e.g., 10×), resolving the diffraction spots by the detector becomes more challenging and thus the overall resolution is dependent on the detector properties–more specifically, the size of the detector surface and its pixels. The detector surface size is commonly given as the diagonal measure in inches (e.g., 1/3" and 2/3") and the detector pixel size in micrometers (e.g., 6.45 µm), from which the total number of pixels can be derived (Nakamura 2005).

Table 1. Critical sampling requirements for detector pixel size. The objective lens specifications are based on plan-apochromatic structures and the light uses reference mid-spectrum wavelength of 0.55 µm. The maximum detector pixel size is defined according to the Nyquist criterion.

Lens magnification	Lens NA	Resolution limit (µm)	Projected Airy disk radius (µm)	Maximum detector pixel size (µm)
4×	0.20	1.68	6.72	3.36
10×	0.45	0.75	7.50	3.75
20×	0.75	0.45	9.00	4.50
40×	0.95	0.35	14.00	7.00
60×*	1.40	0.24	14.40	7.20
100×*	1.40	0.24	24.00	12.00

* with immersion oil (refractive index ~1.51)

2.2.7 Spatial calibration

Matching the size of the produced digital image to the specimen is achieved via spatial calibration (Wu *et al.* 2008). Spatial calibration produces an image scale (typically in µm/pixel), which is beneficial in downstream image processing and analysis. The calibration is done by calculating the image scale *s* of the specimen, such that

$$s = \frac{\Delta x}{M}, \tag{8}$$

where Δx is the detector pixel size (i.e., the sampling spacing) and M is the total magnification of the optical system. Alternatively, the image scale can be measured using a pre-calibrated target, such as a stage micrometer, which contains a scale bar etched on its surface. By measuring the distance D between two points on the stage micrometer, the image scale s can be calculated by

$$s = \frac{D}{\sqrt{(x_2 - x_1)^2 + (y_2 - y_1)^2}}, \tag{9}$$

where (x_1,y_1) and (x_2,y_2) are the pixel locations of the two points within the image.

2.3 Overview of diagnostic pathology

One of the largest medical disciplines to routinely employ light microscopes is pathology, which uses them in the examination of organs, tissues, and body fluids (Kumar *et al.* 2007). Pathology is divided into several subspecialties, such as surgical, molecular, and forensic pathology. However, within the scope of the present study, I use a generalized term *diagnostic pathology*, which encompasses various methods from the subspecialties, with the emphasis on clinical aspects and microscopy. The software applications described in the present study are all targeted for diagnostic pathology and the biological sample material is mainly derived from clinical pathology archives. Thus, a brief summary of the involved pathological methodology is in order.

2.3.1 Histopathological specimen preparation

Histopathology, that is, the *in vitro* examination of diseased tissue specimens with a light microscope, is a widely applied technique in diagnostic pathology (Gross & Steinman 2009). The specimens are sections from a gross tissue sample, which can be either a surgically removed tumor or a biopsy sample. After extraction, the gross sample is fixed to preserve it close to its natural state and to prevent degradation. If rapid processing time is required, the fixation is done using a frozen section technique (Taxy *et al.* 2009), but in other cases the fixation is done using chemical substances (e.g., formalin). After chemical fixation, the gross sample is embedded in a solid medium, such as a paraffin wax block, which is then sectioned into 1–10 µm thick slices using a microtome. Each slice is subsequently mounted on a transparent microscope glass slide and a protective coverslip is ultimately attached on top of the slide. However, before attaching the coverslip, the contrast of the tissue section has to be artificially improved by the means of staining, since the cellular structures appear transparent and colorless.

2.3.2 Tissue section staining

The most common way to increase the contrast of the cellular structures is to stain the tissue section with dyes, which selectively attach to different cellular components (Gross & Steinman 2009). Several stains have been developed, of which the most frequently used is the hematoxylin–eosin (H&E). In an H&E stain, the hematoxylin colors the cell nuclei blue, followed by the eosin counterstain, which colors the cytoplasm and extracellular matrix in various hues of red (Figure 9a). Another alternative to stain the section is to use immunohistochemical (IHC) techniques, which utilize the cell antigen–antibody binding interaction to localize various proteins (Renshaw 2007). In the context of the present study, the most relevant IHC staining is based on diaminobenzidine (DAB) chromogen, which, in the presence of a peroxidase enzyme, produces a brown precipitate either within the cell nuclei, cytoplasm, or cell membranes. The staining is finalized by complementing the DAB with a blue hematoxylin counterstain (Figure 9b).

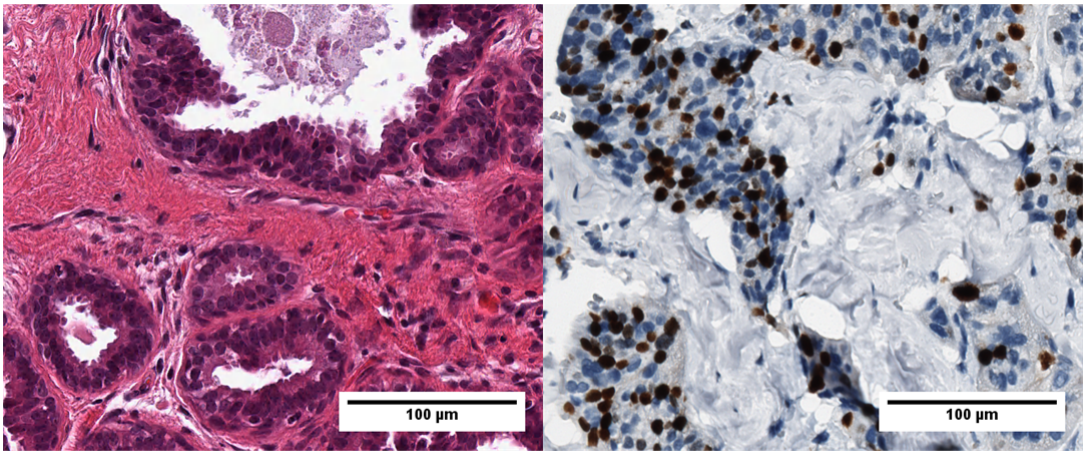

Figure 9. Micrographs of two stained histological tissue sections. Exemplified with hematoxylin–eosin in basic histopathology (a) and diaminobenzidine–hematoxylin nuclear staining for ER, PR, and Ki-67 in immunohistochemistry (b).

2.3.3 Breast cancer biomarkers

The stained tissue sections can be used to diagnose the tumor's type, grade, stage, and, of increasing importance, the expression of various disease-related biological

features, *biomarkers* (Jain 2010). Cancer-related biomarkers are commonly classified as either *predictive* or *prognostic*, but in many cases they are both. Predictive biomarkers provide information on how a patient will respond to a given therapy, whereas prognostic biomarkers reveal information on the overall clinical outcome of the patient with regard to mortality and the risk of disease recurrence.

A considerable amount of literature has been published on breast cancer-specific biomarkers (Weigel & Dowsett 2010, Stuart-Harris *et al.* 2008, Harris *et al.* 2007). Among the strong predictive biomarkers are estrogen receptor (ER) and progesterone receptor (PR), which provide tumor status information for determining the patient's eligibility for endocrine therapy (Allred *et al.* 2009). Current recommendations of the American Society of Clinical Oncology and College of American Pathologists (ASCO/CAP) set guidelines for performing the ER and PR IHC assays (Hammond *et al.* 2010). First, measuring the ER and PR status is done, for instance, with a validated IHC assay, which stains the positive cell nuclei with brown DAB (Figure 9b). Second, the fraction of positive invasive tumor cells must be quantified either by visual estimation or automatically with image analysis software. Third, the staining intensity should be classified as weak, moderate, or strong. Finally, the interpretation of the assay should be as receptor positive (≥1% positive), receptor negative (<1% negative), or uninterpretable. Although there is no golden standard assay available for IHC testing of ER and PR, several inter-laboratory quality assurance studies have provided high reproducibility and repeatability of staining procedures (UK NEQAS 2011, NordiQC 2011).

Another important predictive, as well as prognostic, biomarker for breast cancer is the oncogene Human Epidermal growth factor Receptor 2 (HER2) (Köninki *et al.* 2009). Overexpression of HER2 is an indication that the patient will more likely benefit from trastuzumab-based chemotherapy (Mass *et al.* 2005). On the other hand, HER2 positivity is also associated with shorter overall patient survival (Press *et al.* 1993). Similar to ER and PR, the ASCO/CAP has compiled recommendations for the assessment of HER2 status (Wolff *et al.* 2007). The HER2 expression is measured, for example, with a validated IHC assay, which stains the positive cell membranes with brown DAB (Figure 10). The tumor is scored either visually or semi-quantitatively with a digital analysis software as IHC negative (0/1+), IHC equivocal (2+), or IHC positive (3+). The negative score is given if the cellular membrane contains no staining or has weak and incomplete staining in any propor-

tion of tumor cells. The positive score is given if the membrane staining is uniform and intense in >30% of invasive tumor cells. The equivocal score is assigned if the membrane staining is complete, but is either non-uniform or weak in intensity (with obvious circumferential distribution in at least 10% of cells). In addition, in the case of equivocal score, the HER2 status should be confirmed using fluorescence *in situ* hybridization (FISH) or chromogenic *in situ* hybridization (CISH) (Riethdorf *et al.* 2011).

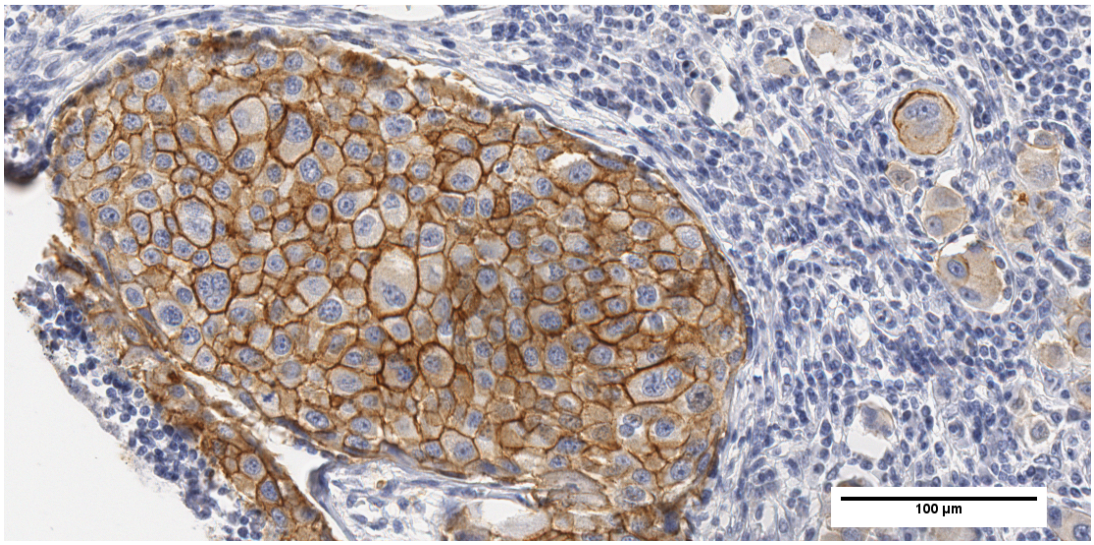

Figure 10. Immunohistochemical HER2 staining of breast cancer tissue section. Complete and intense brown diaminobenzidine staining is observed in the cellular membrane regions. The sample is counterstained with blue hematoxylin.

An emerging prognostic biomarker for breast cancer is the proliferation antigen Ki-67 (Yerushalmi *et al.* 2010). The expression of Ki-67 is measured with IHC by quantifying the percentage of positively stained (brown DAB) cell nuclei out of total nuclei (Figure 9b); the percentage is referred to as *labeling index*. High Ki-67 labeling index is linked with rapidly proliferating tumors, and patients with such tumors are shown to endure poorer outcomes than those with tumors exhibiting low proliferation (de Azambuja *et al.* 2007). However, wide adaptation of Ki-67 is hindered by the lack of uniformly accepted cut-off points for defining low- and high-risk patient groups, and as such, is not currently recommended as a routine biomarker by the ASCO/CAP. Nevertheless, the prognostic role of Ki-67 has been confirmed with meta-analyses including several thousand patients (Stuart-Harris *et al.* 2008, Urruticoechea *et al.* 2005).

2.3.4 Accuracy of visual biomarker assessment

Regardless of the biomarker expression being assessed, it is well-known that pathologists' visual interpretations may lead to significant inter- and intra-observer variability. For example, a German-wide study with 172 pathologists revealed that with six IHC biomarkers (CD45, pankeratin, chromogranin, smooth muscle actin, ER, and Ki-67), the correct positive recognition (sensitivity) of the participants was as low as 20%, averaging to 72%, whereas the correct recognition of negative samples (specificity) was averaged at 89% (Table 2; samples stained in each participant's laboratory) (Rüdiger *et al.* 2002). With regard to ER, 24% of stains were interpreted as false negatives. In the case of HER2, the equivocal (2+) category is particularly problematic, as evident by the poor inter-observer agreement in several studies (Gavrielides *et al.* 2011, Lacroix-Triki *et al.* 2006).

Table 2. Sensitivity of biomarker assessment and errors in interpretation of stained IHC slides compared with an expert panel review (172 participant pathologists, 6 slides per participant to be stained for six antibodies, 30 tumor tissue cores per slide, totaling 29,040 analyzable data spots). Modified from Rüdiger *et al.* 2002.

Biomarker (antibody)	Participant sensitivity	False negative *	False positive **
CD45	96%	4%	19%
Chromogranin	65%	3%	2%
Keratin	73%	3%	4%
Ki-67	84%	1%	1%
ER	83%	24%	1%
SMA	48%	10%	24%

* only cases with expected positive staining were evaluated

** only cases with expected negative staining were evaluated

2.4 Virtual microscopy

Virtual microscopy began to develop in the early 2000s, when several research groups started to experiment on emulating the usage of light microscope on a computer by semi-automatically digitizing the whole microscope specimen area into a virtual slide and subsequently viewing it on a computer display (Glatz-Krieger *et al.* 2003, Lundin *et al.* 2004a, Weinstein 2005). The challenges at the time were many, including poor hardware computational power, low digital camera frame rates, mediocre image quality, improper image stitching algorithms, and the high cost of storage capacity, thus making the process relatively slow and cumbersome (Kayser *et al.* 2006). However, with the advent of inexpensive, high-quality camera equipment, continually improving computational resources, and lowered storage costs, scanning virtual slides and disseminating them through the networks has become feasible in routine practice (Della Mea 2011).

2.4.1 Virtual slide scanning

In order to create virtual slides which resemble real microscopy viewing, specimens must be scanned at high spatial resolution. Resolutions from 0.20 to 0.40 µm per pixel (typically obtained using 40× and 20× objective lenses, respectively) are generally considered necessary for sufficient image quality (Rojo *et al.* 2006). However, using resolution ranges this high, the microscope's field of view covers only a fraction of the whole specimen area, and therefore the image acquisition has to be done sequentially, on a tile-by-tile basis (Figure 11). The sequential acquisition is performed by a controller software, which systematically moves the motorized specimen stage under the objective lens. Most imaging systems employ the so-called *area scanning* technique, in which an initial field of view is captured, the stage is then moved to an adjacent field in the X/Y direction, the field is focused in the Z direction (Sun *et al.* 2005), and the process is repeated until the whole specimen area, or a selected region (Oger *et al.* 2008), is imaged. Finally, a downstream image processing software is used to combine, or *stitch*, the generated image tiles together to form one large image montage (i.e., the virtual slide). The scanner manufacturer DMetrix (Tucson, AZ, US) has developed an area scanner variant based on an 80-

element microlens array in lieu of the objective lens, thereby capturing a larger field of view with a single exposure (Weinstein et al. 2006).

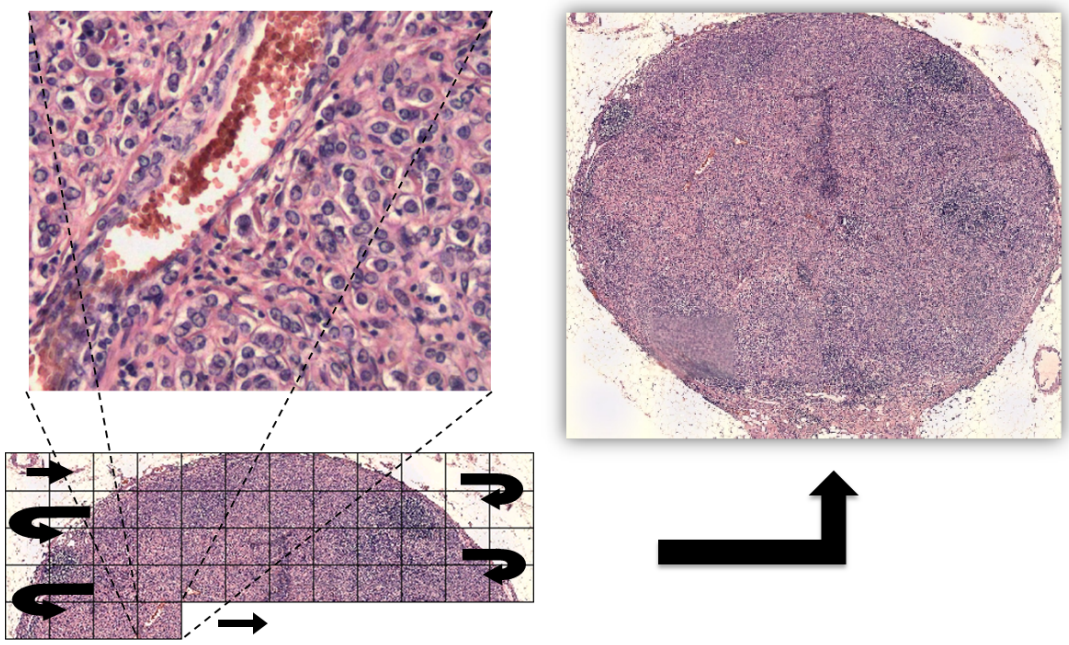

Figure 11. Virtual slide acquisition using the area scanning technique. Several thousands of individual image tiles are systematically captured from the specimen glass slide and stitched together to form a large image montage–the virtual slide. Hematoxylin–eosin staining of a cancerous lymph node.

Area scanning produces a vast amount of image tiles, which cause computational overhead and are more difficult to stitch together by the software. To overcome these problems, some scanner manufacturers have adopted an alternative acquisition approach called *line scanning* (Rojo *et al.* 2006). Line scanners employ a linear array camera sensor, which collects several image stripes from the continuously moving slide. By using image stripes, the image tile number is significantly lower and the image stitching becomes more straightforward. However, since the photon collecting capability of these sensors is weaker, the scanning speed becomes slower. The sensitivity of the detector can be increased by using a time-delay-and-integration (TDI) sensor architecture, which combines several linear array sensors, as demonstrated by the scanner manufacturer Hamamatsu Photonics (Hamamatsu, Japan).

2.4.2 Image tile stitching

Regardless of the scanning technique used, a common problem with the downstream image stitching is the discontinuity in the boundary regions of the image tiles (Figure 12). These stitching artifacts are mainly caused by the inaccuracy of the motorized specimen stage movement. A naïve correction method is to process the tile boundaries, for instance, with image convolution filtering, which blend and smooth the overlapping regions. However, several more advanced methods to remove the artifacts have been developed. Early stitching techniques were described by Dani & Chaudhuri (1995) for satellite imagery, and later Beck *et al.* (2000) for confocal microscope imagery. With regard to virtual microscopy, Appleton *et al.* (2005) described a method based on dynamic programming, Sun *et al.* (2006) developed a stitching algorithm based on global geometric and radiometric corrections, and more recently Steckhan *et al.* (2008) have developed a global registration method based on weighted least squares. Thévenaz *et al.* (1998) describe a generalized registration solution, which locates landmarks from adjacent tiles in the boundary regions and transforms (e.g., translation, scaled rotation, and/or rigid body) the images with respect to each other.

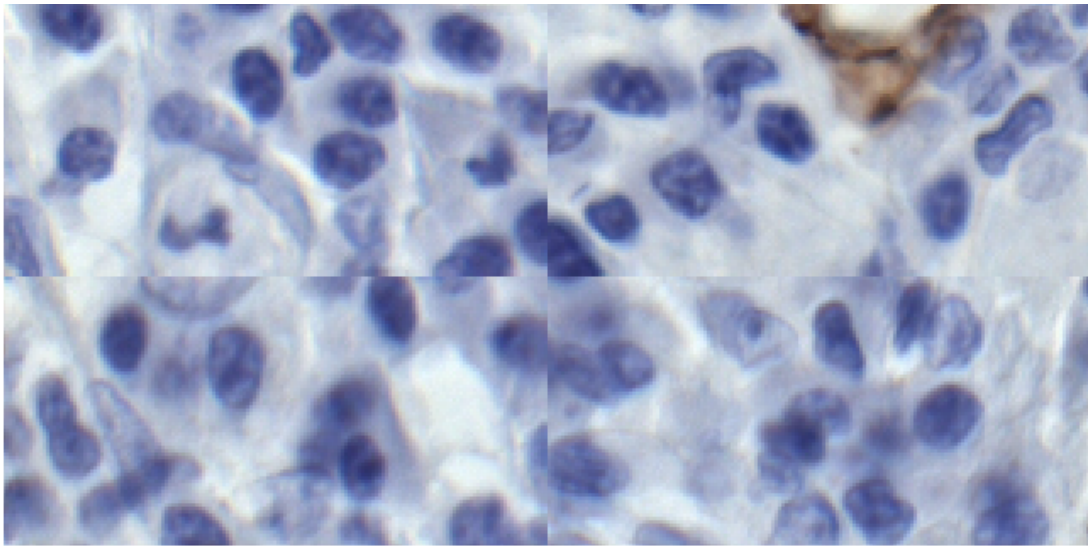

Figure 12. Visible stitching artifacts near the image tile boundaries due to mechanical inaccuracy in the movement of the specimen stage. Immunohistochemical diaminobenzidine–hematoxylin staining.

2.4.3 Capturing multi-layer image stacks

When digitizing thick tissue sections, cytological smears, or fluorescence specimens, most biologically relevant information is scattered along a relatively wide distance in the Z axis (Dee *et al.* 2007, Kalinski *et al.* 2008). By capturing only one focal plane, some of the objects of interest appear as blurred and out of focus, producing an overall low-quality image. Therefore, it is often beneficial to digitize several focal planes in the Z axis. The amount of in-focus information that can be captured per focal plane is measured with the optical system property called *depth-of-field*. The depth-of-field *z* refers to the distance along the Z axis within which the specimen is in focus, and is dependent on the objective lens, such that

$$z = \frac{n\lambda}{NA^2}, \tag{10}$$

where n is the refractive index of the surrounding medium, λ is the wavelength of light, and NA is the numerical aperture of the objective lens. Consequently, lenses with higher NA (i.e., large acceptance angle) have lower depth-of-field and lenses with lower NA have higher depth-of-field.

Ideally one would capture several focal planes from all specimens and store them as an image stack for downstream volumetric processing and viewing (Figure 13a). However, this significantly increases both the complexity of the scanning and the amount of data to be stored. To achieve best of both worlds, that is, to acquire 2D images containing all biologically relevant information of a 3D data set, several so-called *extended depth-of-field* methods have been developed (Bradley *et al.* 2005). Hardware-based techniques include wavefront coding, in which the image is artificially distorted with an optical filter and subsequently corrected with an inverse digital filter (Dowski & Cathey 1995). Software-based methods are more common and most are based on digital image fusion, in which optical sections are acquired along the Z axis with a spacing Δx, such that $\Delta x \leq z$, and processed with a software algorithm that identifies regions containing most in-focus information and combines these region into a single composite image (Figure 13b). These methods include pixel-based image fusion (Pieper & Korpel 1983), neighborhood-based image fusion (Tympel 1996), complex wavelet-based transformation (Forster *et al.* 2004), and,

more recently, model-based methods using the point spread function (Aguet *et al.* 2008).

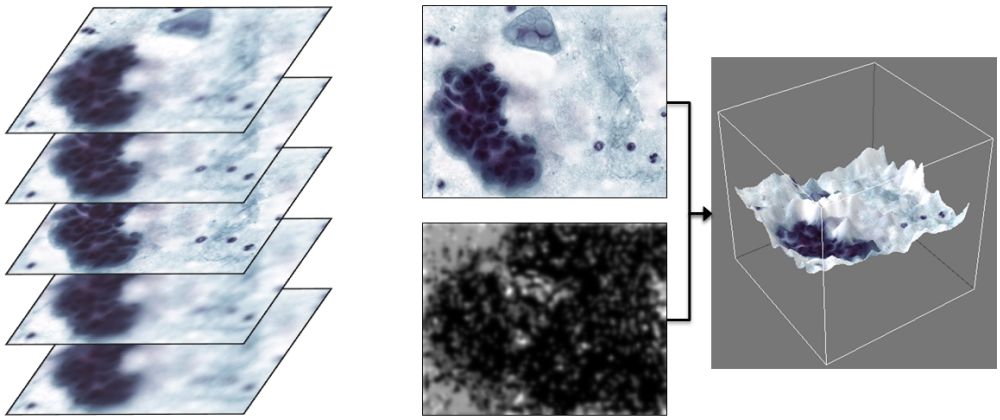

Figure 13. Multi-layer image stack acquired from a cytological specimen with Papanicolaou staining (a). Same image stack processed with an extended depth-of-field technique for generating a composite 2D image with combined in-focus regions from the stack layers (b) (BIG 2011). Additionally shown the focus topology and its volumetric visualization using the original image as an overlay texture.

2.4.4 Color normalization

Normalizing the color acquisition of the virtual slide scanner and the color reproduction of the computer display is an important aspect in the clinical application of virtual microscopy (Yagi & Gilbertson 2005). Other factors affecting the slide color properties are the thickness of the specimen section and the varying laboratory staining practices, but these types of variation can be reduced by employing standardized tissue preparation and staining protocols (NordiQC 2011). Normalizing the color reproduction of a display can be done using customized ICC profiles, generated with peripheral calibration instruments, such as the Spyder™ sensor by Datacolor Inc. (Lawrenceville, NJ, US). The color calibration of the scanning hardware can be performed with standardized IT8 calibration targets, such as the ColorChecker color rendition chart (also known as Macbeth chart), which contains an arrangement of color patches with spectral properties mimicking those of natural objects (McCamy *et al.* 1976). If the virtual slide scanner does not support ICC profiling, the calibration can be done manually by scanning a slide with an embedded color chart. The scanned chart is viewed with a calibrated display, compared against a golden stand-

ard target, and adjusting the acquisition parameters as needed for a better match (Yagi 2011).

2.4.5 Data processing and storage requirements

Virtual slide scanning produces vast amounts of information. For example, a typical microscope specimen of size 20 × 15 mm results in a 50,000 × 37,500 pixel virtual slide when digitized using resolution 0.40 µm/pixel. With three 8-bit color channels, the raw, uncompressed size of the virtual slide would be ~5 GB. With a slightly larger specimen of size 20 × 30 mm and the digitization made using resolution 0.20 µm/pixel, the resulting virtual slide would be 100,000 × 150,000 pixels in size and would require ~42 GB of storage space. An extreme example of a 25 × 50 mm specimen filling nearly the entire slide area, captured using an immersion oil objective lens and with resolution 0.10 µm/pixel, would result in a virtual slide of 250,000 × 500,000 pixels and ~349 GB. Furthermore, if a multi-plane Z stack is captured, the total virtual slide size is multiplied by the number of planes. For instance, if 10 focal planes are captured from the specimen in the previous example, the total size of the virtual slide would be ~3.4 TB. Considering that a pathology laboratory may produce thousands of slides per day, it is clear that processing and handling the amount of digitized data requires customized software and hardware solutions, which are not typical for other medical imaging specialties (Huang 2010).

First and foremost, virtual slides have to be stored using lossy instead of lossless compression algorithms, which are commonly employed in medical imaging (Gonzalez & Woods 2008). Lossless algorithms, such as the LZW (Welch 1984), yield compression ratios up to 2:1 with natural images, whereas lossy algorithms, such as the baseline JPEG (ISO/IEC 10918-1), result in ratios tens of times higher (Taubman & Marcellin 2002). With currently available hardware, storing slides with lossless compression would be costly, and transmitting the data over the Internet would require considerably more bandwidth than with lossy compressed virtual slides. Kalinski *et al.* (2009, 2011) and Sharma *et al.* (2011) have shown that lossy compression does not significantly affect the diagnostic resolution of pathological specimens, and is therefore readily applicable to virtual slides.

2.4.6 Virtual slide image formats

A major challenge arising from the large size of virtual slides is finding a suitable image file format to store the slides. Although several conventional image file formats do support lossy compression, they have an inherent image pixel and/or bit size restrictions in the specifications, thus making them inapplicable to virtual slides. For example, the JPEG standard uses 16-bit addressing for the image width and height, thereby limiting them to 65,535 (2^{16}–1). As a solution, nearly all scanner manufacturers have developed their own proprietary virtual slide formats, such as *SVS* by Aperio Technologies (Vista, CA, US); *MRXS* by 3DHISTECH (Budapest, Hungary); and *NDPI* by Hamamatsu Photonics (Hamamatsu, Japan). However, these formats are closed and non-compatible with each other. Moreover, there are no guarantees that a vendor-specific file format will be supported in the future, posing a significant risk for long-term virtual slide archives, accumulated over decades. Satyanarayanan *et al.* (2011) have described a software library *OpenSlide* for the interchange of several commercial slide formats. On the whole, the ideal virtual slide format should support the handling of large-sized imagery, be open and/or international standards-based, interchangeable, and have a guaranteed longevity. A promising candidate format is the JPEG2000 (reviewed in detail in Section 2.5), which features numerous advantages for virtual slide processing and storage.

2.4.7 Virtual slide viewing

Virtual slides can be viewed on a conventional computer workstation with a color display (Weinstein 2005), on a tablet computer (Stoner 2011), or on a mobile device (Ramey *et al.* 2011). Virtual slides can reside in a local storage or, more conveniently, in a remote storage, which is accessed through the Internet (Lundin *et al.* 2004a, Rojo *et al.* 2008). The slides are typically viewed by panning through the slide at a low resolution and when encountering an area of diagnostic interest, the resolution is increased by "zooming in" (Gómez *et al.* 2011). Most common navigation instruments on a workstation are keyboard and mouse, but more specialized controller devices have been described, such as the SmartMove by Leica Microsystems (Wetzlar, Germany). However, owing to the large size of virtual slides–up to terabytes of uncompressed data per slide, the viewing cannot be made using conventional image

viewing applications, which require the whole image data to be loaded into the computer memory. Instead, the slide viewing follows the *on-demand* principle, that is, the server sends the client only the content of the currently active image region (Kayser *et al.* 2006). When inspecting the slide at lower magnifications, the server dynamically reduces the image resolution, thereby optimizing the amount of data to be transferred. When viewing virtual slides from a local storage, without an image server, a similar partitioned image loading approach is taken.

Virtual slide viewing software is commonly bundled with a slide scanner (Rojo *et al.* 2006). The viewing software can be categorized into native applications (e.g., *NDP.view* by Hamamatsu Photonics, Hamamatsu, Japan; and *OlyVIA* by Olympus Corporation, Tokyo, Japan) or web browser-based applications. Della Mea *et al.* (2008) present a survey of readily available, platform-dependent virtual slide viewers. For web browser-based viewers, Rojo *et al.* (2008) have presented a review of three commercial solutions. Web browser-based viewers can be further divided into applications that are based on Adobe® Flash® (e.g., *WebScope* by Aperio Technologies, Vista, CA, US; and *Zoomify* by Zoomify, Santa Cruz, CA, US), the Java platform (e.g., *mScope*® by AuroraMSC, Montreal, Canada), a browser and platform-specific plugin (e.g., *ERDAS APOLLO* by Hexagon, Stockholm, Sweden), or approaches based on dynamic HTML (e.g., *BrainMaps* by Mikula *et al.* 2008).

2.4.8 Applications and benefits over traditional microscopy

There are numerous issues regarding the use of physical specimen glass slides. They are fragile, the tissue deteriorates and the staining fades over time (especially immunofluorescence dyes), sending an interesting slide back and forth between several pathologists is tedious and time-consuming, borrowed slides have a risk to be misplaced, and there are significant overhead costs associated with the upkeep of slide storage archives (Kayser *et al.* 2006). By using virtual slides, long-term centralized digital archives can be formed, which provide rapid, networked, and practically unlimited multi-user access to all sample material, including rare cases, and require relatively low upkeep costs compared to physical archives (Pantanowitz *et al.* 2011). Virtual slide archives are beneficial, for example, in tissue biobanking (Isa-

belle *et al.* 2006), as comprehensive digital atlases, such as brain (Mikula *et al.* 2008) and breast (Lundin *et al.* 2004b), in medical student education (Kumar *et al.* 2006, Paulsen *et al.* 2010, Kayser *et al.* 2011, Szymas & Lundin 2011), pathologist training (Helin *et al.* 2005, Dee 2009), scientific research (Lundin *et al.* 2004a), national and international consultation and collaboration (Wilbur *et al.* 2009, Lundin *et al.* 2009), and in inter-laboratory quality assurance (Linder *et al.* 2008, Graham *et al.* 2009). In clinical environments, virtual slides can improve the operational measures, such as cost, time, and patient care, as discussed by Isaacs *et al.* (2011).

Studies show that virtual slides are easily readable by a pathologist and that the viewing is equivalent, and in some cases even better, than traditional, manual microscopy (Della Mea *et al.* 2006, Nassar *et al.* 2011). Moreover, virtual slides provide numerous additional benefits compared to traditional microscopy. The viewing ergonomics of a computer workstation are more freely adjustable then the fixed slide viewing via the ocular, which is shown to be fatiguing in long-term use (James *et al.* 2000). The usage of multi-resolution, always in-focus virtual slides eliminate the need to continuously change objective magnifications, realign the focus, and adjust the microscope lamp voltage (Rojo *et al.* 2009). A low-resolution overview image of the whole specimen can be simultaneously displayed alongside the high-resolution main view, thereby providing valuable context-related information to the user (Della Mea *et al.* 2008). With the use of digital image metadata, region-specific annotations and textual information, such as the organ, diagnosis, copyright, and ICC color profiles, can be embedded within the virtual slide (Wang *et al.* 2011). By utilizing multiple displays, several virtual slides can be opened side-by-side for comparative analysis (Kayser *et al.* 2006). Moreover, virtual slides enable simultaneous, linked viewing of specimens stained for different biomarkers without the need to switch slides (Helin *et al.* 2006). When the slide acquisition is multi-planar, the tissue architecture can viewed as a volume, rotated and reoriented by the means of 3D reconstruction (Wu *et al.* 2005). Lastly, and of increasing interest, virtual slides are readily quantifiable by automated image analysis methods due to their discrete nature (Laurinavicius *et al.* 2011).

2.5 JPEG2000 image compression standard

The JPEG2000 is a multimedia compression standard, which describes an image coding system and several auxiliary techniques (Skodras *et al.* 2001, Taubman & Marcellin 2002). The standard is being developed collaboratively by the International Organization of Standardization (ISO), the International Electrotechnical Commission (IEC), and the International Telecommunications Union (ITU), which have formed the Joint Photographic Experts Group (JPEG) committee to steer the development process (JPEG 2011). JPEG2000 was initially designed to supersede the old discrete cosine transformation-based JPEG standard by introducing an advanced image coding system utilizing the discrete wavelet transformation (DWT) (Mallat 1989). In contrast to JPEG, JPEG2000 performs lossless *and* lossy compression using the same algorithm, and is based on a principle of compressing the image once and decoding it in many ways for different purposes, such as at a reduced resolution for a mobile device (Rabbani & Joshi 2002). Therefore, JPEG2000 is readily usable in various technical fields and multimedia applications, for instance, in 3D imaging (Schelkens *et al.* 2003), video compressing (Forssel *et al.* 2003), and in satellite and aerial photography (Liu *et al.* 2005). Since satellite and aerial photography share similarities with virtual microscopy, JPEG2000 is a promising candidate as an open and vendor-neutral virtual slide format.

2.5.1 Suitability for virtual microscopy

At the time of writing, the JPEG2000 standard family consists of twelve parts, of which the most relevant with regard to virtual microscopy are Part 1 (Core Coding System; ISO/IEC 15444-1, ITU-T Recommendation T.800), Part 2 (Extensions; ISO/IEC 15444-2, ITU-T Recommendation T.801), and Part 9 (Interactivity tools, APIs and protocols; ISO/IEC 15444-9, ITU-T Recommendation T.808). Together these parts form a comprehensive set of features, which contain numerous advantages for virtual slides. Part 1 specifies the core features, including support for large-scale imagery with a limit of $(2^{32}–1) \times (2^{32}–1)$ pixels, the spatial random access of image information, progressive transmission based on resolution and image quality, efficient lossy compression, especially with low bit-rates, predetermined

target file size, and the JP2 container file format for single images (with a common file extension *jp2*). Part 2 extends the first part by introducing the JPX multi-image container file format and enables the embedding of rich metadata. Part 9 specifies the JPEG2000 Interactive Protocol (JPIP), an error-resilient network protocol for transmitting compressed image data.

2.5.2 Compression algorithm overview

As is customary with compression standards, the JPEG2000 standard specification describes only the encoded bit-stream syntax and a decoder. However, it is often more practical to describe a reference encoder. The JPEG2000 Part 1 encoding system consists of several steps, which are outlined in Figure 14 and described briefly in the following paragraphs. For a more comprehensive treatment, the reader is referred to Taubman & Marcellin (2002) and Rabbani & Joshi (2002).

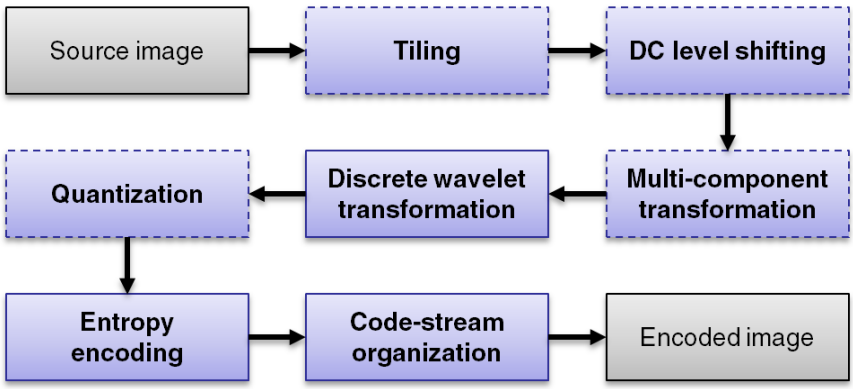

Figure 14. A flowchart describing the JPEG2000 Part 1 encoding system. Steps marked with solid line are mandatory, whereas steps marked with dashed line are optional. Modified from Acharya & Tsai 2005.

The encoding process begins with splitting the image into (color) components, which are then optionally partitioned into a number of image tiles, effectively corresponding to an inverse image stitching process. Rabbani & Joshi (2002) have shown that the smaller the selected tile size, the lower the image fidelity due to tile boundary artifacts. For simplicity, the following steps assume that the tiling is skipped and that each component is treated as a single tile. To ease the computation, the dynamic range of the component pixel values are centered around the zero with a process

called DC level shifting. Should there exist any correlations between the components, the multi-component transformation is used to reduce them, thus gaining an increased compression performance. Two transformations modes are supported: the Reversible Color Transformation (RCT) for lossless and lossy compression, and the Irreversible Color Transformation (ICT) exclusively for lossy compression. Quality and compression-wise, Skodras *et al.* (2001) have shown that the ICT produces substantially better results than RCT.

After the three optional steps, each component is transformed from spatial domain into DWT domain by decomposing them into a number of sub-bands at different levels of resolution (Figure 15) (Vetterli 2001). The first decomposition level contains four sub-bands, LL_1, HL_1, LH_1, and HH_1, of which the LL_1 represents a 2:1 sub-sampled version of the original component and the other contain corresponding residual versions of the component, needed for reconstruction. Higher number of decomposition levels can be achieved by performing DWT on the low-resolution LL_1 image and continuing the process recursively (up to a maximum of 32 levels in Part 1). The DWT is performed using either the reversible Le Gall spline filter (Gall & Tabatabai 1988) or the irreversible biorthogonal Daubechies spline filter (Antonini *et al.* 1992). Rabbani & Joshi (2002) have shown that the Daubechies filter yields better image quality, but at the expense of compression complexity. Ortiz *et al.* (2007) have experimented performing virtual slide stitching during the DWT and shown that it improves the overall scanning time.

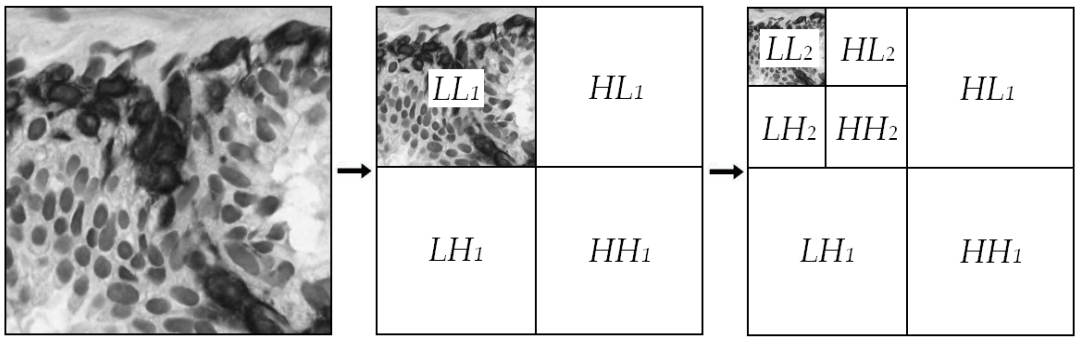

Figure 15. Discrete wavelet transformation of a color component image. The image is decomposed into n successively lower resolution levels, each consisting of four sub-bands: LL_n, HL_n, LH_n, and HH_n. Sub-band LL_n represents a half-resolution version of LL_{n-1} (LL_0 being the original image), whereas the other sub-bands contain residual information used for reconstructing the original image.

After the DWT, the next step is quantization, which is performed only during lossy compression and is responsible for the most information loss during the compression process. Each sub-band generated during the DWT is processed with a custom quantization step size. The coarser the step size, the greater the compression and lower the image quality. The (possibly quantized) wavelet coefficients are then prepared for entropy encoding by sectioning them into rectangular *precincts*, which are further split into smaller rectangular *code-blocks* with a dimension of power of 2. Rabbani & Joshi (2002) have found the optimal code-block size to be 32 × 32 or 64 × 64, other sizes either degrading the image quality or hindering compression performance. The entropy encoding is done using Embedded Block Coding with Optimized Truncation (EBCOT) algorithm (Taubman 2000) as the bit-plane coding scheme and the MQ coder (ISO/IEC 14492) as the arithmetic coding scheme. As a result, the entropy encoding produces a compressed bit-stream for each code-block. The code-block bit-streams in a single precinct form a *packet*. Likewise, the packets from each precinct of a single resolution level form a *layer*. As such, a packet contributes one quality increment for a given resolution level at one spatial location, and a layer contributes one quality increment for the whole image.

The packets are arranged in a nested loop structure to facilitate scalability based on quality layer (L), resolution level (R), spatial position (P), and/or color component (C) (Taubman & Marcellin 2002). The five possible *progression orders* are LRCP (the default), RLCP, RPCL, PCRL, and CPRL. For example, the LRCP provides scalability primarily by quality layer and secondarily by resolution level. Finally, the arranged packets are inserted into a self-contained *code-stream* along with various mandatory and optional markers and marker segments. Code-streams can be directly treated as compressed images or, more typically, embedded in a container file format, such as the JP2, which enables the usage of additional image properties and metadata, or JPX, which enables several code-streams to be embedded as image layers (e.g., as a Z stack).

2.5.3 Image quality with lossy compression

The image quality, or fidelity, of lossy JPEG2000 compression can be measured subjectively by using a simple Mean Opinion Score (MOS) method (Ebrahimi *et al.*

2004). However, subjective evaluation is often inadequate and methods based on objective measurements are required. Two common methods for objective image quality assessment are the Root Mean Squared Error (RMSE) and the peak signal-to-noise-ratio (PSNR) (Sayood 2006). The RMSE is defined as

$$RMSE = \sqrt{\frac{1}{MN}\sum_{x=1}^{M}\sum_{y=1}^{N}[I(x,y) - I'(x,y)]^2}\,, \tag{11}$$

where M is the width of the image in pixels, N is the height of the image in pixels, I is the original image, I' is the lossy-compressed image and (x,y) specifies the image pixel coordinates. The RMSE can be used as such or incorporated into the PSNR measurement, which is measured in decibels (dB), such that

$$PSNR = 20\log_{10}\frac{(2^D - 1)}{RMSE}\,, \tag{12}$$

where D is the image bit-depth. A typical, good-quality natural image has a PSNR value of at least 30 dB (Taubman & Marcellin 2002).

Using the PSNR quality metric, lossy JPEG2000 compression is shown to outperform the baseline JPEG compression with all compression ratios (Skodras *et al.* 2001, Rabbani & Joshi 2002, Santa-Cruz *et al.* 2002). However, if the quality evaluation is performed with a subjective method, the superiority of JPEG2000 becomes evident only at compression ratios over 20:1 (Ebrahimi *et al.* 2004). Figure 16 shows a comparison between lossy JPEG2000 and baseline JPEG compression with a relatively high compression ratio of 60:1. With high compression ratios, JPEG begins to exhibit blocking artifacts due to discontinuities created at the independently processed 8 × 8 block boundaries, whereas the JPEG2000 version has an overall smoother visual result because of applying the DWT over the whole image.

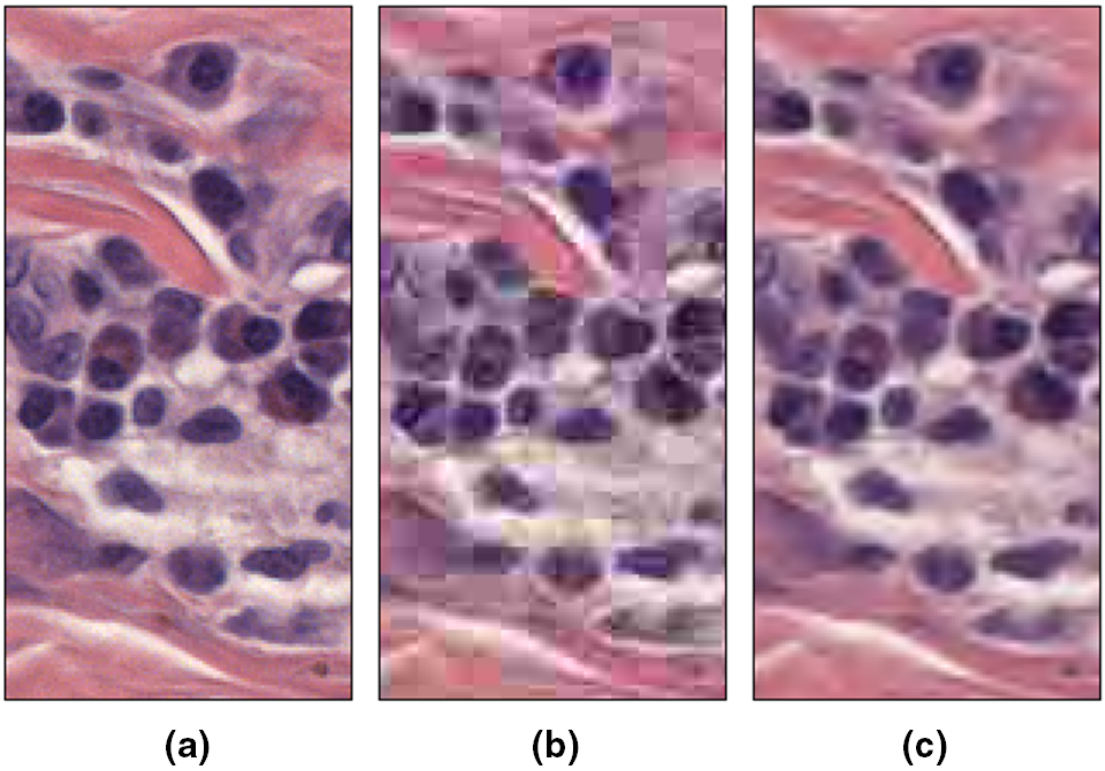

Figure 16. Lossy JPEG2000 compression compared to baseline JPEG compression. The original, uncompressed image (a), which is compressed with baseline JPEG using 0.39 bits per pixel (b) and with JPEG2000 using the same bit-rate (c). Breast cancer tissue section, stained with hematoxylin–eosin.

2.5.4 Image transmission over networks

The Part 9 of the JPEG2000 standard family describes the JPIP protocol for client–server network transmission of JPEG2000 imagery (Taubman & Prandolini 2003). Instead of directly accessing the remote JPEG2000 content, the client requests a specific region of interest (ROI) from the server (Figure 17). As a response, the server encapsulates the code-stream packets corresponding to the requested ROI into a collection of *data-bins* and transmits, or streams, them to the client in arbitrary order. The principal data transport protocol of JPIP is the HTTP/1.1 (RFC 2616), but the lower level TCP (RFC 793) and UDP (RFC 768) protocols are also directly supported. Due to the self-contained nature of data-bins, JPIP streaming is highly robust to errors during the data transport. Furthermore, the standard specification allows the server to maintain a model of the client cache, to alter the sequence in which the data-bins are delivered, and even to transcode the original code-stream to

use difference precinct size, thus optimizing the delivery speed for single and multiple simultaneous users.

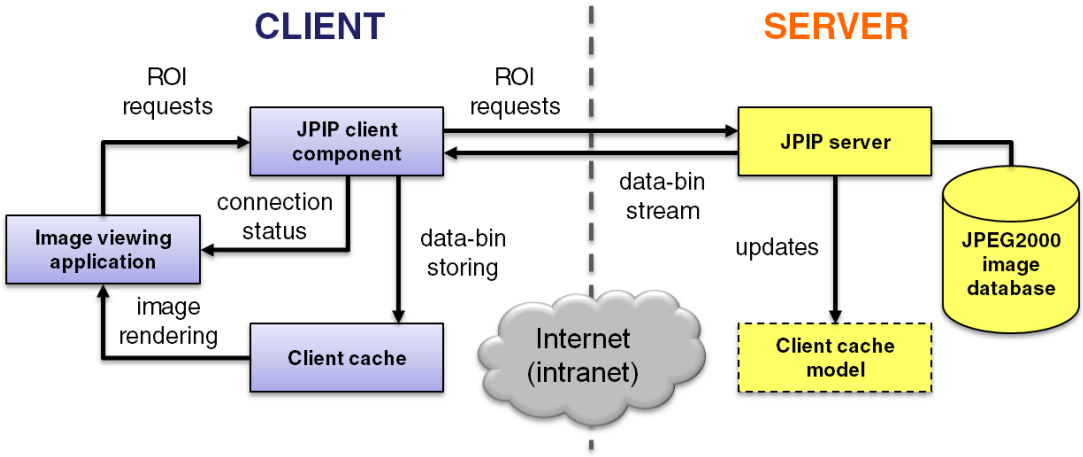

Figure 17. The client–server architecture and information flow of JPEG2000 Interactive Protocol (JPIP) in network-based image data transmission. Modified from Taubman & Prandolini 2003.

2.5.5 Clinical application of JPEG2000 virtual slides

Clinical application of virtual slides requires conforming to existing medical standards, including DICOM. Standardized software interfaces allow developers to link various hospital information systems (HIS) together. For example, connecting the laboratory information system (LIS) of a clinical chemistry or a pathology department with the radiology information system (RIS) in a radiology department, both the pathologists and the radiologists can view breast ultrasound and X-ray images simultaneously with corresponding histological specimens. However, up until recently, the DICOM standard lacked of basic pathological concepts, such as specimen identification, and was not fully compatible with the common workflow of a pathology laboratory. Moreover, due to the image size, data storage, and processing issues related to virtual slides, and since they are primarily used only in pathology (and related subspecialties), virtual slides are not currently used in existing DICOM-based PACS systems. To address these issues, the DICOM Working Group for Pathology (WG-26) was formed in 2005.

During the past years, WG-26 has described two extensions to the core standard. The Supplement 122 (*Specimen Module and Revised Pathology SOP Classes*) de-

scribes a specimen-centric data model for pathology image interpretation and establishes uniform definitions for all major pathological concepts. The Supplement 145 (*Whole Slide Microscopic Image IOD and SOP Classes*) describes a recommendation for the mechanism of using virtual slides with DICOM. At the time of planning Study II, the Supplement 145 was still in formulation and there was debate on what would the preferable method be for storing and accessing virtual slides using DICOM (WG-26 Meeting Minutes, May 17, 2008, Toledo, Spain). Two possible candidate solutions to link virtual slides with a DICOM-based PACS existed, from which the first one, the so-called *pyramidal approach*, was chosen as the primary method for the final version of the Supplement. The pyramidal approach is a legacy-type solution involving splitting the virtual slide into a multi-resolution image tile pyramid, which is embedded into the PACS using existing DICOM mechanisms. More specifically, the pyramidal approach stores the tiles of a given layer as individual frames in a DICOM multi-frame image object, and the layers as DICOM Series (Figure 18).

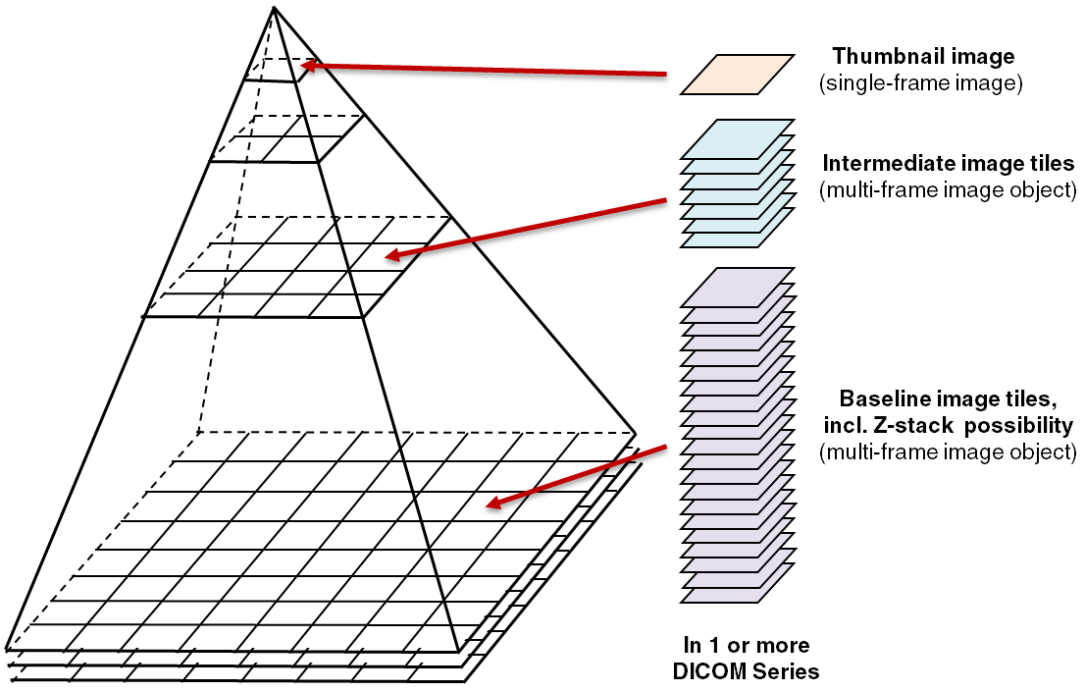

Figure 18. The standardized method for linking virtual slides with DICOM, in which the virtual slide is mapped as a pyramid into a DICOM Series. Modified from DICOM Supplement 145; Final Text 2010/08/24.

The other candidate solution for linking virtual slides with DICOM was based on JPEG2000 and is the so-called *JPIP-based approach*. Although the DICOM standard includes the core parts of JPEG2000 in Supplements 61 (*JPEG 2000 Transfer Syntaxes*) and 105 (*JPEG 2000 Part 2 Multi-component Transfer Syntaxes*), it is not practical to transmit the whole virtual slide content during a DICOM Retrieve operation. Therefore, the JPEG2000 imagery has to be transmitted using the JPIP protocol, for which the Supplement 106 (*JPEG 2000 Interactive Protocol*) describes two Transfer Syntaxes as methods of delivering image pixel data apart from patient data: the non-compressed *JPIP Referenced Transfer Syntax* and the deflate-compressed *JPIP Referenced Deflate Transfer Syntax*. When using virtual slides with the JPIP Transfer Syntaxes in a DICOM-based PACS, a DICOM server sends its client a Uniform Resource Locator (URL) string that refers to the virtual slide pixel data provider (i.e., a JPIP server), together with the image name, which can be arbitrary and unrelated to patient data (Figure 19). Upon receiving the pixel data provider reference, the client DICOM workstation can either use a built-in JPIP viewer or invoke an external one for retrieving the virtual slide from the specified JPIP server. The network messaging between the PACS and the client end is done according to the DICOM protocol, except the JPIP transmission, which is performed using the methods described in Section 2.5.4. Although the JPIP-based approach was not included in the Supplement 145 for the reasons explained earlier, it is nevertheless still a valid method due to the presence of Supplement 106.

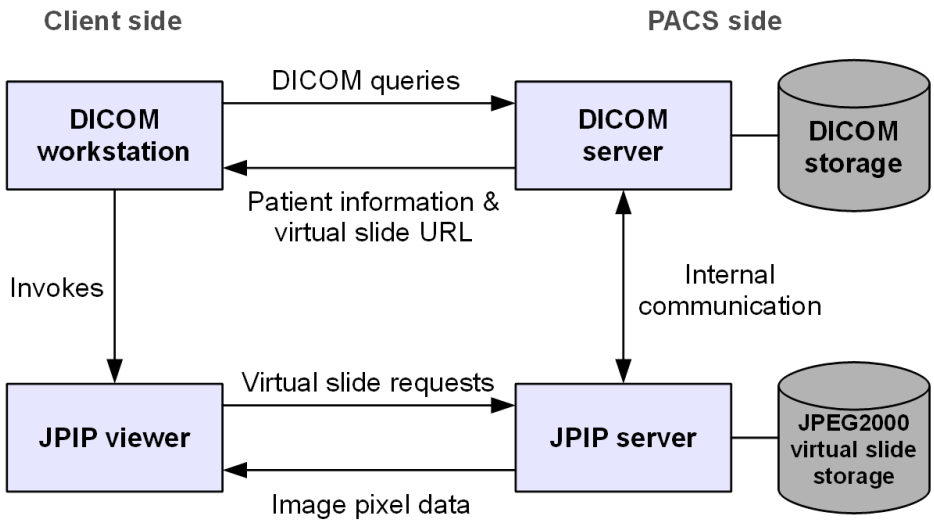

Figure 19. An alternative, JPIP-based method for linking virtual slides with DICOM. Not included in the DICOM Supplement 145; Final Text 2010/08/24.

2.6 Digital microscope image analysis

Digital image analysis of microscope specimens not only reduces inter- and intra-observer variability due to its objective nature, but also provides quantifiable, traceable and repeatable measurements. Moreover, digital analysis is capable of detecting image features that cannot be distinguished with visual interpretation, such as minor differences in gray-level intensities. The analysis can be applied to single micrographs or entire virtual slide areas can be analyzed. Alternatively, as an intermediate approach, several representative fields of the specimen can be captured and analyzed, and the individual field results are averaged to obtain a sample-specific result. Several commercial image analysis and processing software for medical imagery are available, such as MATLAB® (by MathWorks, Natick, MA, US) and Wolfram Mathematica® (by Wolfram Research, Champaign, IL, US). Papademetris *et al.* (2006) describe an open, academia-based medical analysis software, the BioImage Suite. For the analysis and visualization of multi-dimensional microscope images, Kankaanpää *et al.* (2008) have developed the BioImageXD software. The analysis software used in the present study are primarily based on ImageJ, which is a public domain (free) and easily expandable image processing package, used in numerous fields of science (Rasband 2011).

2.6.1 Contrast expansion

Regardless of the available dynamic range of the microscope camera, the actual dynamic range of the digitized image may be narrow, which manifests itself as poor contrast (Russ 2007). To resolve image details visually or, for example, to perform automated image segmentation with global, fixed thresholding (reviewed in Section 2.6.5), it is necessary to improve, or expand, the image contrast with global image enhancement techniques. Global contrast expansion can be implemented in various ways, two of the most common ones being *contrast normalization* (Wu *et al.* 2008) and *histogram equalization* (Stark & Fitzgerald 1996) (Figure 20). Contrast normalization shifts the image pixel intensities to span a desired range of values by applying a linear scaling function, such that

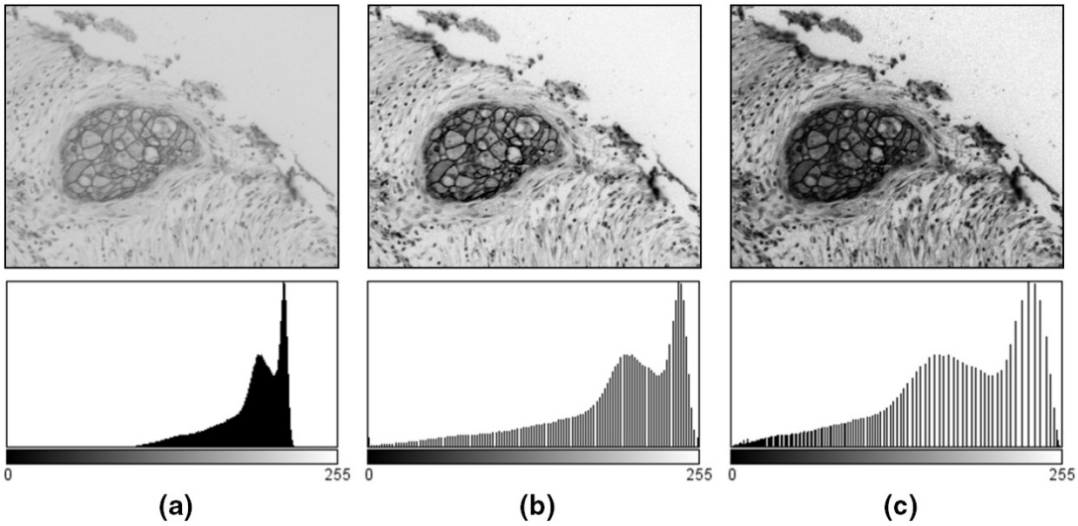

Figure 20. Contrast expansion performed on a single color channel of a microscope image. The original image with low contrast and dynamic range (a), original image processed with contrast normalization (b), and with histogram equalization (c). Single core of a breast cancer tissue microarray, IHC-stained for HER2.

$$P' = \frac{(I_{max} - I_{min})}{(i_2 - i_1)}(P - i_1) + I_{min}\,, \tag{13}$$

where P is the original pixel intensity, P' is the transformed pixel intensity, I_{max} and I_{min} the maximum and minimum intensity values, respectively, over which the image is to be normalized, and i_1 the lowest and i_2 the highest intensity value present in the image. In practice, to reduce the impact of outlier presence on the normalization process, a more robust approach is to select i_1 and i_2 at a lower and an upper histogram percentile (e.g., 5^{th} and 95^{th}). Histogram equalization employs a monotonic, non-linear mapping function to redistribute the pixel intensity values so that all the available gray-level steps are used. A given ith gray level in the original image is mapped into a new gray level s_i such that

$$s_i = \sum_{j=0}^{i} \frac{n_i}{n}\,, \qquad 0 \le i < L \tag{14}$$

where n_i is the number of occurrences of gray level i, n is the total number of pixels, and L is the total number of gray levels available. Stark (2000) extends the basic his-

togram equalization by describing a parameterized and adaptive expansion scheme. Other contrast expansion methods described in the literature include wavelet and curvlet-transform based methods (Starck *et al.* 2003), and local methods, such as constrained equalization (Zhu *et al.* 1999).

2.6.2 Noise reduction

Image noise can arise from several sources, such as the camera detector hardware during the digitization process, existing low noise levels may be multiplied and brought visible as a result of a contrast expansion operation, and the instability of the light source may produce a non-random, periodic noise patterns (Murphy 2001). In light microscopy with brightfield illumination, camera noise is seldom an issue due to low exposure times, but in fluorescence imaging with darkfield illumination and relatively long exposures, the issue is more prevalent. The classical reduction method for random noise is to average a number of frames from the same field of view, resulting in improved image PSNR (Russ 2007). This, however, can be problematic during high-throughput virtual slide scanning, in which the speed is a critical factor. Therefore, other noise reducing techniques have to be used, which are categorized into *spatial* and *frequency domain filters*.

Image noise reduction in the spatial domain can be achieved by using non-linear *median filtering* (Gallagher & Wise 1981) or linear *convolution* (Wu *et al.* 2008), both of which are based on extracting information from the pixel neighborhood with a given block size (e.g., 3 × 3). Median filtering replaces each pixel value with the median of the neighborhood, whereas convolution assigns an intensity weight mask, or *kernel*, on to the neighborhood. In the case of noise reduction, the convolution kernel represents a low-pass filter, usually either a simple average filter (also known as *mean filter*) or a Gaussian filter with the kernel weights approximating the profile of a Gaussian function (Berry 2008) (Table 3). During the convolution operation, each pixel of the image is replaced by the weighted sum of the pixels within the kernel window. Convolution $g(x,y)$ of the image $f(x,y)$ can be expressed as

$$g(x,y) = f(x,y) * h\,, \tag{15}$$

where *x* and *y* are the image pixel coordinates and *h* is the used kernel. Mean and Gaussian filtering are applicable for all types of image noise, but at a cost of reduced image resolution, thereby making small details indiscernible. Median filtering, on the other hand, has less impact on the image resolution, but is primarily applicable only for reducing impulse, or "speckle", noise, characterized by having intensity much higher or lower than the surrounding pixels.

Table 3. Commonly used convolution kernel masks for image noise reduction (Mean & Gaussian) and for sharpening (Laplacian). Modified from Berry 2008.

Mean (low-pass filter)	**Gaussian (low-pass filter)**	**Laplacian (high-pass filter)**
$h = 1/9\begin{bmatrix}1 & 1 & 1\\ 1 & 1 & 1\\ 1 & 1 & 1\end{bmatrix}$	$h = \begin{bmatrix}0.2098 & 0.4580 & 0.2098\\ 0.4580 & 1 & 0.4580\\ 0.2098 & 0.4580 & 0.2098\end{bmatrix}$	$h = \begin{bmatrix}0 & 1 & 0\\ 1 & -4 & 1\\ 0 & 1 & 0\end{bmatrix}$

A common issue with spatial domain filtering is that, as the convolution kernel size increases, so does the overall number of multiplication operations needed. Luckily, we are able to achieve the same result with frequency domain filtering, but with less arithmetic operations. The *convolution theorem* states that the multiplied inverse Fourier transforms of two functions in the frequency domain equals the convolution operation between the same two functions in the spatial domain (Gonzalez & Woods 2008). Therefore, it is often computationally less intensive and faster to perform the convolution in the frequency domain. Detailed treatment of frequency domain filtering can be found in Petrou & Petrou (2010) and Shih (2010).

2.6.3 Shading correction

Microscope images often contain some degree of artificial, unwanted intensity variation, which is known as the *shading* phenomenon (Tomaževic *et al.* 2002). Shading is caused by, for example, vignetting, uneven illumination intensity or color temperature of the light source, misaligned microscope components with respect to each other, or the sensitivity variations of the camera detector elements. The phe-

nomenon can be hard to detect visually, but may significantly affect the result of an automated analysis algorithm (Parker 1991). Therefore, it is imperative to correct the shading prior to performing automated analyses. Several methods have been described in the literature to correct the shading, which are either applied during image acquisition (*a priori*) or after the acquisition (*a posteriori*).

Shading correction methods done *a priori* are preferred, and the most prominent one is based on capturing a single blank image field, or a *blankfield image*, before acquiring the specimen image (Figure 21) (Russ 2007). Both images are then combined by processing each color channel such that

$$I' = \frac{I}{B} k \,, \tag{16}$$

where I' is the corrected image, I is the original image, B is the blankfield image, and k is the image bit-depth (e.g., 255 for 8-bit color images).

Figure 21. Shading correction performed *a priori* with a blankfield image. The resulting corrected image has an even illumination and a neutral color temperature. IHC staining of breast cancer tissue section for Ki-67.

Shading correction methods performed *a posteriori* include morphological *rolling ball* algorithm (Sternberg 1983), homomorphic filtering (Young *et al.* 1998), non-parametric non-uniformity intensity normalization (also known as the N3 method) (Sled *et al.* 1998), background estimation with entropy minimization (Likar *et al.* 2000), large-kernel Gaussian low-pass filtering (Leong *et al.* 2003), linear edge interpolation (Russ 2007), rank-based filtering (Russ 2007), fitting a polynomial surface to a number of sample points (Russ 2007), and signal envelope estimation (Reyes-Aldasoro 2009).

2.6.4 Stain separation

Digital differentiation, or separation, of the staining components in a microscope image is often an important pre-processing step before the segmentation and classification. For example, for the separation of stains used in IHC, several image processing techniques have been described: texture analysis with a color feature set (Kostopoulos *et al.* 2007), color difference discrimination based on cyan-magenta-yellow-black (CMYK) color model (Pham *et al.* 2007), CIE 1976 L*u*v (CIELUV) color model-based component thresholding (Rexhepaj *et al.* 2008), and chromacity–intensity-based separation using L*a*b* color space (Kostopoulos *et al.* 2008). The disadvantage of methods based on color-transformations is that they fail to take into account the contributions of two or more overlapping stains.

For differentiating co-localized, overlapping stains, Ruifrok & Johnston (2001) have described the *color deconvolution* algorithm. Color deconvolution analyzes the absorption spectra and the relative contributions of each overlapping stain. Prior to decomposing multiple stains, each pure stain is imaged, analyzed, and characterized with a 3 × 1 vector of *optical density* values, one for each of the three color channels R, G, and B. The optical densities are derived from the *Beer–Lambert law* (Fuwa & Valle 1963), which describes a non-linear relationship between the detected light intensity and the stain concentration, such that

$$I_c = I_{0,c} exp(-Ar_c) , \qquad c = R, G, B \tag{17}$$

where c is the color channel, I_c is the intensity of light after passing the specimen, $I_{0,c}$ is the intensity of light entering the specimen, and A is the amount of stain with the absorption factor r. The optical density, or absorbance, OD, has a linear relationship with the stain concentration and thus can be readily used to separate the contributions of multiple stains, and can be specified as

$$OD_c = -ln\left(\frac{I_c}{I_{0,c}}\right) = Ar_c , \qquad c = R, G, B . \tag{18}$$

Finally, the stain decomposition is performed by normalizing the optical density vectors for each pure stain and using them to perform an orthonormal transformation to the original RGB color image.

The color deconvolution can be applied, for example, to separate hematoxylin and DAB stains in IHC. However, van der Loos (2008) shows that the DAB stain does not follow the Beer–Lambert law, but instead produces a different spectral shape depending on the stain concentration, and thus cannot be used to reliably quantify the stain intensity. As a consequence, the intensity of DAB staining should only be assessed semi-quantitatively, for example, to categorize the staining intensity as *weak*, *moderate*, or *strong*, or to discriminate negatively and positively stained cell nuclei (Figure 22).

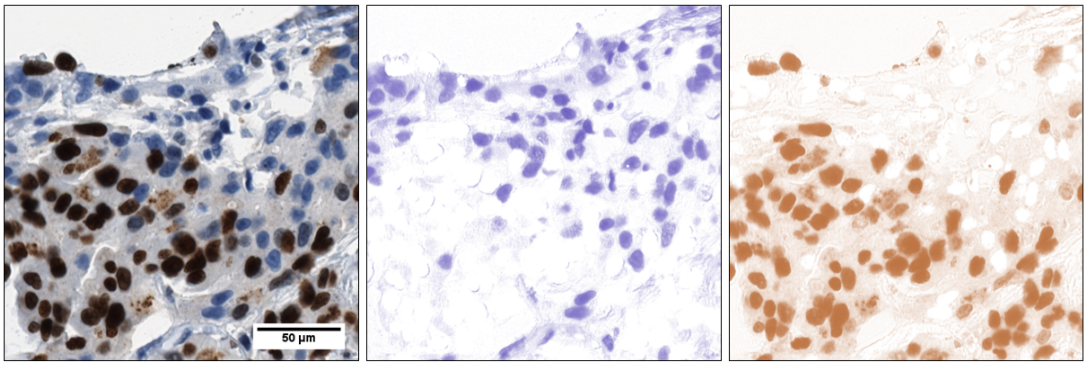

Figure 22. Color deconvolution performed on a breast cancer IHC specimen stained for Ki-67 with hematoxylin and DAB. The original image (a), the hematoxylin stain component of the original image (b), and the corresponding DAB component (c). ImageJ plugin *Colour Deconvolution* (Landini 2011).

2.6.5 Segmentation and classification

The goal of automated microscope image analysis is typically the identification of certain cellular structures, such as nuclei, and their subsequent measurement. To achieve this, the image has to be *segmented* by separating objects of interest from non-relevant information and *classified* by assigning these objects into classes based on their features (Wu *et al.* 2008). Segmentation can be manual, for example, drawing close contour shapes with area selection tools (Smith *et al.* 2010). However, manual methods are often tedious, prone to error, and subjective in nature, and thus,

automated segmentation methods are preferable. The most commonly used automated segmentation is *thresholding*, in which a grayscale image is converted into a binary image. Thresholding can be either fully automated or user-assisted. User-assisted thresholding requires a manually specified pixel intensity value, which acts a cut-point for discarding pixels with lower intensity (background), while including pixels with higher intensity (foreground), or vice versa. In many cases, however, it is preferable to use automated algorithms in defining the intensity cut-point (Sezgin & Sankur 2004). Figure 23 exemplifies several of the most well-known and widely applied thresholding algorithms in the literature: *Huang's fuzzy thresholding* (Huang & Wang 1995), *Intermodes* (Prewitt & Mendelsohn 1966), *IsoData* (Ridler & Calvard 1978), *Li's Minimum Cross Entropy* (Li & Lee 1993), *Kapur–Sahoo–Wong Maximum Entropy* (Kapur *et al.* 1985), *Mean* (Glasbey 1993), *Minimum Error* (Kittler & Illingworth 1986), *Minimum* (Prewitt & Mendelsohn 1966), *Moment-preserving thresholding* (Tsai 1985), *Otsu* (Otsu 1979), *Percentile* (Doyle 1962), *Kapur–Sahoo–Wong Renyi Entropy* (Kapur *et al.* 1985), *Shanbhag* (Shanbhag & Abhijit 1994), and *Triangle* (Zack *et al.* 1977).

Since thresholding is based on histogram segmentation, it lacks spatial information. Thresholded image can be further processed with morphological techniques, such as the *watershed algorithm* (Vincent & Soille 1991), which separates the boundaries of touching objects within the binary image. Alternative segmentation methods to thresholding include *region growing* by Pavlidis & Liow (1990), which uses spatial context information in grouping adjacent pixels or regions together. An opposite method called *region splitting* (Chen *et al.* 1991) hierarchically partitions the image into separate regions based on their similarity (e.g., texture and color properties). Kirsch (1971) describes a boundary-based segmentation method, which uses gradient image thresholding to extract image edge points.

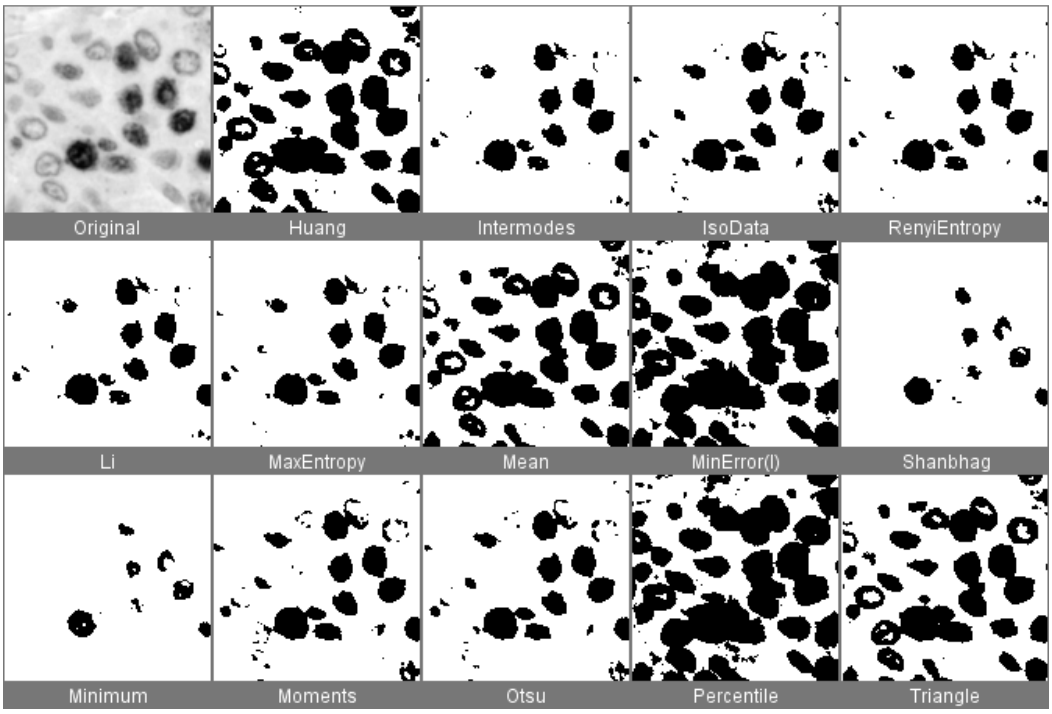

Figure 23. Comparison of 14 grayscale thresholding algorithms applied on a single color channel of a hematoxylin–DAB-stained IHC image with non-complete nuclear staining. Performed using *Auto Threshold* ImageJ plugin (Landini 2011b).

The classification, or labeling, is done with a specific *classifier*–an algorithm that categorizes the segmented image objects into classes based on a set of descriptive features. Classifiers are either *unsupervised* (Jain *et al.* 1999) with no prior knowledge on the features used for classification, or, more commonly, *supervised* (Kotsiantis *et al.* 2006). Supervised classifiers require training from a user with knowledge on the subject at hand, for example, by generating an image training set with manually identified features. Wu *et al.* (2008) describe a maximum-likelihood method with the minimum Bayes risk classifier, Misselwitz *et al.* (2010) have developed a software tool for multi-class classification of micrographs based on Support Vector Machines, and Walkowski & Szymas (2011) have described a structural analysis and shape descriptor-based classification of histopathologic virtual slides. Shih (2010) presents a distinct approach to classification by using artificial neural networks (ANNs), consisting of layers of inter-connected nodes. Each node in a layer processes its input with a modifiable weighting factor (adjusted according to a pre-classified training set) and generates a weighted sum as an output for the subsequent layer; the output of the final layer assigning the object to a class.

2.6.6 Software for IHC biomarker quantification

The development of automated analysis methods for IHC biomarkers are primarily driven by commercial virtual slide scanner manufacturers (Rojo *et al.* 2009). For the analysis of ER, PR, Ki-67, and HER2, currently available solutions include ACIS® III (Dako Denmark; Glostrup, Denmark), Ariol (Molecular Devices; Hampshire, UK), Aperio Digital IHC (Aperio Technologies; Vista, CA, US), HistoQuant (3DHISTECH; Budapest, Hungary), and Virtuoso™ (Ventana Medical Systems, Tucson, AZ, US). However, because these methods are proprietary, the algorithms employed are closed source and their functionality is hidden from the user. Moreover, the commercial packages generally lack of transparent and extensive clinical validation.

Analysis tools described in the academic literature offer a more open and transparently validated approach for the quantification of IHC biomarkers. The number of studies describing novel methodologies has been rapidly rising within the past few years. Analysis tools for ER, PR, and Ki-67 include Mofidi *et al.* (2003), Pham *et al.* (2007), Rexhepaj *et al.* (2008), Gustavson *et al.* (2009), and Konsti *et al.* (2011). For the analysis of HER2, the literature includes methods by Joshi *et al.* (2007), Hall *et al.* (2008), Masmoudi *et al.* (2009), and Brügmann *et al.* (2011). However, the software applications described in these studies are mainly for research purposes and have not been released for public use. In addition, many of the methods may require considerable work if employed in a routine clinical process, requiring dedicated imaging and/or analysis equipment. Furthermore, as the information technological infrastructures in hospital and laboratory environments are often highly restricted, prohibiting the installation and usage of external software, the testing and adaptation of new digital image analysis methods can be cumbersome. Therefore, to increase the clinical adoption of digital image analysis techniques, there is a demand for software that is freely available, open source, clinically validated, and easy to use and install.

3. AIMS OF THE STUDY

The central aim of the present study was to design and implement an open software platform for virtual microscopy in order to facilitate its widespread adoption in clinical, educational, and research environments. All the applications and algorithms developed during the experiments have been published as open source and/or free software, thereby supporting further academic research.

More specifically, the aims of the study were:

- To develop controller software for automated virtual slide scanning and image tile stitching. (Not included in the original communications)

- To design and develop JPEG2000 standard-based software tools for virtual slide viewing, serving, conversion, metadata, and storage. (I)

- To design and develop a proof-of-concept software package for linking JPEG2000 virtual slides with the DICOM standard in a clinical environment. (II)

- To design and develop web applications for quantitative digital image analysis of breast cancer biomarkers ER, PR, Ki-67, and HER2. (III, IV)

4. MATERIALS AND METHODS

4.1 Sample material

According to the Finnish legislation regarding the usage of human organs, tissues, and cells in medical research (101/2001 and 594/2001), the digitization of specimen slides into virtual slides does not require explicit permission from the Finnish National Supervisory Authority for Welfare and Health (Valvira) or a separate statement from an ethical committee responsible for the sample material. Furthermore, as long as the sample material is anonymized, the patient privacy is not compromised (785/1992 and 523/1999).

4.1.1 Histological and radiological imagery (I, II)

The sample material of studies I and II were primarily used for technical testing and reference purposes, and the imagery was not subjected to automated image analysis. Thus, a detailed description of the sample preparation is not relevant. For study I, in addition to routine formalin-fixed, paraffin-embedded histological samples, cytological slides were scanned using a multiple focus layer image acquisition option (Z-stack). For study II, anonymized reference material representing typical diagnostic imagery of breast cancer was obtained from the Imaging Centre of Tampere University Hospital, Finland. The material covered two patients, consisting of radiographs of tumor marking under ultrasound control, mammograms of surgically removed tumors, thorax imagery, bone gamma structure scans, and magnetic resonance images. Histological specimen material (H&E-stained slides, CISH samples, and intraoperative frozen sections) matching the same tumors were collected from the Department of Pathology of Tampere University Hospital, Finland.

4.1.2 Immunohistochemistry (III, IV)

In study III, formalin-fixed and paraffin-embedded tissue sections from invasive breast cancers were derived from the archive of the Department of Pathology, Seinäjoki Central Hospital, Finland. Immunohistochemical stainings of ER, PR, and Ki-67 tissue sections followed the recommended staining protocols (NordiQC 2011). The slides were stained using the BondMax staining robot (Leica Microsystems, Wetzlar, Germany). ER was detected using monoclonal antibody 6F11 (diluted 1:300, Leica Biosystems, Newcastle, UK), PR was detected using monoclonal antibody PgR636 (diluted 1:600, Leica Biosystems, Newcastle, UK), and Ki-67 was detected using monoclonal antibody MIB-1 (diluted 1:100, Dako, Carpinteria, CA, US). Antigen retrieval was performed in Tris-EDTA buffer (pH 9, 100°C for 40 minutes). Bound antibodies were visualized using Bond Refine Detection kit (Leica Biosystems, Newcastle, UK). Immunoreaction was intensified using 0.5% copper sulfate (5 minutes). Hematoxylin counterstaining (1 minutes in ChemMate, diluted 1:6; Dako, Carpinteria, CA, US) was performed using PBS as bluing reagent. The samples were cleared with ethanol and xylene and mounted using standard procedures.

In study IV, formalin-fixed and paraffin-embedded tissue sections from invasive breast cancers were derived from earlier studies. The training set consisted of tissue microarrays (TMA) of 220 breast cancers (Tanner *et al.* 2006) and the validation set of whole sections of 144 invasive breast cancers (Gong *et al.* 2009). Immunohistochemical staining of HER2 was done using the HercepTest® kit (Dako, Copenhagen, Denmark) according to manufacturer's instructions using Lab Vision Autostainer® (Lab Vision, Fremont, CA, US). Gene amplification status of the tumors was verified with both fluorescence and chromogenic in situ hybridization (SPoT-Light® HER2 CISH kit by Life Technologies, Carlsbad, CA, US; and PathVysion® FISH kit by Abbott Laboratories, Chicago, IL, US).

4.2 Digital image acquisition

4.2.1 Study I

Specimen images were acquired using a Zeiss Axioskop40 microscope (Carl Zeiss MicroImaging, Jena, Germany), which was equipped with 10×, 20× and oil-40× objectives and a motorized specimen stage (Märzhäuser Wetzlar, Wetzlar, Germany). The images were captured with a CCD color camera (QICAM Fast, QImaging, Vancouver, Canada; 24-bit color depth; resolution 1,388 × 1,036 pixels, 4.65 pixels/µm). The camera was attached to the microscope with a 1× phototube. Image acquisition was controlled by the Surveyor imaging system (Objective Imaging, Cambridge, UK). The Surveyor software controls for stage and focus movements matched with automated image acquisition. Cytological slide material was scanned using a multiple focus layer image acquisition option (Z-stack). Image tiles were primarily saved in an uncompressed bitmap format and stitched as a contiguous montage either using the built-in function of Surveyor, or using the LargeMontage software, described in the present study (Section 5.2).

4.2.2 Study II

The standard-sized slides (75 × 25 mm) were scanned with Aperio ScanScope® XT (Aperio Technologies, Vista, CA, US; 20× objective lens, 2.0 pixels/µm) using uncompressed BigTIFF (Aperio 2011) as the primary output format. Whole-mount section slides (75 × 50 mm) were acquired with a Zeiss Axioskop40 microscope (Carl Zeiss MicroImaging, Jena, Germany) as described equipped with a CCD color camera (QICAM Fast; QImaging, Vancouver, Canada) and a motorized specimen stage (Märzhäuser Wetzlar, Wetzlar, Germany). The automated image acquisition was controlled by the Surveyor imaging system (Objective Imaging, Cambridge, UK) using uncompressed bitmap as the primary output format. The developed JVS-dicom Compressor application (described in the present study in Section 5.4.1) was used to convert the histological reference material into the DICOM-compatible JPEG2000 virtual slide format.

4.2.3 Study III

The training and validation image sets were captured using a Leica DM3000 microscope (Leica Microsystems, Wetzlar, Germany) equipped with 10×, 20×, and 40× objective lenses, a 1× phototube, and a Scion CFW-1612C digital color camera (Scion Corporation, Frederick, MD, US; 24-bit color depth; resolution 1,600 × 1,200 pixels, 4.40 pixels/µm). The images were stored using an uncompressed bitmap image file format. For every imaging session, an image from empty slide background area was acquired (blankfield image), which was used to correct image color balance and uneven illumination. Optimal image brightness and contrast were determined by using the Camera Adjustment Wizard, which was developed as an incorporated function of the analysis software (ImmunoRatio) described in the present study. The Camera Adjustment Wizard measures the brightness of the blankfield image and performs a contrast analysis using an image containing hematoxylin-stained cells. An optimal brightness (mean gray intensity) of the blankfield image is considered to be in the range of 200 to 250 (available range 0 to 255, black being 0). The contrast analysis segments the hematoxylin-stained cells (foreground) and analyzes their mean gray intensity, which is then divided by the background mean gray intensity. The contrast is considered to be optimal if the foreground mean gray intensity is 50 to 80% of the background mean gray intensity.

4.2.4 Study IV

The training image set was scanned using Aperio ScanScope® XT (Aperio Technologies, Vista, CA, US; 20× objective lens, 2.0 pixels/µm). Image stripes were stitched internally by the scanning software, stored in a lossless BigTIFF format (Aperio 2011), and subsequently converted into lossless JPEG2000 using the JVScomp software described in the present study (Section 5.3.2). The validation image set was imaged using Scion CFW-1612C camera (Scion Corporation, Frederick, MD, US; 1/1.8” sensor, 10× objective lens, 1× phototube, 1,600 × 1,200 pixels, 2.15 pixels/µm). For every imaging session, an image from empty slide background area was acquired (blankfield image), which was used to correct image color balance and uneven illumination.

4.3 Software development

Before preparing studies I–IV, there was a need for an image tile stitching solution suitable for large-sized imagery, such as virtual slides, and a controller software for linking and synchronizing the stitching with the scanning process, downstream image conversion, and other auxiliary steps (e.g., barcode reading). For these reasons, we developed an automated virtual slide acquisition controller software (Section 4.3.1) and a virtual slide stitching application (Section 4.3.2), which have not been published in scientific journals, but have their source code and binaries released for public usage.

4.3.1 Automated virtual slide acquisition controller

The automated virtual slide acquisition controller, entitled *DirObserver*, was developed using the C++ programming language (ISO/IEC 14882:1998 and ISO/IEC 14882:2003; C++03) and the Microsoft Foundation Classes (MFC) library (Microsoft Corporation, Redmond, WA, US). The program code was created and compiled using the Visual Studio 2005 integrated development environment (Microsoft Corporation, Redmond, WA, US), targeting the 32-bit Microsoft Windows® operating systems.

4.3.2 Virtual slide stitching application

In order to facilitate cross-platform compatibility, the virtual slide stitching software, entitled *LargeMontage*, was developed using the Java programming language (Oracle Corporation, Redwood City, CA, US; version 1.5.0). The application uses the Java Advanced Imaging (Oracle Corporation, Redwood City, CA, US; version 1.3.3-alpha) and Java Advanced Imaging Image I/O Tools (Oracle Corporation, Redwood City, CA, US; version 1.1-alpha) image processing libraries. In addition, the image registration functionality is performed with the TurboReg plugin (Thévenaz 2011). LargeMontage is designed as a standalone, command line-based application, but can also be used as a plugin for the ImageJ image processing software.

The program code was created and compiled using the Eclipse integrated development environment (Eclipse Foundation, Ottawa, Canada).

4.3.3 JPEG2000 virtual slide software package (I)

The JPEG2000 virtual slide software package, or the *JVS software package*, was written with the C++ programming language (ISO/IEC 14882:1998 and ISO/IEC 14882:2003; C++03) and built for 32-bit Microsoft Windows® platforms, but can be run under 64-bit platforms via a legacy translation layer (such as WoW64) as well. The package consists of three applications: *JVScomp*–a compression application for creating optimally parameterized JPEG2000 virtual slides; *JVSview*–a viewer application capable of viewing both local and remote JPEG2000 virtual slides; and *JVSserv*–a JPIP server for remote serving of JPEG2000 virtual slides. In addition, the package contains an XML schema, *JVSschema*, for describing the image metadata content. JVSschema was developed using the W3C XML Schema standard (XSD 1.0; W3C 2011). JVScomp is built on the ECW JPEG 2000 SDK (Hexagon, Stockholm, Sweden; versions 2.0–3.3), whereas JVSview and JVSserv are built on the Kakadu JPEG2000 Framework (NewSouth Innovations, Sydney, Australia; versions 5.0–6.4). The program code was created and compiled using the Visual Studio 2005 integrated development environment (Microsoft Corporation, Redmond, WA, US).

4.3.4 Virtual slide–DICOM integration software (II)

An integration software package for linking JPEG2000 virtual slides with DICOM, entitled *JVSdicom*, consists of three applications: *JVSdicom Compressor*–a compression application for creating JPIP-linked JPEG2000 virtual slides, *JVSdicom Server*–a DICOM PACS server application, *JVSdicom Workstation*–a DICOM PACS client application. An open-source DICOM library (OFFIS DCMTK DICOM toolkit; OFFIS, Oldenburg, Germany; version 3.5.4) was modified by adding support for JPIP, as described in the DICOM Supplement 106. The modified library was used to embed DICOM functionality to the developed JVSdicom software package. JVSdicom Compressor is based on our previously described JPEG2000

compression application (JVScomp, version 2.1). JVSdicom Server and Workstation utilize the Qt open-source software framework (Qt Development Frameworks, Oslo, Norway; version 4.3) for core application functionality and the Tango Icon Library (Tango Desktop Project, Portland, OR, US) for graphical user interface elements. The software package was written in C++ programming language (ISO/IEC 14882:1998 and ISO/IEC 14882:2003; C++03) and built for 32-bit Microsoft Windows® platforms but can be run under 64-bit platforms as well.

4.3.5 Analysis software for ER, PR, and Ki-67 IHC (III)

Quantitative IHC analysis software for hormone receptors (ER and PR) and Ki-67, entitled *ImmunoRatio*, was first developed as a plugin for the ImageJ image analysis software (Rasband 2011; version 1.42m) using the Java programming language (Oracle Corporation, Redwood City, CA, US; version 1.6.0). In addition to built-in ImageJ functions, the ImmunoRatio analysis algorithm uses the Calculator Plus plugin (Landini 2011b) for blankfield correction, the Rolling Ball algorithm (Sternberg 1983) for background subtraction, the Color Deconvolution plugin (Landini 2011a) for DAB and hematoxylin stain separation, the IsoData algorithm (Ridler & Calvard 1978) for adaptive thresholding, and the Watershed algorithm (Vincent & Soille 1991) for nucleus segmentation. The analysis algorithm steps are presented in Figures 24–26. The ImmunoRatio plugin was embedded into a Java servlet-based web application. The web application was developed using Google Web Toolkit (Google, Mountain View, CA, US; version 1.7.0), Apache Commons FileUpload package (Apache Software Foundation, Forest Hill, MD, US; version 1.2.1), Apache Commons IO library (Apache Software Foundation, Forest Hill, MD, US; version 1.4), Laboratory for Optical and Computational Instrumentation Bio-Formats package (University of Wisconsin–Madison, Madison, WI, US; version 4.1), and Apache Tomcat servlet container (Apache Software Foundation, Forest Hill, MD, US; version 6.0). The program code was created and compiled using the Eclipse integrated development environment (Eclipse Foundation, Ottawa, Canada).

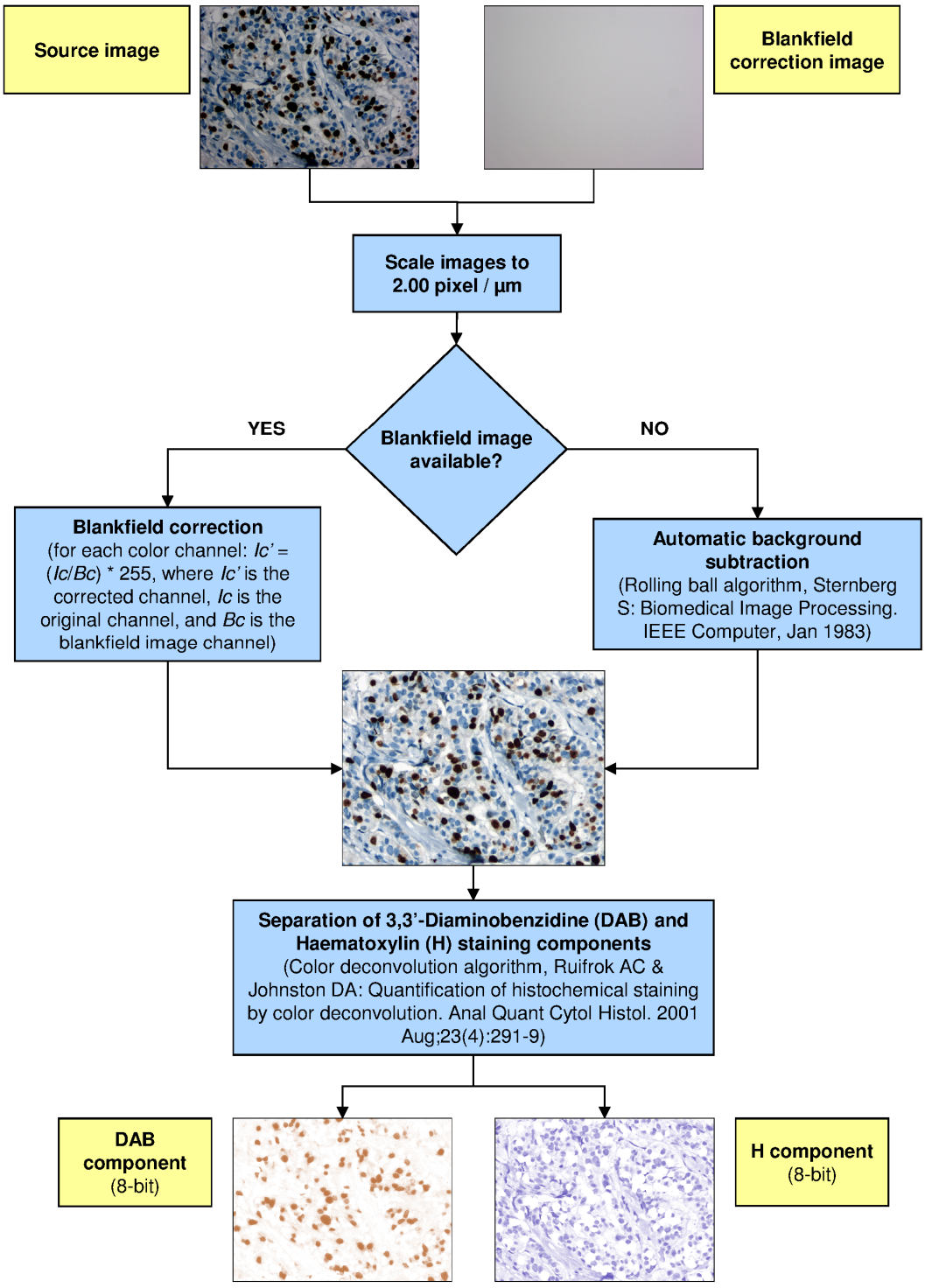

Figure 24. The ImmunoRatio analysis algorithm flowchart – part 1/3.

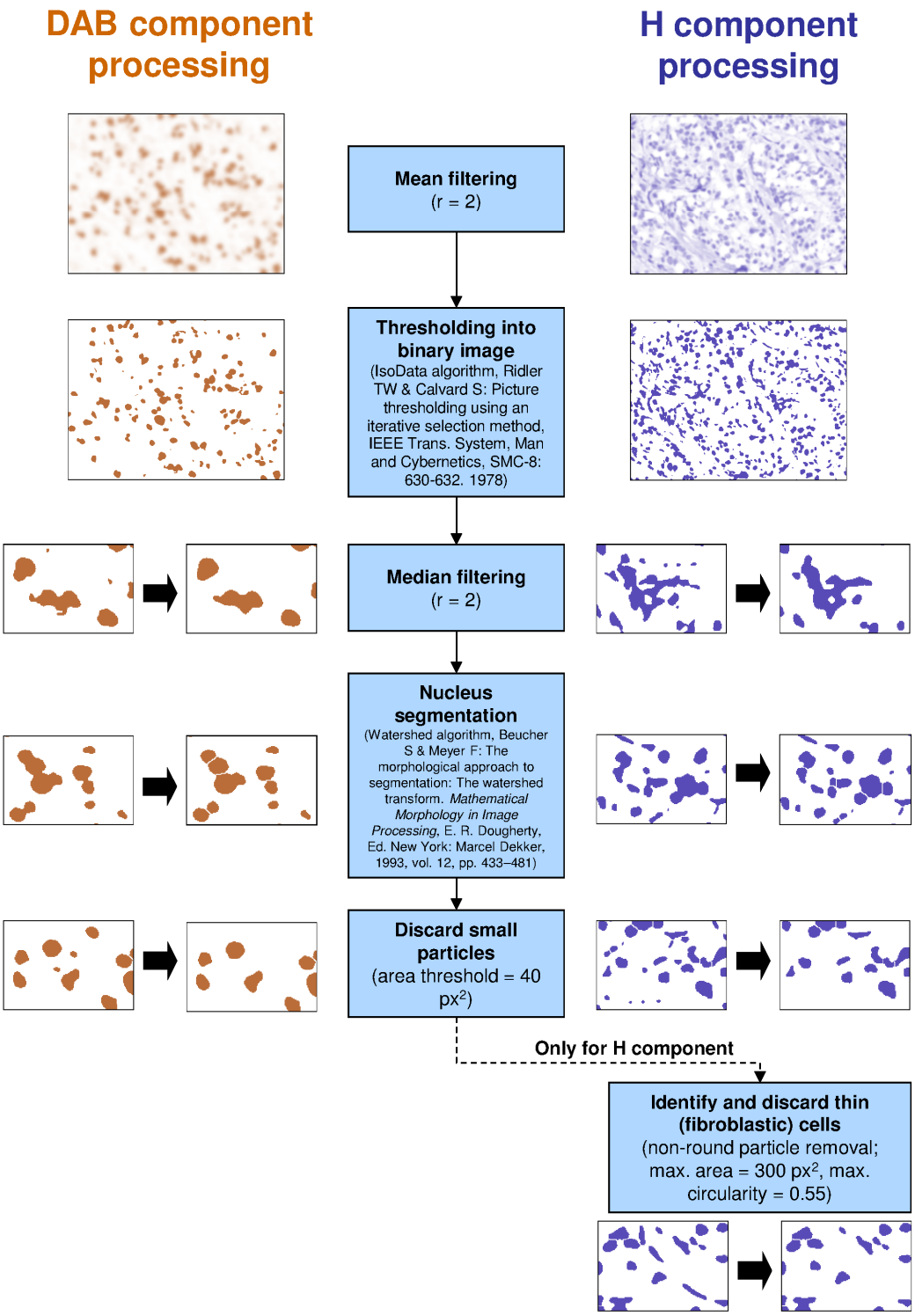

Figure 25. The ImmunoRatio analysis algorithm flowchart – part 2/3.

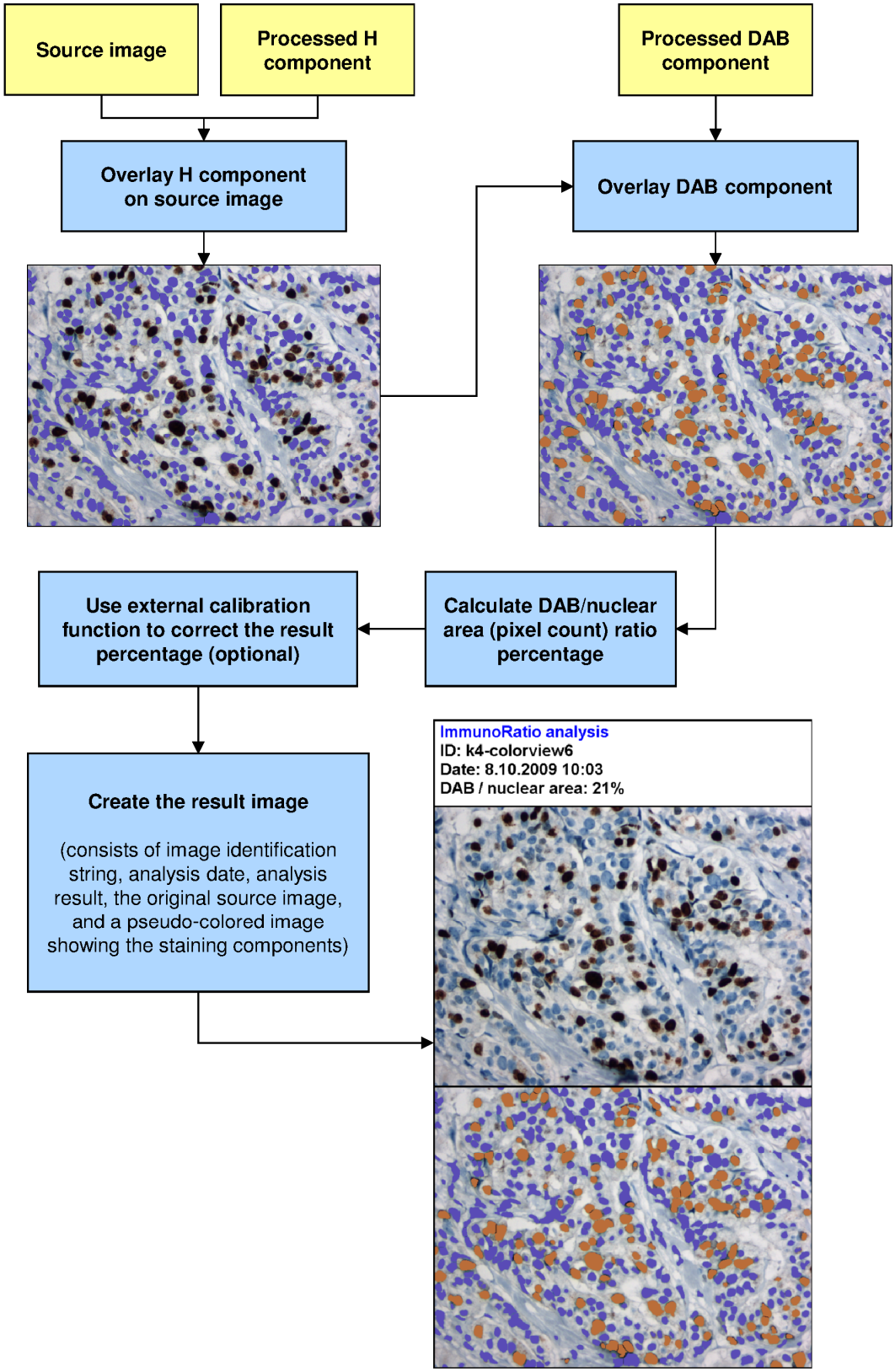

Figure 26. The ImmunoRatio analysis algorithm flowchart – part 3/3.

4.3.6 Analysis software for HER2 IHC (IV)

Semi-quantitative IHC analysis software for breast cancer biomarker HER2, entitled *ImmunoMembrane*, was first developed as a plugin for the ImageJ image analysis software (Rasband 2011; version 1.45b) using the Java programming language (Oracle Corporation, Redwood City, CA, US; version 1.6.0). In addition to built-in ImageJ functions, ImmunoMembrane uses the Calculator Plus plugin (Rasband 2011b) for blankfield correction, the Color Deconvolution plugin (Rasband 2011a) for DAB stain separation, and the Particles4 & Particles8 plugins (Rasband 2011b) for cell membrane segmentation. The analysis algorithm steps are presented in Figures 27–29. The ImmunoMembrane plugin was embedded into a Java servlet-based web application. The web application was developed using Google Web Toolkit (Google, Mountain View, CA, US; version 1.7.1), Apache Commons FileUpload package (Apache Software Foundation, Forest Hill, MD, US; version 1.2.1), Apache Commons IO library (Apache Software Foundation, Forest Hill, MD, US; version 1.4), Laboratory for Optical and Computational Instrumentation Bio-Formats package (University of Wisconsin–Madison, Madison, WI, US; version 4.1), and Apache Tomcat servlet container (Apache Software Foundation, Forest Hill, MD, US; version 6.0). The program code was created and compiled using the Eclipse integrated development environment (Eclipse Foundation, Ottawa, Canada).

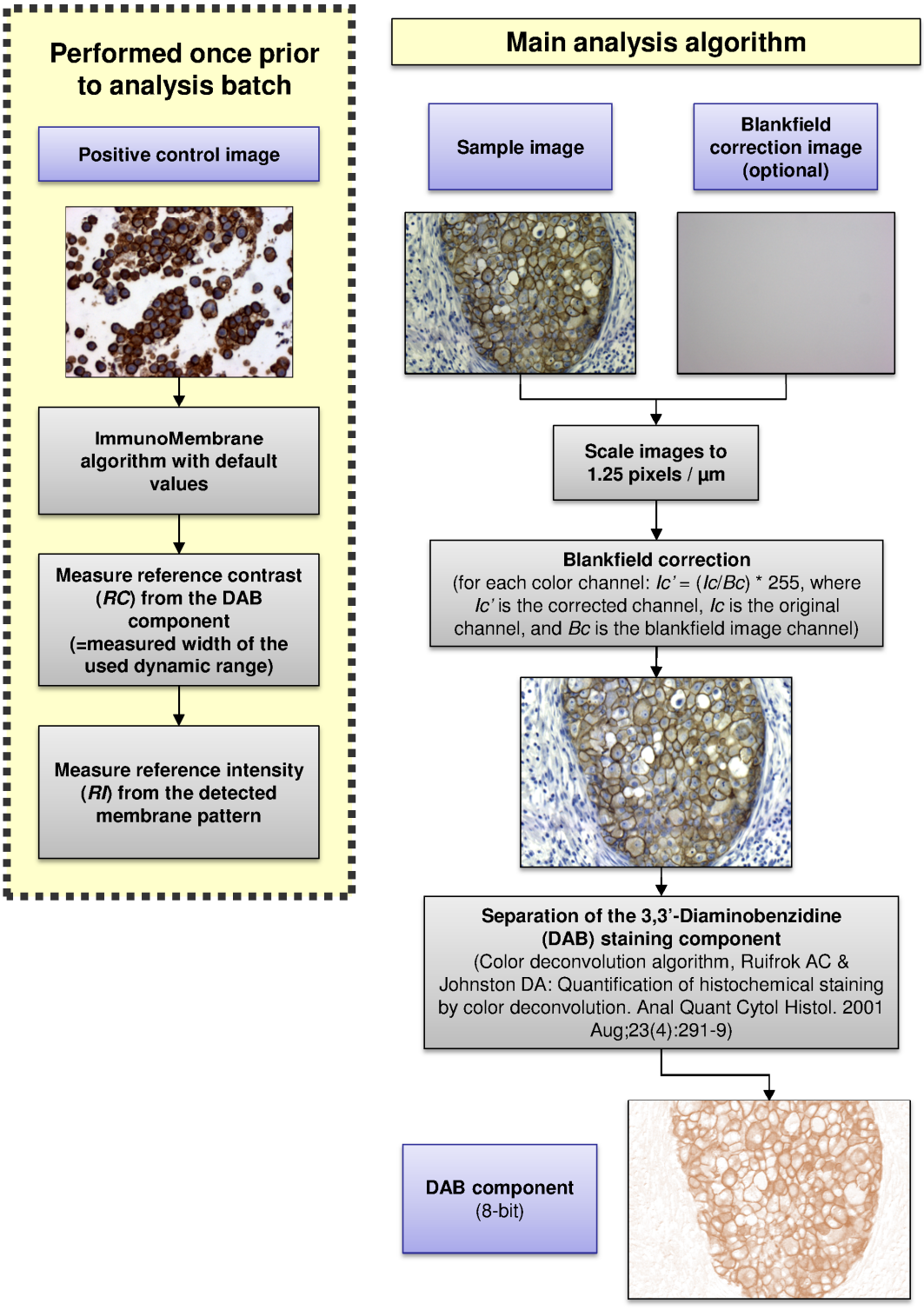

Figure 27. The ImmunoMembrane analysis algorithm – part 1/3.

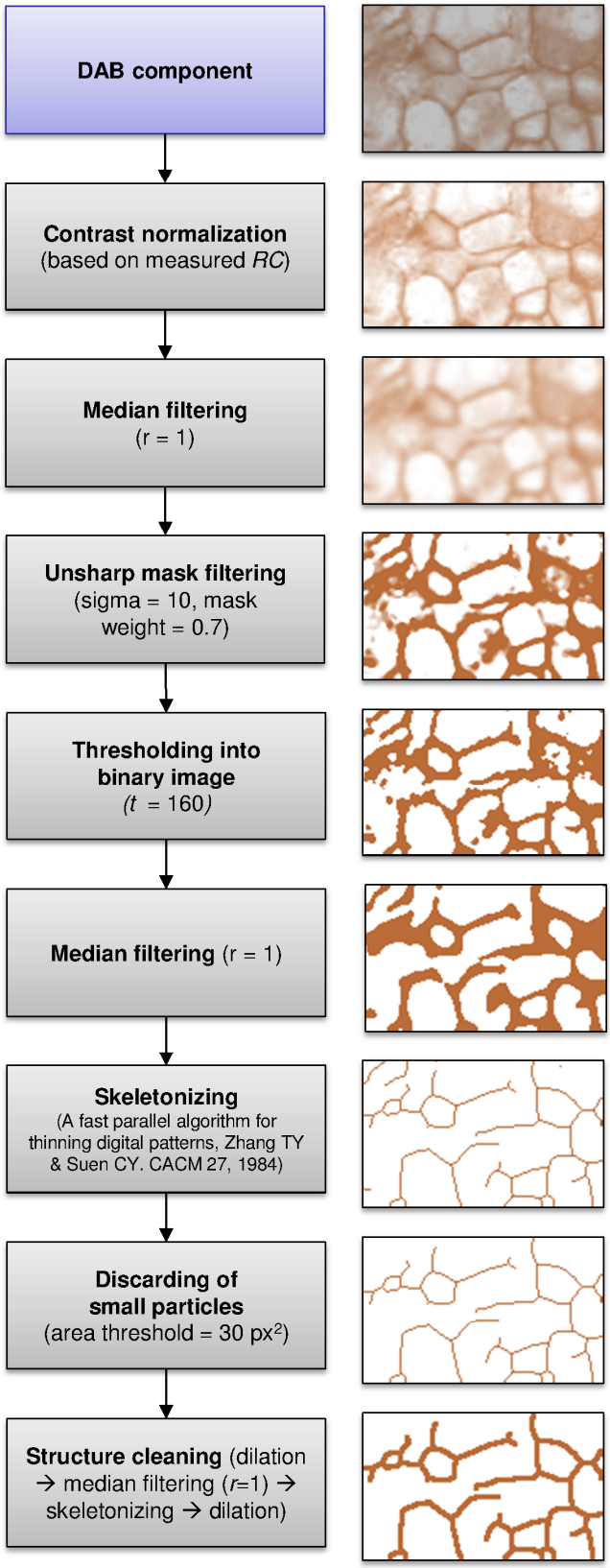

Figure 28. The ImmunoMembrane analysis algorithm – part 2/3.

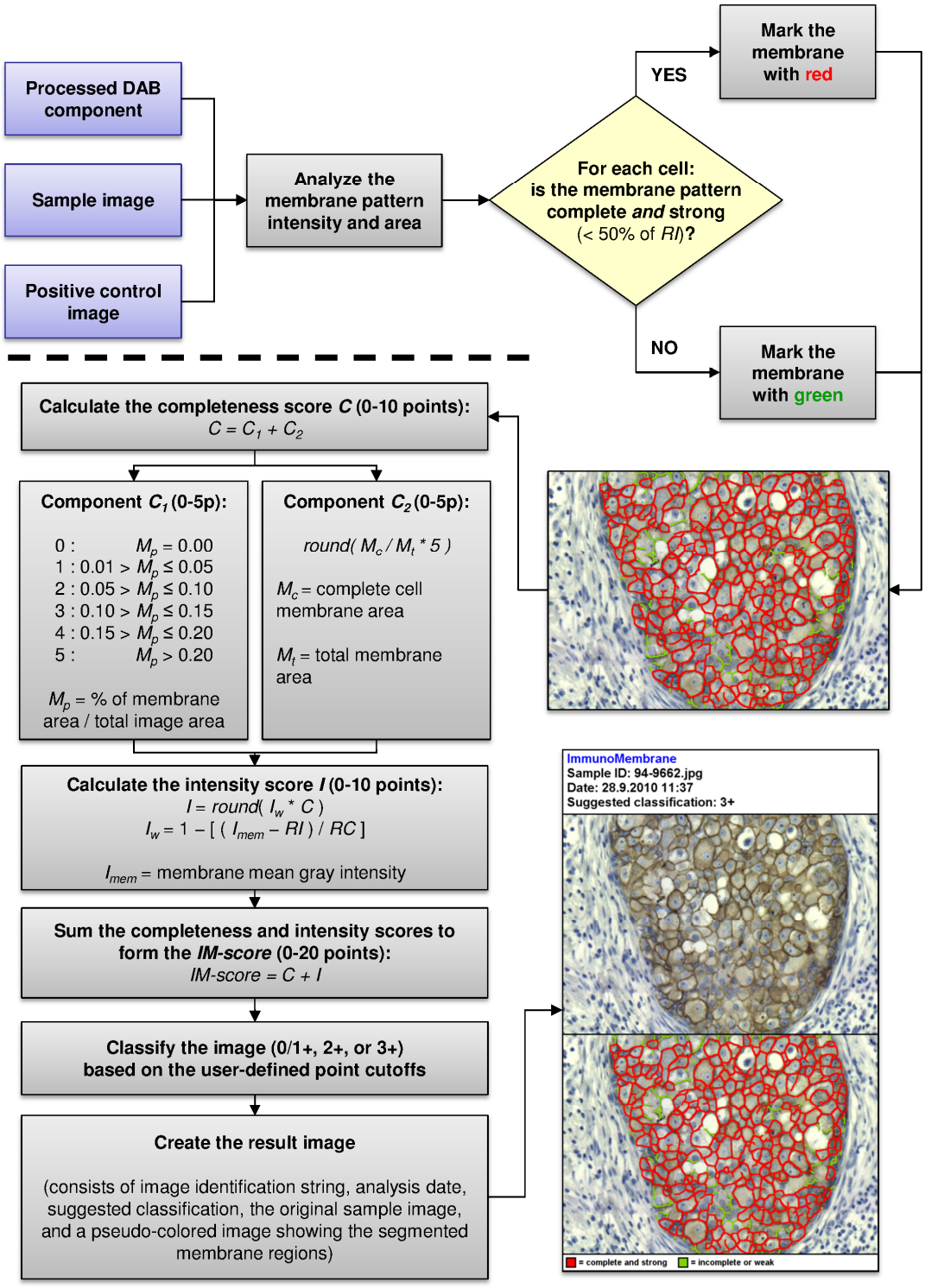

Figure 29. The ImmunoMembrane analysis algorithm – part 3/3.

4.4 Software calibration

Both the analysis algorithms described in studies III and IV were calibrated. The calibration process consisted of a training step and a validation step.

4.4.1 Algorithm training (III, IV)

In study III, a training set consisting of 50 IHC-stained slides was formed by semi-randomly selecting them from a pool of 100 slides (25 stained for Ki-67, 13 for PR, and 12 for ER). The labeling indexes (percentage of positively stained nuclei by visual assessment) were evenly distributed, ranging from 0 to 100%. From each training set slide, one image representative for invasive carcinoma was acquired. Each acquired image was analyzed visually by counting positively and negatively stained carcinoma cells on a computer screen (a minimum of 500 cells total per image). The percent of DAB-stained nuclei out of the total nuclei (DAB- and hematoxylin-stained) was calculated as the labeling index. This result was used as the gold standard for the algorithm training. The images were then analyzed using the non-trained algorithm, and the results were compared with visual counting in a scatter plot. Owing to the non-linear relation, a third degree polynomial was fitted to the data. The training was completed by embedding the fitted polynomial as a correction function into the analysis algorithm.

In study IV, the training image set consisted of 220 breast cancer samples on TMA slides, stained with HercepTest® (Dako, Copenhagen, Denmark). The training set was used to specify pre-defined category cut-offs for the algorithm (to match the 0/1+, 2+, and 3+ ASCO/CAP classification). From each tissue core, one representative snapshot (1,596 × 1,116 pixels) was selected for analysis. The analysis was done first visually by an expert pathologist (JI) and then automatically by the non-trained algorithm. Using the pathologist's visual classification as golden standard, the optimal IM-score cut-offs were defined by searching the peak weighted (equally-spaced) kappa agreement κ_w (Cohen 1968).

4.4.2 Algorithm validation (III, IV)

In study III, to validate the training and demonstrate the accuracy of the analysis, the remaining 50 samples (25 stained for Ki-67, 13 for PR, and 12 for ER) of the training set pool were used as a test set, which was analyzed using the trained algorithm. In the final step of the validation, the minimum number of images needed to be averaged from a typical tumor sample (diameter 1 to 2 cm) was defined. From 10 samples, 12 images per sample representing central and peripheral tumor areas were acquired using 20× objective.

In study IV, to validate the analysis algorithm training, first the optimal required number of image fields to be captured and averaged from a typical tumor sample (diameter 1 to 2 cm) was defined. For this purpose, 10 images per sample representing central and peripheral tumor areas were selected from a non-negative set of 13 breast cancer samples, and analyzed using the trained algorithm. After specifying the optimal field count, a separate validation set consisting of whole sections of 144 HercepTest®-stained invasive breast cancers was analyzed using the trained algorithm and compared against the visual assessment of an expert pathologist (JI). Finally, the disagreement rate of the IHC classifications was compared with the results obtained with FISH and CISH.

4.5 Software testing

4.5.1 JPEG2000 code-stream parameter optimization (I)

The JPEG2000 code-stream parameter optimization was based on theoretical assumptions of the JPEG2000 code-stream properties, visual assessment of the time needed to initially load the image, the time needed for image refreshment during magnification change and navigation within the specimen, and to lesser extent, the compression execution time. Tests were performed using the Kakadu pre-compiled binaries for image compression and viewing (NewSouth Innovations, Sydney, Australia; version 5.2.2.20).

4.5.2 JPEG2000 performance evaluation (I)

The performance of JPEG2000 was evaluated using JPIP image serving speed and compression execution time as outcome measures. The tests were carried out on a Microsoft Windows® XP workstation, equipped with a dual-core processor, 3 gigabytes of RAM, two ATA hard disks, and a 100 Mbit network link. The used main test virtual slide image can be seen on our website (http://jvsmicroscope.uta.fi/examples/). The slide had 42,865 × 57,222 pixels, three 8-bit color channels, totaling 6.9 gigabytes uncompressed, and it was stored as a binary encoded PPM (Poskanzer 2011). An additional set of test images was created by extracting sub-resolutions from the original image, halving the resolution in each step. The compression tests were performed using our JVScomp application. During these tests, we monitored the processor load, RAM usage, disk usage percentage, and the average disk read and write queue lengths. The image serving performance of JPIP was evaluated with our JVSserv application, in comparison to the Zoomifyer EZ™ (Zoomify, Aptos, CA, US; version 3.0.9). Whereas JVSserv is a standalone server application, Zoomifyer requires an external HTTP server underneath it. The Apache HTTP server (Apache Software Foundation, Forest Hill, MD, US; version 2.2.4) was selected for this. The evaluation and comparison were performed by simulation in which 10 local area network workstations with a 100 Mbit/s connection were each simulating 10 clients, yielding a 100-client pool. Each client had their own test image, which was duplicated from the main test image. Server and client caches were disabled. During these simulations, we monitored the server's average disk read queue length, processor load, network bandwidth usage, RAM usage, and subjectively evaluated the clients' viewing interactivity.

4.5.3 Algorithm robustness assessment (III, IV)

In study III, the ImmunoRatio algorithm was initially developed and calibrated using ER-, PR-, and Ki-67-stained slides, which were considered optimal by an external quality assurance program (NordiQC 2011). To simulate inter-laboratory variability in staining results, the effect of suboptimal primary antibody (Ki-67 MIB-1) dilution and hematoxylin counterstaining intensity was studied. The robustness of ImmunoRatio to variations in image acquisition settings was examined by compar-

ing the optical resolutions provided by 10×, 20×, and 40× microscope objectives, and by comparing the analysis results obtained with six microscope cameras: Scion CFW-1612C (Scion Corporation, Frederick, MD, US), Altra 20 (Olympus Corporation, Tokyo, Japan), ColorView II (Olympus Corporation, Tokyo, Japan), Leica DFC290 HD (Leica Microsystems, Wetzlar, Germany), Mightex 3MP Color CMOS (Mightex Systems, Pleasanton, CA, US), and Nikon DS-Fi1 (Nikon Corporation, Tokyo, Japan). Uncompressed, lossless file format was selected as the primary output for each camera. Images were also acquired using JPEG file format (quality factors 10, 20, 40, 60, 80, and 100) to study the suitability of lossy compression for ImmunoRatio analysis. In addition, for each camera, the average diameter (pixels per µm) of a hematoxylin-stained nucleus was measured. Linear regression was used to fit a first degree polynomial to the data and the polynomial was then embedded into the Scale Finder function of ImmunoRatio. The Scale Finder assists the user in determining a rough scale estimate for the microscope setup, if not known prior to analysis.

In study IV, the algorithm robustness was tested using 41 non-negative breast cancer TMA cores, which were digitized with six different camera models: ColorView II (Olympus Corporation, Tokyo, Japan); Leica DFC310 FX (Leica Microsystems, Wetzlar, Germany); OptixCam OCD-3.3-ICE (The Microscope Store, VA, US); QICAM Fast1394 (QImaging, Surrey, Canada); Scion CFW-1612C (Scion Corporation, Frederick, MD, US); and the virtual microscope scanner camera of Aperio ScanScope® XT (Aperio Technologies, Vista, CA, US). To simulate real-life diagnostic environment, the cameras were attached to workstations using LCD displays from various manufacturers (all set to factory default settings). Camera illumination was fixed (auto-exposure disabled) and adjusted to match with the image seen through microscope oculars. Non-linear image intensity and contrast corrections, as well as additional software image enhancements, were set as low as possible. Each camera's scale (in pixels per µm) was measured by using a stage micrometer and recorded for usage during analysis. After these initial configurations, the actual testing was split into several steps. First, to normalize camera intensity and contrast variation, a blankfield and a positive control image were captured for each camera model. Second, with each camera, a fixed area from each sample was imaged using 10× objective lens (Aperio 20×) and subsequently analyzed using ImmunoMembrane. Third, all result IM-scores obtained for a sample were averaged

into a sample-specific reference score. For each camera–sample pair, the absolute difference of the camera-specific IM-score and the sample reference score was measured (=error value). Finally, the error values of each camera were averaged and their equivalence was statistically compared using variance analysis (Kruskal–Wallis non-parametric test, $\alpha = 0.05$).

4.6 Prognostic validation (III)

Prognostic validation of ImmunoRatio was performed with a sample set consisting of 123 primary breast cancer patients, derived from the archives of the Department of Pathology (Tampere University Hospital, Tampere, Finland). Permission for using the samples were received from the National Supervisory Authority for Welfare and Health (Köninki *et al.* 2011: *Analysis of PIK3CA mutations and protein expression in breast cancer*, submitted for publication). Survival rates of all patients were calculated by the method of Kaplan and Meier. Data on breast cancer-specific mortality was obtained from Finnish Cancer Registry. Up to 20-year follow-up was available for this patient cohort (cancers diagnosed between 1988 and 1992). The IHC staining for Ki-67 was carried out as described above, except that PowerVision+ kit (ImmunoVision, Springdale, AZ, US) was used for antibody detection and LabVision Autostainer (Lab-Vision, Fremont, CA, US) for staining automation. Informed consent in very old retrospective patient cohorts was deemed unnecessary, since the study was approved by the local hospital ethics committee and the National Supervisory Authority for Welfare Health.

5. RESULTS

5.1 DirObserver – a microscope image acquisition controller

The DirObserver software was developed for linking and synchronizing several external processing steps (e.g., virtual slide stitching) with the scanning process. The software monitors a given directory and responds to the inclusion of new files and/or sub-directories by invoking external programs and executing a series of user-specific commands. The graphical user interface of the application is presented in Figure 30 and the execution flow of the software is presented in Algorithm 1.

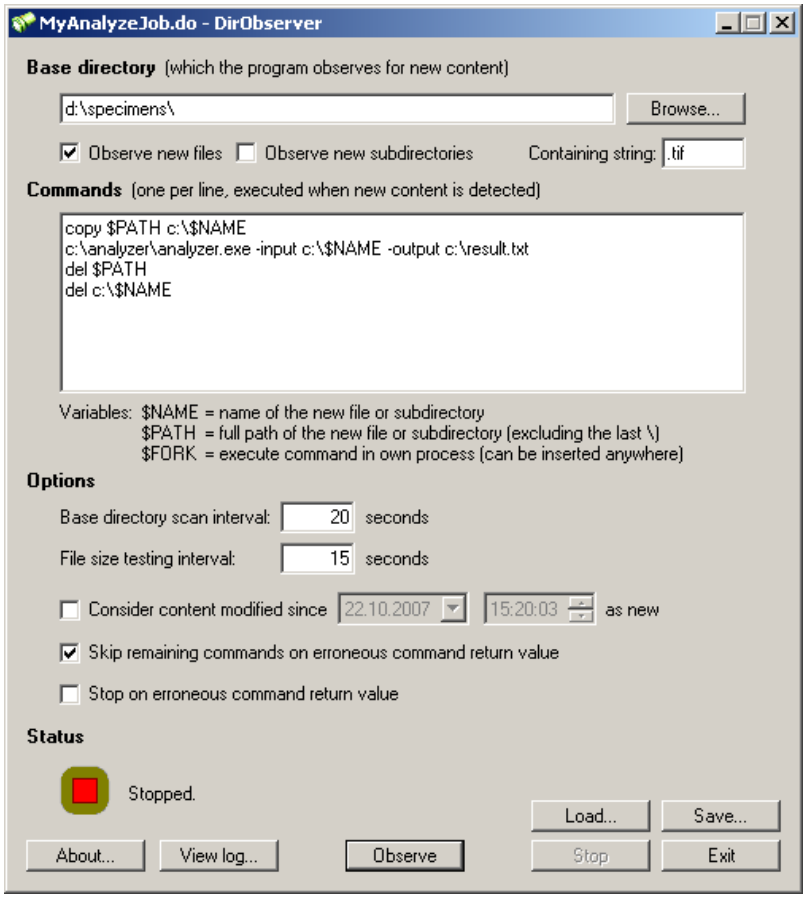

Figure 30. The graphical user interface of the DirObserver software application.

Algorithm 1. The execution flow of the DirObserver software for synchronizing external processing steps of automated virtual slide scanning.

```
1: if user has specified to include existing content based on modification time then
2:     startTimestamp ⟵ user-specified modification time
3: else
4:     startTimestamp ⟵ system time
5: readyList ⟵ the base directory files and sub-directories, which modification time is
       older than startTimestamp
6: loop each n second, where n is user-specified base directory scan interval
7:     observationList ⟵ the base directory files and sub-directories, which modification
           time is equal or newer than startTimestamp
8:     for each file or sub-directory x ∈ observationList do
9:         if x has changed since last iteration then
10:            if the file (or the newest file within the sub-directory) x is not
                   modified in m seconds, where m is the user-specified file size
                   testing interval then
11:                execute the user-specified command chain
12:                remove x from the observationList
13:                readyList ⟵ x
```

Content (i.e., new files and sub-directories) can be filtered using string matching. For example, you can filter only files containing string *.tif*, effectively making DirObserver to react whenever a new TIFF image file appears into the base directory. When DirObserver has successfully detected new content, it starts to execute the user-specified commands, which are inserted within the program one per line. The commands are given with a conventional command-line syntax and a separate command interpreter window is opened for console applications. The command return values are captured and can be used to stop DirObserver, if necessary. By default, DirObserver ignores erroneous return values and continues to execute the commands line by line. The program can be instructed to stop on erroneous command return value, and, in addition, it can be instructed to skip remaining commands on erroneous command return value, that is, if a command returns an erroneous value, the program skips the remaining commands and moves on to the next new file or sub-directory. Successfully and unsuccessfully executed commands are displayed in a log window, which shows the command execution starting time, as well as the return value (a return value 0 is commonly interpreted as success). The

commands are shown in their actual form, having their command variables already translated.

The software features a set of special command variables, which are translated to strings during the command execution. The following variables can be used within the commands:

- *$NAME* – name of the new file or sub-directory, without file extension
- *$FILE* – name of the new file, with file extension
- *$PATH* – full path of the new file or sub-directory
- *$FORK(n)* – executes a command in own process and returns immediately; can be inserted anywhere in the command string; *n* is the number of maximum simultaneous commands

DirObserver has been released under the GNU General Public License (GPL) v2.0 and the executable 32-bit Microsoft Windows® binaries as well as the source code are available on our website http://jvsmicroscope.uta.fi/dirobserver/.

5.2 LargeMontage – a virtual slide stitching application

The LargeMontage software was developed to stitch the image tiles generated during virtual slide scanning. The design of the application allows the building of very large montage images, that is, those that cannot be processed in memory due to their size. The stitching is done using image registration to aid in aligning the tiles with respect to each other, thereby creating no visible discontinuities in the tile boundary regions (Figure 31). If the registration operation is not perfect, the boundary regions can be further processed with spatial mean filtering. LargeMontage processes the image tiles from a directory either in a unidirectional, raster or in a bidirectional order. The user can specify fixed overlap values or alternatively employ automated registration, which is performed using the TurboReg software library (Thévenaz 2011), embedded within LargeMontage. During the processing, the image tiles can be optionally processed with unsharp mask filtering to enhance the sharpness and visual clarity.

LargeMontage can be used in batch mode from command line or interactively via the graphical user interface (Figure 32a). Additionally, since the application is also a functional ImageJ plugin, it can be invoked from within ImageJ and included in macro scripts. Prior to processing the image tiles, the user specifies to the program

- the location of the base image file,
- the location and file format of the final output montage file,
- the number of rows and columns in the image tile grid,
- the horizontal (X) and vertical (Y) overlap of the tiles (in pixels),
- the X and Y cumulative shift (in pixels),
- the level of unsharp mask filtering applied,
- the mean (convolution) filter weight for boundary smoothing,
- the level of JPEG2000 lossy compression,
- whether and where to apply the automated image registration,
- the default image tile order, and
- other minor auxiliary features, such as logging and debug mode.

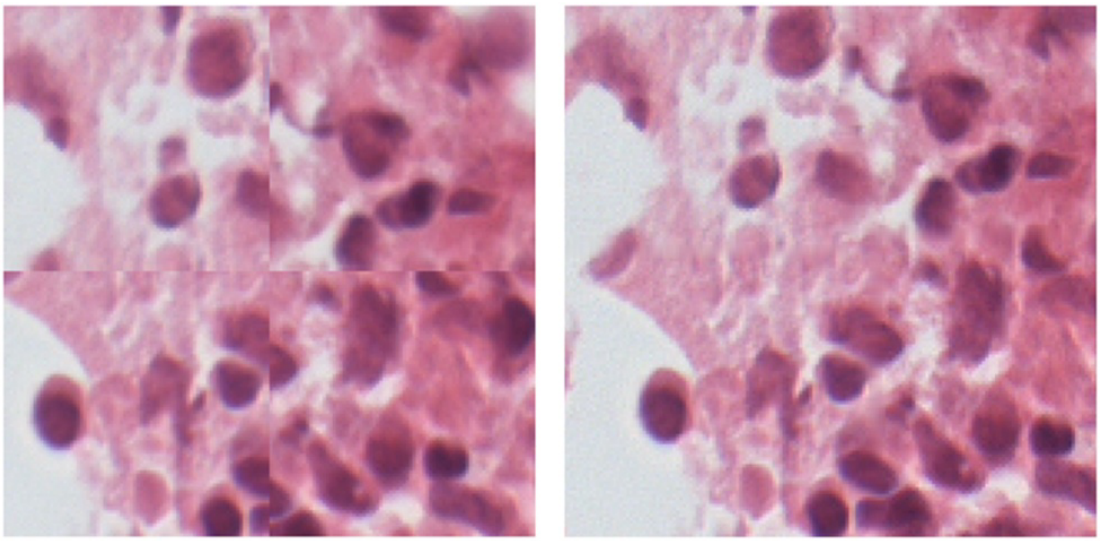

Figure 31. Visible discontinuity at the border of four image tiles due to improper tile alignment (a); the same tile set processed with LargeMontage, resulting in near-invisible border artifacts (b). H&E staining of a breast cancer tissue section.

If the automated registration method is being used, the user-specified Y overlap value is treated as an approximation. The accuracy of the registration is dependent on the amount of distinguishable landmark information visible within the overlapping tile boundary regions, and the overlap has to be at least 30–50 pixels (when using a reference resolution of 4.0 pixels/µm). The calculation of each row's Y overlap is done by matching two montages vertically adjacent source images together (Figure 32b). The program can identify if these two images contain registrable data or not, and if not, the matching is done to a different image pair from the same row. The X overlap will always be set to a fixed, user defined value. The X shift is a correction value for each row that is applied only to the first image of a row and it is recalculated for each row. Similarly, the Y shift is a correction value for each column that is applied cumulatively, that is,

$$Y_c = (n-1) * Y_o \,, \tag{19}$$

where Y_c is the current row's shift value, n is the row number, and Y_o is the original, user-specified shift value.

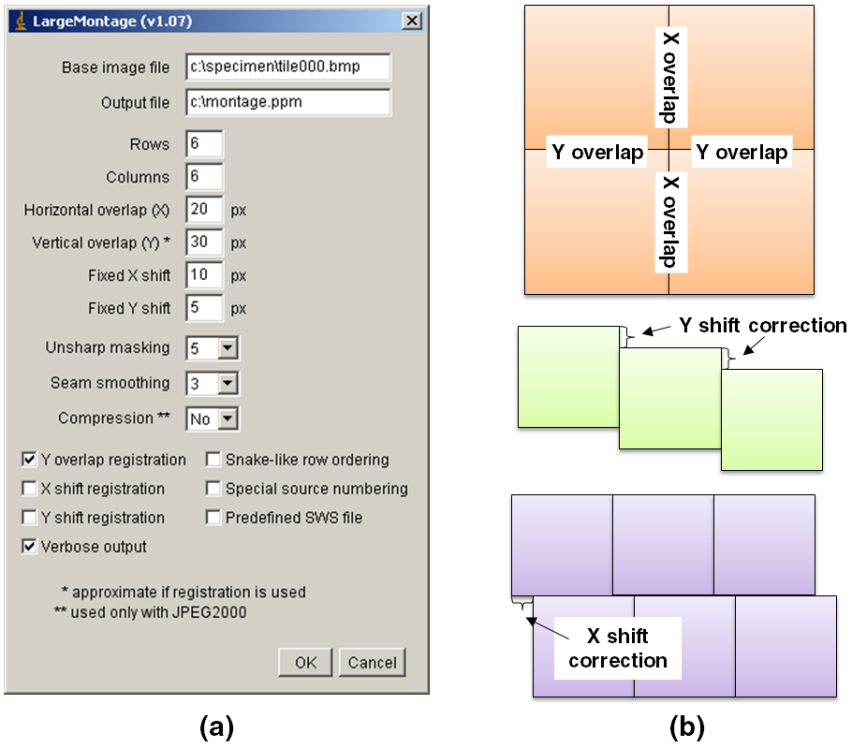

Figure 32. The graphical user interface of the LargeMontage software (a) and image tile alignment parameters used during the stitching process (b).

Supported input file formats are JPG, BMP, PNG, PNM and TIFF, and supported output formats are PNM (PBM/PGM/PPM; uncompressed, raw/binary formatted, over 4 GB output file support), TIFF (uncompressed, untiled & stripped, output file size limited to 4 GB), and JPEG2000 (lossless- or lossy-compressed, tiled, RPCL progression order). Input format is assumed to be grayscale (8-bit, 16-bit, or 32-bit) or to use the RGB color model (24-bit).

LargeMontage has been released under the GNU GPL v2.0 and the compiled Java class files as well as the source code are available as a Java Archive (JAR) container on our website http://jvsmicroscope.uta.fi/largemontage/.

5.3 JPEG2000 virtual slide software package (I)

5.3.1 Optimal JPEG2000 code-stream parameterization

In order to effectively employ JPEG2000 in virtual microscopy, we found the code-stream parameterization to be of critical importance. The optimal parameterization based on our experiments is summarized in Table 4.

Table 4. Optimal JPEG2000 code-stream parameterization for virtual slide.

JPEG2000 code-stream parameter	Parameter value
Compression ratio (lossy)	25:1 to 30:1
Wavelet filter	Irreversible
Wavelet decomposition levels	10
Tiling	Not needed
Tile-parts	1
Precinct size	128 × 128
Code-block size	64 × 64
Progression order	RPCL
Quality layers	1
PLT pointer marker segments	Inserted always

5.3.2 JVScomp – a virtual slide converter

JVScomp is a JPEG2000 virtual slide compression application capable of creating virtual slides that follow the parameterization described in Section 5.3.1. The generated virtual slides are optimized for viewing and serving with the JVSview and the JVSserv software applications, described in the following sections. At the time of writing Study I, JVScomp was capable of compressing only commonly used input file formats, such as PPM, BMP, and JPEG, and the software supported only dual-processor workstation environments. The file format support has been later enhanced to cover various virtual slide scanner manufacturer formats, such as NDP (Hamamatsu Photonics, Hamamatsu, Japan) and MRXS (3DHISTECH, Budapest, Hungary), as well as to support multi-core processors. Likewise, the default user interface for the initially released version of the software was command line-based, but has later been upgraded with a graphical user interface (Figure 33). By default, JVScomp employs a rate control policy that yields as efficient a compression as possible. If an image contains areas that are substantially responsive to compression, for example, homogenous areas of virtual slide glass background with no tissue section, a higher compression ratio is applied to these areas. Thus, a greater overall compression ratio and a smaller file size can be achieved.

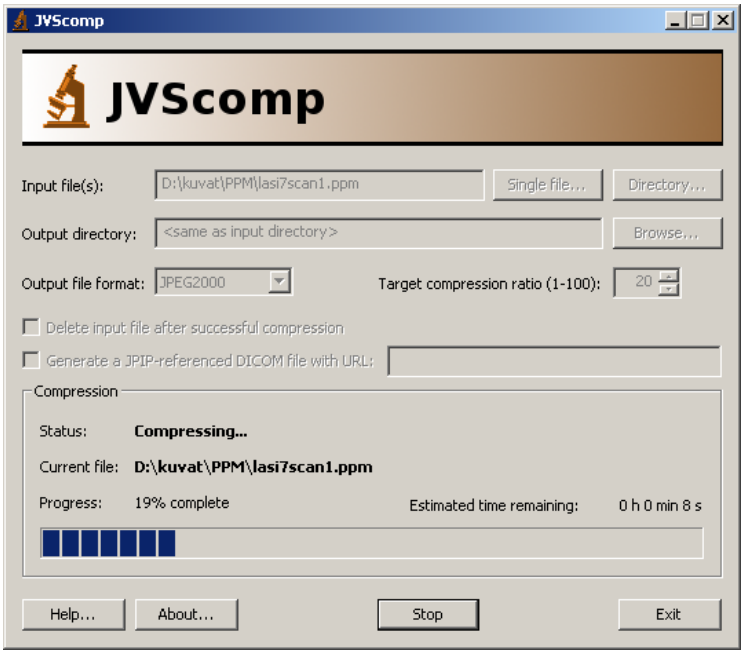

Figure 33. The graphical user interface of the JVScomp JPEG2000 virtual slide compression software. Pre-release version.

The initial version of JVScomp is released under the GNU GPL v2.0 license and the later versions under a customized end-user license agreement. The executable binaries for 32-bit Microsoft Windows® and source code is freely available on our website http://jvsmicroscope.uta.fi/jvscomp/.

5.3.3 JVSview – a virtual slide viewer

JVSview is a JPEG2000 virtual slide viewer capable of displaying slides from a local storage or a remote, JPIP-accessed network storage (Figure 34). The basic features of JVSview include a main image display window for showing the currently active field of view (or region of interest), and an auxiliary overview window for showing the whole specimen at a low resolution (Table 5). Using the overview window, users can quickly see the context what is being shown on the main window. The main window is capable of displaying the slide at several different resolution levels, which mimic the objective lens magnifications, such as 20× or 40×.

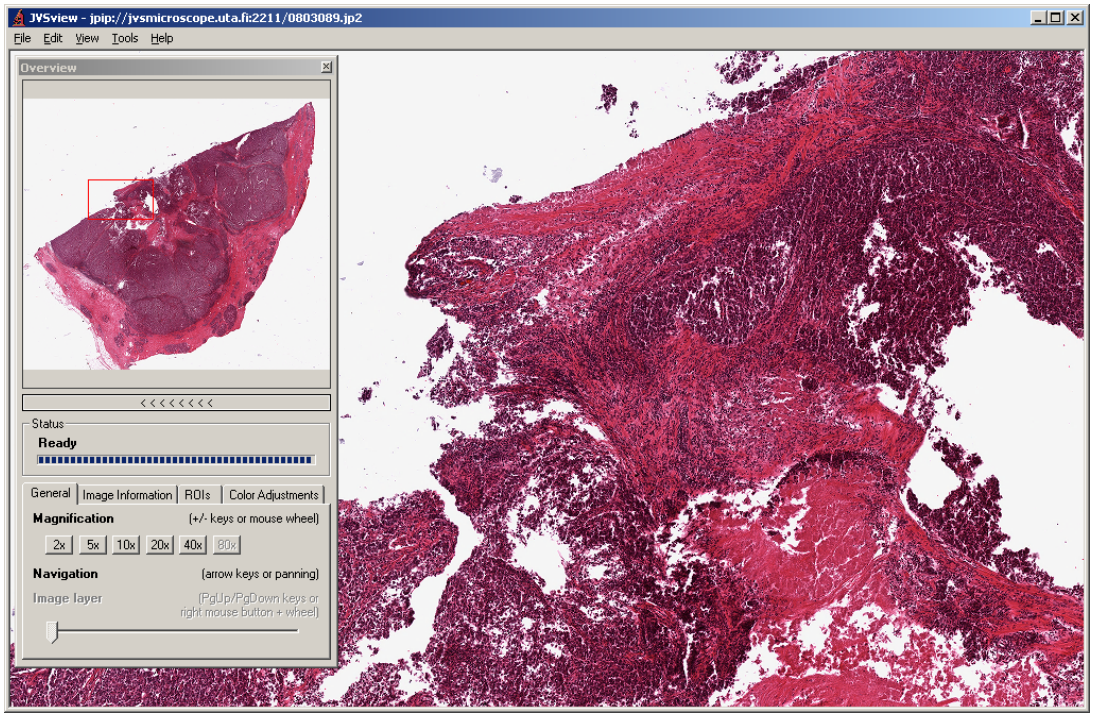

Figure 34. The graphical user interface of the JVSview JPEG2000 virtual slide viewing software displaying an overview window, navigation controls, and the main view.

Table 5. The main features of the JVSview JPEG2000 virtual slide viewing software.

List of features
Local image viewing & remote image viewing over JPIP
Overview window representing the entire specimen
Magnifications resembling common microscope objectives
Interactive panning with mouse or keyboard
Image brightness, contrast & color saturation adjustments
Multi-display full screen viewing
Support for multiple image layers (e.g., focus layers)
Storing image information and regions of interest (ROIs) as XML metadata
A functional link with image analysis software (ImageJ)

More advanced features of JVSview include the possibility to dynamically adjust the image brightness, contrast and color saturation. In addition, the software supports multi-layer images (e.g., focus Z stacks or different fluorochromes in FISH samples) through the usage of the JPX container file format. Image layers are treated as semi-transparent overlay images with an associated transparency value. The switching between the layers can be done freely with a slider control and the image rendered visible to the user is an interpolated version of two adjacent layers, weighted according to the transparency values. Example slides multi-layer slides are presented on our website http://jvsmicroscope.uta.fi/examples/. Image metadata can be embedded within the virtual slides by following the JVSschema (presented in Section 5.3.5). JVSview also allows specifying and storing regions of interest (ROIs), which can then be retrieved from a ROI list by the clients. For image measurements, JVSview provides a functional link with ImageJ, providing an easy way to measure lengths and areas as well as to count particles, such as cells and nuclei, using a click-and-count feature.

The executable binaries for 32-bit Microsoft Windows® have been released for free non-commercial purposes and are available on our website http://jvsmicroscope.uta.fi/jvsview/.

5.3.4 JVSserv – a virtual slide server

JVSserv is server application for network distribution of JPEG2000 virtual slides. The software features a command line-based interface as well as a graphical user interface (Figure 35). JVSserv utilizes the JPIP protocol as its principal data transfer technique. JVSserv supports multiple simultaneous client connections and uses a *first-in-first-out* (FIFO) caching policy, which is used to maintain the most frequently accessed data in memory. JVSserv also supports load balancing for dividing the workload of the main server onto several sub-servers, thereby allowing the system to handle more simultaneous clients.

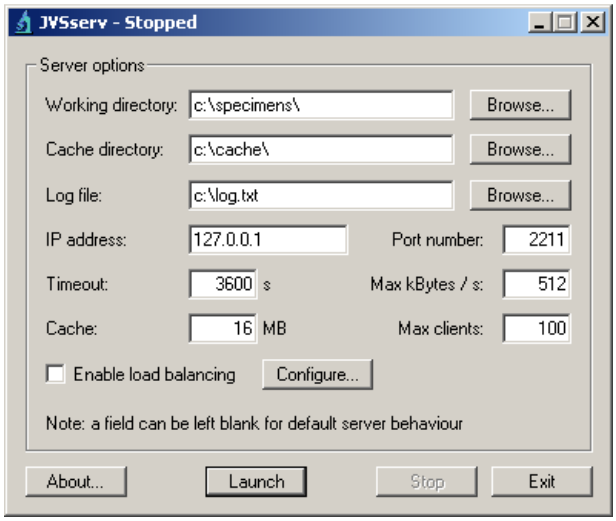

Figure 35. Graphical user interface of the JVSserv server software for network distribution of JPEG2000 virtual slides.

The executable binaries for 32-bit Microsoft Windows® have been released for free non-commercial purposes and are available on our website http://jvsmicroscope.uta.fi/jvsserv/.

5.3.5 JVSschema – a metadata XML schema

Short textual information and image ROIs are embedded as metadata within the header of the JPEG2000 virtual slide file (Figure 36). The textual information can contain, for example, information on the scanning resolution, organ and histopathologic diagnosis, and the staining method. The metadata is internally stored in XML

format and its structure is formally described with the JVSschema–a W3C XML Schema-based specification. The metadata is primarily for the purposes of image collections, for which the associated patient data is irrelevant (e.g., those used in teaching). The current version (1.0.2) of JVSschema is presented in Appendix A.

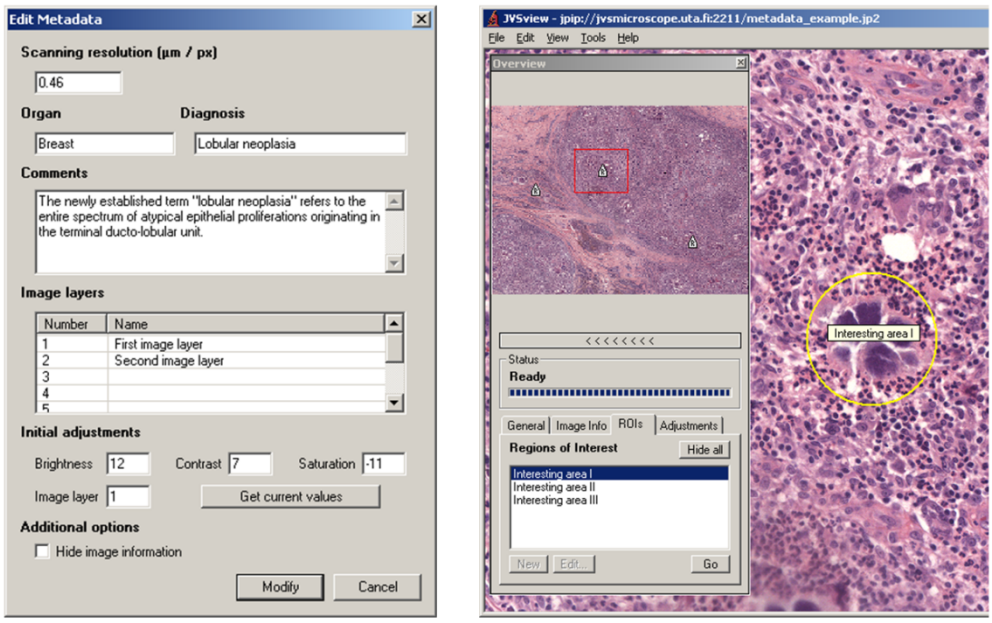

Figure 36. Embedding textual image information (a) and regions of interest (b) as JVSschema-formatted metadata within JPEG2000 virtual slides.

The specification of JVSschema and an example instance are released on our website http://jvsmicroscope.uta.fi/jvsschema/.

5.3.6 Computational performance of JPEG2000 and JPIP

We found the duration of the JPEG2000 compression to be linearly dependent on the original virtual slide image size. In our tests, the RAM usage was relatively low, as during the compression of a 7-gigabyte virtual slide the memory footprint of JVScomp constantly remained around 70 megabytes. JVScomp reached a compression speed of 50 gigabytes per hour on a dual-processor workstation. The limiting factor was the processor performance, as the source hard disk could have effectively processed over twice the number of read requests.

We found that the virtual slide serving performance of both the JPIP protocol and the Zoomifyer EZ™ to be limited by the speed of the hard disk; the processor load was constantly under 50%, as was the RAM allocation. The network bandwidth was utilized only about 25% of the maximum transmission rate (100 Mbit/s). As the number of clients increased, the average disk read queue lengths quickly reached the effective performance limits (an average of 2.0 was considered to be a suitable limit). With the main test virtual slide, which was duplicated for every client, JVSserv could effectively handle about 30 simultaneous clients, while the Zoomifyer (run on top of the Apache HTTP server) had its limit at around 20 simultaneous clients. Because of caching policies, both servers would have benefited for clients that browse the same image simultaneously. Therefore, assuming that some clients are usually viewing the same image, JVSserv could easily serve 50 simultaneous clients. In addition, JVSserv features a load balancing function, which can be used to distribute clients to several sub-servers. Thus, we estimate that a standard JVSserv workstation behind a 100 Mbit/s network link could handle 200 to 300 simultaneous clients when supplemented with 4 to 5 sub-servers.

5.4 DICOM software package (II)

5.4.1 JVSdicom Compressor – a DICOM image converter

JVSdicom Compressor is a command line-based image compression application capable of converting multiple image formats into the DICOM-compatible, JPIP-linked JPEG2000 virtual slide format (Table 6). JVSdicom Compressor is an extension of the JVScomp application, described in Section 5.3.2. As such, JVSdicom Compressor supports several input image file formats, such as BMP, PPM, and BigTIFF. In addition to the output JPEG2000 file, JVSdicom Compressor can produce an accompanying DICOM file, which uses the General Microscopy modality, Visible Light Microscopic Image IOD (with minimal set of attributes), and the JPIP Referenced Transfer Syntax. The DICOM file contains a URL reference to a JPIP server, from which the JPEG2000 can be accessed.

Table 6. The main features of the JVSdicom Compressor for the conversion of DICOM-based JPEG2000 virtual slides.

List of features
Optimized parameterization for virtual microscopy
Efficient rate control policy for virtual microscopy
Support for multi-processor environments
Support for the following input file formats: PPM, BMP, JPEG, JPEG2000, ECW, and TIFF (with BigTIFF support)
Produces DICOM-tagged JPEG2000 images with GM modality and JPIP Referenced Transfer Syntax

JVSdicom Compressor is released under a customized end-user license agreement. The executable binaries for Microsoft Windows® 32-bit and 64-bit architectures are freely available on our website http://jvsmicroscope.uta.fi/ jvsdicom_compressor/.

5.4.2 JVSdicom Workstation – a DICOM PACS client

JVSdicom Workstation is a DICOM PACS client program that acts as a Query/Retrieve Service SCU and a Storage Service SCU (Table 7). With it, users can query and retrieve images from a PACS server (preferably from the JVSdicom Server, described in Section 5.4.2). The user can view a summary of the patient- and treatment-related information and analyze the image by measuring distance, rotating the image arbitrarily, and adjusting width and center values (Figure 36). JVSdicom Workstation interacts with a PACS server as a conventional DICOM client, but upon receiving a JPIP reference to a JPEG2000 virtual slide, it invokes an external JPEG2000 viewing program. The external viewer displays the image pixel data, while JVSdicom displays the associated DICOM medical information. Thus, by having an external viewer for virtual slides, users can simultaneously view conventional DICOM imagery and corresponding histopathologic specimens. The external JPEG2000 viewing program can be chosen arbitrarily. However, JVSdicom uses JVSview (described in Section 5.3.3) as the default viewer application. The DICOM conformance statements for the supported SOP classes of JVSdicom Workstation as

an SCP are presented in Appendix B and as an SCU in Appendix C. In general, JVSdicom Workstation will prefer transfer syntaxes having an explicit encoding over the default implicit transfer syntax, and does not support extended negotiation.

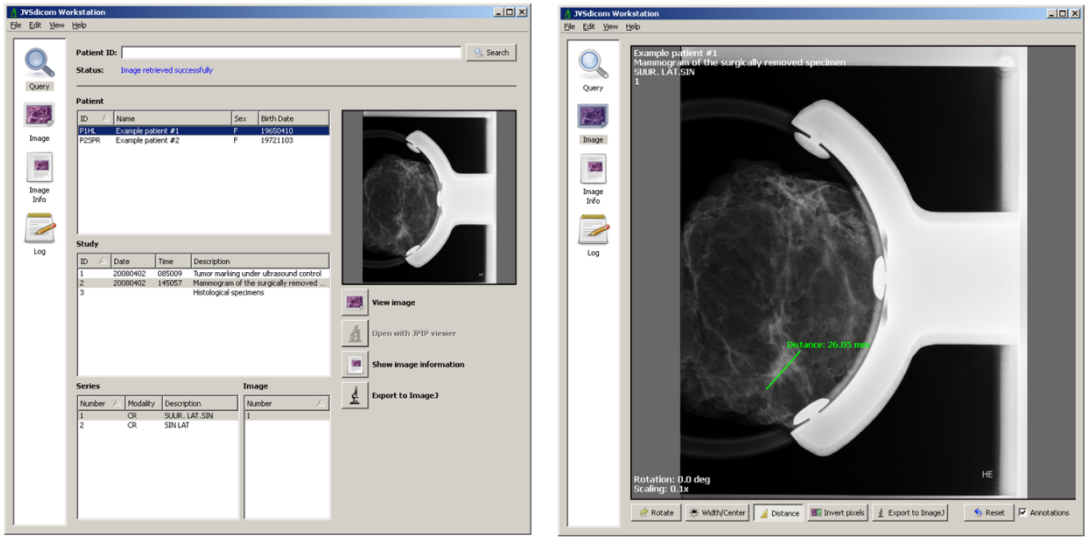

(a) (b)

Figure 36. The graphical user interface of the JVSdicom Workstation. The query view for Patient, Study, Series, and Image data (a) and the specimen image view with embedded measurement tools (b).

Table 7. The main features of the JVSdicom Workstation for viewing JPEG2000 virtual slides using the DICOM standard.

List of features
Fully DICOM-compliant PACS client
Support for JPEG2000 virtual slides with JPIP Referenced Transfer Syntax virtual slides
Simultaneous viewing of radiological images and corresponding histological virtual slides
Compatibility with commercial PACS servers
A functional link with public domain image analysis software (ImageJ)
Open-source

JVSdicom Workstation has been released under the GNU General Public License (GPL) v2.0 and the executable 32-bit and 64-bit Microsoft Windows® binaries as well as the source code are available on our website http://jvsmicroscope.uta.fi/jvsdicom_workstation/.

5.4.3 JVSdicom Server – a DICOM PACS server

JVSdicom Server is a DICOM PACS server application that acts as a Storage Service SCP and as a Query/Retrieve Service SCP (Table 8). The server is capable of accepting multiple associations simultaneously, preferably those using JVSdicom Workstation (described in Section 5.4.2). The server's administrators can configure it to contain several file system-based storage areas (with different AE Titles), as well as to limit access to these areas from a pre-defined AE network (Figure 37). Alternatively, the server features a public mode, which can be used to grant open access to the server. For open access, the calling AE is assumed to have a receiving Storage SCP set up. New DICOM entries can be imported into the server with pixel data either coming from image files, or replaced with a JPIP reference (i.e., in case of JPEG2000 virtual slides). The DICOM conformance statements for the supported SOP classes of JVSdicom Server as an SCP are presented in Appendix D and as an SCU in Appendix E. In general, JVSdicom Server will prefer transfer syntaxes having an explicit encoding over the default implicit transfer syntax, and does not support extended negotiation.

Table 8. The main features of the JVSdicom Server for distributing JPEG2000 virtual slides using the DICOM standard.

List of features
Fully DICOM-compliant PACS server
Support for JPEG2000 virtual slides with JPIP Referenced Transfer Syntax
Support for several Storage SOP Classes
Public mode with open access to server
Can be used as a DICOM–JPEG2000 virtual slide server for JVSdicom Workstation
Open-source

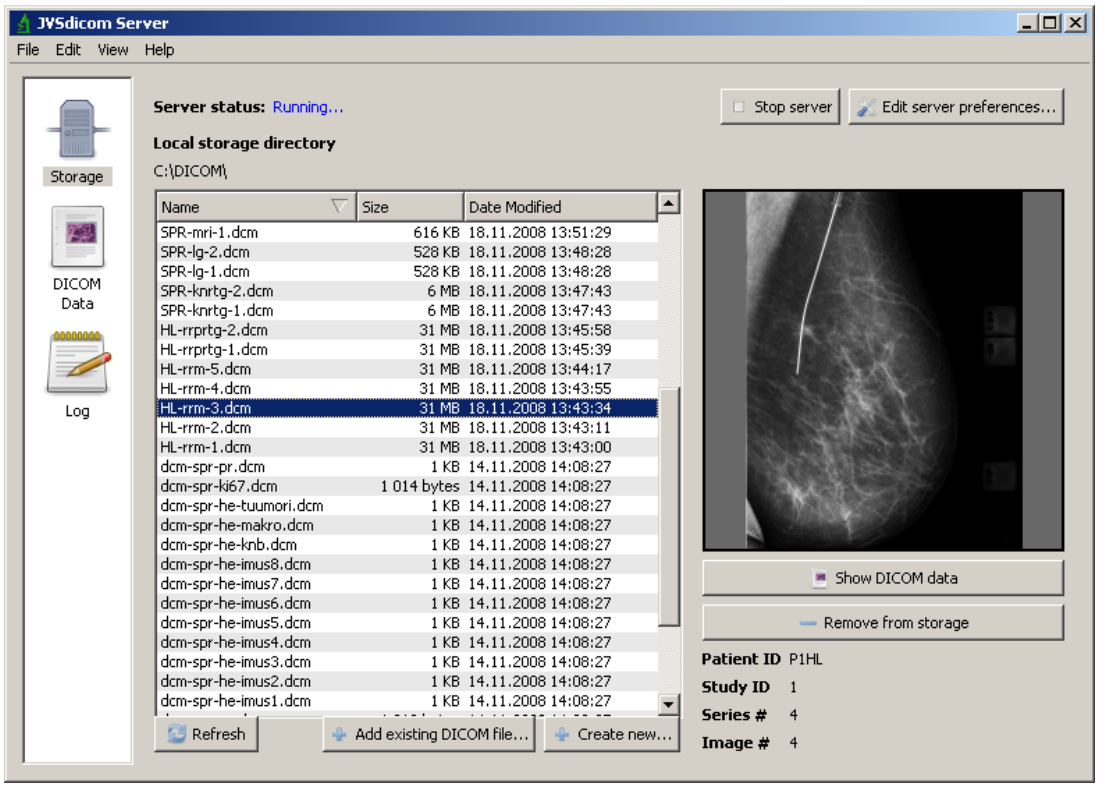

Figure 37. The server administration interface of the JVSdicom Server.

JVSdicom Server has been released under the GNU General Public License (GPL) v2.0 and the executable 32-bit and 64-bit Microsoft Windows® binaries as well as the source code are available on our website http://jvsmicroscope.uta.fi/jvsdicom_server/.

5.5 ImmunoRatio & ImmunoMembrane – software for IHC breast cancer biomarker analysis (III, IV)

We developed the ImmunoRatio software for quantitative image analysis of ER, PR, and Ki-67 IHC breast cancer samples (III), and the ImmunoMembrane software for semi-quantitative analysis of HER2 IHC breast cancer samples (IV). Both software applications were first implemented as ImageJ plugins, which were subsequently embedded within publicly open web applications.

5.5.1 ImageJ plugins

ImmunoRatio segments the DAB- and hematoxylin-stained nuclei areas from a microscope image, calculates the labeling index (i.e., the percent of DAB-stained area out of the total nuclear area), and generates a pseudo-colored result image matching the segmentation and classification (Figure 38a), whereas ImmunoMembrane segments DAB-stained cell membrane regions from the sample image, classifies the image into 0/1+, 2+, or 3+ (according to the ASCO/CAP guidelines) based on the membrane staining completeness and intensity, and generates a pseudo-colored overlay image matching the membrane segmentation (Figure 38b). The ImageJ plugin versions of the software provide graphical user interfaces, as well as the possibility to use it with ImageJ macro language. Multiple images from the same specimen can be analyzed at once, resulting in a montage containing all of the analyzed images. The plugin versions enable a direct link to image capture either by using the driver plugins provided by the camera vendors or via standardized imaging protocols, such as TWAIN (TWAIN Working Group, international). Open source versions of ImmunoRatio and ImmunoMembrane plugins are available for free download on our website http://jvsmicroscope.uta.fi/immunoratio-plugin/ and http://jvsmicroscope.uta.fi/ immunomembrane-plugin/, respectively.

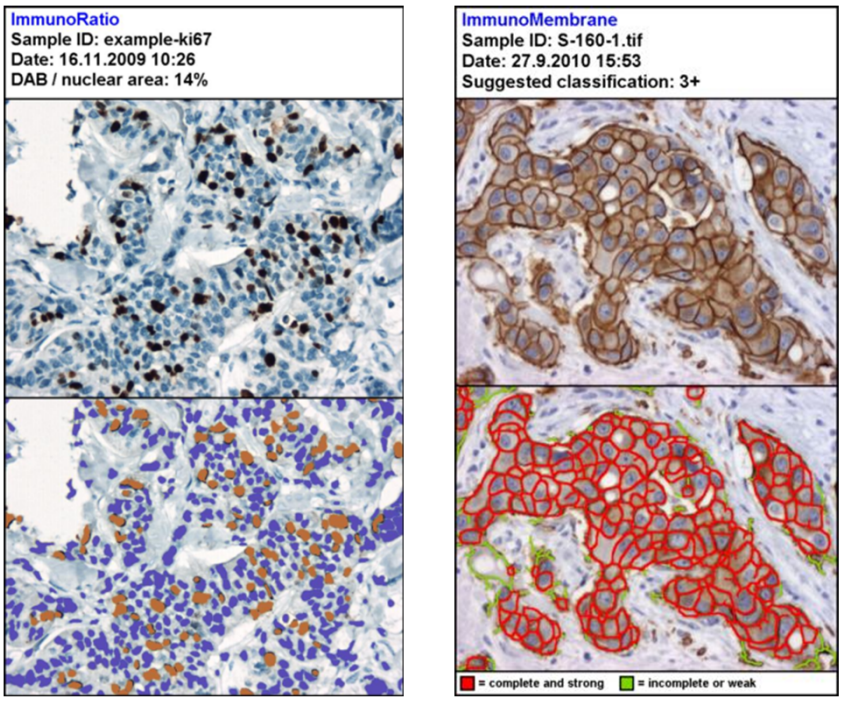

Figure 38. An example IHC breast cancer section stained for Ki-67 and analyzed with ImmunoRatio image analysis software (a), and another stained for HER2 and analyzed with ImmunoMembrane (b). The result images include a sample identifier, the analysis date, the resulting labeling index (ImmunoRatio) or the suggested classification (ImmunoMembrane), the original image, and a pseudo-colored image showing the segmentation and classification results.

5.5.2 Web applications

The plugin versions of ImmunoRatio and ImmunoMembrane were used as a basis in developing two cross-platform web applications (Figure 39). The web applications reside in a remote server and are accessed over the Internet with a web browser, without any software downloads or installations. They support all modern web browsers (e.g., Windows Internet Explorer, Mozilla Firefox, Safari, and Google Chrome) and all operating systems (e.g., Microsoft Windows®, Linux distributions, and Mac OS). The main features of the software are summarized in Table 9. The analysis can be made either to the whole image, a series of images (from which an average is calculated), or to an interactively defined ROI. The analysis adapts to various combinations of microscope objective lenses, phototubes, and camera resolutions by using either an exact or an estimated image scale (pixels per µm). The esti-

mation can be performed using the Scale Finder function. Both ImmunoRatio and ImmunoMembrane support most existing camera models and their output images, including JPEG, JPEG2000, TIFF, BMP, and PNG. For demonstrational and first-time analyses, the applications offer an introductory basic mode, which has a simplified user interface with minimal required functionality. In ImmunoMembrane, users can calibrate the software by specifying custom classification category cut-offs, allowing the software to be integrated more easily with a custom diagnostic process. ImmunoRatio offers a similar option, allowing the users to calibrate the software with their own visually determined labeling index data and derive a suitable result correction equation (a third degree polynomial). In addition, users can fine-adjust the hematoxylin- and DAB-thresholding parameters.

In ImmunoRatio, the optimal camera brightness and contrast settings can be defined using the assistance of the Camera Adjustment Wizard. The wizard measures a user-provided reference image and either accepts it or recommends the user to alter some specific setting. If the camera settings and/or the staining protocol remains unchanged, the wizard needs to be run only once. In ImmunoMembrane, the variation between different camera models and settings is minimized by employing the positive control slide for contrast and intensity normalization.

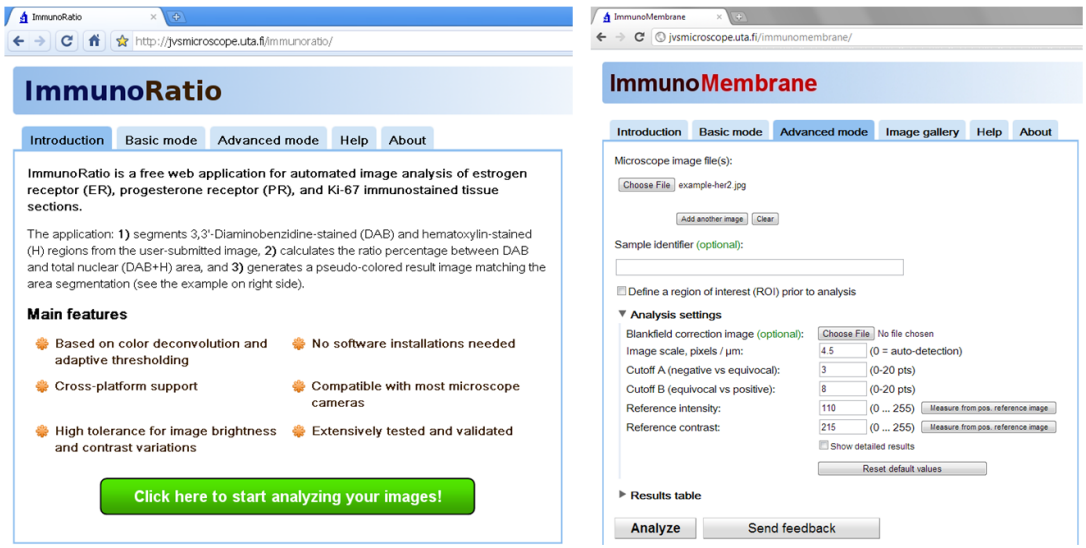

(a) **(b)**

Figure 39. Screenshots of the cross-platform compatible web applications ImmunoRatio and ImmunoMembrane, developed for the quantitative analysis of ER, PR, Ki-67, and HER2 IHC samples. The introductory view of ImmunoRatio (a) and the Advanced usage view of ImmunoMembrane (b).

Table 9. The main features of the ImmunoRatio (IR) and ImmunoMembrane (IR) image analysis web applications.

Feature	Description
Robust analytical principle	▪ Analyzes immunostained slides (ER, PR, Ki-67, and HER2) using color deconvolution for stain separation ▪ Users can analyze a single image, a series of images, and/or image regions of interest
Cross-platform compatible	▪ Runs within the web browser, requiring no additional program or plugin installations ▪ Is compatible with all modern web browsers and operating systems
Usable with various microscope setups	▪ Adapts to several combinations of microscope objective lenses, phototubes, and camera resolutions ▪ Supports most existing camera models and image formats (e.g., JPEG, JPEG2000, TIFF, BMP, PNG) ▪ Users can define optimal camera brightness and contrast settings with the Camera Adjustment Wizard (IR) ▪ Contrast and intensity normalization (IM)
User-calibratable	▪ Users can train the software to match with their own visual cell counting data (IR) or category cut-offs (0/1+, 2+, and 3+) (IM)
Easy to use	▪ Includes a basic usage mode for introductory analyses and a full-featured, advanced mode

Both the ImmunoRatio and the ImmunoMembrane web applications are freely accessible on our website http://jvsmicroscope.uta.fi/immunoratio/ and http://jvsmicroscope.uta.fi/immunomembrane/, respectively. Uploaded specimen images and related information are not archived or used for any purposes other than the user-requested image analysis operation. The imagery is erased from the server in a 24-hour cycle.

5.5.3 Robustness to variation in staining and image acquisition settings

Based on our software testing, in order to obtain a representative result for stained breast tumor slides, the minimum number of images needed to be captured and analyzed with ImmunoRatio was found to be three (20× microscope objective, 1× phototube, camera resolution 1,600 × 1,200 pixels, 4.40 pixels/µm), and with Im-

munoMembrane four to five (10× objective lens, 1× phototube, 2 megapixel 1/1.8” CCD camera). Averaging data from a higher number of images was found to have a minimal impact on the mean labeling index and the mean IM-score. Owing to the image scale information, which is entered either manually or by using the Scale Finder function, the analyses were highly similar with all common microscope objective lenses. However, when using a 10× objective with ImmunoRatio, considerably more non-carcinomatous cells were often included in the analysis. To circumvent this, the developed ROI functionality can be used to exclude unwanted regions.

As with all IHC image analysis systems, a prerequisite of valid and consistent analysis is good-quality staining. Tissue morphology should be optimally preserved, and the slide should be free of non-specific staining or other well-known IHC artifacts. For ER, PR, and Ki-67 samples, an optimally titrated primary antibody (1:100 for MIB-1 Ki-67) resulted in the best match with visual cell counting. Weak counterstaining was found to cause nuclear segmentation to fail, whereas overly concentrated counterstaining led to false segmentation of the cytoplasmic structures. For HER2 samples, we recommend the usage of the HercepTest® kit (Dako, Copenhagen, Denmark) and the accompanying guidelines, although ImmunoMembrane is readily applicable to be used with other staining kits as well.

We found both ImmunoRatio and ImmunoMembrane to be robust to the differences in the analysis results between the tested camera models, and that the variation between repeated staining batches was small (data not shown). Variation in image brightness and uneven illumination can be accurately corrected with a blankfield image. However, greatly underexposed images (blankfield image mean gray intensity <200) as well as overly overexposed images (blankfield image mean gray intensity >250) may cause false analysis results. For accurate nuclei segmentation, the image contrast must be relatively high; the foreground mean gray intensity should be 50 to 80% of the background mean gray intensity. In ImmunoRatio, users can validate their image acquisition settings by using the Camera Adjustment Wizard function of ImmunoRatio, whereas in ImmunoMembrane, the contrast and intensity normalization feature aims at automatically reducing the camera-related variations.

To minimize the data uploaded to the server during web application analysis, it is advantageous to use lossy image file formats, such as JPEG. We found that using lossy JPEG compression with quality factors 50 to 100 had no significant effect on the accuracy of ImmunoRatio analysis results. This compression level allows a typi-

cal 5 megabyte uncompressed image to be compressed into 250 kilobytes (about 20:1 compression ratio), enabling rapid image transfer with almost any network bandwidth. Using very low JPEG quality factors (<50) can cause image distortion and artifacts, making the analysis unreliable.

5.5.4 Calibration and prognostic validation

Due to the non-linearity between visual cell nuclei counting and non-calibrated ImmunoRatio (Figure 40a), a third degree polynomial was fitted to the data and used as a default correction function to calibrate ImmunoRatio (Figure 40b). The analysis of the separate test set with calibrated ImmunoRatio had a strong linear relation with visual cell counting, showing a near-perfect correlation *(r* = 0.98). The test set included two outlier observations, which were detected by visually inspecting the pseudo-color result images. The first outlier had weak DAB-staining intensity, making interpretation based on visual counting difficult. The second outlier had too low image contrast, as demonstrated by using the Camera Adjustment Wizard feature of ImmunoRatio.

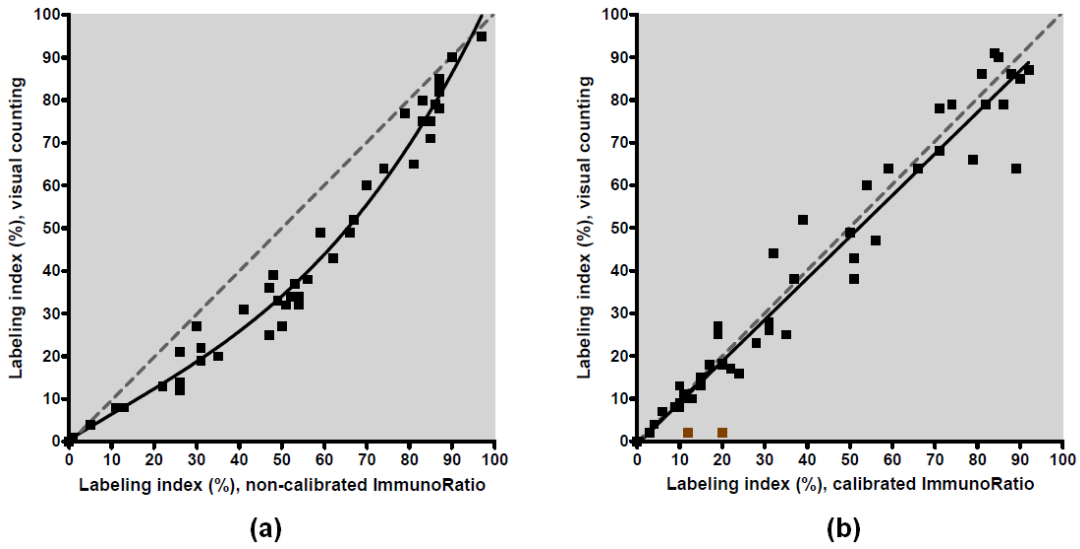

Figure 40. Comparisons of labeling indices obtained with visual nuclei counting against non-calibrated ImmunoRatio (a) and calibrated ImmunoRatio (b). The calibration was done by fitting a third degree polynomial (solid black line) to the training set. The validation set included two outliers (marked with brown).

For ImmunoMembrane, the calibration was performed by analyzing the training set and searching the optimal IM-score cut-off values. Using the visual classification of the training set as golden standard, the optimal cut-off values were found to be three and eight points (weighted kappa coefficient κ_w = 0.91, ASE = 0.08). Accordingly, the default classification of ImmunoMembrane uses the following category division: 0–2 points = negative (0 / 1+, 3–7 points = equivocal (2+) and 8–20 points = positive (3+). The analysis of the validation set (*n* = 144) showed very good agreement with the pathologist assessment (weighted kappa coefficient κ_w = 0.80, ASE = 0.08). The FISH–IHC disagreement was 3.5% (calculated from the total number of cases), containing false IHC-positive in two cases (1.4%) and false IHC-negative in three cases (2.1%). Similarly, the CISH–IHC disagreement was 2.8%, containing false IHC-positive in two cases (1.4%) and false IHC-negative in two cases (1.4%).

In the prognostic validation of ImmunoRatio, breast cancer-specific survival of patients with high Ki-67 tumors was significantly shorter than low Ki-67 during 20-year follow-up. Labeling index values of 15%, 20%, and 25% were tested as cut-off. Of those, 20% (the median in this material), gave a hazard ratio (HR) of 2.2 (P = 0.01 by log rank test). Cut-off values 15% and 25% yielded similar results (HR = 2.1 and HR = 2.4, respectively).

6. DISCUSSION

To facilitate the widespread usage of virtual microscopy in clinical, educational, and research environments, the present study describes the design and implementation of an open software platform, directly applicable to diagnostic pathology. The platform consists of several proof-of-concept applications, which can be considered novel, as–at the time of their development–there were no equivalent software described in the academic literature nor were there similar commercial products available.

6.1 Viability of JPEG2000 as the universal standard format for virtual slides (I)

The amount of information generated during virtual slide scanning is vast, posing a significant problem for data management and, in particular, for the image file format. Currently there is no universally accepted image file format for virtual slides. Instead, there is a plethora of proprietary, vendor-specific formats, which may be constantly modified as new scanner and imaging equipment are introduced to the market. As such, these formats have no guarantees for backwards compatibility in the years to come. As we have demonstrated in the present study, JPEG2000 is a feasible candidate, which is independent, open, and standards-based, thus guaranteeing the longevity and backwards compatibility in the future. The standard is readily capable of providing all the basic functionalities required by virtual microscopy, and thus can be utilized in the construction of long-lasting virtual slide collections, which are accumulated over decades. Furthermore, the standard makes it possible to set up centralized virtual slide registries, which are accessed in a unified manner. To index the metadata within these slide registries, one possibility would be the usage of the JPSearch standard (ISO/IEC TR 24800-1), which is a framework for interoperability for still image search and retrieval.

We have also shown in our computational performance tests with multi-core processor workstations that JPEG2000 is readily applicable in image conversion, viewing, and serving using consumer-grade computer hardware. However, should the need to enhance the computational performance arise, Very Large Scale Integration (VSLI) hardware solutions for performing the DWT–the most computationally demanding part of JPEG2000 encoding–have been described by the signal processing and electronics community (Acharya & Tsai 2005). In addition, the Compute Unified Device Architecture (CUDA, by Nvidia, Santa Clara, CA, US) can be used as a platform for leveraging the performance power of graphical processing units found on the video display cards, as demonstrated by the CUJ2K implementation of JPEG2000 on CUDA (Balevic *et al.* 2011).

As with all modern multimedia standards, it is practically impossible to completely avoid the possibility of a patent infringement amidst the current software patent legislation. To circumvent this, all patent-holding members of the JPEG committee have made a reciprocal agreement, in line with the patent policies of ISO and ITU, to offer a royalty and fee-free license for the baseline implementation (Part 1) of JPEG2000 (Minutes of 33rd JPEG committee meeting, Redmond, WA, US, July 19–23, 2004).

As an alternative to JPEG2000 in virtual microscopy, some discussions have suggested the usage of JPEG XR (ISO/IEC 29199-2), which is a standard family for still-image coding by the JPEG committee, intended to provide an intermediate solution for JPEG and JPEG2000, compression- and quality-wise. The technology behind the standard is originally created and patented by Microsoft (Redmond, WA, US) as Windows Media Photo, which was later renamed to HD Photo. However, although the standard specifies the image width and height as 32-bit integers (thereby allowing very large imagery), the container file format specified in Annex A of the standard is based on TIFF, and therefore inherits all of its limitations, including the 32-bit file size (i.e., the maximum of 4 GB). Recently, the JPEG committee also formed the Advanced Image Coding and Evaluation Methodologies ad-hoc group (ISO/IEC 29170 – AIC), which has issued a proposal call for novel medical imaging codecs (JPEG committee press release, 49th WG1 meeting, Sardinia, Italy, July 17, 2009), possibly resulting in a format suitable for virtual slides in the future. Another interesting alternative, albeit not an image file format per se, is the Open Microcopy Environment's OMERO project (University of Dundee, Dundee, Scotland, UK),

which is an effort to provide a complete, centralized microscopy image platform with multi-format support. As of version 4.3 (June 2011), OMERO began to support large-scale imagery, such as virtual slides, by using a tile-based approach, similar to the image pyramid described in the present study in Section 2.5.5.

6.2 Virtual slides as an integrated part of clinical information systems (I, II)

The widespread utilization of virtual microscopy in routine diagnostics requires standardized integration with clinical information systems, such as HIS and LIS. Since pathology is currently the dominant discipline to employ virtual microscopy, the integration process is largely done in the context of pathology laboratory workflow. Early on, Zwönitzer *et al.* (2007) proposed an information model for the pathology laboratory workflow with integrated virtual slides. However, this model is, for the most part, superseded by the finalized DICOM Supplements 122 and 145. These supplements contain a unified workflow model and virtual slide integration technique representing the consensus of both the industry and the academia, and as such, can be expected to become the *de facto* model in the future. To further facilitate interoperability between different standards, such as DICOM and Health Level Seven (HL7), the Integrating the Healthcare Enterprise (IHE) has recently launched an initiative to define basic image acquisition and reporting processes in pathology laboratories, and to describe a standard solution for exchanging structured pathological reports with linked virtual slides (Daniel *et al.* 2011). Recently, the DICOM WG-26 made a consensus decision to pursue the use HL7 v2.x messaging rather than DICOM services for device control and integration in the workflow management across all clinical and pathology laboratories, whereas DICOM would be used to exchange imagery and related metadata (WG-26 Meeting Minutes, October 30, 2011, San Diego, CA, US).

At the time of writing Study II, no standard for virtual slide integration with clinical information systems existed, and because of that, we described a proof-of-concept solution to link JPEG2000 virtual slides with a DICOM PACS. Based on the developed software, a comprehensive, DICOM-compatible virtual slide imaging system can be constructed by combining the JVSdicom software with JVSview

JPEG2000 viewing application and JVSserv JPIP network serving application (Figure 41). In this model system, a virtual slide scanner produces raw image data, which is processed by JVSdicom Compressor. The JVSdicom Compressor produces a JPEG2000 file containing the actual virtual slide image data and a DICOM file containing the associated medical data (i.e., patient information) as well as some mandatory image properties, such as width and height. By default, the produced DICOM file contains anonymized DICOM entries, but it could readily be linked with a LIS or a HIS for retrieving patient information. A straightforward way to name the JPEG2000 virtual slide file is to use the microscope slide label identification string, which can be read automatically if bar-coded labels are used. The JPEG2000 virtual slide file is then moved into a JVSserv server, and the DICOM file is moved into a JVSdicom Server, which both are parts of the same PACS. Both files can be stored separately inside a server-specific storage area within the PACS. JVSdicom can also receive imagery from other imaging modalities, which are in turn linked with the LIS or HIS. End-users (e.g., pathologists or physicians) query the JVSdicom Server with a JVSdicom Workstation and retrieve patient-linked image objects. They can view and analyze conventional DICOM imagery within JVSdicom Workstation, while virtual slides are opened with JVSview in another viewing window. The DICOM data is transmitted using the JPIP Referenced Transfer Syntax, and the JPEG2000 virtual slide data is transmitted via an auxiliary channel over JPIP. The system architecture makes it possible to use JVSserv separately outside the PACS, since virtual slide do not contain any DICOM references.

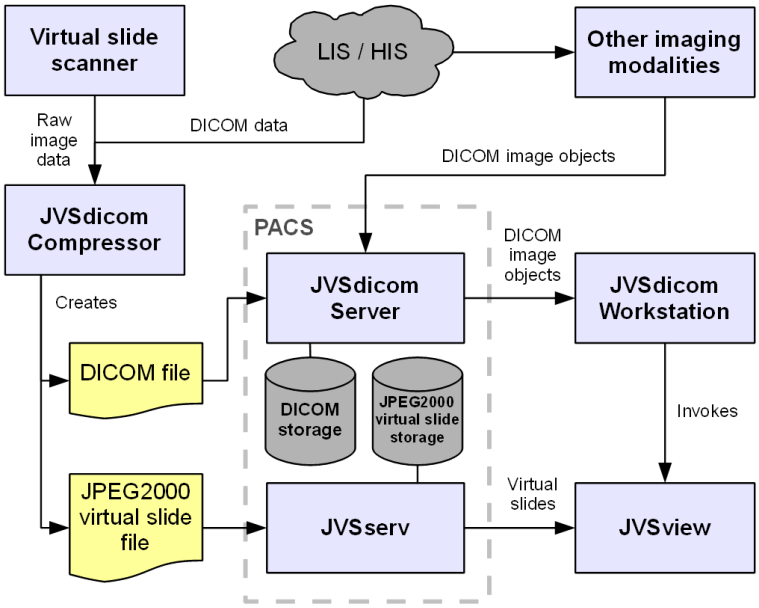

Figure 41. The dataflow of a model system for linking virtual slides with DICOM by using JPEG2000 and JVS software. The virtual slide scanner produces raw image data for JVSdicom Compressor, which produces a DICOM and a JPEG2000 virtual slide file, which are moved into the PACS to JVSdicom Server and JVSserv, from which they are queried with JVSdicom Workstation and viewed with JVSview.

6.3 Diagnostic application of ImmunoRatio and ImmunoMembrane software (III, IV)

The ImmunoRatio and ImmunoMembrane analysis applications described in the present study provide a comprehensive software suite for the digital image analysis of IHC breast cancer biomarkers. The software is designed to be used as a diagnostic aid by a trained pathologist. The analysis results should always be interpreted together with the pseudo-colored result images and the original histology of the slides.

Ideally all end-users should calibrate the ImmunoRatio and ImmunoMembrane software to suit their laboratory staining protocols and/or image acquisition settings. For ImmunoRatio, this can be done by first measuring the correct image scale and then by using the Image Calibration Wizard to find the acceptable staining and image acquisition settings, which in turn are used to define the visually correct threshold parameter settings. After this, a group of trained pathologists or clinicians manually click-and-count the cell nuclei of a laboratory-specific training image set and

compare those results against the analysis results of non-calibrated ImmunoRatio. Finally, the end-users fit a third degree polynomial to the training data and use that as the result correction equation. This procedure has been described in the present study in Section 4.4. For ImmunoMembrane, laboratories using other HER2 IHC staining than the HercepTest® kit (used in developing the software), such as the AB-HER2 IHC kit (Alper Biotech, Rockville, MD, US) or custom staining protocols, can calibrate the software prior to routine usage following the guidelines described in Section 4.4.

6.4 Benefits and issues of automated image analysis of breast cancer biomarkers (III, IV)

In the validation of the calibration process, the segmentation and classification of ER, PR, and Ki-67 by ImmunoRatio and HER2 IHC by ImmunoMembrane matched very well with the visual assessment made by expert pathologists. The advantages of using automated image analysis software include shorter overall analysis time and improved reproducibility and repeatability of the analysis. By utilizing the Image Calibration Wizard (in ImmunoRatio) or by using an image captured from the positive staining control slide as a normalization reference (in ImmunoMembrane), the inter- and intra-observer variability can be decreased significantly. Moreover, when using web-based image analysis, many of the laboratory- and hospital-specific information system restrictions can be circumvented, and since there are no software downloads or installations involved, the barrier for adopting new technologies by the pathologists is most likely lower, thereby enhancing the widespread adoption of digital tools in clinical diagnostics.

The current criteria for HER2 tumor positivity assessment is based on the ASCO/CAP guidelines released in 2007. These guidelines were formed by modifying those of the US Food and Drug Administration (FDA) based on an extensive literature review by a panel of experts. However, Perez *et al.* (2011) have shown that with a nearly 3,000 patient cohort, the retrospective survival rate was similar among patients treated with trastuzumab under either set of criteria, but if the decision-making followed the ASCO/CAP guidelines, a small but meaningful group of patients were denied of the therapy. Therefore, the ASCO/CAP guidelines may need

some revising in the future. However, since the HER2 classification is always a compromise, perfect accuracy can never be achieved.

Defining the optimal Ki-67 cut-off for prognostic assessment can be problematic, since no universally accepted guidelines exist. We tested this with a retrospective analysis of data from 123 primary breast cancer patients followed up for 20 years. The Ki-67 labeling index 20% (the median value in this material) gave a strong prognostic discrimination (HR = 2.2). Although cut-off values 15% and 25% yielded similar prognostication in this patient material, we recommend each laboratory to define their own cut-off value.

6.5 Clinical usage regulation of virtual slides and medical image analysis software (I–IV)

The current regulations governing the acquisition, display, and validation of virtual slides in clinical pathology use are fragmented and unclear (Pantanowitz *et al.* 2011). The consensus appears to be that virtual slides are treated as medical devices, and are therefore under the US Food and Drug Administration (FDA) regulation, but before any clear guidelines or legislation can be formulated, there are a number of issues to be clarified — namely, are the hardware and software components of a virtual slide system regulated separately or as a whole? How is distributed slide processing (e.g., staining in one laboratory, scanning in another) treated? Does the regulatory approval cover all types of diagnostic work, or are some entities excluded? And lastly, how is the validation criteria selected?

With regard to the regulation of IHC image analysis software, the situation is somewhat clearer. However, although the IHC analysis software described in the present study is intended for clinical diagnostics, regulations governing the usage of automated image analysis systems vary between countries. For example, in the United States the software would require clearance from the FDA. Although some of the commercially available digital image analysis packages have been cleared by FDA with the 510(k) premarket notification process (FDA 2011), an expert panel from Institute of Medicine–an independent, non-profit organization–has criticized the opaqueness and the validity of the process, and suggested abandoning it altogether (IOM 2011).

In Europe, medical image analysis software is regulated by the legislation of the European Union. The *Medical Devices Directive* 93/42/EC (MDD) and, more importantly, its amendment 2007/47/EC (AMDD) specifies that a stand-alone (i.e., without any hardware integration) medical software can be treated as a medical device, and thus is applicable for the Conformité Européenne (CE) conformity marking procedure. In addition, medical devices used for *in vitro* diagnostics are covered by the *In Vitro Diagnostic Medical Devices Directive* 98/79/EC (IVD MDD), which categorizes the devices into four classes (General, Self-testing, Annex II List B, and Annex II List A) based on their relative risk. The class General has the lowest risk and its conformance is self-declared, whereas the other three classes require the intervention of a national regulatory body, which, in case of Finland, is Valvira. However, the IVD MDD contains only vague guidelines with regard to image analysis software, and since the AMDD–containing more explicit rulings for medical software–came into effect on 2010, the legislation as a whole is relatively new and leaves room for interpretation. For example, medical devices released prior to 2010 are not covered by the AMDD, and since this also includes their subsequent version upgrades, it raises an interesting question of what differentiates a version upgrade from a completely new software, especially in the case of web applications? Consequently, to the best of my knowledge, there are currently no CE-marked IVD image analysis software applications available on the market. Should the ImmunoRatio and ImmunoMembrane software described in the present study–or other similar diagnostics image analysis applications–be brought under the regulation, they would most likely fall into the General class, since they are not explicitly covered by the Annex II of IVD MDD and they are not intended for self-testing.

7. SUMMARY AND CONCLUSIONS

Virtual microscopy offers a novel way of interacting with microscope specimen information. Compared to traditional light microscopy, virtual microscopy offers unlimited lifespan for the specimens, remote slide sharing, centralized slide repositories and biobanks with lower archival costs, generation of rare-case atlases, practical tools for research and educational purposes, effective inter-laboratory quality assurance, and lastly the possibility to perform traceable, repeatable, and quantifiable image analysis. Especially in pathology, all this leads into more accurate and reliable histopathological diagnosis and ultimately into better patient care.

However, the application of virtual microscopy requires considerable efforts from hardware and software point of view. In order to overcome the elementary issues involved in the automated virtual slide scanning and image tile stitching, we have developed and described an automated controller and stitching software, DirObserver and LargeMontage, which are both released as open source applications and are currently being used world-wide.

Our studies indicate that JPEG2000 is a well-suited image format for virtual microscopy, enabling effective compression, viewing, and serving of the large image files produced by the modern microscope slide scanners. This is also evident from the wide adoption and usage of the JVS software package described in the present study; we have been receiving positive feedback from several academic and clinical institutions in Finland, and there has also been significant interest from abroad.

The JPEG2000-format virtual slides can be readily integrated into clinical information systems, as we have demonstrated with the JVSdicom software package described in the present study. The package is the first practical solution to overcome the limitations of DICOM in virtual microscopy. Although the JPIP-based approach for linking virtual slides with DICOM is now superseded by the pyramidal approach, the DICOM standard specification continues to support JPIP, and thus the two approaches are not mutually exclusive and can be used simultaneously within the same PACS.

To the best of our knowledge, ImmunoRatio and ImmunoMembrane are the first free, ready-to-use web application for analyzing ER, PR, Ki-67, and HER2 IHC. The applications are hardware-independent and robust for variations in the camera settings and laboratory-specific staining practices. We anticipate that publicly available and open source image analysis applications will accelerate the adoption of automated analysis techniques in clinical diagnostics of breast cancer biomarkers. All the developed software for the present study is freely available at our website http://jvsmicroscope.uta.fi/.

The usage of virtual slides in diagnostic pathology is increasing, although compared to radiology, the process of laboratory-wide integration with hospital information systems is still years behind. Clinical application of virtual microscopy requires the development of standards, regulation, workflow specifications, and the assessment of the added benefit and cost effectiveness virtual microscopy has to offer. A probable scenario for the current decade is that the large hospital information system providers will adopt virtual slides as a core part of their product lines and begin to offer a unified healthcare system that covers all imaging modalities throughout the hospital, thereby digitizing the laboratories employing light microscopes, such as pathology. The interfacing and data exchange between different systems will most likely be performed using messaging, which follows the specifications devised by DICOM, HL7, and IHE standardization bodies. In the more distant future, the standardized laboratory workflow may very well consist of digital-only specimen processing and analysis, bypassing the usage of traditional glass slides.

ACKNOWLEDGEMENTS

I'll try to keep this short. First and foremost, I wish to express my deepest gratitude to my supervisor Prof. Jorma Isola for giving me the opportunity to accomplish one of the greatest milestones of my life. Your professional expertise and endless stream of fresh ideas have been a source of great inspiration and have provided me a solid foundation to work upon. I wish to equally thank the rest of our Cancer Biology research group (including former and partial members): laboratory technicians Mrs. Sari Toivola, Mrs. Kristiina Salonoja, Mrs. Mariitta Vakkuri, and Mrs. Eeva Pesonen for providing me the raw material to digitize and process with my software (and Kristiina for being a tough board game opponent!); and researchers Dr. Teemu Tolonen, Dr. Laura Partanen, Dr. Katri Köninki, Docent Minna Tanner, Mr. Arttu Viitanen, Mr. Visa Manni, Ms. Satu Luhtala, Dr. Synnöve Staff, Dr. Mark Barok, Ms. Sofia Heinonen, and Dr. Joanna Ilvesaro for giving me valuable insight into the world of biology and medicine. I have not only loved working with all of you, but also thoroughly enjoyed our countless off-work activities, which have taught me a great deal of life in general (such as why champagne might very well be the best thing that has happened to humanity). I truly cannot imagine a better work group!

I am also grateful to all my co-authors and colleagues not already mentioned for their valuable contributions and assistance: Ms. Sanna Ruotoistenmäki, Dr. Mervi Jumppanen, Dr. Saara Lehmusvaara, Dr. Heini Kallio, Prof. Anne Kallioniemi, Dr. Emma-Leena Alarmo, Dr. Johanna Ketolainen, Mr. Henrik Helin, and Mr. Mauro Scaravilli.

I want to thank my thesis committee members, Prof. Tapio Visakorpi and Dr. Merja Helenius for guidance and supervision throughout the whole project. Likewise, the official reviewers of this study, Prof. Martti Juhola and Prof. Tuomo Karttunen, are acknowledged for their valuable comments and suggestions.

I also wish to warmly thank all our collaborators: Dr. Paula Kujala, Dr. Mika Tirkkonen, Dr. Hannu Haapasalo, and Dr. Anna-Leena Lääperi from the Tampere University Hospital; Dr. Marcial Garcia Rojo from the Hospital General Universi-

tario de Ciudad Real, Spain; Dr. Johan Lundin, Dr. Mikael Lundin, and Dr. Juho Konsti from the Institute for Molecular Medicine Finland; Mrs. Satu Remes from the Hospital District of Helsinki and Uusimaa; and Prof. Gabriel Landini from the University of Birmingham, UK.

And of course my work couldn't have been possible without proper support functions from our institute. My special thanks go to technical support Mr. Toni Vormisto, laboratory equipment manager Dr. Anja Rovio, personnel administrators Mrs. Kaarin Forsman and Mrs. Merja Koivula, the coordinator of the TGPBB school Dr. Henna Mattila, the institute's director Dr. Hannu Hanhijärvi, and to all members of the maintenance and cleaning staff.

This study has been financially supported by the following organizations: Finnish Cancer Foundation, Sigrid Juselius Foundation, Biocenter Finland, Pirkanmaa Hospital District, Tampere University Hospital, Seinäjoki Central Hospital, and the EU COST Action IC604: Eurotelepath ("Telepathology Network in Europe") initiative.

Lastly, I wish to heartily thank my parents Leena and Kai, sisters Viivi and Vilma, grandparents Eila, Mikko, Airi (Mumma) and Reijo, family-in-law Merja, Harri and Janne, godchildren Jesse and Juulia, relatives and friends who are too many to be listed, and, above all, my loving wife Elina. You all are the core of my world.

REFERENCES

Abbe E (1887): On improvements of the microscope with the aid of new kinds of optical glass. J Roy Microscop Soc February:20–34.

Abramowitz M (1987): Contrast Methods in Microscopy: Transmitted Light. Olympus America, Inc., Melville, New York.

Acharya T and Tsai PS (2005): JPEG2000 Standard for Image Compression: Concepts, Algorithms and VLSI Architectures. John Wiley & Sons, Inc., Hoboken, New Jersey.

Aguet F, Van De Ville D, and Unser M (2008): Model-based 2.5-D deconvolution for extended depth-of-field in brightfield microscopy. IEEE Trans Image Process 17(7):1144–1153.

Airy GB (2007): On the Diffraction of an Object-Glass with Circular Aperture. SPIE milestone series, Society of Photo-optical Instrumentation Engineers.

Allred DC, Carlson RW, Berry DA, Burstein HJ, Edge SB, Goldstein LJ, Gown A, Hammond ME, Iglehart JD, Moench S, Pierce LJ, Ravdin P, Schnitt SJ, and Wolff AC (2009): NCCN Task Force Report: Estrogen Receptor and Progesterone Receptor Testing in Breast Cancer by Immunohistochemistry. J Natl Compr Canc Netw 7:S1-S21, quiz S22-23.

Antonini M, Barlaud M, Mathieu P, and Daubechies I (1992): Image coding using the wavelet transform. IEEE Trans Image Processing 1(2):205–220.

Aperio (2011): BigTIFF image library. Aperio Technologies Inc., Vista, CA, US. Available at: http://www.aperio.com/bigtiff/. Accessed 18.1.2012.

Appleton B, Bradley AP, and Wildermoth M (2005): Towards optimal image stitching for virtual microscopy. Digital Image Computing: Techniques and Applications. IEEE, Cairns, Australia, pp. 299–306.

Ash EA and Nicholls G (1972): Super-resolution aperture scanning microscope. Nature 237:510.

Balevic A, Fürst N, Weiß A, Heide M, and Papandreou S (2011): CUJ2K – JPEG2000 on CUDA software. University of Stuttgart, Stuttgart, Germany. Available at: http://cuj2k.sourceforge.net/. Accessed 18.1.2012.

Bayer BE (1976): Color imaging array. US Patent 3,971,065.

Beck J, Murray J, Willows A, and Cooper M (2000): Computer-assisted visualizations of neural networks: expanding the field of view using seamless confocal montaging. J Neurosci Meth 98(2):155–163.

Berry E (2008): A Practical Approach to Medical Image Processing. Taylor & Francis, Boca Raton, FL.

BIG (2011): Extended Depth of Field algorithm. Biomedical Imaging Group, École polytechnique fédérale de Lausanne, Lausanne, Switzerland. Available at: http://bigwww.epfl.ch/demo/edf/. Accessed 18.1.2012.

Born M and Wolf E (2000): Principles of Optics: Electromagnetic Theory of Propagation, Interference and Diffraction of Light. Cambridge University Press, Cambridge, UK, 7th edition.

Brügmann A, Eld M, Lelkaitis G, Nielsen S, Grunkin M, Hansen JD, Foged NT, and Vyberg M (2011): Digital image analysis of membrane connectivity is a robust measure of HER2 immunostains. Breast Cancer Res Treat; Epub ahead of print.

Bradbury S and Bracegirdle B (1998): Introduction to Light Microscopy, RMS Microscopy Handbooks, Vol. 42. BIOS Scientific Publishers, Ltd., Oxford, UK, pp. 59–61

Bradley AP, Wildermoth M, and Mills P (2005): Virtual microscopy with extended depth of field. Digital Image Computing: Techniques and Applications, IEEE, Cairns, Australia, pp. 235–242.

Chen S, Lin W, and Chen C (1991): Split-and-merge image segmentation based on localized feature analysis and statistical tests. CVGIP: Graphical Models and Image Processing 53(5):457–475.

Coates C, Fowler B, and Holst G (2009): sCMOS-Scientific CMOS technology: a high-performance imaging breakthrough. White paper; Andor Technology, Belfast, Ireland; Fairchild Imaging, Milpitas, CA, US; PCO AG, Kelheim, Germany.

Cohen J (1968): Weighted kappa: nominal scale agreement with provision for scaled disagreement or partial credit. Psychol Bull 70:213–220.

Dani P and Chaudhuri S (1995): Automated assembling of images: Image montage preparation. Patt Recog 28(3):431–445.

de Azambuja E, Cardoso F, de Castro G Jr, Colozza M, Mano MS, Durbecq V, Sotiriou C, Larsimont D, Piccart-Gebhart MJ, and Paesmans M (2007): Ki-67 as prognostic marker in early breast cancer: a meta-analysis of published studies involving 12,155 patients. Br J Cancer 96:1504–1513.

Dee FR (2009): Virtual microscopy in pathology education. Hum Pathol 40(8):1112–21.

Dee FR, Donnelly A, Radio S, Leaven T, Zaleski MS, and Kreiter C (2007): Utility of 2-D and 3-D virtual microscopy in cervical cytology education and testing. Acta Cytol 51:523–529.

Della Mea V (2011): 25 years of telepathology research: a bibliometric analysis. Diagn Pathol 6 Suppl 1:S26.

Della Mea V, Demichelis F, Viel F, Dalla Palma P, and Beltrami CA (2006): User attitudes in analyzing digital slides in a quality control test bed: a preliminary study. Comput Methods Programs Biomed 82(2):177–86.

Della Mea V, Bortolotti N, and Beltrami CA (2008): A survey on non specialized off-the-shelf JPEG2000 viewers for digital microscopy use. Diagn Pathol 2008 3 Suppl 1:S20.

Dowski ER and Cathey WT (1995): Extended Depth of Field through Wavefront Coding. Applied Optics 34(11):1859–1866.

Doyle W (1962): Operation useful for similarity-invariant pattern recognition. Journal of the Association for Computing Machinery 9:259–267.

Ebrahimi F, Chamik M, and Winkler S (2004): JPEG vs. JPEG2000: An Objective Comparison of Image Encoding Quality. Proc of SPIE 5558:300–308.

FDA (2011): 510(k) process overview. US Food and Drug Administration. Available at: http://www.fda.gov/MedicalDevices/ProductsandMedicalProcedures/DeviceApprovalsandClearances/510kClearances/. Accessed 18.1.2012.

Fossel S, Fottinger G, and Mohr J (2003): Motion JPEG2000 for high quality video systems. IEEE Trans Cons Electr 49(4):787–791.

Forster B, Van De Ville D, Berent J, Sage D, and Unser M (2004): Complex Wavelets for Extended Depth-of-Field: A New Method for the Fusion of Multichannel Microscopy Images. Microsc Res Tech, 65(1–2):33–42.

Fuwa K and Valle BL (1963): The Physical Basis of Analytical Atomic Absorption Spectrometry. The Pertinence of the Beer-Lambert Law. Anal Chem 35(8):942–946.

Gómez F, Marín D, and Romero E (2011): A soft-cache strategy for pathologist's navigation in virtual microscopy. Microsc Res Tech 74(5):401–14.

Gage SH and Gage HP (1914): Optic Projection. Comstock Publishing, Co., Ithaca, New York.

Gall DL and Tabatabai A (1988): Subband Coding of Digital Images Using Symmetric Short Kernel Filters and Arithmetic Coding Techniques. Proc. of IEEE International Conference Acoustics, Speech, and Signal Processing 2:761–764.

Gallagher N Jr, Wise G (1981): A theoretical analysis of the properties of median filters. Acoustics, Speech and Signal Processing, IEEE Transactions 29(6):1136–1141.

Gavrielides MA, Gallas BD, Lenz P, Badano A, and Hewitt SM (2011): Observer variability in the interpretation of HER2/neu immunohistochemical expression with unaided and computer-aided digital microscopy. Arch Pathol Lab Med 135(2):233–42.

Glasbey CA (1993): An analysis of histogram-based thresholding algorithms. CVGIP: Graphical Models and Image Processing 55:532–537.

Glatz-Krieger K, Glatz D, and Mihatsch MJ (2003): Virtual slides: high-quality demand, physical limitations, and affordability. Hum Pathol 34(10):968–74.

Goldstein DJ (1999): Understanding the Light Microscope: A Computer-Aided Introduction. Academic Press, London.

Gong Y, Sweet W, Duh YJ, Greenfield L, Fang Y, Zhao J, Tarco E, Symmans WF, Isola J, and Sneige N (2009): Chromogenic in situ hybridization is a reliable method for detecting HER2 gene status in breast cancer: a multicenter study using conventional scoring criteria and the new ASCO/CAP recommendations. Am J Clin Pathol 131:490–497.

Gonzalez RC and Woods RE (2008): Digital Image Processing. Pearson Education, New Jersey, Pearson International 3rd Edition.

Graham AR, Bhattacharyya AK, Scott KM, Lian F, Grasso LL, Richter LC, Carpenter JB, Chiang S, Henderson JT, Lopez AM, Barker GP, and Weinstein RS (2009): Virtual slide telepathology for an academic teaching hospital surgical pathology quality assurance program. Hum Pathol 40(8):1129–36.

Gross K and Steinman HK (2009): Mohs Surgery and Histopathology: Beyond the Fundamentals. Cambridge University Press, Cambridge.

Gustavson MD, Bourke-Martin B, Reilly DM, Cregger M, Williams C, Tedeschi G, Pinard R, and Christiansen J. (2009): Development of an unsupervised pixel-based clustering algorithm for compartmentalization of immunohistochemical expression using Automated QUantitative Analysis. Appl Immunohistochem Mol Morphol 17(4):329–37.

Hall BH, Ianosi-Irimie M, Javidian P, Chen W, Ganesan S, and Foran DJ (2008): Computer-assisted assessment of the human epidermal growth factor receptor 2 immunohistochemical assay in imaged histologic sections using a membrane isolation algorithm and quantitative analysis of positive controls. BMC Med Imaging 8:11.

Hammond ME, Hayes DF, Dowsett M, Allred DC, Hagerty KL, Badve S, Fitzgibbons PL, Francis G, Goldstein NS, Hayes M, Hicks DG, Lester S, Love R, Mangu PB, McShane L, Miller K, Osborne CK, Paik S, Perlmutter J, Rhodes A, Sasano H, Schwartz JN, Sweep FC, Taube S, Torlakovic EE, Valenstein P, Viale G, Visscher D, Wheeler T, Williams RB, Wittliff JL, and Wolff AC (2010): American Society of Clinical Oncology/College of American Pathologists guideline recommendations for immunohistochemical testing of estrogen and progesterone receptors in breast cancer. J Clin Oncol 28(16):2784–95.

Harris L, Fritsche H, Mennel R, Norton L, Ravdin P, Taube S, Somerfield MR, Hayes DF, and Bast RC Jr; American Society of Clinical Oncology (2007): American Society of Clinical Oncology 2007 Update of Recommendations for the Use of Tumor Markers in Breast Cancer. J Clin Oncol 25(33):5287–312.

Hecht E (2002): Optics. Addison-Wesley, Boston.

Helin H, Lundin M, Lundin J, Martikainen P, Tammela T, Helin H, van der Kwast T, and Isola J (2005): Web-based virtual microscopy in teaching and standardizing Gleason grading. Hum Pathol 36(4):381–6.

Helin HO, Lundin ME, Laakso M, Lundin J, Helin HJ, and Isola J (2006): Virtual microscopy in prostate histopathology: simultaneous viewing of biopsies stained sequentially with hematoxylin and eosin, and alpha-methylacyl-coenzyme A racemase/p63 immunohistochemistry. J Urol 175(2):495–9.

Hooke R (1665). Micrographia. Jo. Martyn and Ja. Allestry, London.

Huang LK and Wang MJJ (1995): Image thresholding by minimizing the measure of fuzziness. Pattern Recognition 28(1):41–51.

Huang HK (2010): PACS and Imaging Informatics. John Wiley & Sons, Inc., New Jersey.

Inoué S and Spring KR (1997): Video Microscopy: The Fundamentals. Plenum, New York, 2nd edition.

IOM (2011): Medical Devices and the Public's Health: The FDA 510(k) Clearance Process at 35 Years. Consensus report, Institute of Medicine of the National Academies. July 29 2011.

Irie K, McKinnon AE, Unsworth K, and Woodhead IM (2008): A model for measurement of noise in CCD digital-video cameras. Meas Sci Technol 19(4).

Isaacs M, Lennerz JK, Yates S, Clermont W, Rossi J, and Pfeifer JD (2011): Implementation of whole slide imaging in surgical pathology: A value added approach. J Pathol Inform 2:39.

Isabelle M, Teodorovic I, Oosterhuis JW, Riegman PH, Passioukov A, Lejeune S, Therasse P, Dinjens WN, Lam KH, Oomen MH, Spatz A, Ratcliffe C, Knox K, Mager R, Kerr D, Pezzella F, Van Damme B, Van de Vijver M, Van Boven H, Morente MM, Alonso S, Kerjaschki D, Pammer J, López-Guerrero JA, Llombart-Bosch A, Carbone A, Gloghini A, and Van Veen EB; Tubafrost Consortium (2006): Virtual microscopy in virtual tumor banking. Adv Exp Med Biol 587:75–86.

Jain KK (2010): The Handbook of Biomarkers. Springer, New York.

Jain AK, Murty MN, and Flynn P (1999): Data clustering: a review. ACM Comput Surveys 31(3):264–323.

Jain AK, Figueiredo M, and Zerubia J (2001): Energy Minimization Methods in Computer Vision and Pattern Recognition. Springer, New York.

James T, Lamar S, Marker T (2000): An intervention study comparing traditional and ergonomic microscopes. Human Factors and Ergonomics Society Annual Meeting Proceedings 44(32):31–34.

Jerri AJ (1977): The Shannon sampling theorem—Its various extensions and applications: A tutorial review. Proceedings of the IEEE 1565–1596.

Joshi AS, Sharangpani GM, Porter K, Keyhani S, Morrison C, Basu AS, Gholap GA, Gholap AS, and Barsky SH (2007): Semi-automated imaging system to quantitate Her-2/neu membrane receptor immunoreactivity in human breast cancer. Cytometry A 71:273–285.

JPEG (2011): The JPEG committee home page. Available at: http://www.jpeg.org/. Accessed 19.1.2012.

Köhler A (1893): A new system of illumination for photomicrographic purposes. Z. Wiss. Mikroskopie 10, 433–440. Translated in Royal Microscopical Society—Koehler Illumination Centenary, 1994.

Köninki K, Tanner M, Auvinen A, and Isola J (2009): HER-2 positive breast cancer: decreasing proportion but stable incidence in Finnish population from 1982 to 2005. Breast Cancer Res 11(3):R37.

Kalinski T, Zwönitzer R, Sel S, Evert M, Guenther T, Hofmann H, Bernarding J, and Roessner A (2008): Virtual 3D microscopy using multiplane whole slide images in diagnostic pathology. Am J Clin Pathol 130(2):259–64.

Kalinski T, Zwönitzer R, Grabellus F, Sheu SY, Sel S, Hofmann H, Bernarding J, and Roessner A (2009): Lossy compression in diagnostic virtual 3-dimensional microscopy--where is the limit? Hum Pathol 40(7):998–1005.

Kalinski T, Zwönitzer R, Grabellus F, Sheu SY, Sel S, Hofmann H, and Roessner A (2011): Lossless Compression of JPEG2000 Whole Slide Images Is Not Required for Diagnostic Virtual Microscopy. Am J Clin Pathol 136(6):889–95.

Kankaanpää PP, Pahajoki KA, Marjomäki VS, White DJ, and Heino J (2008): BioImageXD - Free Microscopy Image Processing Software. Microscopy and Microanalysis 14:724–725.

Kapur JN, Sahoo PK, and Wong ACK (1985): A New Method for Gray-Level Picture Thresholding Using the Entropy of the Histogram. Graphical Models and Image Processing 29(3):273–285.

Kayser K, Molnar B, Weinstein RS (2006): Virtual microscopy – fundamentals, applications, perspectives of electronic tissue-based diagnosis. VSV Interdisciplinary Medical Publishing, Berlin.

Kayser K, Ogilvie R, Borkenfeld S, and Kayser G (2011): E-education in pathology including certification of e-institutions. Diagn Pathol 30:6 Suppl 1:S11.

Kirsch R (1971): Computer determination of the constituent structure of biological images. Computers and Biomedical Research 4:315–328.

Kittler J and Illingworth J (1986): Minimum error thresholding. Pattern Recognition 19:41–47.

Konsti J, Lundin J, Jumppanen M, Lundin M, Viitanen A, and Isola J (2008): A public-domain image processing tool for automated quantification of fluorescence in situ hybridisation signals. J Clin Pathol 61(3):278–82.

Konsti J, Lundin M, Joensuu H, Lehtimäki T, Sihto H, Holli K, Turpeenniemi-Hujanen T, Kataja V, Sailas L, Isola J, and Lundin J (2011): Development and evaluation of a virtual microscopy application for automated assessment of Ki-67 expression in breast cancer. BMC Clin Pathol 11:3.

Kostopoulos S, Cavouras D, Daskalakis A, Bougioukos P, Georgiadis P, Kagadis GC, Kalatzis I, Ravazoula P, and Nikiforidis G (2007): Colour-texture based image analysis method for assessing the hormone receptors status in breast tissue sections. Conf Proc IEEE Eng Med Biol Soc 2007:4985–4988.

Kostopoulos S, Cavouras D, Daskalakis A, Kagadis GC, Kalatzis I, Georgiadis P, Ravazoula P, and Nikiforidis G (2008): Cascade pattern recognition structure for improving quantitative assessment of estrogen receptor status in breast tissue carcinomas. Anal Quant Cytol Histol 30(4):218–25.

Kotsiantis SB, Zaharakis ID, and Pintelas PE (2006): Machine learning: a review of classification and combining techniques. Artif Intell Rev 26:159–190.

Kumar RK, Freeman B, Velan GM, and De Permentier PJ (2006): Integrating histology and histopathology teaching in practical classes using virtual slides. Anat Rec B New Anat 289(4):128–133.

Kumar V, Abbas AK, Fausto N, and Mitchell R (2007): Robbins Basic Pathology. Saunders, Philadelphia, 8th edition.

Lacroix-Triki M, Mathoulin-Pelissier S, Ghnassia JP, Macgrogan G, Vincent-Salomon A, Brouste V, Mathieu MC, Roger P, Bibeau F, Jacquemier J, Penault-Llorca F, and Arnould L (2006): High inter-observer agreement in immunohistochemical evaluation of HER-2/neu expression in breast cancer: a multicentre GEFPICS study. Eur J Cancer 42(17):2946–53.

Landini G (2011a): The Color Deconvolution ImageJ plugin. Available at: http://www.dentistry.bham.ac.uk/landinig/software/cdeconv/cdeconv.html. Accessed 19.1.2012.

Landini G (2011b): ImageJ plugin software. Available at: http://www.dentistry.bham.ac.uk/landinig/software/software.html. Accessed 19.1.2012.

Laurinavicius A, Laurinaviciene A, Dasevicius D, Elie N, Plancoulaine B, Bor C, and Herlin P (2011): Digital image analysis in pathology: Benefits and obligation. Anal Cell Pathol (Amst) Epub ahead of print.

Leeuwenhoek AV (1673): The figures of some of Mr. Leeuwenhoek's microscopical observations. London.

Legault R (1973): The aliasing problems in two-dimensional sampled imagery; in Perception of displayed information. Plenum Press, New York.

Leong FJ, Brady M, and McGee JO (2003): Correction of uneven illumination (vignetting) in digital microscopy images. J Clin Pathol 56:619–621.

Li CH and Lee CK (1993): Minimum Cross Entropy Thresholding. Pattern Recognition 26(4):617–625.

Likar B, Maintz JBA, Viergever MA, and Pernus F (2000): Retrospective shading correction by entropy minimization. J Microsc 197:285–295.

Linder E, Lundin M, Thors C, Lebbad M, Winiecka-Krusnell J, Helin H, Leiva B, Isola J, and Lundin J (2008): Web-based virtual microscopy for parasitology: a novel tool for education and quality assurance. PLoS Negl Trop Dis 2(10):e315.

Liu JK, Wu HC, and Shih TY (2005): Effects of JPEG2000 on the Information and Geometry Content of Aerial Photo Compression. Photogrammetric Engineering & Remote Sensing 71(2):157–168.
Lundin M, Lundin J, and Isola J (2004a): Virtual microscopy. J Clin Pathol 57(12):1250–1.
Lundin M, Lundin J, Helin H, and Isola J (2004b): A digital atlas of breast histopathology: an application of web based virtual microscopy. J Clin Pathol 57(12):1288–91.
Lundin M, Szymas J, Linder E, Beck H, de Wilde P, van Krieken H, García Rojo M, Moreno I, Ariza A, Tuzlali S, Dervisoglu S, Helin H, Lehto VP, and Lundin J (2009): A European network for virtual microscopy–design, implementation and evaluation of performance. Virchows Arch 454(4):421–9.
Mallat S (1989): A Theory of Multiresolution Signal Decomposition: The Wavelet Representation. IEEE Trans on Pattern Analysis and Machine Intelligence 11(7):674–693.
Masmoudi H, Hewitt SM, Petrick N, Myers KJ, and Gavrielides MA (2009): Automated quantitative assessment of HER-2/neu immunohistochemical expression in breast cancer. IEEE Trans Med Imaging 28:916–925.
Mass RD, Press MF, Anderson S, Cobleigh MA, Vogel CL, Dybdal N, Leiberman G, and Slamon DJ (2005): Evaluation of clinical outcomes according to HER2 detection by fluorescence in situ hybridization in women with metastatic breast cancer treated with trastuzumab. Clinical Breast Cancer 6:240–246.
McCamy CS, Marcus H, and Davidson JG (1976): A Color-Rendition Chart. Journal of Applied Photographic Engineering 2(3):95–99.
Mikula S, Stone JM, and Jones EG (2008): BrainMaps.org – Interactive High-Resolution Digital Brain Atlases and Virtual Microscopy. Brains Minds Media 2008;3:bmm1426.
Mofidi R, Walsh R, Ridgway PF, Crotty T, McDermott EW, Keaveny TV, Duffy MJ, Hill AD, and O'Higgins N (2003): Objective measurement of breast cancer oestrogen receptor status through digital image analysis. Eur J Surg Oncol 29(1):20–4.
Murphy DB (2001): Fundamentals of Light Microscopy and Electronic Imaging. John Wiley & Sons, Inc., New York.
Nakamura J (2005): Image Sensors and Signal Processing for Digital Still Cameras. CRC Press, Boca Raton, FL.
Nassar A, Cohen C, Albitar M, Agersborg SS, Zhou W, Lynch KA, Heyman ER, Lange H, and Siddiqui MT (2011): Reading immunohistochemical slides on a computer monitor--a multisite performance study using 180 HER2-stained breast carcinomas. Appl Immunohistochem Mol Morphol 19(3):212–7.
NordiQC (2011): Nordic immunohistochemical Quality Control (NordiQC). Available at: http://www.nordiqc.org/. Accessed 20.1.2012.
Ortiz JP, Ruiz VG, and Garcia I (2007): Efficient Virtual Slide Telepathology Systems with JPEG2000. Conf Proc IEEE Eng Med Biol Soc 2007:880–883.
Otsu N (1979): A threshold selection method from gray-level histograms. IEEE Trans Sys, Man, Cyber 9:62–66.
Pantanowitz L, Valenstein PN, Evans AJ, Kaplan KJ, Pfeifer JD, Wilbur DC, Collins LC, and Colgan TJ (2011): Review of the current state of whole slide imaging in pathology. J Pathol Inform 2:36.
Papademetris X, Jackowski M, Rajeevan N, DiStasio M, Okuda H, Constable RT, Staib L (2006): BioImage Suite: An integrated medical image analysis suite: An update. The Insight Journal – 2006 MICCAI Open Science Workshop.
Parker JR (1991): Grey level thresholding in badly illuminated images. IEEE Trans Pattern Anal Machine Intell 13:813–819.
Parulski KA, Nutting TC, Moore G (1990): Color sequential optical offset image sampling system. US Patent 4,967,264.
Paulsen FP, Eichhorn M, and Bräuer L (2010): Virtual microscopy-The future of teaching histology in the medical curriculum? Ann Anat 192(6):378–82.
Pavlidis T and Liow YT (1990): Integrating Region Growing and Edge Detection. IEEE Trans on Pattern Analysis and Machine Intelligence PAMI-12:225–233.

Petrou M and Petrou C (2010): Image Processing - The Fundamentals. John Wiley & Sons, Inc., New York, 2nd edition.

Pham NA, Morrison A, Schwock J, Aviel-Ronen S, Iakovlev V, Tsao MS, Ho J, and Hedley DW (2007): Quantitative image analysis of immunohistochemical stains using a CMYK color model. Diagn Pathol 2:8.

Pieper RJ and Korpel A (1983): Image Processing for Extended Depth of Field. Applied Optics 22:1449–1453.

Pluta M (1988): Advanced Light Microscopy, Volume 1: Principles and Basic Optics. Elsevier, Amsterdam.

Poskanzer J (2011): PBM file format specification. Available at: http://netpbm.sourceforge.net/doc/pbm.html. Accessed 20.1.2012.

Press MF, Pike MC, Chazin VR, Hung G, Udove JA, Markowicz M, Danyluk J, Godolphin W, Sliwkowski M, Akita R, Paterson MC, and Slamon J (1993): Her-2/neu expression in node-negative breast cancer: direct tissue quantitation by computerized image analysis and association of overexpression with increased risk of recurrent disease. Cancer Res 53(20):4960–70.

Prewitt JMS and Mendelsohn ML (1966): The analysis of cell images. Annals of the New York Academy of Sciences 128:1035–1053.

Rüdiger T, Höfler H, Kreipe HH, Nizze H, Pfeifer U, Stein H, Dallenbach FE, Fischer HP, Mengel M, von Wasielewski R, and Müller-Hermelink HK (2002): Quality assurance in immunohistochemistry: results of an interlaboratory trial involving 172 pathologists. Am J Surg Pathol 26(7):873–82.

Rabbani M and Joshi R (2002): An overview of the JPEG 2000 still image compression standard. Signal Process: Image Comm 17(1):3–48.

Ramanath R, Snyder WE, Bilbro GL (2002): Demosaicking methods for Bayer color arrays. J Electronic Imaging 11(3):306–315.

Ramey J, Fung KM, and Hassell LA (2011): Use of mobile high-resolution device for remote frozen section evaluation of whole slide images. J Pathol Inform 2:41.

Rasband WS (2011): ImageJ software, National Institutes of Health, Bethesda, Maryland, US. Available at: http://imagej.nih.gov/ij/. Accessed 20.1.2012.

Rayleigh L (1896): On the Theory of Optical Images, with Special Reference to the Microscope. Philosophical Magazine 42(5):167.

Renshaw S (2007): Immunohistochemistry: Methods Express Series. Scion Publishing Ltd, Bloxham.

Rexhepaj E, Brennan DJ, Holloway P, Kay EW, McCann AH, Landberg G, Duffy MJ, Jirstrom K, and Gallagher WM (2008): Novel image analysis approach for quantifying expression of nuclear proteins assessed by immunohistochemistry: application to measurement of oestrogen and progesterone receptor levels in breast cancer. Breast Cancer Res 10:R89.

Reyes-Aldasoro CC (2009): Retrospective shading correction algorithm based on signal envelope estimation. Electronic Letters 45(9):454–456.

Ridler TW and Calvard S (1978): Picture thresholding using an iterative selection method. IEEE Trans Sys, Man, Cyber 8:630–632.

Riethdorf S, Hoegel B, John B, Ott G, Fritz P, Thon S, Loening T, and Pantel K (2011): Prospective multi-centre study to validate chromogenic in situ hybridisation for the assessment of HER2 gene amplification in specimens from adjuvant and metastatic breast cancer patients. J Cancer Res Clin Oncol 137(2):261–9.

Rojo MG, García GB, Mateos CP, García JG, Vicente MC (2006): Critical comparison of 31 commercially available digital slide systems in pathology. Int J Surg Pathol 14(4):285–305.

Rojo MG, Gallardo AJ, González L, Peces C, Murillo C, González J, and Sacristán J (2008): Reading virtual slide using web viewers: results of subjective experience with three different solutions. Diagn Pathol 3 Suppl 1:S23.

Rojo MG, Bueno G, and Slodkowska J (2009): Review of imaging solutions for integrated quantitative immunohistochemistry in the Pathology daily practice. Folia Histochem Cytobiol 47:349–354.
Ruifrok AC and Johnston DA (2001): Quantification of histochemical staining by color deconvolution. Anal Quant Cytol Histol 23:291–299.
Russ JC (2007): Image Processing Handbook. CRC Press, Boca Raton, FL, 5th edition.
Santa-Cruz D, Grosbois R, Ebrahimi T (2002): JPEG 2000 performance evaluation and assessment. Signal Process: Image Comm 17(1):113–130.
Satyanarayanan M and Goode A (2001): A Vendor-Neutral Library and Viewer for Whole-Slide Images. Technical Report CMU-CS-08-136, Computer Science Department, Carnegie Mellon University.
Sayood K (2006): Introduction to Data Compression. Morgan Kaufmann, San Francisco, 3rd edition.
Schelkens P, Munteanu A, and Cornelis J (2003): Wavelet coding of volumetric medical datasets. IEEE Trans Med Imag 22(3):441–458.
Sezgin M and Sankur B (2004): Survey over Image Thresholding Techniques and Quantitative Performance Evaluation. Journal of Electronic Imaging 13(1):146–165.
Shanbhag AG and Abhijit G (1994): Utilization of information measure as a means of image thresholding. Graph Models Image Process 56(5):414–419.
Shannon CE (1948): A Mathematical Theory of Communication. The Bell System Technical Journal 27(3):379–423.
Sharma A, Bautista P, and Yagi Y (2011): Balancing image quality and compression factor for special stains whole slide images. Anal Cell Pathol (Amst); Epub ahead of print.
Shih FY (2010): Image Processing and Pattern Recognition: Fundamentals and Techniques. John Wiley & Sons, Inc., Hoboken New Jersey.
Skodras A, Christopoulos C, and Ebrahimi T (2001): The JPEG 2000 Still Image Compression Standard. IEEE Signal Proc Mag 18(5):36–58.
Sled JG, Zijdenbos AP, and Evans AC (1998): A nonparametric method for automatic correction of intensity nonuniformity in MRI data. IEEE Trans Med Imaging 17:87–97.
Smith MB, Li H, Shen T, Huang X, Yusuf E, and Vavylonis D (2010): Segmentation and tracking of cytoskeletal filaments using open active contours. Cytoskeleton (Hoboken) 67(11):693–705.
Smith W (1992): Modern Lens Design: A Resource Manual. McGraw-Hill, New York.
Starck JL, Murtagh F, Candès EJ, and Donoho DL (2003): Gray and color image contrast enhancement by the curvelet transform. IEEE Trans Image Process 12(6):706–17.
Stark JA and Fitzgerald WJ (1996): An alternative algorithm for adaptive histogram equalization. Computer Vision Graphics Image Process 56:180–185.
Stark JA (2000): Adaptive image contrast enhancement using generalizations of histogram equalization. IEEE Trans Image Process 9(5):889–96.
Steckhan D, Bergen T, Wittenberg T, and Rupp S (2008): Efficient large scale image stitching for virtual microscopy. Conf Proc IEEE Eng Med Biol Soc 2008:4019–23.
Sternberg S (1983): Biomedical Image Processing. IEEE Computer 16(1):22–34.
Stoner R (2011): WholeSlide iOS application. Available at: http://wholeslide.com/. Accessed 9.11.2011.
Stuart-Harris R, Caldas C, Pinder SE, and Pharoah P (2008): Proliferation markers and survival in early breast cancer: a systematic review and meta-analysis of 85 studies in 32,825 patients. Breast 17:323–334.
Sun Y, Duthaler S, and Nelson BJ (2005): Autofocusing algorithm selection in computer microscopy. IROS 2005:70–76.
Szymas J and Lundin M (2011): Five years of experience teaching pathology to dental students using the WebMicroscope. Diagn Pathol 6 Suppl 1:S13.
Tanner M, Isola J, Wiklund T, Erikstein B, Kellokumpu-Lehtinen P, Malmström P, Wilking N, Nilsson J, and Bergh J; Scandinavian Breast Group Trial 9401 (2006): Topoisomerase IIalpha gene amplification predicts favorable treatment response to tailored and dose-

escalated anthracycline-based adjuvant chemotherapy in HER-2/neu-amplified breast cancer: Scandinavian Breast Group Trial 9401. J Clin Oncol 24:2428–2436.
Taubman DS and Marcellin MW (2002): JPEG2000: Image Compression Fundamentals, Standards and Practice. Springer, New York.
Taubman DS and Prandolini R (2003): Architecture, Philosophy and Performance of JPIP: Internet Protocol Standard for JPEG2000. Proc of SPIE 5150:791–805.
Taubman DS (2000): High Performance Scalable Image Compression with EBCOT. IEEE Trans Image Processing 9(7):1158–1170.
Taxy JB, Husain AN, and Montag AG (2009): Biopsy Interpretation: The Frozen Section. Lippincott Williams & Wilkins, Philadelphia.
Thévenaz P (2011): TurboReg ImageJ plugin website. Available at: http://bigwww.epfl.ch/thevenaz/turboreg/. Accessed 20.1.2012.
Thévenaz P, Ruttimann UE, Unser M (1998): A Pyramid Approach to Subpixel Registration Based on Intensity. IEEE Transactions on Image Processing 7(1):27–41.
Tomaževic D, Likar B, and Pernus F (2002): Comparative evaluation of retrospective shading correction methods. J Microsc 208(Pt 3):212–23.
Tsai W (1985): Moment-preserving thresholding: a new approach. Computer Vision, Graphics, and Image Processing 29:377–393.
Tympel VA (1996): New High-Level Image Capture System for Conventional Light Microscopy. Proc SPIE 2707:529–536.
UK NEQAS (2011): United Kingdom National External Quality Assessment Service (UK NEQAS). Available at: http://www.ukneqas.org.uk/. Accessed 20.1.2012.
Urruticoechea A, Smith IE, and Dowsett M (2005): Proliferation marker Ki-67 in early breast cancer. J Clin Oncol 23:7212–7220.
van der Loos CM (2008): Multiple immunoenzyme staining: methods and visualizations for the observation with spectral imaging. J Histochem Cytochem 56:313–328.
Vetterli M (2001): Wavelets, approximation and compression. IEEE Signal Processing Mag 18:59–73.
Vincent L and Soille P (1991): Watersheds in Digital Spaces: An Efficient Algorithm Based on Immersion Simulations. IEEE Trans Pattern Anal Mach Intell 13(6):583–598.
W3C (2011): World Wide Web Consortium (W3C) XML Schema. Available at: http://www.w3.org/XML/Schema. Accessed 20.1.2012.
Walkowski S and Szymas J (2011): Histopathologic patterns of nervous system tumors based on computer vision methods and whole slide imaging (WSI). Anal Cell Pathol (Amst); Epub ahead of print.
Walter RJ Jr and Berns MW (1986): Digital image processing and analysis. In: Video Microscopy. Plenum Press, New York.
Wang F, Kong J, Cooper L, Pan T, Kurc T, Chen W, Sharma A, Niedermayr C, Oh TW, Brat D, Farris AB, Foran DJ, and Saltz J (2011): A data model and database for high-resolution pathology analytical image informatics. J Pathol Inform 2:32.
Wayne R (2009): Light and Video microscopy. Academic Press, London.
Weigel MT and Dowsett M (2010): Current and emerging biomarkers in breast cancer: prognosis and prediction. Endocr Relat Cancer 17(4):R245–62.
Weinstein RS (2005): Innovations in medical imaging and virtual microscopy. Hum Pathol 36(4):317–9.
Weinstein RS, Descour MR, Liang C, Barker G, Scott KM, Richter L, Krupinski EA, Bhattacharyya AK, Davis JR, Graham AR, Rennels M, Russum WC, Goodall JF, Zhou P, Olszak AG, Williams BH, Wyant JC, and Bartels PH (2006): An array microscope for ultrarapid virtual slide processing and telepathology. Design, fabrication, and validation study. Hum Pathol 35:1303–1314.
Weiss DG, Maile W, and Wick RA (1989): Video Microscopy. In: Light Microscopy in Biology. A Practical Approach. ILR Press, Oxford.
Welch TA (1984): A technique for high-performance data compression. IEEE Computer 17(6):8–19.

Wilbur DC, Madi K, Colvin RB, Duncan LM, Faquin WC, Ferry JA, Frosch MP, Houser SL, Kradin RL, Lauwers GY, Louis DN, Mark EJ, Mino-Kenudson M, Misdraji J, Nielsen GP, Pitman MB, Rosenberg AE, Smith RN, Sohani AR, Stone JR, Tambouret RH, Wu CL, Young RH, Zembowicz A, and Klietmann W (2009): Whole-slide imaging digital pathology as a platform for teleconsultation: a pilot study using paired subspecialist correlations. Arch Pathol Lab Med 133(12):1949–53.

Wolff AC, Hammond ME, Schwartz JN, Hagerty KL, Allred DC, Cote RJ, Dowsett M, Fitzgibbons PL, Hanna WM, Langer A, McShane LM, Paik S, Pegram MD, Perez EA, Press MF, Rhodes A, Sturgeon C, Taube SE, Tubbs R, Vance GH, van de Vijver M, Wheeler TM, and Hayes DF; American Society of Clinical Oncology; College of American Pathologists (2007): American Society of Clinical Oncology/College of American Pathologists guideline recommendations for human epidermal growth factor receptor 2 testing in breast cancer. J Clin Oncol 25(1):118–45.

Wootton C (2005): A Practical Guide to Video and Audio Compression: From Sprockets and Rasters to Macroblocks. Focal Press, Oxford.

Wu ML, Varga VS, Kamaras V, Ficsor L, Tagscherer A, Tulassay Z, and Molnar B (2005): Three-dimensional virtual microscopy of colorectal biopsies. Arch Pathol Lab Med 129:507–510.

Wu Q, Merchant FA, Castleman KA (2008): Microscope image processing. Academic Press, Burlington, MA.

Yagi Y and Gilbertson J (2005): Digital imaging in pathology: The case for standardization, Journal of Telemedicine and Telecare 11:109–116.

Yagi Y (2011): Color standardization and optimization in whole slide imaging. Diagn Pathol 6 Suppl 1:S15.

Yerushalmi R, Woods R, Ravdin PM, Hayes MM, and Gelmon KA (2010): Ki67 in breast cancer: prognostic and predictive potential. Lancet Oncol 11(2):174–83.

Young IT, Gerbrands JJ, and Vliet LJ (1998): Image Processing Fundamentals. The Digital Signal Processing Handbook. CRC Press, Boca Raton, FL.

Zack GW, Rogers WE, and Latt SA (1977): Automatic measurement of sister chromatid exchange frequency. J Histochem Cytochem 25(7):741–53.

Zhu H, Chan FHY, and Lam FK (1999): Image Contrast Enhancement by Constrained Local Histogram Equalization. Computer Vision and Image Understanding 73(2): 281–290.

Zwönitzer R, Kalinski T, Hofmann H, Roessner A, and Bernarding J (2007): Digital pathology: DICOM-conform draft, testbed, and first results. Comput Methods Programs Biomed 87(3):181–8.

APPENDICES

Appendix A: JVSschema, version 1.0.2

```
<?xml version="1.0" encoding="ISO-8859-1"?>
<xsd:schema
  version="1.0.2"
  xmlns:xsd="http://www.w3.org/2001/XMLSchema"
  xmlns:jvs="http://jvsmicroscope.uta.fi/JVSschema"
  targetNamespace="http://jvsmicroscope.uta.fi/JVSschema"
  elementFormDefault="qualified"
  attributeFormDefault="unqualified">

  <xsd:element name="ImageInformation" type="jvs:ImageInformationType"/>

  <xsd:complexType name="ImageInformationType">
    <xsd:annotation>
      <xsd:documentation xml:lang="en">
        The root element for image information.
      </xsd:documentation>
    </xsd:annotation>
    <xsd:sequence>
      <xsd:element name="SchemaVersion" type="xsd:string" minOccurs="1" maxOccurs="1">
        <xsd:annotation>
          <xsd:documentation xml:lang="en">
            Used JVSschema version.
         </xsd:documentation>
        </xsd:annotation>
      </xsd:element>
      <xsd:element name="ScanningResolution" type="jvs:PositiveDecimal" minOccurs="0" maxOccurs="1"/>
      <xsd:element name="Organ" type="xsd:string" minOccurs="0" maxOccurs="1">
        <xsd:annotation>
          <xsd:documentation xml:lang="en">
            The organ from which the specimen is from, expressed with few words.
         </xsd:documentation>
        </xsd:annotation>
      </xsd:element>
      <xsd:element name="Diagnosis" type="xsd:string" minOccurs="0" maxOccurs="1">
        <xsd:annotation>
          <xsd:documentation xml:lang="en">
            The diagnosis, expressed with few words.
         </xsd:documentation>
        </xsd:annotation>
      </xsd:element>
      <xsd:element name="Comments" type="xsd:string" minOccurs="0" maxOccurs="1">
        <xsd:annotation>
          <xsd:documentation xml:lang="en">
            Additional comments, expressed with few sentences.
         </xsd:documentation>
        </xsd:annotation>
      </xsd:element>
      <xsd:element name="ROIs" type="jvs:ROIsType" minOccurs="0" maxOccurs="1"/>
      <xsd:element name="ImageLayerInformation" type="jvs:ImageLayerInformationType" minOccurs="0" maxOccurs="1">
        <xsd:unique name="layer_number">
          <xsd:selector xpath="Layer"/>
          <xsd:field xpath="Number"/>
        </xsd:unique>
```

```
    </xsd:element>
    <xsd:element name="InitialAdjustments" type="jvs:InitialAdjustmentsType" minOccurs="0" maxOccurs="1"/>
    <xsd:element name="HideImageInformation" type="xsd:boolean" minOccurs="0" maxOccurs="1">
      <xsd:annotation>
        <xsd:documentation xml:lang="en">
          Should the image information be hidden (e.g., in JVSview application for educational purposes).
       </xsd:documentation>
      </xsd:annotation>
    </xsd:element>
  </xsd:sequence>
</xsd:complexType>

<xsd:complexType name="ROIsType">
  <xsd:annotation>
    <xsd:documentation xml:lang="en">
      Image regions of interest.
    </xsd:documentation>
  </xsd:annotation>
  <xsd:sequence>
    <xsd:element name="ROI" type="jvs:ROIType" minOccurs="1" maxOccurs="unbounded"/>
  </xsd:sequence>
</xsd:complexType>

<xsd:complexType name="ROIType">
  <xsd:annotation>
    <xsd:documentation xml:lang="en">
      One elliptical region of interest. Contains a textual description, a color, the bounding rectangle
      of the ellipse within the image coordinate system, as well as scale information on how to display
      the ROI properly.
    </xsd:documentation>
  </xsd:annotation>
  <xsd:sequence>
    <xsd:element name="Description" type="xsd:string" minOccurs="0" maxOccurs="1"/>
    <xsd:element name="Color" type="jvs:ROIColorType" minOccurs="0" maxOccurs="1"/>
    <xsd:element name="Left" type="xsd:integer" minOccurs="1" maxOccurs="1">
      <xsd:annotation>
        <xsd:documentation xml:lang="en">
          The x-coordinate of the upper-left corner of the bounding rectangle.
       </xsd:documentation>
      </xsd:annotation>
    </xsd:element>
    <xsd:element name="Top" type="xsd:integer" minOccurs="1" maxOccurs="1">
      <xsd:annotation>
        <xsd:documentation xml:lang="en">
          The y-coordinate of the upper-left corner of the bounding rectangle.
       </xsd:documentation>
      </xsd:annotation>
    </xsd:element>
    <xsd:element name="Right" type="xsd:integer" minOccurs="1" maxOccurs="1">
      <xsd:annotation>
        <xsd:documentation xml:lang="en">
          The x-coordinate of the lower-right corner of the bounding rectangle.
       </xsd:documentation>
      </xsd:annotation>
    </xsd:element>
    <xsd:element name="Bottom" type="xsd:integer" minOccurs="1" maxOccurs="1">
      <xsd:annotation>
        <xsd:documentation xml:lang="en">
          The y-coordinate of the lower-right corner of the bounding rectangle.
       </xsd:documentation>
      </xsd:annotation>
    </xsd:element>
    <xsd:element name="Scale" type="jvs:PositiveDecimal" minOccurs="1" maxOccurs="1">
      <xsd:annotation>
        <xsd:documentation xml:lang="en">
          The scale to be used when viewing the ROI. Note: this is NOT to be used as a coefficient
          for the bounding rectangle coordinates.
       </xsd:documentation>
      </xsd:annotation>
```

```
    </xsd:element>
    <xsd:element name="ImageLayer" type="xsd:positiveInteger" minOccurs="1" maxOccurs="1">
      <xsd:annotation>
        <xsd:documentation xml:lang="en">
          The image layer on which the ROI is located. Number 1 represents the first layer.
       </xsd:documentation>
      </xsd:annotation>
    </xsd:element>
  </xsd:sequence>
</xsd:complexType>

<xsd:simpleType name="ROIColorType">
  <xsd:annotation>
    <xsd:documentation xml:lang="en">
      The color of a region of interest.
    </xsd:documentation>
  </xsd:annotation>
  <xsd:restriction base="xsd:string">
    <xsd:enumeration value="Red"/>
    <xsd:enumeration value="Green"/>
    <xsd:enumeration value="Blue"/>
    <xsd:enumeration value="Yellow"/>
    <xsd:enumeration value="Black"/>
    <xsd:enumeration value="White"/>
  </xsd:restriction>
</xsd:simpleType>

<xsd:complexType name="ImageLayerInformationType">
  <xsd:annotation>
    <xsd:documentation xml:lang="en">
      Information regarding different image layers (which can represent, for example, different staining).
    </xsd:documentation>
  </xsd:annotation>
  <xsd:sequence>
    <xsd:element name="Layer" type="jvs:LayerType" minOccurs="1" maxOccurs="unbounded"/>
  </xsd:sequence>
</xsd:complexType>

<xsd:complexType name="LayerType">
  <xsd:annotation>
    <xsd:documentation xml:lang="en">
      One image layer, consisting of an unique number and a name.
    </xsd:documentation>
  </xsd:annotation>
  <xsd:sequence>
    <xsd:element name="Number" type="xsd:positiveInteger" minOccurs="1" maxOccurs="1">
      <xsd:annotation>
        <xsd:documentation xml:lang="en">
          The layer number. Layer 1 represents the first layer. Must be unique (i.e., no two layers with
          same number can exist).
       </xsd:documentation>
      </xsd:annotation>
    </xsd:element>
    <xsd:element name="Name" type="xsd:string" minOccurs="0" maxOccurs="1"/>
  </xsd:sequence>
</xsd:complexType>

<xsd:complexType name="InitialAdjustmentsType">
  <xsd:annotation>
    <xsd:documentation xml:lang="en">
      Initial image adjustments for JVSview (i.e., brightness, contrast, saturation, and image layer).
    </xsd:documentation>
  </xsd:annotation>
  <xsd:sequence>
    <xsd:element name="Brightness" type="jvs:AdjustmentInteger" minOccurs="0" maxOccurs="1"/>
    <xsd:element name="Contrast" type="jvs:AdjustmentInteger" minOccurs="0" maxOccurs="1"/>
    <xsd:element name="Saturation" type="jvs:AdjustmentInteger" minOccurs="0" maxOccurs="1"/>
    <xsd:element name="ImageLayer" type="xsd:positiveInteger" minOccurs="0" maxOccurs="1">
      <xsd:annotation>
```

```
          <xsd:documentation xml:lang="en">
            Specifies the initially visible image layer (e.g., a focus layer), in case multiple layers are
            used. Layer 1 represents the first layer.
          </xsd:documentation>
        </xsd:annotation>
      </xsd:element>
    </xsd:sequence>
  </xsd:complexType>

  <xsd:simpleType name="AdjustmentInteger">
    <xsd:annotation>
      <xsd:documentation xml:lang="en">
        An integer in the range [-100,100].
      </xsd:documentation>
    </xsd:annotation>
    <xsd:restriction base="xsd:integer">
      <xsd:minInclusive value="-100"/>
      <xsd:maxInclusive value="100"/>
    </xsd:restriction>
  </xsd:simpleType>

  <xsd:simpleType name="PositiveDecimal">
    <xsd:annotation>
      <xsd:documentation xml:lang="en">
        A positive decimal.
      </xsd:documentation>
    </xsd:annotation>
    <xsd:restriction base="xsd:decimal">
      <xsd:minExclusive value="0.00"/>
    </xsd:restriction>
  </xsd:simpleType>

</xsd:schema>
```

Appendix B: JVSdicom Workstation DICOM SCP conformance

JVSdicom Workstation supports the following SOP Classes as an SCP:

VerificationSOPClass	1.2.840.10008.1.1
FINDPatientRootQueryRetrieveInformationModel	1.2.840.10008.5.1.4.1.2.1.1
FINDPatientStudyOnlyQueryRetrieveInformationModel	1.2.840.10008.5.1.4.1.2.3.1
FINDStudyRootQueryRetrieveInformationModel	1.2.840.10008.5.1.4.1.2.2.1
GETPatientRootQueryRetrieveInformationModel	1.2.840.10008.5.1.4.1.2.1.3
GETPatientStudyOnlyQueryRetrieveInformationModel	1.2.840.10008.5.1.4.1.2.3.3
GETStudyRootQueryRetrieveInformationModel	1.2.840.10008.5.1.4.1.2.2.3
MOVEPatientRootQueryRetrieveInformationModel	1.2.840.10008.5.1.4.1.2.1.2
MOVEPatientStudyOnlyQueryRetrieveInformationModel	1.2.840.10008.5.1.4.1.2.3.2
MOVEStudyRootQueryRetrieveInformationModel	1.2.840.10008.5.1.4.1.2.2.2
StoredPrintStorage	1.2.840.10008.5.1.1.27
HardcopyGrayscaleImageStorage	1.2.840.10008.5.1.1.29
HardcopyColorImageStorage	1.2.840.10008.5.1.1.30
ComputedRadiographyImageStorage	1.2.840.10008.5.1.4.1.1.1
DigitalXRayImageStorageForPresentation	1.2.840.10008.5.1.4.1.1.1.1
DigitalXRayImageStorageForProcessing	1.2.840.10008.5.1.4.1.1.1.1.1
DigitalMammographyXRayImageStorageForPresentation	1.2.840.10008.5.1.4.1.1.1.2
DigitalMammographyXRayImageStorageForProcessing	1.2.840.10008.5.1.4.1.1.1.2.1
DigitalIntraOralXRayImageStorageForPresentation	1.2.840.10008.5.1.4.1.1.1.3

DigitalIntraOralXRayImageStorageForProcessing	1.2.840.10008.5.1.4.1.1.1.3.1
GrayscaleSoftcopyPresentationStateStorage	1.2.840.10008.5.1.4.1.1.11.1
XRayAngiographicImageStorage	1.2.840.10008.5.1.4.1.1.12.1
XRayFluoroscopyImageStorage	1.2.840.10008.5.1.4.1.1.12.2
PETImageStorage	1.2.840.10008.5.1.4.1.1.128
PETCurveStorage	1.2.840.10008.5.1.4.1.1.129
CTImageStorage	1.2.840.10008.5.1.4.1.1.2
EnhancedCTImageStorage	1.2.840.10008.5.1.4.1.1.2.1
NuclearMedicineImageStorage	1.2.840.10008.5.1.4.1.1.20
RETIRED_UltrasoundMultiframeImageStorage	1.2.840.10008.5.1.4.1.1.3
UltrasoundMultiframeImageStorage	1.2.840.10008.5.1.4.1.1.3.1
MRImageStorage	1.2.840.10008.5.1.4.1.1.4
EnhancedMRImageStorage	1.2.840.10008.5.1.4.1.1.4.1
MRSpectroscopyStorage	1.2.840.10008.5.1.4.1.1.4.2
RTImageStorage	1.2.840.10008.5.1.4.1.1.481.1
RTDoseStorage	1.2.840.10008.5.1.4.1.1.481.2
RTStructureSetStorage	1.2.840.10008.5.1.4.1.1.481.3
RTBeamsTreatmentRecordStorage	1.2.840.10008.5.1.4.1.1.481.4
RTPlanStorage	1.2.840.10008.5.1.4.1.1.481.5
RTBrachyTreatmentRecordStorage	1.2.840.10008.5.1.4.1.1.481.6
RTTreatmentSummaryRecordStorage	1.2.840.10008.5.1.4.1.1.481.7
RETIRED_UltrasoundImageStorage	1.2.840.10008.5.1.4.1.1.6
UltrasoundImageStorage	1.2.840.10008.5.1.4.1.1.6.1
RawDataStorage	1.2.840.10008.5.1.4.1.1.66
SpatialRegistrationStorage	1.2.840.10008.5.1.4.1.1.66.1
SpatialFiducialsStorage	1.2.840.10008.5.1.4.1.1.66.2
SecondaryCaptureImageStorage	1.2.840.10008.5.1.4.1.1.7
MultiframeSingleBitSecondaryCaptureImageStorage	1.2.840.10008.5.1.4.1.1.7.1
MultiframeGrayscaleByteSecondaryCaptureImageStorage	1.2.840.10008.5.1.4.1.1.7.2
MultiframeGrayscaleWordSecondaryCaptureImageStorage	1.2.840.10008.5.1.4.1.1.7.3
MultiframeTrueColorSecondaryCaptureImageStorage	1.2.840.10008.5.1.4.1.1.7.4
VLEndoscopicImageStorage	1.2.840.10008.5.1.4.1.1.77.1.1
VideoEndoscopicImageStorage	1.2.840.10008.5.1.4.1.1.77.1.1.1
VLMicroscopicImageStorage	1.2.840.10008.5.1.4.1.1.77.1.2
VideoMicroscopicImageStorage	1.2.840.10008.5.1.4.1.1.77.1.2.1
VLSlideCoordinatesMicroscopicImageStorage	1.2.840.10008.5.1.4.1.1.77.1.3
VLPhotographicImageStorage	1.2.840.10008.5.1.4.1.1.77.1.4
VideoPhotographicImageStorage	1.2.840.10008.5.1.4.1.1.77.1.4.1
Ophthalmic8BitPhotographyImageStorage	1.2.840.10008.5.1.4.1.1.77.1.5.1
Ophthalmic16BitPhotographyImageStorage	1.2.840.10008.5.1.4.1.1.77.1.5.2
StereometricRelationshipStorage	1.2.840.10008.5.1.4.1.1.77.1.5.3
BasicTextSR	1.2.840.10008.5.1.4.1.1.88.11
EnhancedSR	1.2.840.10008.5.1.4.1.1.88.22
ComprehensiveSR	1.2.840.10008.5.1.4.1.1.88.33
ProcedureLogStorage	1.2.840.10008.5.1.4.1.1.88.40
MammographyCADSR	1.2.840.10008.5.1.4.1.1.88.50
KeyObjectSelectionDocument	1.2.840.10008.5.1.4.1.1.88.59
ChestCADSR	1.2.840.10008.5.1.4.1.1.88.65
TwelveLeadECGWaveformStorage	1.2.840.10008.5.1.4.1.1.9.1.1
GeneralECGWaveformStorage	1.2.840.10008.5.1.4.1.1.9.1.2
AmbulatoryECGWaveformStorage	1.2.840.10008.5.1.4.1.1.9.1.3
HemodynamicWaveformStorage	1.2.840.10008.5.1.4.1.1.9.2.1
CardiacElectrophysiologyWaveformStorage	1.2.840.10008.5.1.4.1.1.9.3.1
BasicVoiceAudioWaveformStorage	1.2.840.10008.5.1.4.1.1.9.4.1

JVSdicom Workstation will accept presentation contexts for all of the above mentioned supported SOP Classes using any of the transfer syntaxes:

LittleEndianImplicitTransferSyntax	1.2.840.10008.1.2
LittleEndianExplicitTransferSyntax	1.2.840.10008.1.2.1
BigEndianExplicitTransferSyntax	1.2.840.10008.1.2.2

With VLMicroscopicImageStorage SOP Class, the JPIP referenced TS is also supported:

JPIPReferencedTransferSyntax	1.2.840.10008.1.2.4.94

Appendix C: JVSdicom Workstation DICOM SCU conformance

JVSdicom Workstation supports the following SOP Classes as an SCU:

VerificationSOPClass	1.2.840.10008.1.1
StoredPrintStorage	1.2.840.10008.5.1.1.27
HardcopyGrayscaleImageStorage	1.2.840.10008.5.1.1.29
HardcopyColorImageStorage	1.2.840.10008.5.1.1.30
ComputedRadiographyImageStorage	1.2.840.10008.5.1.4.1.1.1
DigitalXRayImageStorageForPresentation	1.2.840.10008.5.1.4.1.1.1.1
DigitalXRayImageStorageForProcessing	1.2.840.10008.5.1.4.1.1.1.1.1
DigitalMammographyXRayImageStorageForPresentation	1.2.840.10008.5.1.4.1.1.1.2
DigitalMammographyXRayImageStorageForProcessing	1.2.840.10008.5.1.4.1.1.1.2.1
DigitalIntraOralXRayImageStorageForPresentation	1.2.840.10008.5.1.4.1.1.1.3
DigitalIntraOralXRayImageStorageForProcessing	1.2.840.10008.5.1.4.1.1.1.3.1
StandaloneModalityLUTStorage	1.2.840.10008.5.1.4.1.1.10
EncapsulatedPDFStorage	1.2.840.10008.5.1.4.1.1.104.1
StandaloneVOILUTStorage	1.2.840.10008.5.1.4.1.1.11
GrayscaleSoftcopyPresentationStateStorage	1.2.840.10008.5.1.4.1.1.11.1
ColorSoftcopyPresentationStateStorage	1.2.840.10008.5.1.4.1.1.11.2
PseudoColorSoftcopyPresentationStateStorage	1.2.840.10008.5.1.4.1.1.11.3
BlendingSoftcopyPresentationStateStorage	1.2.840.10008.5.1.4.1.1.11.4
XRayAngiographicImageStorage	1.2.840.10008.5.1.4.1.1.12.1
EnhancedXAImageStorage	1.2.840.10008.5.1.4.1.1.12.1.1
XRayFluoroscopyImageStorage	1.2.840.10008.5.1.4.1.1.12.2
EnhancedXRFImageStorage	1.2.840.10008.5.1.4.1.1.12.2.1
RETIRED_XRayAngiographicBiPlaneImageStorage	1.2.840.10008.5.1.4.1.1.12.3
PETImageStorage	1.2.840.10008.5.1.4.1.1.128
PETCurveStorage	1.2.840.10008.5.1.4.1.1.129
CTImageStorage	1.2.840.10008.5.1.4.1.1.2
EnhancedCTImageStorage	1.2.840.10008.5.1.4.1.1.2.1
NuclearMedicineImageStorage	1.2.840.10008.5.1.4.1.1.20
RETIRED_UltrasoundMultiframeImageStorage	1.2.840.10008.5.1.4.1.1.3
UltrasoundMultiframeImageStorage	1.2.840.10008.5.1.4.1.1.3.1
MRImageStorage	1.2.840.10008.5.1.4.1.1.4
EnhancedMRImageStorage	1.2.840.10008.5.1.4.1.1.4.1
MRSpectroscopyStorage	1.2.840.10008.5.1.4.1.1.4.2
RTImageStorage	1.2.840.10008.5.1.4.1.1.481.1
RTDoseStorage	1.2.840.10008.5.1.4.1.1.481.2
RTStructureSetStorage	1.2.840.10008.5.1.4.1.1.481.3
RTBeamsTreatmentRecordStorage	1.2.840.10008.5.1.4.1.1.481.4
RTPlanStorage	1.2.840.10008.5.1.4.1.1.481.5
RTBrachyTreatmentRecordStorage	1.2.840.10008.5.1.4.1.1.481.6
RTTreatmentSummaryRecordStorage	1.2.840.10008.5.1.4.1.1.481.7
RETIRED_NuclearMedicineImageStorage	1.2.840.10008.5.1.4.1.1.5
RETIRED_UltrasoundImageStorage	1.2.840.10008.5.1.4.1.1.6
UltrasoundImageStorage	1.2.840.10008.5.1.4.1.1.6.1
RawDataStorage	1.2.840.10008.5.1.4.1.1.66
SpatialRegistrationStorage	1.2.840.10008.5.1.4.1.1.66.1
SpatialFiducialsStorage	1.2.840.10008.5.1.4.1.1.66.2
RealWorldValueMappingStorage	1.2.840.10008.5.1.4.1.1.67

SecondaryCaptureImageStorage	1.2.840.10008.5.1.4.1.1.7
MultiframeSingleBitSecondaryCaptureImageStorage	1.2.840.10008.5.1.4.1.1.7.1
MultiframeGrayscaleByteSecondaryCaptureImageStorage	1.2.840.10008.5.1.4.1.1.7.2
MultiframeGrayscaleWordSecondaryCaptureImageStorage	1.2.840.10008.5.1.4.1.1.7.3
MultiframeTrueColorSecondaryCaptureImageStorage	1.2.840.10008.5.1.4.1.1.7.4
RETIRED_VLImageStorage	1.2.840.10008.5.1.4.1.1.77.1
VLEndoscopicImageStorage	1.2.840.10008.5.1.4.1.1.77.1.1
VideoEndoscopicImageStorage	1.2.840.10008.5.1.4.1.1.77.1.1.1
VLMicroscopicImageStorage	1.2.840.10008.5.1.4.1.1.77.1.2
VideoMicroscopicImageStorage	1.2.840.10008.5.1.4.1.1.77.1.2.1
VLSlideCoordinatesMicroscopicImageStorage	1.2.840.10008.5.1.4.1.1.77.1.3
VLPhotographicImageStorage	1.2.840.10008.5.1.4.1.1.77.1.4
VideoPhotographicImageStorage	1.2.840.10008.5.1.4.1.1.77.1.4.1
OphthalmicPhotography8BitImageStorage	1.2.840.10008.5.1.4.1.1.77.1.5.1
OphthalmicPhotography16BitImageStorage	1.2.840.10008.5.1.4.1.1.77.1.5.2
StereometricRelationshipStorage	1.2.840.10008.5.1.4.1.1.77.1.5.3
RETIRED_VLMultiFrameImageStorage	1.2.840.10008.5.1.4.1.1.77.2
StandaloneOverlayStorage	1.2.840.10008.5.1.4.1.1.8
DRAFT_SRTextStorage	1.2.840.10008.5.1.4.1.1.88.1
DRAFT_SRAudioStorage	1.2.840.10008.5.1.4.1.1.88.2
DRAFT_SRDetailStorage	1.2.840.10008.5.1.4.1.1.88.3
DRAFT_SRComprehensiveStorage	1.2.840.10008.5.1.4.1.1.88.4
BasicTextSR	1.2.840.10008.5.1.4.1.1.88.11
EnhancedSR	1.2.840.10008.5.1.4.1.1.88.22
ComprehensiveSR	1.2.840.10008.5.1.4.1.1.88.33
ProcedureLogStorage	1.2.840.10008.5.1.4.1.1.88.40
MammographyCADSR	1.2.840.10008.5.1.4.1.1.88.50
KeyObjectSelectionDocument	1.2.840.10008.5.1.4.1.1.88.59
ChestCADSR	1.2.840.10008.5.1.4.1.1.88.65
XRayRadiationDoseSR	1.2.840.10008.5.1.4.1.1.88.67
StandaloneCurveStorage	1.2.840.10008.5.1.4.1.1.9
DRAFT_WaveformStorage	1.2.840.10008.5.1.4.1.1.9.1
TwelveLeadECGWaveformStorage	1.2.840.10008.5.1.4.1.1.9.1.1
GeneralECGWaveformStorage	1.2.840.10008.5.1.4.1.1.9.1.2
AmbulatoryECGWaveformStorage	1.2.840.10008.5.1.4.1.1.9.1.3
HemodynamicWaveformStorage	1.2.840.10008.5.1.4.1.1.9.2.1
CardiacElectrophysiologyWaveformStorage	1.2.840.10008.5.1.4.1.1.9.3.1
BasicVoiceAudioWaveformStorage	1.2.840.10008.5.1.4.1.1.9.4.1

JVSdicom Workstation will propose presentation contexts for all of the abovementioned supported SOP Classes using the transfer syntaxes:

LittleEndianImplicitTransferSyntax	1.2.840.10008.1.2
LittleEndianExplicitTransferSyntax	1.2.840.10008.1.2.1
BigEndianExplicitTransferSyntax	1.2.840.10008.1.2.2
JPIPReferencedTransferSyntax	1.2.840.10008.1.2.4.94

Appendix D: JVSdicom Server DICOM SCP conformance

JVSdicom Server supports the following SOP Classes as an SCP:

VerificationSOPClass	1.2.840.10008.1.1
FINDPatientRootQueryRetrieveInformationModel	1.2.840.10008.5.1.4.1.2.1.1
FINDPatientStudyOnlyQueryRetrieveInformationModel	1.2.840.10008.5.1.4.1.2.3.1
FINDStudyRootQueryRetrieveInformationModel	1.2.840.10008.5.1.4.1.2.2.1

GETPatientRootQueryRetrieveInformationModel	1.2.840.10008.5.1.4.1.2.1.3
GETPatientStudyOnlyQueryRetrieveInformationModel	1.2.840.10008.5.1.4.1.2.3.3
GETStudyRootQueryRetrieveInformationModel	1.2.840.10008.5.1.4.1.2.2.3
MOVEPatientRootQueryRetrieveInformationModel	1.2.840.10008.5.1.4.1.2.1.2
MOVEPatientStudyOnlyQueryRetrieveInformationModel	1.2.840.10008.5.1.4.1.2.3.2
MOVEStudyRootQueryRetrieveInformationModel	1.2.840.10008.5.1.4.1.2.2.2
StoredPrintStorage	1.2.840.10008.5.1.1.27
HardcopyGrayscaleImageStorage	1.2.840.10008.5.1.1.29
HardcopyColorImageStorage	1.2.840.10008.5.1.1.30
ComputedRadiographyImageStorage	1.2.840.10008.5.1.4.1.1.1
DigitalXRayImageStorageForPresentation	1.2.840.10008.5.1.4.1.1.1.1
DigitalXRayImageStorageForProcessing	1.2.840.10008.5.1.4.1.1.1.1.1
DigitalMammographyXRayImageStorageForPresentation	1.2.840.10008.5.1.4.1.1.1.2
DigitalMammographyXRayImageStorageForProcessing	1.2.840.10008.5.1.4.1.1.1.2.1
DigitalIntraOralXRayImageStorageForPresentation	1.2.840.10008.5.1.4.1.1.1.3
DigitalIntraOralXRayImageStorageForProcessing	1.2.840.10008.5.1.4.1.1.1.3.1
GrayscaleSoftcopyPresentationStateStorage	1.2.840.10008.5.1.4.1.1.11.1
XRayAngiographicImageStorage	1.2.840.10008.5.1.4.1.1.12.1
XRayFluoroscopyImageStorage	1.2.840.10008.5.1.4.1.1.12.2
PETImageStorage	1.2.840.10008.5.1.4.1.1.128
PETCurveStorage	1.2.840.10008.5.1.4.1.1.129
CTImageStorage	1.2.840.10008.5.1.4.1.1.2
EnhancedCTImageStorage	1.2.840.10008.5.1.4.1.1.2.1
NuclearMedicineImageStorage	1.2.840.10008.5.1.4.1.1.20
RETIRED_UltrasoundMultiframeImageStorage	1.2.840.10008.5.1.4.1.1.3
UltrasoundMultiframeImageStorage	1.2.840.10008.5.1.4.1.1.3.1
MRImageStorage	1.2.840.10008.5.1.4.1.1.4
EnhancedMRImageStorage	1.2.840.10008.5.1.4.1.1.4.1
MRSpectroscopyStorage	1.2.840.10008.5.1.4.1.1.4.2
RTImageStorage	1.2.840.10008.5.1.4.1.1.481.1
RTDoseStorage	1.2.840.10008.5.1.4.1.1.481.2
RTStructureSetStorage	1.2.840.10008.5.1.4.1.1.481.3
RTBeamsTreatmentRecordStorage	1.2.840.10008.5.1.4.1.1.481.4
RTPlanStorage	1.2.840.10008.5.1.4.1.1.481.5
RTBrachyTreatmentRecordStorage	1.2.840.10008.5.1.4.1.1.481.6
RTTreatmentSummaryRecordStorage	1.2.840.10008.5.1.4.1.1.481.7
RETIRED_UltrasoundImageStorage	1.2.840.10008.5.1.4.1.1.6
UltrasoundImageStorage	1.2.840.10008.5.1.4.1.1.6.1
RawDataStorage	1.2.840.10008.5.1.4.1.1.66
SpatialRegistrationStorage	1.2.840.10008.5.1.4.1.1.66.1
SpatialFiducialsStorage	1.2.840.10008.5.1.4.1.1.66.2
SecondaryCaptureImageStorage	1.2.840.10008.5.1.4.1.1.7
MultiframeSingleBitSecondaryCaptureImageStorage	1.2.840.10008.5.1.4.1.1.7.1
MultiframeGrayscaleByteSecondaryCaptureImageStorage	1.2.840.10008.5.1.4.1.1.7.2
MultiframeGrayscaleWordSecondaryCaptureImageStorage	1.2.840.10008.5.1.4.1.1.7.3
MultiframeTrueColorSecondaryCaptureImageStorage	1.2.840.10008.5.1.4.1.1.7.4
VLEndoscopicImageStorage	1.2.840.10008.5.1.4.1.1.77.1.1
VideoEndoscopicImageStorage	1.2.840.10008.5.1.4.1.1.77.1.1.1
VLMicroscopicImageStorage	1.2.840.10008.5.1.4.1.1.77.1.2
VideoMicroscopicImageStorage	1.2.840.10008.5.1.4.1.1.77.1.2.1
VLSlideCoordinatesMicroscopicImageStorage	1.2.840.10008.5.1.4.1.1.77.1.3
VLPhotographicImageStorage	1.2.840.10008.5.1.4.1.1.77.1.4
VideoPhotographicImageStorage	1.2.840.10008.5.1.4.1.1.77.1.4.1
Ophthalmic8BitPhotographyImageStorage	1.2.840.10008.5.1.4.1.1.77.1.5.1
Ophthalmic16BitPhotographyImageStorage	1.2.840.10008.5.1.4.1.1.77.1.5.2
StereometricRelationshipStorage	1.2.840.10008.5.1.4.1.1.77.1.5.3
BasicTextSR	1.2.840.10008.5.1.4.1.1.88.11
EnhancedSR	1.2.840.10008.5.1.4.1.1.88.22
ComprehensiveSR	1.2.840.10008.5.1.4.1.1.88.33
ProcedureLogStorage	1.2.840.10008.5.1.4.1.1.88.40
MammographyCADSR	1.2.840.10008.5.1.4.1.1.88.50
KeyObjectSelectionDocument	1.2.840.10008.5.1.4.1.1.88.59
ChestCADSR	1.2.840.10008.5.1.4.1.1.88.65
TwelveLeadECGWaveformStorage	1.2.840.10008.5.1.4.1.1.9.1.1
GeneralECGWaveformStorage	1.2.840.10008.5.1.4.1.1.9.1.2
AmbulatoryECGWaveformStorage	1.2.840.10008.5.1.4.1.1.9.1.3
HemodynamicWaveformStorage	1.2.840.10008.5.1.4.1.1.9.2.1
CardiacElectrophysiologyWaveformStorage	1.2.840.10008.5.1.4.1.1.9.3.1

BasicVoiceAudioWaveformStorage	1.2.840.10008.5.1.4.1.1.9.4.1

JVSdicom Server will accept presentation contexts for all of the above mentioned supported SOP Classes using any of the transfer syntaxes:

LittleEndianImplicitTransferSyntax	1.2.840.10008.1.2
LittleEndianExplicitTransferSyntax	1.2.840.10008.1.2.1
BigEndianExplicitTransferSyntax	1.2.840.10008.1.2.2

With VLMicroscopicImageStorage SOP Class, the JPIP referenced TS is also supported:

JPIPReferencedTransferSyntax	1.2.840.10008.1.2.4.94

Appendix E: JVSdicom Server DICOM SCU conformance

JVSdicom Server supports the following SOP Classes as an SCU:

VerificationSOPClass	1.2.840.10008.1.1
StoredPrintStorage	1.2.840.10008.5.1.1.27
HardcopyGrayscaleImageStorage	1.2.840.10008.5.1.1.29
HardcopyColorImageStorage	1.2.840.10008.5.1.1.30
ComputedRadiographyImageStorage	1.2.840.10008.5.1.4.1.1.1
DigitalXRayImageStorageForPresentation	1.2.840.10008.5.1.4.1.1.1.1
DigitalXRayImageStorageForProcessing	1.2.840.10008.5.1.4.1.1.1.1.1
DigitalMammographyXRayImageStorageForPresentation	1.2.840.10008.5.1.4.1.1.1.2
DigitalMammographyXRayImageStorageForProcessing	1.2.840.10008.5.1.4.1.1.1.2.1
DigitalIntraOralXRayImageStorageForPresentation	1.2.840.10008.5.1.4.1.1.1.3
DigitalIntraOralXRayImageStorageForProcessing	1.2.840.10008.5.1.4.1.1.1.3.1
StandaloneModalityLUTStorage	1.2.840.10008.5.1.4.1.1.10
EncapsulatedPDFStorage	1.2.840.10008.5.1.4.1.1.104.1
StandaloneVOILUTStorage	1.2.840.10008.5.1.4.1.1.11
GrayscaleSoftcopyPresentationStateStorage	1.2.840.10008.5.1.4.1.1.11.1
ColorSoftcopyPresentationStateStorage	1.2.840.10008.5.1.4.1.1.11.2
PseudoColorSoftcopyPresentationStateStorage	1.2.840.10008.5.1.4.1.1.11.3
BlendingSoftcopyPresentationStateStorage	1.2.840.10008.5.1.4.1.1.11.4
XRayAngiographicImageStorage	1.2.840.10008.5.1.4.1.1.12.1
EnhancedXAImageStorage	1.2.840.10008.5.1.4.1.1.12.1.1
XRayFluoroscopyImageStorage	1.2.840.10008.5.1.4.1.1.12.2
EnhancedXRFImageStorage	1.2.840.10008.5.1.4.1.1.12.2.1
RETIRED_XRayAngiographicBiPlaneImageStorage	1.2.840.10008.5.1.4.1.1.12.3
PETImageStorage	1.2.840.10008.5.1.4.1.1.128
PETCurveStorage	1.2.840.10008.5.1.4.1.1.129
CTImageStorage	1.2.840.10008.5.1.4.1.1.2
EnhancedCTImageStorage	1.2.840.10008.5.1.4.1.1.2.1
NuclearMedicineImageStorage	1.2.840.10008.5.1.4.1.1.20
RETIRED_UltrasoundMultiframeImageStorage	1.2.840.10008.5.1.4.1.1.3
UltrasoundMultiframeImageStorage	1.2.840.10008.5.1.4.1.1.3.1
MRImageStorage	1.2.840.10008.5.1.4.1.1.4
EnhancedMRImageStorage	1.2.840.10008.5.1.4.1.1.4.1

MRSpectroscopyStorage	1.2.840.10008.5.1.4.1.1.4.2
RTImageStorage	1.2.840.10008.5.1.4.1.1.481.1
RTDoseStorage	1.2.840.10008.5.1.4.1.1.481.2
RTStructureSetStorage	1.2.840.10008.5.1.4.1.1.481.3
RTBeamsTreatmentRecordStorage	1.2.840.10008.5.1.4.1.1.481.4
RTPlanStorage	1.2.840.10008.5.1.4.1.1.481.5
RTBrachyTreatmentRecordStorage	1.2.840.10008.5.1.4.1.1.481.6
RTTreatmentSummaryRecordStorage	1.2.840.10008.5.1.4.1.1.481.7
RETIRED_NuclearMedicineImageStorage	1.2.840.10008.5.1.4.1.1.5
RETIRED_UltrasoundImageStorage	1.2.840.10008.5.1.4.1.1.6
UltrasoundImageStorage	1.2.840.10008.5.1.4.1.1.6.1
RawDataStorage	1.2.840.10008.5.1.4.1.1.66
SpatialRegistrationStorage	1.2.840.10008.5.1.4.1.1.66.1
SpatialFiducialsStorage	1.2.840.10008.5.1.4.1.1.66.2
RealWorldValueMappingStorage	1.2.840.10008.5.1.4.1.1.67
SecondaryCaptureImageStorage	1.2.840.10008.5.1.4.1.1.7
MultiframeSingleBitSecondaryCaptureImageStorage	1.2.840.10008.5.1.4.1.1.7.1
MultiframeGrayscaleByteSecondaryCaptureImageStorage	1.2.840.10008.5.1.4.1.1.7.2
MultiframeGrayscaleWordSecondaryCaptureImageStorage	1.2.840.10008.5.1.4.1.1.7.3
MultiframeTrueColorSecondaryCaptureImageStorage	1.2.840.10008.5.1.4.1.1.7.4
RETIRED_VLImageStorage	1.2.840.10008.5.1.4.1.1.77.1
VLEndoscopicImageStorage	1.2.840.10008.5.1.4.1.1.77.1.1
VideoEndoscopicImageStorage	1.2.840.10008.5.1.4.1.1.77.1.1.1
VLMicroscopicImageStorage	1.2.840.10008.5.1.4.1.1.77.1.2
VideoMicroscopicImageStorage	1.2.840.10008.5.1.4.1.1.77.1.2.1
VLSlideCoordinatesMicroscopicImageStorage	1.2.840.10008.5.1.4.1.1.77.1.3
VLPhotographicImageStorage	1.2.840.10008.5.1.4.1.1.77.1.4
VideoPhotographicImageStorage	1.2.840.10008.5.1.4.1.1.77.1.4.1
OphthalmicPhotography8BitImageStorage	1.2.840.10008.5.1.4.1.1.77.1.5.1
OphthalmicPhotography16BitImageStorage	1.2.840.10008.5.1.4.1.1.77.1.5.2
StereometricRelationshipStorage	1.2.840.10008.5.1.4.1.1.77.1.5.3
RETIRED_VLMultiFrameImageStorage	1.2.840.10008.5.1.4.1.1.77.2
StandaloneOverlayStorage	1.2.840.10008.5.1.4.1.1.8
DRAFT_SRTextStorage	1.2.840.10008.5.1.4.1.1.88.1
DRAFT_SRAudioStorage	1.2.840.10008.5.1.4.1.1.88.2
DRAFT_SRDetailStorage	1.2.840.10008.5.1.4.1.1.88.3
DRAFT_SRComprehensiveStorage	1.2.840.10008.5.1.4.1.1.88.4
BasicTextSR	1.2.840.10008.5.1.4.1.1.88.11
EnhancedSR	1.2.840.10008.5.1.4.1.1.88.22
ComprehensiveSR	1.2.840.10008.5.1.4.1.1.88.33
ProcedureLogStorage	1.2.840.10008.5.1.4.1.1.88.40
MammographyCADSR	1.2.840.10008.5.1.4.1.1.88.50
KeyObjectSelectionDocument	1.2.840.10008.5.1.4.1.1.88.59
ChestCADSR	1.2.840.10008.5.1.4.1.1.88.65
XRayRadiationDoseSR	1.2.840.10008.5.1.4.1.1.88.67
StandaloneCurveStorage	1.2.840.10008.5.1.4.1.1.9
DRAFT_WaveformStorage	1.2.840.10008.5.1.4.1.1.9.1
TwelveLeadECGWaveformStorage	1.2.840.10008.5.1.4.1.1.9.1.1
GeneralECGWaveformStorage	1.2.840.10008.5.1.4.1.1.9.1.2
AmbulatoryECGWaveformStorage	1.2.840.10008.5.1.4.1.1.9.1.3
HemodynamicWaveformStorage	1.2.840.10008.5.1.4.1.1.9.2.1
CardiacElectrophysiologyWaveformStorage	1.2.840.10008.5.1.4.1.1.9.3.1
BasicVoiceAudioWaveformStorage	1.2.840.10008.5.1.4.1.1.9.4.1

JVSdicom Server will propose presentation contexts for all of the abovementioned supported SOP Classes using the transfer syntaxes:

LittleEndianImplicitTransferSyntax	1.2.840.10008.1.2
LittleEndianExplicitTransferSyntax	1.2.840.10008.1.2.1
BigEndianExplicitTransferSyntax	1.2.840.10008.1.2.2
JPIPReferencedTransferSyntax	1.2.840.10008.1.2.4.94

ORIGINAL COMMUNICATIONS

The Application of JPEG2000 in Virtual Microscopy

Vilppu J Tuominen[1] and Jorma Isola[2]

[1] Institute of Medical Technology, University of Tampere and Tampere University Hospital, 33014 Tampere, Finland (vilppu.tuominen@uta.fi)

[2] Institute of Medical Technology, University of Tampere and Tampere University Hospital, 33014 Tampere, Finland (jorma.isola@uta.fi)

J Digit Imaging. 2009 Jun;22(3):250-8.

AUTHOR PRE-PRINT VERSION

Address for correspondence

Prof. Jorma Isola
Institute of Medical Technology, University of Tampere,
33014 Tampere, Finland.

Email: Jorma.Isola@uta.fi
Tel. +358-3-35516729
Fax. +358-3-35518923

ABSTRACT

Virtual microscopy (i.e., the viewing of entire microscope specimens on a computer display) is becoming widely applied in microscopy teaching and clinical laboratory medicine. Despite rapidly increasing use, virtual microscopy currently lacks of a universally accepted image format. A promising candidate is JPEG2000, which has potential advantages for handling gigabyte-sized virtual slides. To date, no JPEG2000-based software has been specifically suited for virtual microscopy. To study the utility of JPEG2000 in virtual microscopy, we first optimized JPEG2000 code-stream parameters for virtual slide viewing (i.e., fast navigation, zooming, and use of an overview window). Compression using ratios 25:1–30:1 with the irreversible wavelet filter were found to provide the best compromise between file size and image quality. Optimal code-stream parameters also consisted of 10 wavelet decomposition levels, progression order Resolution-Position-Component-Layer (RPCL), a precinct size of 128×128, and code-block size of 64×64. Tiling and the use of multiple quality layers were deemed unnecessary. A compression application (JVScomp) was developed for creating optimally parameterized JPEG2000 virtual slides. A viewing application (JVSview) was developed specifically for virtual microscopy, offering all of the basic viewing functions. JVSview also supports viewing of focus stacks, embedding of textual descriptions, and defining regions of interest as metadata. Combined with our server application (JVSserv), virtual slides can be viewed over networks by employing the JPEG2000 Interactive Protocol (JPIP). The software can be tested using virtual slide examples located on our public JPIP server (http://jvsmicroscope. uta.fi/). The software package is freely downloadable and usable for non-commercial purposes.

Keywords: JPEG2000, JPIP, telepathology, digital pathology, virtual slide

BACKGROUND

Virtual slides are digitized versions of whole microscope specimens that can be viewed on a computer display.[1] Virtual slide image files can be accessed from the computer hard disk, transportable media (e.g., a USB memory stick or a DVD), or, more practically, over networks.[2] Within the internal network of a hospital or pathology department, virtual slides can be used for case meetings, slide seminars, and didactic live audience presentations.[3] By allowing access over the internet, virtual slides can be used more widely for national and international conferences and in inter-laboratory quality assurance programmes.[4] Feedback from microscopists shows that virtual microscopy can be regarded as a significant improvement over digital snapshot images and the use of multi-headed microscopes.[5,6]

To create virtual slides that resemble real microscopy viewing experiences, specimens must be scanned at high optical resolution. Image resolutions from 0.20 to 0.40 μm per pixel are considered necessary for sufficient image quality.[7] Since microscope specimens are often up to 20×30 mm in size, a virtual slide can contain up to 40 gigabytes of uncompressed image data (with three 8-bit colour channels). When virtual slides are applied in cytopathology or hematology, a higher optical magnification (scanning with oil-40×, oil-60×, or oil-100× lens) is often needed.[8] This multiplies the amount of image data produced when compared to standard scanning. Moreover, when several focus planes (along Z-axis) are digitized, the resulting data amount is further multiplied by the number of planes. Due to the large size of the virtual slide files, it is not possible to use conventional image viewing software (such as Photoshop®), which requires the image data to be loaded entirely into computer's memory (RAM). For this reason, the virtual slide viewing systems described to date apply the on-demand principle, that is, the viewing software decodes and displays only a user-requested area of the virtual slide at the requested resolution. When using JPEG-compressed images, this requires splitting the virtual slide image data into tens of thousands of very small image files, which are uploaded to the client on demand (e.g., Zoomify).[9] Proprietary

image formats provided with commercial slide scanners (e.g., Mirax by Carl Zeiss MicroImaging, USA; dotSlide by Olympus UK, UK; and ScanScope® by Aperio Technologies, USA) also follow this principle in their web viewing solutions. Due to competition, it is unlikely that any of the proprietary industry-based image formats will become universally accepted in virtual microscopy.

A promising candidate for a universal image format for virtual microscopy is JPEG2000, which is a family of standards, developed by the Joint Photographic Experts Group.[10] It is based on a wavelet-based compression scheme that is defined in the core part of the standard series (published as International Standard ISO/IEC 15444-1 | ITU-T Rec. T.800).[11] JPEG2000 provides many features that support scalable and interactive access to large-sized images such as virtual slides. These include an efficient and unified compression architecture, especially at low bit-rates, resolution and quality scalability, region of interest coding, spatial random access, and effective error resiliency.[12–14] Currently, the JPEG2000 standard consists of 11 parts, which describe techniques that are useful in various areas of imaging. Part 1 (Core Coding System),[11] Part 2 (Extensions),[15] and Part 9 (Interactivity Tools, APIs and Protocols)[16] are the most essential for virtual microscopy. The first part specifies the JPEG2000 code-stream syntax and the JP2 file format ("jp2" as the common file extension), which offers, for example, the possibility of adding textual metadata into the image header. The second part specifies the JPX file format ("jpx" and "jpf" as the common file extensions), which contains more advanced features, such as building stacks of images (e.g., for specimens scanned at multiple focal depths), and associating textual and graphical metadata with spatial regions. The ninth part defines the JPEG2000 Interactive Protocol (JPIP), which provides a client–server architecture for network-based remote viewing of JPEG2000 family images.[17] Currently, web browsers do not have direct, built-in support for JPIP. For this reason, internet-based viewing of virtual slides over JPIP requires external viewing software, which is, for example, invoked automatically from the browser upon clicking on a virtual slide URL link.

Although JPEG2000 has theoretical advantages for application in virtual microscopy, no efficient application software has been described so far. The computational demands of virtual microscopy images differ to a large extent from that of radiology and other medical imaging because of the larger size of the image files (up to tens of gigabytes). In this study, we first searched for an optimal parameterization of JPEG2000 for virtual microscopy and constructed a JPEG2000-based software package entitled JVS (for JPEG2000 Virtual Slide), consisting of image compression, viewing, and network server applications. The performance of JPEG2000 was evaluated using JPIP image serving speed and compression execution time as outcome measures. In addition, the performance of our network server application (JVSserv) was compared against the commonly used virtual slide server solution Zoomify.[9] Finally, we present a model for a simple, scalable, and inexpensive JPEG2000-based virtual microscopy system.

MATERIALS AND METHODS

Image Acquisition

We acquired test images by using a Zeiss Axioskop40 microscope (Carl Zeiss MicroImaging, USA) which was equipped with 10×, 20× and oil-40× objectives and a motorized specimen stage (Märzhäuser Wetzlar GmbH, Germany). The images were captured with a CCD colour camera (QICAM Fast, QImaging, Canada; 24-bit colour depth; resolution 1,388×1,036 pixels, pixel size 4.65 μm). The camera was attached to the microscope with a 1× phototube. Image acquisition was controlled by the Surveyor imaging system (Objective Imaging, UK, software version 5.03) running on a standard Windows® XP workstation. The Surveyor software controls for stage and focus movements matched with automated image acquisition. In addition to standard histological samples, cytological slides were scanned using a multiple focus layer image acquisition option (Z-stack). Image tiles (up to 5,000 per scanned slide) were primarily saved in an uncompressed file format (BMP) and stitched as a contiguous montage either using the built-in function of Surveyor, or using the LargeMontage plugin[18] of the publicly available image analysis software ImageJ.[19]

JPEG2000 Code-Stream Parameter Optimization

The JPEG2000 code-stream parameter optimization was based on theoretical assumptions of the JPEG2000 code-stream properties, visual assessment of the time needed to initially load the image, the time needed for image refreshment during magnification change and navigation within the specimen, and to lesser extent, the compression execution time. Tests were performed using the highly configurable Kakadu kdu_compress and kdu_show applications, version 5.2.2.[20]

JPEG2000 Performance Evaluation

The performance of JPEG2000 was evaluated using JPIP image serving speed and compression execution time as outcome measures. The tests were carried out on a Windows® XP workstation, equipped with a dual-core processor, 3 gigabytes of RAM, two ATA hard disks, and a 100 Mbit network link. The used main test virtual slide image can be seen on our website (http://jvsmicroscope.uta.fi/examples/). The image had 42,865×57,222 pixels, three 8-bit colour channels, totalling 6.9 gigabytes uncompressed, and it was stored as a binary encoded PPM file. An additional set of test images was created by extracting sub-resolutions from the original image, halving the resolution in each step.

The compression tests were performed using our JVScomp application. During these tests, we monitored the processor load, RAM usage, disk usage percentage, and the average disk read and write queue lengths. The image serving performance of JPIP was evaluated with our JVSserv application, in comparison to the Zoomifyer EZ™, version 3.0.9 While JVSserv is a standalone server application, Zoomifyer requires an external HTTP server underneath it. The Apache HTTP server, version 2.2.4,[21] was selected for this. The evaluation and comparison were performed by simulation, in which 10 local area network workstations were each simulating 10 clients, yielding a 100-client pool. Each client had their own test image, which was duplicated from the main test image. Server and client caches were disabled. During these simulations, we monitored the server's average disk read queue length, processor load, network bandwidth usage, RAM usage, and subjectively evaluated the clients' viewing interactivity.

Software Package Development

The demonstrational software package was written with the C++ programming language and built for 32-bit Windows® platforms, but can be run under a 64-bit Windows® platform as well. The package consists of three applications: JVScomp—a compression application for creating optimally parameterized JPEG2000 virtual slides; JVSview—a viewer application capable of viewing both local and remote JPEG2000 virtual slides; and JVSserv—a JPIP server for remote serving of JPEG2000 virtual slides. JVScomp is built on the ECW JPEG 2000 SDK,[22] while JVSview and JVSserv are built on the Kakadu JPEG2000 Framework.[20]

RESULTS

JPEG2000 Code-Stream Parameter Optimization

To fully utilize the advantages of JPEG2000 in virtual microscopy, we first searched for an optimal combination of JPEG2000 code-stream parameters. The findings are summarized in Table 1. In virtual microscopy, lossy compression is mandatory due to the large amount of image data. It is shown that highly compressed JPEG2000 images can be used for pathological diagnostic studies.[23] We found compression ratios ranging from 25:1 to 30:1 in areas containing cells or tissue sections to produce virtual slides without disturbing visible image compression artefacts at the original image resolution. A comparison of the image quality between different JPEG2000 lossy compression ratios is demonstrated on our website (http://jvsmicroscope.uta.fi/examples/).

Of the two alternative wavelet filters (reversible and irreversible), the irreversible filter yielded somewhat better visual quality, but at the expense of compression speed. The Discrete Wavelet Transform (DWT) process decomposes the original image into several low-resolution versions. To

extract an overview image, we found 10 DWT levels to be sufficient for even the largest virtual slides, although this creates redundant resolution levels for smaller slides. Tiling and the use of multiple tile-parts were not found to be useful in virtual slides. Technically, an untiled JPEG2000 image actually contains a single tile whose size is identical to the image size. We found precincts to be a more useful alternative for partitioning the JPEG2000 code-stream for random access. A precinct size of 128×128 was a suitable average for all resolution levels. Precincts are further divided into code-blocks, the optimal size of which was 64×64. The progression order defines how packets—the basic segments of a JPEG2000 code-stream—are prioritized. We found the Resolution-Position-Component-Layer (RPCL) order most useful, since it allowed the fastest access to different image resolutions, as well as fast spatial random access. No particular advantages were found for multiple quality layers, since the gradual image quality improvement after navigation or zooming became noticeable only with very slow-speed JPIP connections. The JPEG2000 code-stream headers are composed of so-called markers and marker segments, which are used, for example, to specify the image size and to offer pointers to the code-stream. To further increase the code-stream random access, we found it advantageous to use packet length pointer marker segments within the tile-part header (PLT).

Table 1. JPEG2000 code-stream parameters found optimal for virtual microscopy.

JPEG2000 code-stream parameter	Parameter value
Compression ratio (lossy)	25:1 to 30:1
Wavelet filter	Irreversible
Wavelet decomposition levels	10
Tiling	Not needed
Tile-parts	1
Precinct size	128 × 128
Code-block size	64 × 64
Progression order	RPCL
Quality layers	1
PLT pointer marker segments	Inserted always

JPEG2000 Compression Performance

We performed various compression speed tests to ensure that JPEG2000 can be used within a real virtual microscopy scanning system. The duration of the compression process was linearly dependent on the original virtual slide image size. RAM usage was relatively low, as during the compression of a 7-gigabyte virtual slide the memory footprint of JVScomp constantly remained around 70 megabytes. JVScomp reached a compression speed of 50 gigabytes per hour on a dual-processor workstation. The limiting factor was the processor performance, as the source hard disk could have effectively processed over twice the number of read requests.

JPIP Image Serving Performance

We evaluated the serving performance of the JPIP protocol using our JVSserv application. In addition, a comparison was made to the commonly used Zoomifyer EZ™ virtual slide server solution. On both systems, virtual slide serving was limited by the speed of the hard disk; the processor load was constantly under 50%, as was the RAM allocation. The network bandwidth (100 Mbit/s in our tests) was utilized only about 25% of the maximum transmission rate. As the number of clients increased, the average disk read queue lengths quickly reached the effective performance limits (an average of 2.0 was considered to be a suitable limit).

With the main test virtual slide, which was duplicated for every client, JVSserv could effectively handle about 30 simultaneous clients, while the Zoomifyer (run on top of the Apache HTTP server) had its limit at around 20 simultaneous clients. The difference can be explained by the fact that Zoomifyer splits the image into tens of thousands of small JPEG files, which the HTTP server (Apache) then serves to the clients. Because of caching policies, both servers would have benefited for clients that browse the same image simultaneously. Thus, assuming that some clients are usually viewing the same image, JVSserv could easily serve 50 simultaneous clients.

Furthermore, JVSserv features a load balancing function, which can be used to distribute clients to several sub-servers. Thus, we estimate that a standard JVSserv workstation behind a 100 Mbit/s network link could handle 200 to 300 simultaneous clients when supplemented with 4 to 5 sub-servers.

Software Package Description

We developed the demonstrational JVS software package to illustrate the utility of JPEG2000 in virtual microscopy. The package is designed primarily for Windows® 2000 and XP, and is Windows Vista™ compatible. JVScomp is licensed under the GNU General Public License, while the binaries (i.e., the actual executable programs) for JVSview and JVSserv are released for free, non-commercial usage. The software package can be obtained from our website (http://jvsmicroscope.uta.fi/). Our website also features a public JPIP server with several virtual slide collections, which can be viewed using JVSview.

JVSview. This software is a JPEG2000 virtual slide viewer that works identically both in local storage and JPIP-based virtual slide viewing (Table 2). JVSview displays an overview of the entire sample and a detailed microscopic view. The magnifications have been set to mimic commonly used microscope objectives. The user can navigate around the sample using either the arrow keys, mouse panning, or by clicking on a location in the macroscopic view. The application allows the user to interactively adjust brightness, contrast and colour saturation of the main window. Multiple display devices can be used in full screen viewing mode. Viewing interactivity is dependent on the processor performance of the client workstation. Acceptable speed can already be achieved with conventional single-processor computers, although JVSview has an automatic support for multi-processor environments.

To illustrate new functionalities of virtual microscopy, made possible by advanced features of JPEG2000, we included a focus feature, which enables switching between alternative image layers, each representing the cells or tissue scanned

at different focal depth (see the examples on our website http://jvsmicroscope.uta.fi/examples/). We also included the possibility to embed short textual data conveniently within the header of the virtual slide file. The textual data, called metadata, can contain information on the scanning resolution, organ and histopathologic diagnosis, and the staining method, for example. The metadata is written in XML format and its structure is described formally with an XML schema;[24] it can be added and edited within JVSview. The metadata is primarily for the purposes of image collections, where the associated patient data is irrelevant (e.g., those used in teaching). JVSview also allows specifying and storing regions of interest (ROIs), which can then be retrieved from a ROI list by the clients. JVSview also provides a functional link with ImageJ,[19] which is an efficient, feature-rich, public domain image analysis application. The link to ImageJ is an easy way to measure lengths and areas as well as to count particles (e.g., cells and nuclei) using a click-and-count feature.

Table 2. Main features of the JVSview JPEG2000 viewer application.

- Local image viewing & remote image viewing over JPIP
- Overview window representing the entire specimen
- Magnifications resembling common microscope objectives
- Interactive panning with mouse or keyboard
- Image brightness, contrast & colour saturation adjustments
- Multi-display full screen viewing
- Support for multiple image layers (e.g., focus layers)
- Storing information and regions of interest as XML metadata
- A functional link with image analysis software (ImageJ)

JVSserv. This software is a JPEG2000 virtual slide server application, which utilizes the JPIP protocol as its data transfer technique (Table 3). It is based on the kdu_server application by the Kakadu Software.[20] It has been modified by adding a simple graphical user interface, and by modifying image sample count restrictions and the messaging system. Therefore, JVSserv should only be used with the JVSview viewer application. JVSserv supports multiple simultaneous client connections and uses a standard FIFO (First In, First Out) caching policy, which is used to maintain the most frequently accessed data in memory. JVSserv also supports load balancing, which means sharing the main server's workload to several sub-servers, thereby allowing the system to handle more simultaneous clients.

Table 3. Main features of the JVSserv JPEG2000 server application.

- Remote image serving over JPIP
- Graphical user interface for administration
- Support for multiple simultaneous clients
- Multiple server clustering (load balancing)

JVScomp. This software is a JPEG2000 virtual slide compression application capable of creating virtual slides that are optimized for viewing and serving with JVSview and JVSserv (Table 4). It follows the parameterization guidelines described earlier, and it is capable of compressing various input file formats, such as PPM, BMP, and JPEG. It supports dual-processor workstation environments, which are detected automatically. JVScomp utilizes the ECW JPEG 2000 SDK compression algorithm,[22] which employs a rate control policy that yields as efficient a compression as possible. If an image contains areas that are substantially responsive to compression, for example, homogenous areas of virtual slide glass background with no tissue section, a higher compression ratio is applied to these areas. Thus, a greater overall compression ratio and a smaller file size can be achieved.

Table 4. Main features of the JVScomp JPEG2000 compression application.

▪ Optimised parameterisation for virtual microscopy
▪ Efficient rate control policy for virtual microscopy
▪ Support for dual-processor environments
▪ Support for the various input file formats

DISCUSSION

Today many manufacturers of virtual slide scanners use proprietary image formats, which preclude image exchange between different systems. Support of proprietary non-standard image formats may also be short-lived. For these reasons, the use of an open image standard is a prerequisite for large-scale virtual slide collections that are supposed to be accumulated and utilized for years or even decades. Since technical development is likely to continue rapidly in slide scanners, it is advantageous if image acquisition can be decoupled from image archival and delivery. This ensures that virtual slides generated with older generation equipment are compatible with newer ones. All these conditions are met with the JPEG2000 image format, which, based on its advanced features, is in many ways an ideal choice for virtual microscopy. The present study defined optimal code-stream parameters, which are essential for fast viewing of JPEG2000 virtual slides.

Compression of virtual slide image data into JPEG2000 format is a computationally intensive process. As shown in our experiments, the limiting factor with a conventional dual-core processor environment is the processor performance. However, given that JPEG2000 compression software can be designed to efficiently utilize new multiprocessor environments, the hard disk reading performance eventually becomes critical. By utilizing the mirrored RAID data storage scheme, in which multiple hard disks are combined together and data content is duplicated to all disks, the reading performance can be effectively multiplied. Thus, we estimate that a JPEG2000 compression application using a quad-core processor is capable of compressing over 100 gigabytes of image data per hour, which is faster than the time it takes to scan a 20×20-mm tissue section with a 0.23 μm per pixel resolution using current scanners.[7] Therefore, it seems that the computational demands of JPEG2000 image compression can be fulfilled with a software-based solution, and there is probably no need for external JPEG2000 processing hardware.

In general, JPEG2000 differs from its predecessor JPEG in many important ways. With regards to virtual microscopy, the most important improvement over JPEG is the possibility to retrieve any part of the image with random spatial accessing. Moreover, due to the nature of the JPEG2000 data structure, different image resolutions (magnification levels in virtual slides) can be retrieved without compromising viewing speed. A single JPEG2000 file can thus contain the entire virtual slide data, and even data from multiple focus layers, when using the JPX file format. It has been extensively documented that when using the average Peak Signal-to-Noise Ratio (PSNR) image quality metric, JPEG2000 outperforms JPEG at all compression ratios.[13,14,25] If the quality assessment is based on human observations, the superiority of JPEG2000 becomes evident at compression ratios of 20:1 or higher.[26] In practice, an 8-gigabyte uncompressed 50,000×50,000 pixel virtual slide can be readily compressed into a 300-megabyte JPEG2000 image. If the slide contains vast glass background areas, the corresponding file size can be substantially reduced, without compromising the overall image quality of the cells and tissues to be imaged.

Recently, an expansion proposal for the common TIFF file format, entitled BigTIFF,[27] has been suggested as a candidate image format for virtual microscopy. It circumvents the 4-gigabyte file size limitation of TIFF, thereby enabling the manipulation of very large images. BigTIFF does not define a compression scheme of its own. It can contain, for example, several JPEG or LZW compressed image code-streams structured in a tile-like fashion. However, by using JPEG compressed BigTIFF, the benefits of JPEG2000 lossy compression are lost. Incorporating a JPEG2000 code-stream within BigTIFF is questionable, since the

internal structuring of the JPEG2000 code-stream already enables, among many other advantages, an efficient spatial random access. In addition, JPEG2000 specifies the JPIP protocol for image remote viewing, which has not been described for BigTIFF so far.

Due to its demonstrational nature, the current version of JVS software package does not include any encryption scheme for transmitted image data. However, should a need for encrypted network transmission arise, it is possible to use a standard secure network protocol, such as SSH or TLS, to tunnel the unencrypted JPIP traffic through it. For example, use of the TLS protocol with Virtual Private Networking (VPN) requires setting up a VPN server alongside the JPIP server in the server end, and a VPN client alongside the JPEG2000 viewer in the client end. The VPN client would then act as a proxy for the JPEG2000 viewer, redirecting the viewer's requests through the network to the VPN server, and from there to the actual JPIP server, and vice versa.

A Model System for JPEG2000-Based Virtual Microscopy

As shown in our results, JPEG2000 already meets the functional needs of virtual microscopy viewing. We have described a model for an easily upgradeable JPEG2000-based virtual microscopy system that utilizes load balancing (Fig. 1). The system consists of a main JPIP server with two network interfaces: a 100-Mbit link for client accesses (via internet or intranet) and a 1-Gbit local area network (LAN) connection for data traffic between main server and sub-server(s). The images are distributed on the hard disks of the sub-servers. The main server includes a database of the image locations within the sub-server hard disks. The database can also store other relevant information (similar to metadata described earlier). The main server delegates incoming client image requests onwards to the sub-servers according to the image location data. An ideally suited sub-server is an inexpensive workstation equipped with three hard disks (one disk for the images, one disk for their backup, and one disk for system software). The backup disk is an independent hard disk, activated only during a nightly backup. Currently available one terabyte hard disks can contain approximately 3,000 to 4,000 virtual slides. As the sub-server hard disks reach their storage capacity, a new sub-server can be easily inserted into the system. Thus, this represents an efficient and inexpensive upscaling strategy that can be done gradually over time. In addition, the modularity of the system allows parts of the system to be offline without affecting the functionality as a whole.

Figure 1. A model system for JPEG2000-based virtual microscopy.

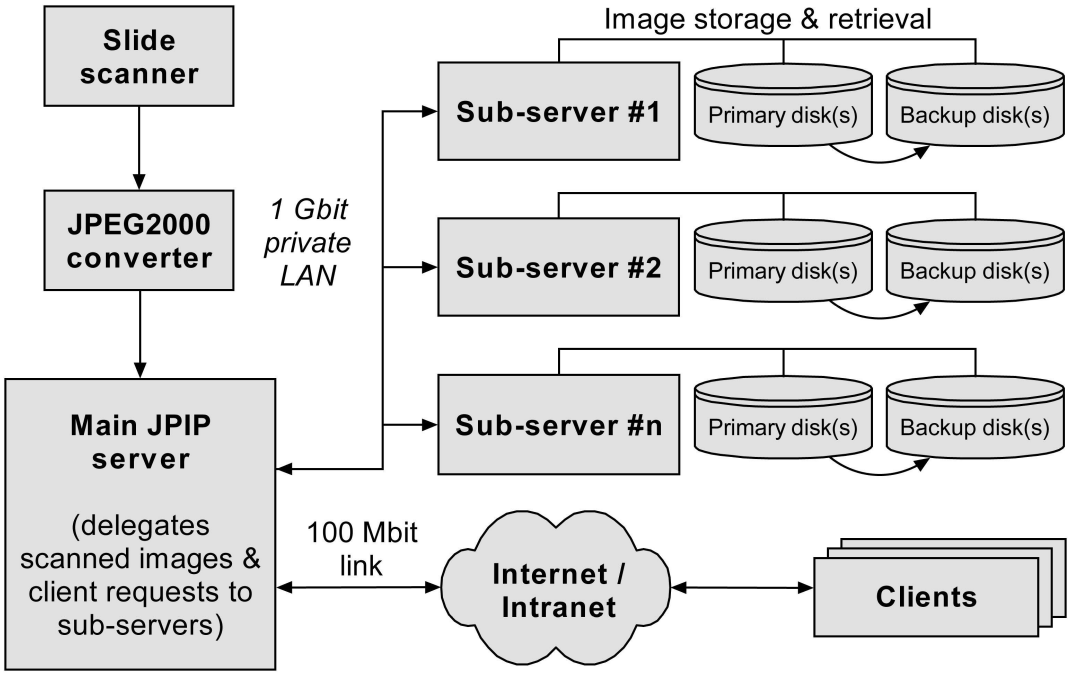

Future Prospects

Large-scale clinical utilization of virtual microscopy requires compatibility with the Digital Imaging and Communications in Medicine (DICOM) standard,[28] which is currently recognized as the standard specification for image archival in clinical medicine. At the present time, DICOM includes some parts of the JPEG2000 standard, the foremost being Part 1, which is included in Supplement 61 (JPEG 2000 Transfer Syntaxes).[29] Recently, Supplement 106 (JPEG 2000 Interactive Protocol)[30] introduced the JPIP protocol as a method of delivering the image pixel data apart from the patient data. A joint international effort towards consolidating pathology concepts and virtual slide imaging with DICOM is currently underway by the DICOM working group for pathology imaging (WG-26).[31] Thus, we assume that the next step towards full implementation of JPEG2000 in clinical pathology and virtual slide imaging requires integration with DICOM.

CONCLUSION

We conclude that JPEG2000 is a well-suited image format for virtual microscopy. It enables compressing, viewing, and serving the large image files produced by the modern microscope slide scanners. We developed a demonstrational software package for JPEG2000 compression, viewing, and JPIP-based network serving, all suited for the needs of virtual microscopy. The package is freely downloadable and usable for non-commercial purposes.

ACKNOWLEDGEMENTS

This study was financially supported by the Finnish Cancer Foundation, Sigrid Juselius Foundation, and an EVO-grant from Tampere University Hospital.

REFERENCES

1. Weinstein RS: Innovations in medical imaging and virtual microscopy. Hum Pathol 36(4):317–319, 2005
2. Lundin M, Lundin J, Helin H, Isola J: A digital atlas of breast histopathology: an application of web based virtual microscopy. J Clin Pathol 57(12):1288–1291, 2004
3. Kumar RK, Freeman B, Velan GM, De Permentier PJ: Integrating histology and histopathology teaching in practical classes using virtual slides. Anat Rec B New Anat 289(4):128–133, 2006
4. Lundin M, Lundin J, Isola J: Virtual microscopy. J Clin Pathol 57(12):1250–1251, 2004
5. Helin H, Lundin M, Lundin J, Martikainen P, Tammela T, Helin H, van der Kwast T, Isola J: Web-based virtual microscopy in teaching and standardizing Gleason grading. Hum Pathol 36(4):381–386, 2005
6. Furness P: A randomized controlled trial of the diagnostic accuracy of internet-based telepathology compared with conventional microscopy. Histopathology 50(2):266–273, 2007
7. Rojo MG, García GB, Mateos CP, García JG, Vicente MC: Critical Comparison of 31 Commercially Available Digital Slide Systems in Pathology. Int J Surg Pathol 14(4):285–305, 2006
8. Burthem J, Brereton M, Ardern J, Hickman L, Seal L, Serrant A, Hutchinson CV, Wells E, McTaggart P, De la Salle B, Parker–Williams J, Hyde K: The use of digital 'virtual slides' in the quality assessment of haematological morphology: results of a pilot exercise involving UK NEQAS(H) participants. Br J Haematol 130(2):293–296, 2005
9. Zoomify, Inc., USA: Zoomify image server software. Available at http://www.zoomify.com/. Accessed 12 July 2007
10. The Joint Photographic Experts Group website. Available at http://www.jpeg.org/. Accessed 12 July 2007
11. Information technology—JPEG 2000 image coding system: Core coding system. ISO/IEC 15444-1, 2000 | ITU-T Recommendation T.800, 2002
12. Taubman DS, Marcellin MW: JPEG2000: Image Compression Fundamentals, Standards and Practice: Springer, 2002
13. Skodras A, Christopoulos C, Ebrahimi T: The JPEG 2000 Still Image Compression Standard. IEEE Signal Proc Mag 18(5):36–58, 2001
14. Rabbani M, Joshi R: An overview of the JPEG 2000 still image compression standard. Signal Process: Image Comm 17 (1):3–48, 2002
15. Information technology—JPEG 2000 image coding system: Extensions. ISO/IEC 15444-2, 2002 | ITU-T Recommendation T.801, 2002
16. Information technology—JPEG 2000 image coding system: Interactivity tools, APIs and protocols. ISO/IEC 15444-9, 2005 | ITU-T Recommendation T.808, 2005
17. Taubman DS, Prandolini R: Architecture, Philosophy and Performance of JPIP: Internet Protocol Standard for JPEG2000. Proc SPIE 5150:791–805, 2003
18. Tuominen VJ, Isola J, University of Tampere, Finland: LargeMontage—a Java application for creating large image montages. Available at http://iki.fi/vtuo/software/largemontage/. Accessed 12 July 2007
19. Rasband WS, U.S. National Institutes of Health, USA: ImageJ image analysis software. Available at http://rsb.info.nih.gov/ij/. Accessed 12 July 2007
20. Taubman DS, The University of New South Wales, Australia: Kakadu JPEG2000 Framework. Available at http://www.kakadusoftware.com/. Accessed 12 July 2007
21. The Apache Software Foundation, USA: The Apache HTTP Server Project. Available at http://httpd.apache.org/. Accessed 12 July 2007
22. Earth Resource Mapping Ltd., Australia: ER Mapper Image Compression SDK. Available at http://www.ermapper.com/. Accessed 12 July 2007
23. Gao M, Bridgman P, Kumar S: Computer Aided Prostate Cancer Diagnosis Using Image Enhancement and JPEG2000. Proc SPIE 5203:323–334, 2003
24. Tuominen VJ, Isola J, University of Tampere, Finland: JVSschema: a metadata XML schema for the JVS software. Available at http://jvsmicroscope.uta.fi/jvsschema/. Accessed 12 July 2007
25. Santa-Cruz D, Grosbois R, Ebrahimi T: JPEG 2000 performance evaluation and assessment. Signal Process: Image Comm 17(1):113–130, 2002

26. Ebrahimi F, Chamik M, Winkler S: JPEG vs. JPEG2000: An Objective Comparison of Image Encoding Quality. Proc SPIE 5558:300–308, 2004
27. Aware Systems, Belgium: The BigTIFF File Format Proposal. Available at http://www.awaresystems.be/imaging/tiff/bigtiff.html. Accessed 10 October 2007
28. Digital Imaging and Communications in Medicine (DICOM). Available at http://medical.nema.org/dicom/2007/. Accessed 12 July 2007
29. Digital Imaging and Communications in Medicine (DICOM), Supplement 61: JPEG 2000 Transfer Syntaxes. Available at ftp://medical.nema.org/medical/dicom/final/sup61_ft.pdf. Accessed 12 July 2007
30. Digital Imaging and Communications in Medicine (DICOM), Supplement 106: JPEG 2000 Interactive Protocol. Available at ftp://medical.nema.org/medical/dicom/final/sup106_ft.pdf. Accessed 12 July 2007
31. Digital Imaging and Communications in Medicine (DICOM), Strategic Document & Principal Contacts. Available at http://medical.nema.org/dicom/geninfo/Strategy.pdf. Accessed 10 October 2007

Linking Whole-Slide Microscope Images with DICOM by Using JPEG2000 Interactive Protocol

Vilppu J Tuominen[1] and Jorma Isola[2]

[1] Institute of Medical Technology, University of Tampere and Tampere University Hospital, 33014 Tampere, Finland (vilppu.tuominen@uta.fi)

[2] Institute of Medical Technology, University of Tampere and Tampere University Hospital, 33014 Tampere, Finland (jorma.isola@uta.fi)

J Digit Imaging. 2010 Aug;23(4):454-62.

AUTHOR PRE-PRINT VERSION

Address for correspondence

Prof. Jorma Isola
Institute of Medical Technology, University of Tampere,
33014 Tampere, Finland.

Email: Jorma.Isola@uta.fi
Tel. +358-3-35516729
Fax. +358-3-35518923

ABSTRACT

The use of digitized histopathologic specimens (also known as whole-slide images (WSIs)) in clinical medicine requires compatibility with the Digital Imaging and Communications in Medicine (DICOM) standard. Unfortunately, WSIs usually exceed DICOM image object size limit, making it impossible to store and exchange them in a straightforward way. Moreover, transmitting the entire DICOM image for viewing is ineffective for WSIs. With the JPEG2000 Interactive Protocol (JPIP), WSIs can be linked with DICOM by transmitting image data over an auxiliary connection, apart from patient data. In this study, we explored the feasibility of using JPIP to link JPEG2000 WSIs with a DICOM-based Picture Archiving and Communications System (PACS). We first modified an open-source DICOM library by adding support for JPIP as described in the existing DICOM Supplement 106. Second, the modified library was used as a basis for a software package (JVSdicom), which provides a proof-of-concept for a DICOM client–server system that can transmit patient data, conventional DICOM imagery (e.g., radiological), and JPIP-linked JPEG2000 WSIs. The software package consists of a compression application (JVSdicom Compressor) for producing DICOM-compatible JPEG2000 WSIs, a DICOM PACS server application (JVSdicom Server), and a DICOM PACS client application (JVSdicom Workstation). JVSdicom is available for free from our Web site (http://jvsmicroscope.uta.fi/), which also features a public JVSdicom Server, containing example X-ray images and histopathology WSIs of breast cancer cases. The software developed indicates that JPEG2000 and JPIP provide a well-working solution for linking WSIs with DICOM, requiring only minor modifications to current DICOM standard specification.

Keywords: digital pathology, telepathology, DICOM, JPEG2000, JPIP, virtual slide, whole-slide imaging, WSI

BACKGROUND

Hospital information systems (HIS) have evolved from closed and proprietary-linked systems into open and standards-based. This change has encouraged medical equipment vendors and software developers to create uniform and interoperable systems. Standardized interfaces let developers link different internal department information systems together: for example, connecting the Laboratory Information System (LIS) of a clinical chemistry or a pathology department with the Radiology Information System in a radiology department. Linked data repositories make all patient-related material (e.g., clinical history and images from different modalities) available to all institution personnel. For instance, pathologists and radiologists can view breast ultrasound and X-ray images simultaneously with corresponding histological specimens.

The most widely used medical imaging standard is the Digital Imaging and Communications in Medicine (DICOM)[1], which is routinely used in several medical specialties, especially radiology. In pathology, digitization of whole microscope specimens has only recently become possible with high-throughput slide scanners[2]. The digitized versions of microscope glass slides are called "virtual slides" or "whole-slide images" (WSIs). Acquiring, handling, and displaying WSIs is commonly called "virtual microscopy" (or whole-slide imaging)[3,4]. WSIs can be used for local viewing or, more practically, for remote viewing by transmitting them over networks[5]. Within the internal network of a hospital or pathology department, personnel can use WSIs in case meetings, slide seminars, and instructional live-audience presentations[6]. By allowing access over the Internet, WSIs can also be used more widely in second-opinion consultations, national and international conferences, and inter-laboratory quality assurance programs[7].

Since microscope specimens are often up to 20×30 mm in size, a WSI can contain up to 40 GB of uncompressed image data (with a scanning resolution 0.2–0.5 μm per pixel)[2]. The amount of data increases further if scanning is done at a

higher optical magnification and/or if several focus layers (along Z-axis) are scanned (e.g., in cytopathology)[8]. Due to the large size of WSIs, all viewing systems described to date apply the "on-demand" principle: that is, only a user-requested area (with a desired resolution) of the WSI is decoded and displayed. Moreover, the large image size necessitates the use of lossy image compression. Lossy compression can yield a 10- to 30-fold compression ratio compared to lossless compression, without affecting the diagnostic properties of a WSI[9]. Thus, a suitable image format for virtual microscopy needs to be based on an effective image compression algorithm, as well as to provide a sophisticated random access technique.

Virtual microscopy currently lacks a universally accepted WSI format. There are several proprietary image formats that are tied to specific scanner vendors, such as SVS (by Aperio Technologies, USA), NDP (by Hamamatsu Photonics, Japan), and Mirax (by Carl Zeiss MicroImaging, USA). The interoperability between different vendor formats and viewing software is practically non-existent. We have previously shown that the open JPEG2000 standard is a suitable format for WSIs, allowing fast random slide access and efficient lossy compression[10]. Although JPEG2000 compression is computationally intensive, the process can be matched with current slide scanner speeds by utilizing multi-core processor environments[10]. JPEG2000 is a family of standards supervised by the Joint Photographic Experts Group standardization committee[11,12]. The standard family currently consists of 13 parts, three of which are essential for virtual microscopy. Part 1 (Core Coding System)[13] specifies the code-stream syntax and the JP2 file format, which uses "jp2" as the common file extension. Part 2 (Extensions)[14] provides extensions for the first part. Part 9 (Interactivity Tools, APIs, and Protocols)[15] introduces the JPEG2000 Interactive Protocol (JPIP) for remote serving and viewing of JPEG2000 images. We have previously developed and released a free JPEG2000 software package (called JVS, for JPEG2000 Virtual Slide) comprising WSI compression, viewing, and network server applications[10]. Della Mea *et al.*[16] have presented a survey of currently available JPEG2000 viewing software.

For clinical diagnostic use, WSIs must be compatible with existing imaging standards, such as DICOM[17]. Although a DICOM Object definition for visible light microscopy exists[18], WSIs are too large (both pixel dimensions and byte size) to be used directly as these objects. A base standard Correction Item (CP 896)[19] to overcome the image dimension limitation was recently rejected by the DICOM Standards Committee[20]. Nevertheless, the committee will continue to consider the possibility of introducing this change to the standard as a supplement. In addition to image size, the access characteristics of WSIs differ from conventional DICOM images. Panning and zooming within a huge WSI require fast random access with on-demand decoding. Currently, the DICOM standard includes the basic parts of the JPEG2000 standard in Supplements 61[21] and 105[22]. Supplement 106 (JPEG 2000 Interactive Protocol)[23] describes two JPIP-based Transfer Syntaxes as methods of delivering image pixel data apart from patient data: the noncompressed JPIP Referenced Transfer Syntax and the Deflate-compressed[24] JPIP Referenced Deflate Transfer Syntax. Thus, the DICOM standard specification already contains necessary elements for transmitting WSIs over JPIP.

When using the JPIP Transfer Syntaxes in a DICOM-based Picture Archiving and Communication System (PACS), a DICOM server sends its client a Uniform Resource Locator (URL) string that refers to the WSI pixel data provider (i.e., a JPIP server), together with the image name, which can be arbitrary and unrelated to patient data (as shown in Fig. 1). Upon receiving the pixel data provider reference, the client DICOM workstation can either use a built-in JPIP viewer or invoke an external one for retrieving the WSI from the specified JPIP server. All network messaging between the PACS and the client end is done according to the DICOM protocol, except the JPIP transmission, which is by default performed on top of the Hypertext Transfer Protocol (HTTP/1.1)[25] for compatibility with existing Web infrastructure, but it can also be done using a lower-level transport protocol (such as Transmission Control Protocol, TCP)[26]. Image serving performance of JPIP has been demonstrated to be excellent and upwards scalable in multi-client systems[10,27].

Figure 1. The principle of transmitting whole-slide images (WSIs) within a DICOM-based PACS by using JPEG2000 Interactive Protocol (JPIP).

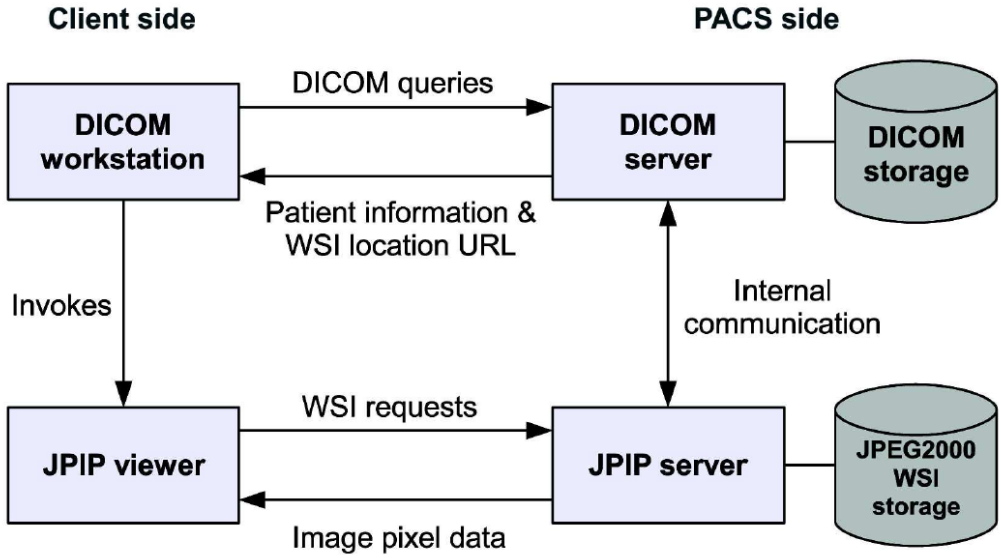

Although JPIP is described in the DICOM standard specification and a brief description of a commercial application exists[28], we are not aware of any open DICOM software solutions or libraries supporting it. In this study, we explore the feasibility of linking JPEG2000 WSIs with a DICOM-based PACS by using JPIP. First, we modified an open-source DICOM library by adding support for JPIP as described in the Supplement 106. Second, the modified library was used as a basis for a software package (JVSdicom), which provides a proof-of-concept for a DICOM client-server system that can transmit patient data, conventional DICOM imagery, and JPEG2000 WSIs over JPIP. The software package consists of a compression application (JVSdicom Compressor) for producing DICOM-compatible JPEG2000 WSIs, a DICOM PACS server application (JVSdicom Server), and a DICOM PACS client application (JVSdicom Workstation). Finally, we present a DICOM-compatible whole-slide imaging system based on the software developed.

MATERIALS AND METHODS

An open-source DICOM library (OFFIS DCMTK DICOM toolkit, version 3.5.4)[29] was modified by adding support for JPIP, as described in the DICOM Supplement 106. The modified library was used to embed DICOM functionality to the developed JVSdicom software package. JVSdicom Compressor is based on our previously described JPEG2000 compression application (JVScomp, version 2.1)[10]. JVSdicom Server and Workstation utilize the Qt open-source software framework (version 4.3)[30] for core application functionality and the Tango Icon Library[31] for graphical user interface elements. The software package was written in C++ programming language and built for 32-bit Windows® platforms but can be run under a 64-bit Windows® platform as well.

Reference material representing typical diagnostic imagery of breast cancer was obtained from Tampere University Hospital. The material comprises radiology imagery (ultrasound, mammography, bone scan, and magnetic resonance imaging) and histological specimen slides (routine H&E stains and immunohistochemistry). The standard-sized slides (75×25 mm) were scanned with Aperio ScanScope® XT (Aperio Technologies, USA) using uncompressed BigTIFF32 as the primary output format. Whole-mount section slides (75×50 mm) were acquired with a Zeiss Axioskop40 microscope (Carl Zeiss MicroImaging, USA) as described equipped with a charge-coupled device color camera (QICAM Fast; QImaging, Canada) and a motorized specimen stage (Märzhäuser Wetzlar GmbH, Germany). The au-

tomated image acquisition was controlled by the Surveyor imaging system (Objective Imaging, UK) using uncompressed bitmap as the primary output format. The developed JVSdicom Compressor application was used to convert the histological reference material into the DICOM-compatible JPEG2000 WSI format.

RESULTS

The JVSdicom software package was developed as a proof-of-concept for a DICOM client–server system that can transmit patient data, conventional DICOM imagery (e.g., radiological), and JPEG2000 WSIs using the JPIP Referenced Transfer Syntax. The software package consists of a compression application (JVSdicom Compressor), a DICOM PACS server application (JVSdicom Server), and a DICOM PACS client application (JVSdicom Workstation).

JVSdicom Compressor is a free, command line-based image compression application capable of converting multiple image formats (e.g., BMP, PPM, and BigTIFF) into the DICOM-compatible JPEG2000 WSI format. The output JPEG2000 file follows the optimized code-stream parameterization we have previously described[10]. In addition to the JPEG2000 WSI file, the application generates a supplementary DICOM file containing medical information, image properties, and a JPIP server reference to the WSI file location, which is used by the DICOM client to access the WSI. The resulting DICOM file uses the General Microscopy modality[18] and Visible Light Microscopic Image Information Object Definition (IOD)[18] with a minimal set of required attributes.

JVSdicom Server is an open-source DICOM PACS server application that acts as a Storage Service Class Provider (SCP) and as a Query/Retrieve SCP (Table 1). The server is capable of accepting multiple associations simultaneously. Server can be configured to contain several filesystem-based storage areas with different Application Entity (AE) Titles, as well as to limit access to these areas from a predefined AE network (Fig. 2). Alternatively, the server features a public mode, which can be used to grant open access to the server. For open access, the calling AE is assumed to have a receiving Storage SCP set up. New DICOM entries can be added into the server storage with pixel data either coming from existing image files or replaced with a JPIP reference (i.e., in case of JPEG2000 WSIs). JVSdicom Server supports several Storage Service Object Pair (SOP) Classes. A comprehensive conformance statement appears in the software documentation.

Figure 2. A screenshot of JVSdicom Server storage management view. DICOM image objects can be added to the storage by importing existing image files or by creating a new JPIP-referenced object.

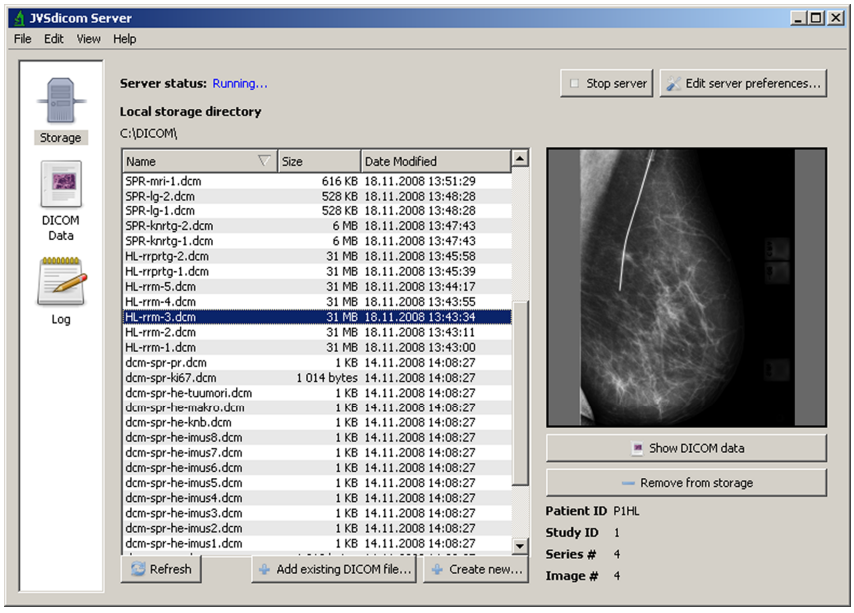

Table 1. Main features of JVSdicom Server.

▪ Fully DICOM-compliant PACS server ▪ Support for several Storage SOP Classes ▪ Support for JPEG2000 WSIs with JPIP Referenced Transfer Syntax ▪ A public mode with open access to server ▪ Can be used as a server for JVSdicom Workstation ▪ Open-source

JVSdicom Workstation is an open-source DICOM PACS client application that acts as a Query/Retrieve Service Class User (SCU) and a Storage SCU (Table 2). With it, users can query and retrieve images from a DICOM-compatible PACS server (Fig. 3). Users can view the images with several image enhancement options, as well as view a summary of patient- and treatment-related information. JVSdicom Workstation interacts with a DICOM server as a conventional DICOM client, but upon receiving a JPIP reference to a JPEG2000 WSI, it invokes an external JPEG2000 viewing application. The external viewing application displays the image pixel data, while JVSdicom displays the associated DICOM medical information. Thus, by having an external viewer for WSIs, users can view conventional DICOM imagery and corresponding histopathologic specimens side by side (Fig. 4). The external viewing application can be chosen by the user. The default viewer is JVSview10. Regions of interests from the DICOM images and WSIs can both be opened in a public domain image analysis software, ImageJ[33], which features a multitude of analysis tools for medical imaging. JVSdicom Workstation is compatible with commercial-grade DICOM servers, supporting several Storage SOP Classes (a comprehensive conformance statement appears in the software documentation).

Figure 3. A screenshot of JVSdicom Workstation showing the PACS query view. Conventional DICOM imagery is displayed in the thumbnail window, while JPEG2000 WSIs are opened in an external JPIP viewer.

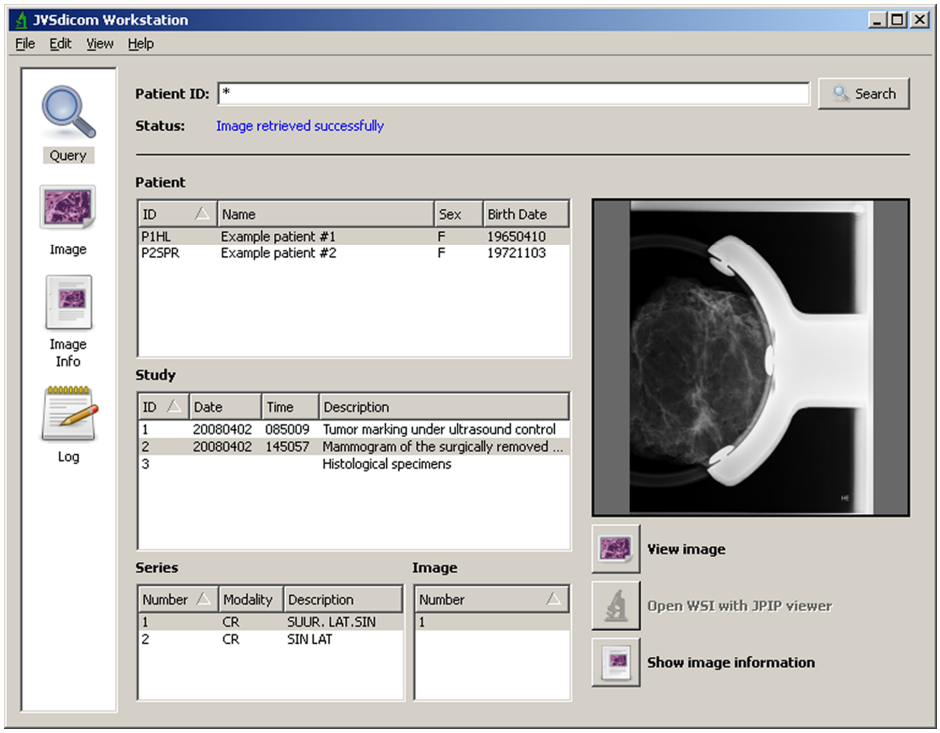

Figure 4. Viewing of a breast cancer specimen X-ray and corresponding histological WSI (whole-mount section) side by side with JVSdicom Workstation and an external JPIP viewer. Within JVSdicom, users can rotate the image, adjust width and center values, and measure distances by using the ruler tool. The JPIP viewer displays the WSI using an overview and a main navigation window.

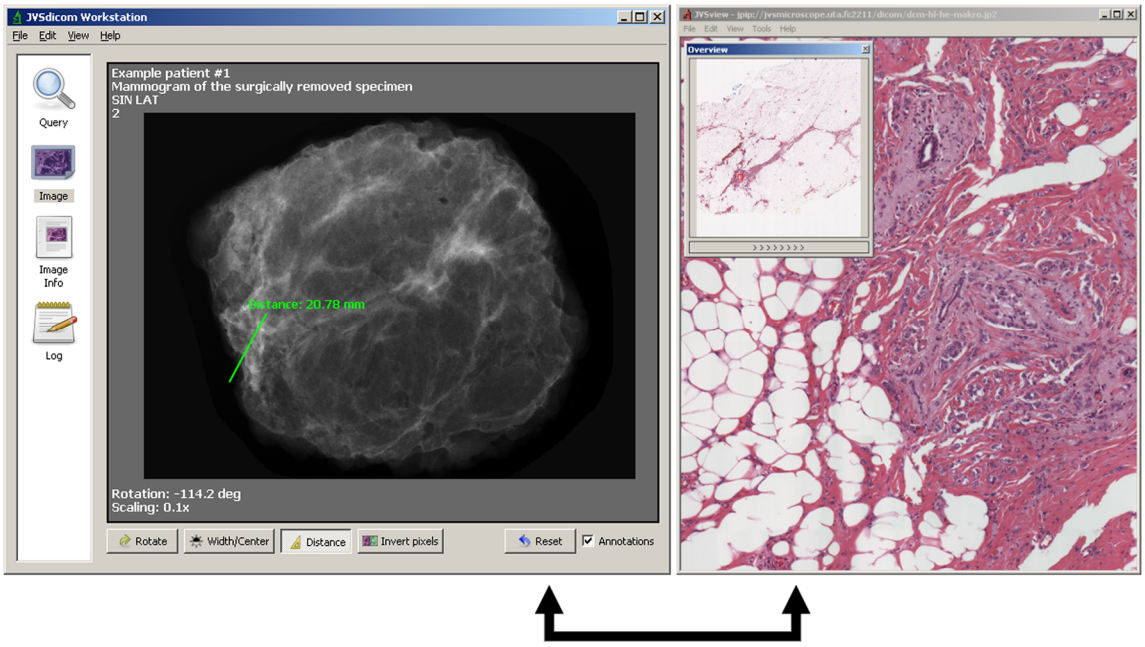

Table 2. Main features of JVSdicom Workstation.

▪ Fully DICOM-compliant PACS client ▪ Support for JPEG2000 WSIs with JPIP Referenced Transfer Syntax ▪ Viewing of radiological images and corresponding histological WSIs side by side ▪ A functional link with public domain image analysis software (ImageJ) ▪ Can be used as a client for JVSdicom Server ▪ Open-source

The JVSdicom software package is fully DICOM-compliant and designed to run on Windows® XP but is also Windows Vista™ compatible. The binaries and source code, as well as a comprehensive conformance statement, are available on our Web site (http://jvsmicroscope.uta.fi/). The Web site also features a public JVSdicom server, containing example images produced in the diagnostics of breast cancer.

DISCUSSION

We developed the JVSdicom software package to study the feasibility of linking JPEG2000 WSIs with a DICOM-based PACS by using JPIP. JVSdicom Compressor is used for creating DICOM-compatible JPEG2000 WSIs, which consist of the actual JPEG2000 image file and a supplementary DICOM file containing patient-related information. The supplementary DICOM file can be served using the JVSdicom Server, while the JPEG2000 image files are served using a separate

JPIP server. Querying and retrieving images from the JVSdicom Server can be done using the JVSdicom Workstation, which handles conventional DICOM imagery directly but uses an external JPIP client application for JPEG2000 WSI viewing.

A complete, DICOM-compatible whole-slide imaging system can be constructed by combining JVSdicom with our previously described JPEG2000 viewing application (JVSview) and JPIP network serving application (JVSserv; Fig. 5). In this model system, a WSI scanner produces raw image data, which is processed by JVSdicom Compressor. JVSdicom Compressor produces a JPEG2000 file containing the actual WSI image data and a DICOM file containing the associated medical data (i.e., patient information) as well as some mandatory image properties, such as width and height. By default, the produced DICOM file contains anonymized DICOM entries, but it could be linked with a LIS or a HIS for retrieving patient information. A straightforward way to name the JPEG2000 WSI file is to use the microscope slide label identification string, which can be read automatically if bar-coded labels are used. The JPEG2000 WSI file is then moved into a JVSserv server, and the DICOM file is moved into a JVSdicom Server, which both are parts of the same PACS. Both files can be stored separately inside a server-specific storage area within the PACS. JVSdicom can also receive imagery from other imaging modalities, which are in turn linked with the LIS or HIS. End-users (e.g., pathologists or physicians) query the JVSdicom Server with a JVSdicom Workstation and retrieve patient-linked image objects. They can view and analyze conventional DICOM imagery within JVSdicom Workstation, while WSIs are opened with JVSview in another viewing window. The DICOM data is transmitted using the JPIP Referenced Transfer Syntax, and the JPEG2000 WSI data is transmitted via an auxiliary channel over JPIP. The system architecture makes it possible to use JVSserv separately outside the PACS, since WSIs do not contain any DICOM references.

Figure 5. A model system for linking whole-slide images (WSIs) with DICOM by using JPEG2000, JPIP, and the JVS software. The WSI scanner produces raw image data, which JVSdicom Compressor processes. The resulting DICOM and JPEG2000 WSI files are moved into the PACS to JVSdicom Server and JVSserv, from which they are queried with JVSdicom Workstation and viewed with JVSview.

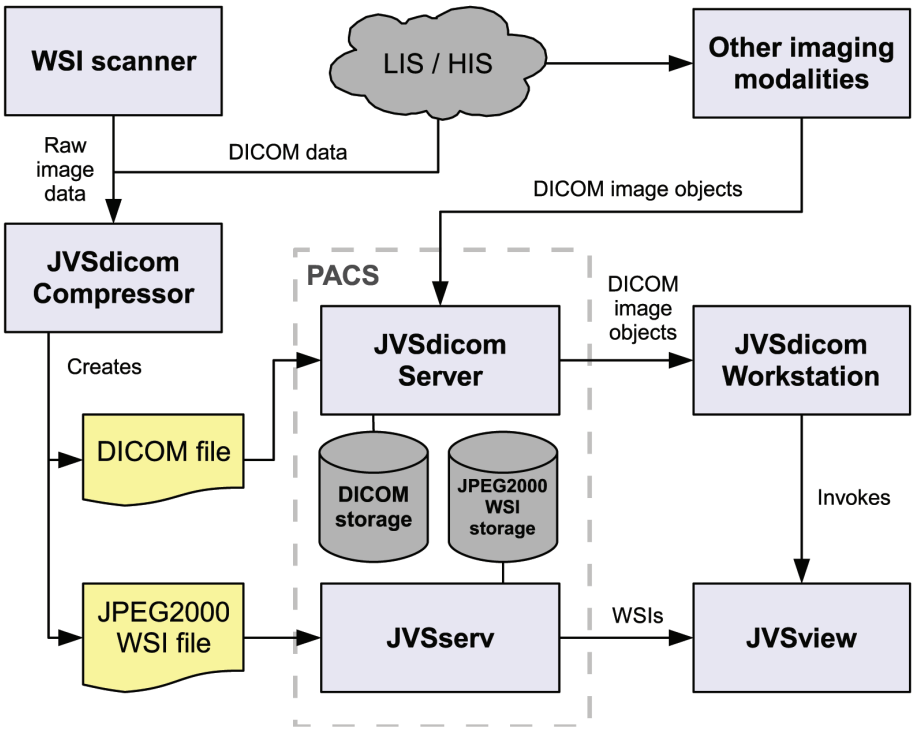

An open issue with using JPEG2000 WSIs and JPIP is the image dimension restriction in the DICOM standard specification. Since image width and height tags are currently described using 16-bit values, oversized (width or height >65,535 pixels) WSIs will show false information with regards to these tags. However, since the definitive image width and height information are always also stored in the JPEG2000 code-stream header, the DICOM counterpart values can be bypassed. This requires the JPIP client software to use the code-stream values instead of the DICOM-specific values. The software described in this study follows this principle. In the future, if a DICOM Supplement equivalent to the CP 896 (to eliminate 16-bit image dimension restrictions) is introduced to the standard, the JPIP viewing software can also operate using the DICOM-specific image dimension tags. Current limitations for DICOM image object size due to 32-bit addressing (4 GB) do not affect JPEG2000 WSIs as long as they are stored in a separate JPIP server, such as the one described in this study. As such, the JPEG2000 standard does not limit individual file size and image dimensions, even in the largest future WSIs[11,13].

The DICOM Working Group for pathology imaging (WG-26) is currently making an effort to consolidate pathology concepts and whole-slide imaging with DICOM[34]. WG-26 has recently finalized Supplement 122 (Specimen Module and Revised Pathology SOP Classes), introducing a new mechanism for pathology specimen identification in DICOM[35]. The new mechanism revises the concept of "specimen" within DICOM framework. Zwönitzer *et al.*[36] have also proposed a similar approach. The scope of our study was to exemplify a DICOM WSI solution based on JPIP. Thus, the software described does not currently implement Supplement 122.

WG-26 has also recently started preparing a draft for a new DICOM Supplement for whole-slide imaging containing an IOD and SOP Classes for WSIs (as discussed in the WG-26 meetings)[37]. At its current state, the supplement utilizes a "pyramidal" approach in which the original resolution WSI is split into small image tiles (usually thousands of them). In addition, a number of successively lower resolution versions of the original tiles may be precomputed, creating a pyramid-shaped resolution structure. All the image tiles are stored as a conventional DICOM Series and accessed with the DICOM WSI object, which provides a mapping between the Series and the conceptual image pyramid. The pyramidal approach is similar to what various WSI scanner vendors have used in their web viewing solutions for several years. Prior to its finalization, the supplement draft is subject to changes.

Both approaches for whole-slide imaging in DICOM, the pyramidal and the JPIP-based, as described in this study, can be implemented with minor modifications to the existing standard specification. An advantage of the pyramidal approach is that WSIs are treated equal to other DICOM imagery residing within the same server. In the JPIP-based approach, an additional JPIP server must be set up within the PACS. However, a disadvantage of the pyramidal approach is that because WSIs are stored in a DICOM-specific data structure using lossy compression, as is required in virtual microscopy, relocating WSIs from the PACS (e.g., for teaching purposes) requires lossy recompression. This results in image quality degradation. In the JPIP-based approach, on the other hand, the JPEG2000 WSIs are not stored using a DICOM-specific data structure, making them directly interchangeable with non-DICOM systems. Moreover, since patient-related DICOM data is not embedded in the JPEG2000 WSI files, the same JPIP server can be readily used inside and outside of a PACS without the need for anonymization.

Since the DICOM standard specification already includes support for JPIP, the pyramidal approach and the JPIP-based approach for whole-slide imaging are not mutually exclusive and can be used simultaneously in the same PACS. Regardless of the approach, changes in existing PACS workstation software are also required because of the WSI-specific image viewing characteristics. At the time of preparation of this article, the detailed contents of the upcoming WG-26 WSI supplement, as well as its expected release date, are open. In the future, when the supplement is finalized and implemented in practice, comparisons between the two WSI approaches might turn out useful.

CONCLUSION

To our knowledge, the software package described in this study is the first practical solution to overcome the limitations of DICOM in virtual microscopy. Compared to other approaches, such as the pyramidal approach of the DICOM WG-26, JPEG2000 with JPIP is a good alternative, enabling use of WSI archives either with or without a linked DICOM system. Further, since JPEG2000 has also many other advantageous features over those of existing WSI image formats, we anticipate that JPEG2000 will become a widely-accepted standard WSI format in virtual microscopy.

ACKNOWLEDGEMENTS

This study was financially supported by the Finnish Cancer Foundation, Sigrid Juselius Foundation, and Tampere University Hospital with a governmental grant (EVO). The authors wish to thank Anna-Leena Lääperi from Tampere University Hospital and COST Action IC604: Eurotelepath ("Telepathology Network in Europe") for supportive collaboration.

REFERENCES

1. Digital Imaging and Communications in Medicine (DICOM). Available at ftp://medical.nema.org/dicom/2008/. Accessed 9 October 2008
2. Rojo MG, García GB, Mateos CP, García JG, Vicente MC: Critical comparison of 31 commercially available digital slide systems in pathology. Int J Surg Pathol 14(4):285–305, 2006
3. Weinstein RS: Innovations in medical imaging and virtual microscopy. Hum Pathol 36(4):317–9, 2005
4. Gilbertson J, Yagi Y: Histology, imaging and new diagnostic work-flows in pathology. Diagn Pathol 3(Suppl 1):S14, 2008
5. Lundin M, Lundin J, Helin H, Isola J: A digital atlas of breast histopathology: an application of web based virtual microscopy. J Clin Pathol 57(12):1288–1291, 2004
6. Lundin M, Lundin J, Isola J: Virtual microscopy. J Clin Pathol 57(12):1250–1, 2004
7. Ho J, Parwani AV, Jukic DM, Yagi Y, Anthony L, Gilbertson JR: Use of whole slide imaging in surgical pathology quality assurance: design and pilot validation studies. Hum Pathol 37(3):322–31, 2006
8. Kalinski T, Zwönitzer R, Sel S, Evert M, Guenther T, Hofmann H, Bernarding J, Roessner A: Virtual 3D microscopy using multiplane whole slide images in diagnostic pathology. Am J Clin Pathol 130(2):259–64, 2008
9. Gao M, Bridgman P, Kumar S: Computer aided prostate cancer diagnosis using image enhancement and JPEG2000. Proc SPIE 5203:323–334, 2003
10. Tuominen VJ, Isola J: The application of JPEG2000 in virtual microscopy. J Digit Imaging, doi:10.1007/s10278-007-9090-z, 2007
11. Taubman DS, Marcellin MW: JPEG2000: Image Compression Fundamentals, Standards and Practice, Boston: Kluwer Academic, 2002
12. The Joint Photographic Experts Group Web site. Available at http://www.jpeg.org/. Accessed 19 October 2008
13. Information technology—JPEG 2000 image coding system: Core coding system. ISO/IEC 15444–1, 2000 | ITU-T Recommendation T.800, 2002
14. Information technology—JPEG 2000 image coding system: Extensions. ISO/IEC 15444–2, 2002 | ITU-T Recommendation T.801, 2002
15. Information technology—JPEG 2000 image coding system: Interactivity tools, APIs and protocols. ISO/IEC 15444–9, 2005 | ITU-T Recommendation T.808, 2005
16. Della Mea V, Bortolotti N, Beltrami CA: A survey on non specialized off-the-shelf JPEG2000 viewers for digital microscopy use. Diagn Pathol 3(Suppl 1):S20, 2008

17. Kayser K, Görtler J, Goldmann T, Vollmer E, Hufnagl P, Kayser G: Image standards in Tissue-Based Diagnosis (Diagnostic Surgical Pathology). Diagn Pathol 3:17, 2008
18. Digital Imaging and Communications in Medicine (DICOM), Part 3: Information Object Definitions. Available at ftp://medical.nema.org/medical/dicom/2008/08_03pu.pdf. Accessed 9 October 2008
19. Digital Imaging and Communications in Medicine (DICOM), Correction Item CP-896: "Eliminate 16 bit row and column image size restrictions" (Letter Ballot). Available at ftp://medical.nema.org/medical/dicom/CP/cp896_lb.pdf. Accessed 23 February 2009
20. Digital Imaging and Communications in Medicine (DICOM), Working Group 6 (Base Standard) meeting minutes, January 19–23, 2009, San Francisco, CA, USA. Available at http://medical.nema.org/Dicom/minutes/WG-06/2009/2009-01-19/WG-06_2009-01-19_Min.doc. Accessed 23 February 2009
21. Digital Imaging and Communications in Medicine (DICOM), Supplement 61: JPEG 2000 Transfer Syntaxes. Available at ftp://medical.nema.org/medical/dicom/final/sup61_ft.pdf. Accessed 9 October
22. Digital Imaging and Communications in Medicine (DICOM), Supplement 105: JPEG 2000 Part 2 Multicomponent Transfer Syntaxes. Available at ftp://medical.nema.org/medical/dicom/final/sup105_ft.pdf. Accessed 9 October 2008
23. Digital Imaging and Communications in Medicine (DICOM), Supplement 106: JPEG 2000 Interactive Protocol. Available at ftp://medical.nema.org/medical/dicom/final/sup106_ft.pdf. Accessed 9 October 2008
24. The Internet Engineering Task Force (IETF), RFC 1951, DEFLATE Compressed Data Format Specification version 1.3. Available at http://www.ietf.org/rfc/rfc1951.txt. Accessed 9 October 2008
25. The Internet Engineering Task Force (IETF), RFC 2616, Hypertext Transfer Protocol – HTTP/1.1. Available at http://www.ietf.org/rfc/rfc2616.txt. Accessed 9 October 2008
26. Taubman DS, Prandolini R: Architecture, philosophy and performance of JPIP: Internet protocol standard for JPEG2000. Proc SPIE 5150:791–805, 2003
27. Tian Y, Cai W, Sun J, Zhang J: A novel strategy to access high resolution DICOM medical images based on JPEG2000 interactive protocol. Proc SPIE 6919:691912, 2008
28. Peces C, García-Rojo M, Sacristán J, Gallardo AJ, Rodríguez A: Serendipia: Castilla-La Mancha telepathology network. Diagn Pathol 15(Suppl 1):S5, 2008
29. Kuratorium OFFIS e.V., Germany: DCMTK DICOM toolkit. Available at http://dicom.offis.de/. Accessed 9 October 2008
30. Qt Software, Norway: Qt cross-platform software development framework. Available at http://trolltech.com/products/. Accessed 9 October 2008
31. Tango Desktop Project, Tango Icon Library. Available at http://tango.freedesktop.org/Tango_Icon_Library. Accessed 9 October 2008
32. Aware Systems, Belgium: The BigTIFF File Format Proposal. Available at http://www.awaresystems.be/imaging/tiff/bigtiff.html. Accessed 9 October 2008
33. Rasband WS, U.S. National Institutes of Health, USA: ImageJ image analysis software. Available at http://rsb.info.nih.gov/ij/. Accessed 9 October 2008
34. Digital Imaging and Communications in Medicine (DICOM), Strategic Document & Principal Contacts. Available at http://medical.nema.org/dicom/geninfo/Strategy.pdf. Accessed 9 October 2008
35. Digital Imaging and Communications in Medicine (DICOM), Supplement 122: Specimen Module and Revised Pathology SOP Classes. Available at ftp://medical.nema.org/medical/dicom/final/sup122_ft2.pdf. Accessed 9 October 2008
36. Zwönitzer R, Kalinski T, Hofmann H, Roessner A, Bernarding J: Digital pathology: DICOM-conform draft, testbed, and first results. Comput Methods Programs Biomed, 87(3):181–8, 2007
37. Digital Imaging and Communications in Medicine (DICOM), Working Group 26 (Pathology) meeting minutes, May 17, 2008, Toledo, Spain. Available at http://medical.nema.org/DICOM/minutes/WG-26/2008/2008-05-17/WG-26_2008-05-17_Min.doc. Accessed 23 February 2009

Breast Cancer RESEARCH

RESEARCH ARTICLE Open Access

ImmunoRatio: a publicly available web application for quantitative image analysis of estrogen receptor (ER), progesterone receptor (PR), and Ki-67

Vilppu J Tuominen[1], Sanna Ruotoistenmäki[1,2], Arttu Viitanen[1], Mervi Jumppanen[2], Jorma Isola[1*]

Abstract

Introduction: Accurate assessment of estrogen receptor (ER), progesterone receptor (PR), and Ki-67 is essential in the histopathologic diagnostics of breast cancer. Commercially available image analysis systems are usually bundled with dedicated analysis hardware and, to our knowledge, no easily installable, free software for immunostained slide scoring has been described. In this study, we describe a free, Internet-based web application for quantitative image analysis of ER, PR, and Ki-67 immunohistochemistry in breast cancer tissue sections.

Methods: The application, named ImmunoRatio, calculates the percentage of positively stained nuclear area (labeling index) by using a color deconvolution algorithm for separating the staining components (diaminobenzidine and hematoxylin) and adaptive thresholding for nuclear area segmentation. ImmunoRatio was calibrated using cell counts defined visually as the gold standard (training set, $n = 50$). Validation was done using a separate set of 50 ER, PR, and Ki-67 stained slides (test set, $n = 50$). In addition, Ki-67 labeling indexes determined by ImmunoRatio were studied for their prognostic value in a retrospective cohort of 123 breast cancer patients.

Results: The labeling indexes by calibrated ImmunoRatio analyses correlated well with those defined visually in the test set (correlation coefficient $r = 0.98$). Using the median Ki-67 labeling index (20%) as a cutoff, a hazard ratio of 2.2 was obtained in the survival analysis ($n = 123$, $P = 0.01$). ImmunoRatio was shown to adapt to various staining protocols, microscope setups, digital camera models, and image acquisition settings. The application can be used directly with web browsers running on modern operating systems (e.g., Microsoft Windows, Linux distributions, and Mac OS). No software downloads or installations are required. ImmunoRatio is open source software, and the web application is publicly accessible on our website.

Conclusions: We anticipate that free web applications, such as ImmunoRatio, will make the quantitative image analysis of ER, PR, and Ki-67 easy and straightforward in the diagnostic assessment of breast cancer specimens.

Introduction

Immunohistochemical staining of the estrogen receptor (ER), progesterone receptor (PR), and proliferation antigen Ki-67 are routinely used in the diagnostic assessment of breast cancer. Positive ER status of a tumor is considered necessary for patients to be eligible for post-surgical hormonal therapies. ER and PR assays are based on immunohistochemistry performed on formalin-fixed and paraffin-embedded tumor tissue blocks [1]. Although the analytical quality of ER and PR assays has been debated for decades, recent results of interlaboratory quality assurance studies provide convincing evidence for the high reproducibility of these laboratory staining procedures [2,3]. The tumor cell proliferation antigen level, as defined by Ki-67 immunostaining, is an auxiliary tool for defining patient prognosis. Patients with rapidly proliferating tumors are predicted to endure poorer outcomes than patients with tumors exhibiting low proliferation [4]. Meta-analyses confirming the role

* Correspondence: jorma.isola@uta.fi
[1]Institute of Medical Technology, University of Tampere, Biokatu 6, 33014 Tampere, Finland

of Ki-67 as a prognostic factor have included more than 15,000 patients [5].

Common practice in pathology laboratories is to score ER-, PR-, and Ki-67-stained slides visually (also termed manually) using light microscopy at medium power magnification (10× or 20× objectives). For ER and PR evaluation, a tumor is scored as negative or positive or, as is currently recommended, by evaluating the percentage of positively stained tumor cell nuclei [6]. A threshold of 10% total stained tumor cells is commonly used as a cut-off for defining positive ER and PR status. A combination of the stained cell percentage and the staining intensity is applied in histoscore and Allred-score methods [7,8]. Whichever scoring method is used, it is well known that microscopic evaluation of ER- and PR-stained slides is subjective and can lead to significant inter-observer variability. For example, in an extensive inter-laboratory study of 172 pathologists, 24% of ER-positive slides were interpreted as falsely negative [9]. Interpretation of Ki-67 staining can be even more difficult, mainly owing to the lack of uniformly accepted cut-off points for defining low- and high-risk patient groups. In most of the published studies included in the meta-analyses, Ki-67 has been evaluated in a single center or by one or very few observers, thereby failing to address the problem of possible inter-observer variability [4,5]. The magnitude of inter-observer variability for Ki-67 scoring is largely unknown, but there is no reason to believe that it would be less than that of ER and PR.

In clinical practice, ER-, PR- and Ki-67-stained slides are interpreted by a pathologist. Careful estimation of the percentage of positively stained cells (labeling index) is not only prone to inter-observer variation, but is also tedious and time-consuming. To overcome this, various digital image analysis methods have been described [10,11]. The principles behind quantitative immunohistochemistry analyses are based on differentiation of the staining components by using, for example, the color deconvolution algorithm [12]. The color deconvolution algorithm detects and separates multiple stains by analyzing their absorption spectra and relative contributions to areas containing two or more overlapping stains. Although the optical density of the immunoreaction product (brown diaminobenzidine (DAB) precipitate) may not accurately reflect the abundance of the antigen (ER, PR, or Ki-67 protein), systems discriminating between negatively and positively stained cells have turned out to be useful [13]. Unfortunately, the image analysis software described in the literature is seldom released for public use. Likewise, the commercially available software is usually proprietary and/or bundled with dedicated analysis equipment or virtual microscopy scanners, making it difficult to compare them [14].

In order to become widely accepted and utilized by pathologists, a digital image analysis system should be easily accessible, not require dedicated equipment or software installation, and be compatible with existing microscope setups. For this purpose, we developed an image analysis application, named ImmunoRatio, which is accessed and used within a web browser. ImmunoRatio supports all modern web browsers and operating systems, requiring no software installation. The application segments immunostained and hematoxylin-stained cellular areas from the user-submitted image and calculates the labeling index (percent of DAB-stained area out of the total nuclear area). ImmunoRatio is free, open source, and publicly available on our research group website [15].

Materials and methods

Immunohistochemistry

Formalin-fixed and paraffin-embedded tissue sections from invasive breast cancers were derived from the archive of the Department of Pathology, Seinäjoki Central Hospital. The study has been approved by the Scientific Committee of Seinäjoki Central Hospital, Finland. According to the Finnish national ethics committee regulations, informed consent was not considered necessary for this study. Immunohistochemical stainings of ER, PR, and Ki-67 tissue sections followed the recommended staining protocols [3]. The slides were stained using the BondMax staining robot (Leica Microsystems, Wetzlar, Germany). In brief, ER was detected using monoclonal antibody 6F11 (diluted 1:300, Leica Biosystems, Newcastle, UK), PR was detected using monoclonal antibody PgR636 (diluted 1:600, Leica Biosystems, Newcastle, UK), and Ki-67 was detected using monoclonal antibody MIB-1 (diluted 1:100, Dako, Carpinteria, CA, USA). Antigen retrieval was performed in Tris-EDTA buffer (pH 9, 100°C for 40 minutes). Bound antibodies were visualized using Bond Refine Detection kit (Leica Biosystems, Newcastle, UK). Immunoreaction was intensified using 0.5% copper sulfate (5 minutes). Hematoxylin counterstaining (1 minutes in ChemMate diluted 1:6, Dako, Carpinteria, CA, USA) was performed using PBS as bluing reagent. The samples were cleared with ethanol and xylene and mounted using standard procedures.

Prognostic validation

Samples from 123 primary breast cancer patients were derived from the archives of the Department of Pathology at Tampere University Hospital, with the permission from National Supervisory Authority for Welfare and Health (Köninki *et al.*: Analysis of PIK3CA mutations and protein expression in breast cancer, submitted).

Survival rates of all patients were calculated by the method of Kaplan and Meier. Data on breast cancer-specific mortality was obtained from Finnish Cancer Registry. Up to 20-year follow-up was available for this patient cohort (cancers diagnosed between 1988 and 1992). The immunohistochemical staining for Ki-67 was carried out as described above, except that PowerVision + kit (ImmunoVision, Springdale, AZ, USA) was used for antibody detection and LabVision Autostainer (LabVision, Fremont, CA, USA) for staining automation. Informed consent in very old retrospective patient cohorts was deemed unnecessary, because the study was approved by the local hospital ethics committee and the National Supervisory Authority for Welfare Health.

Image acquisition

Digital images were captured using a Leica DM3000 microscope (Leica Microsystems, Wetzlar, Germany) equipped with 10×, 20×, and 40× objective lenses, a 1× phototube, and a Scion CFW-1612C digital color camera (Scion Corporation, Frederick, MD, USA; 24-bit color depth; resolution 1,600 × 1,200 pixels, pixel size 4.40 μm). The images were stored using an uncompressed image file format (bitmap). For every imaging session, an image from empty slide background area was acquired (blankfield image), which was used to correct image color balance and uneven illumination. Optimal image brightness and contrast were determined by using the Camera Adjustment Wizard, which was developed as an incorporated function of ImmunoRatio. The Camera Adjustment Wizard measures the brightness of the blankfield image and performs a contrast analysis using an image containing hematoxylin-stained cells. An optimal brightness (mean gray intensity) of the blankfield image is considered to be in the range of 200 to 250 (available range 0 to 255, black being 0). The contrast analysis segments the hematoxylin-stained cells (foreground) and analyzes their mean gray intensity, which is then divided by the background mean gray intensity. The contrast is considered to be optimal if the foreground mean gray intensity is 50 to 80% of the background mean gray intensity.

Software development

ImmunoRatio was first developed as a plugin for the ImageJ image analysis software (1.42 m) [16] using the Java programming language [17]. In addition to built-in ImageJ functions, the ImmunoRatio analysis algorithm uses the Calculator Plus plugin [18] for blankfield correction, the Rolling Ball algorithm [19] for background subtraction, the Color Deconvolution plugin [20] for DAB and hematoxylin stain separation, the IsoData algorithm [21] for adaptive thresholding, and the Watershed algorithm [22] for nucleus segmentation. The analysis algorithm steps are outlined in Figure 1. A more detailed algorithm flowchart is available on our website [15]. The ImmunoRatio plugin was embedded into a Java servlet-based web application. The web application was developed using Google Web Toolkit (1.7.0) [23], Apache Commons FileUpload package (1.2.1) [24], Apache Commons IO library (1.4) [25], Laboratory for Optical and Computational Instrumentation Bio-Formats package (4.1) [26], and Apache Tomcat servlet container (6.0) [27].

Software calibration

From a pool of 100 immunohistochemically stained slides, 50 were selected to be included in the training set (25 stained for Ki-67, 13 for PR, and 12 for ER). The labeling indexes (percentage of positively stained nuclei by visual assessment) were evenly distributed, ranging from 0 to 100%. From each training set slide, one image representative for invasive carcinoma was acquired. Each acquired image was analyzed visually by counting positively and negatively stained carcinoma cells on a computer screen (a minimum of 500 cells total per image). The percent of DAB-stained nuclei out of the total nuclei (DAB- and hematoxylin-stained) was calculated as the labeling index. This result was used as the gold standard for ImmunoRatio calibration. The images were then analyzed using non-calibrated ImmunoRatio, and the results were compared with visual counting in a scatter plot. Owing to the non-linear relation, a third degree polynomial was fitted to the data. ImmunoRatio was then calibrated by embedding the fitted polynomial as a correction function into the analysis algorithm. To validate the calibration and demonstrate the accuracy of the analysis, the remaining 50 samples (25 stained for Ki-67, 13 for PR, and 12 for ER) were used as a test set, which was analyzed using calibrated ImmunoRatio. In the final step of the validation, the minimum number of images needed to be averaged from a typical tumor sample (diameter 1 to 2 cm) was defined. From 10 samples, 12 images per sample representing central and peripheral tumor areas were acquired using 20× objective.

Software testing

ImmunoRatio was initially developed and calibrated using ER-, PR-, and Ki-67-stained slides, which were considered optimal by an external quality assurance program [3]. To simulate interlaboratory variability in staining results, the effect of suboptimal primary antibody (Ki-67 MIB-1) dilution and hematoxylin counterstaining intensity was studied. The robustness of ImmunoRatio to variations in image acquisition settings was examined by comparing the optical resolutions provided by 10×, 20×, and 40× microscope objectives, and by comparing the analysis results obtained with six microscope

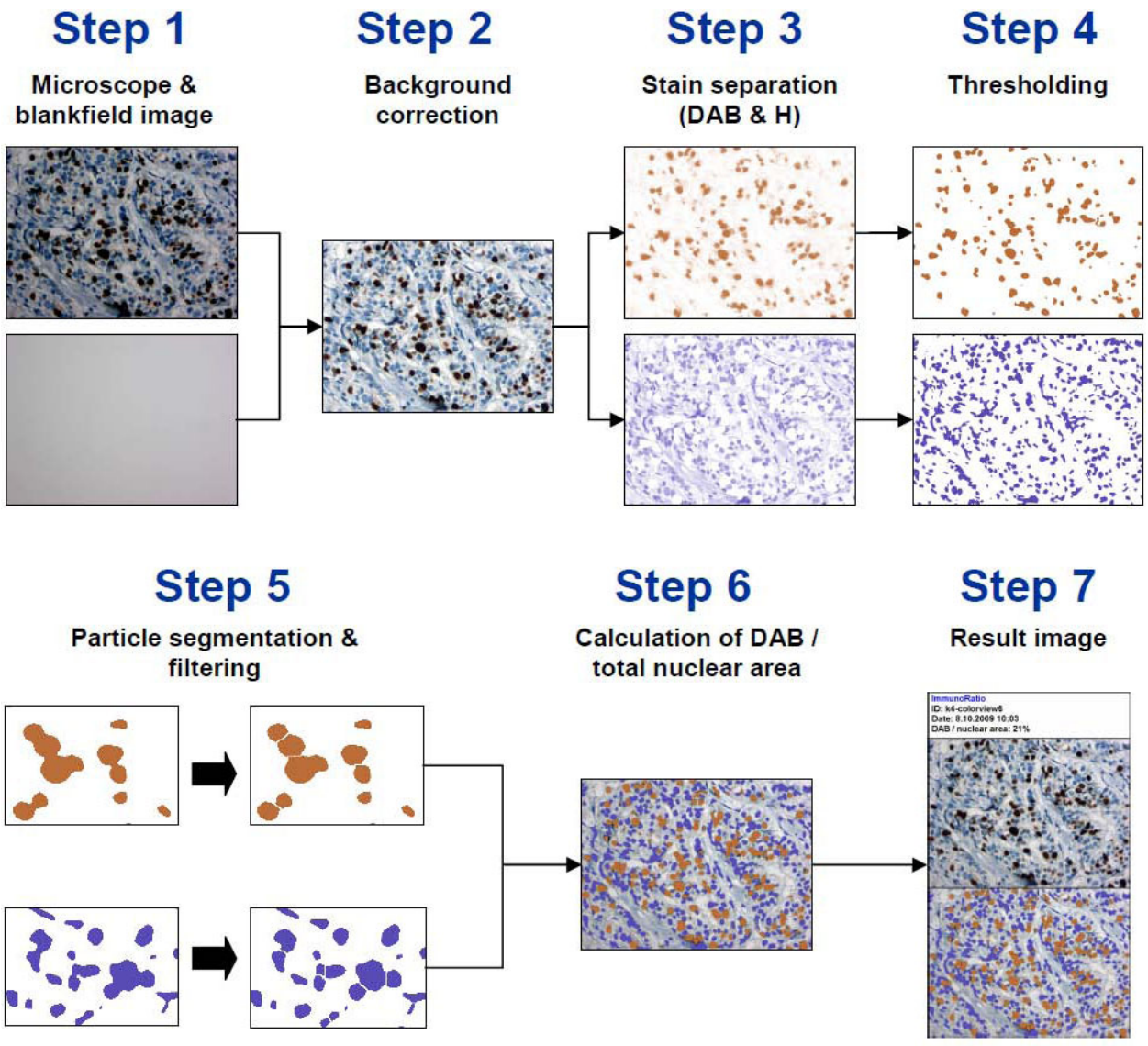

Figure 1 A flowchart outlining the ImmunoRatio analysis algorithm. **Step 1:** A RGB color microscope image, an optional blankfield correction image, and thresholding adjustment parameters are received as an input. **Step 2:** The blankfield image is used to correct uneven illumination and color balance. If a blankfield image is not available, background subtraction is carried out using the Rolling ball algorithm [19]. **Step 3:** The Color Deconvolution plugin [20] is used to separate the stains into two eight-bit component images: diaminobenzidine (DAB) and hematoxylin (H). **Step 4:** The components are processed with a mean filter and binarized using adaptive IsoData thresholding [21]. Component-specific threshold adjustments are applied if defined via input parameters. **Step 5:** The components are processed with a median filter to smooth the thresholding result. Nucleus segmentation is performed on both components by using the Watershed algorithm [22] and small particles are discarded based on their size. For the H component, thin (fibroblastic) cells are identified and discarded using non-round particle removal. **Step 6:** The H and DAB components are overlaid on the source image. The percentage of DAB-stained nuclear area out of the total nuclear area (the labeling index) is calculated. An (optional) external calibration function is used to correct the ratio percentage. **Step 7:** The result image consisting of image identification string, the analysis date, the result labeling index, the original image, and a pseudo-colored image showing the staining components is created. A more detailed algorithm flowchart is available on our research group website [15].

cameras: Scion CFW-1612C (Scion Corporation, Frederick, MD, USA), Altra 20 (Olympus Corporation, Tokyo, Japan), ColorView II (Olympus Corporation, Tokyo, Japan), Leica DFC290 HD (Leica Microsystems, Wetzlar, Germany), Mightex 3MP Color CMOS (Mightex Systems, Pleasanton, CA, USA), and Nikon DS-Fi1 (Nikon Corporation, Tokyo, Japan). The primary output file format used in the acquisition was uncompressed (i.e., lossless). Images were also acquired using JPEG file format (quality factors 10, 20, 40, 60, 80, and 100) to study the suitability of lossy compression for ImmunoRatio analysis. In addition, for each camera, the average diameter

(pixels per μm) of a hematoxylin-stained nucleus was measured. Linear regression was used to fit a first degree polynomial to the data and the polynomial was then embedded into the Scale Finder function of ImmunoRatio. The Scale Finder assists the user in determining a rough scale estimate for the microscope setup, if not known prior to analysis.

Results

ImmunoRatio software

We developed the ImmunoRatio image analysis software, which segments the DAB- and hematoxylin-stained nuclei areas from a microscope image, calculates the labeling index (percent of DAB-stained area out of the total nuclear area), and generates a pseudo-colored result image matching the segmentation. An example analysis output of a Ki-67 image is shown in Figure 2. We first implemented ImmunoRatio as an open source ImageJ plugin, which provides a graphical user interface, as well as the possibility to use it with ImageJ macro language. Multiple images from the same specimen can be analyzed at once, resulting in a montage containing all of the analyzed images. The plugin version enables a direct link to image capture either by using the driver plugins provided by the camera vendors or via the open TWAIN protocol [28]. An open source version of the plugin is available for free download [29].

Based on the plugin described above, we developed a publicly available ImmunoRatio web application (see screenshot in Figure 3). The web application resides in a remote server and is accessed over the Internet with a web browser, without any software downloads or installations. It supports all modern web browsers (e.g., Windows Internet Explorer, Mozilla Firefox, Safari, and Google Chrome) and all operating systems (e.g., Microsoft Windows, Linux distributions, and Mac OS). The main features of the ImmunoRatio web application are summarized in Table 1. The analysis is based on the color deconvolution [12] for stain separation and adaptive IsoData algorithm [21] for thresholding. The analysis can be made either to the whole image or to an interactively defined region of interest (ROI). The analysis adapts to various combinations of microscope objective lenses, phototubes, and camera resolutions by using either an exact or an estimated image scale (pixels per μm). The estimation can be performed using the Scale Finder function. ImmunoRatio supports most existing camera models and their output images, including JPEG, JPEG2000, TIFF, BMP, and PNG. Optimal camera brightness and contrast settings can be defined using the assistance of the Camera Adjustment Wizard. Users can calibrate the software with their own visually determined labeling index data and derive a suitable result correction equation (a third degree polynomial). Users can also fine-adjust the hematoxylin- and DAB-thresholding parameters. For demonstrational analyses, ImmunoRatio offers an introductory basic mode, which has a simplified user interface with minimal required functionality. ImmunoRatio web application is freely accessible on our research group website [15].

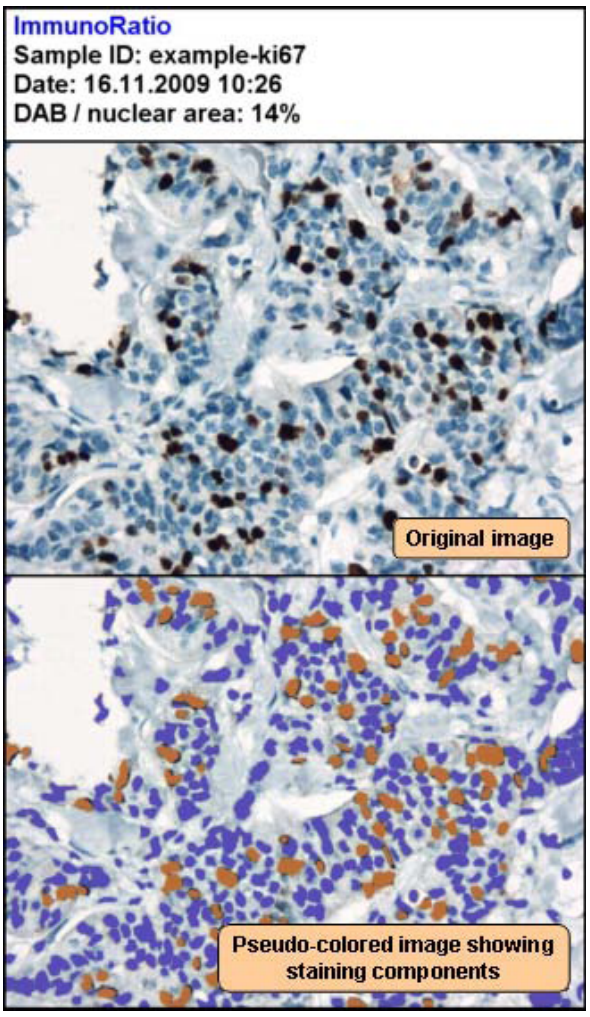

Figure 2 An example result of a Ki-67-stained image processed with ImmunoRatio. The result image includes a sample identifier, the analysis date, the labeling index (percentage of positively stained nuclear area), the original image, and a pseudo-colored image showing the segmented staining components.

Calibration of ImmunoRatio

Although non-calibrated ImmunoRatio correlated well with visual counting of DAB- and hematoxylin-stained cell nuclei (r = 0.97), the results showed an obvious non-linear relation (Figure 4a). Due to this non-linearity, a third degree polynomial was fitted to the data and used as a correction function to calibrate ImmunoRatio. The analysis of the separate test set with calibrated

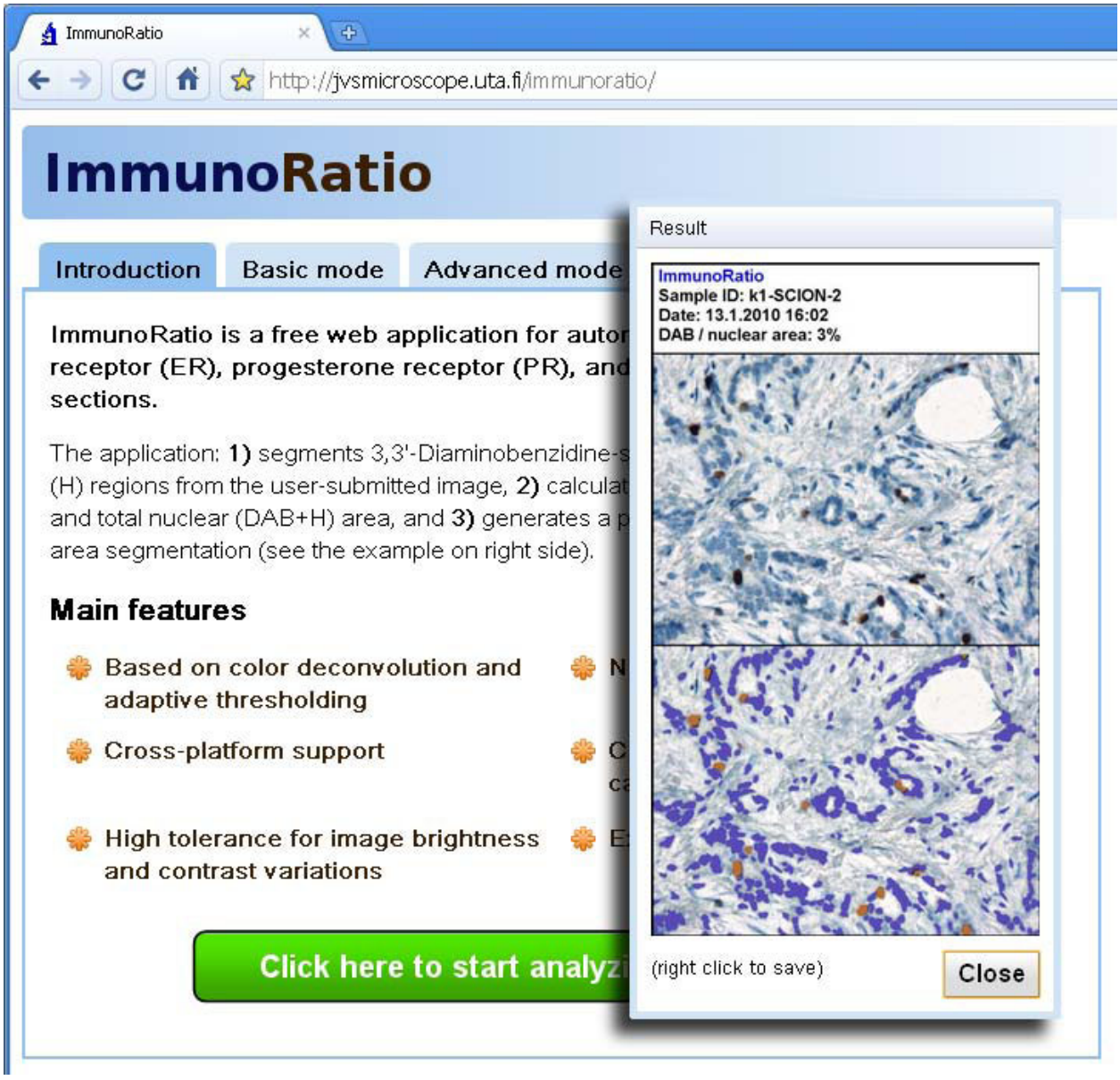

Figure 3 A screenshot of the ImmunoRatio web application. The Result window is shown as an insert in the right panel. The application is publicly available on our jvsmicroscope.uta.fi website, where users can analyze their images freely.

Table 1 Main features of ImmunoRatio web application

Feature	Description
Analytical principle	Analyzes immunostained slides (ER, PR, Ki-67) using color deconvolution [12] for stain separation and adaptive IsoData algorithm [21] for thresholding. Users can analyze either the whole image or a region of interest.
Hardware and software requirements	Runs within the web browser, requiring no additional program or plugin installations. Is compatible with all modern web browsers and operating systems.
Compatibility with different microscope setups	Adapts to various combinations of microscope objective lenses, phototubes, and camera resolutions. Supports most existing camera models and image formats (JPEG, JPEG2000, TIFF, BMP, PNG). Users can define optimal camera brightness and contrast settings with the Camera Adjustment Wizard.
Calibration	Users can calibrate the application to match with their own visual cell counting data.
Usage modes	Includes a basic mode for introductory analyses and a full-featured mode.

ER, estrogen receptor; PR, progesterone receptor.

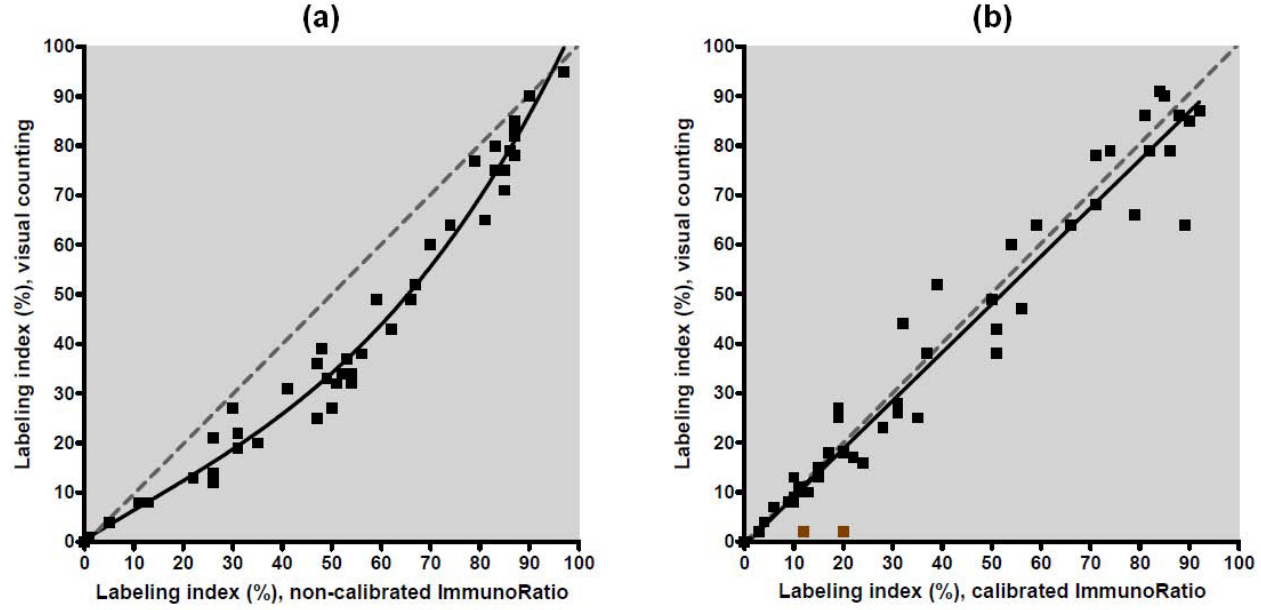

Figure 4 Scatter plots comparing labeling indexes defined by visual cell counting, non-calibrated ImmunoRatio, and calibrated ImmunoRatio. **(a)** The calibration was made using a training set of 50 samples, of which 25 were stained for Ki-67, 13 for progesterone receptor (PR), and 12 for estrogen receptor (ER). To achieve linear relation (dotted line), a correction function was defined by fitting a third degree polynomial (solid black line) to the training set. **(b)** The calibration was validated by using a separate test set of 50 samples (25 stained for Ki-67, 13 for PR, and 12 for ER). The validation test set included two outliers (marked as brown).

ImmunoRatio had a strong linear relation with visual cell counting, showing a near-perfect correlation (r = 0.98; Figure 4b). The test set included two outlier observations, which were detected by visually inspecting the pseudo-color result images. The first outlier had weak DAB-staining intensity, making interpretation based on visual counting difficult. The second outlier had too low image contrast as demonstrated by using the Camera Adjustment Wizard.

In the final step of the validation process, we defined the minimum number of images needed to be captured and analyzed in order to obtain a representative result for the stained breast tumor slides. Using 20× microscope objective, a sufficient number of images per sample for accurate ImmunoRatio analysis was determined to be three (Figure 5). Averaging data from a higher number of images was found to have a minimal impact on the mean labeling index.

The effect of variability in staining and image acquisition settings

The compatibility of ImmunoRatio with variable staining and image acquisition settings is summarized in Table 2. An optimally titrated primary antibody (1:100 for MIB-1 Ki-67) resulted in the best match with visual cell counting. ImmunoRatio tolerated substantial deviations in the antibody dilutions well. A usable antibody dilution was 1:50 to 1:200, because a four-times more diluted antibody (1:400) resulted in labeling indexes that were too low, whereas using very concentrated antibody (1:25) led to cytoplasmic background staining and labeling indexes that were too high. Optimal hematoxylin

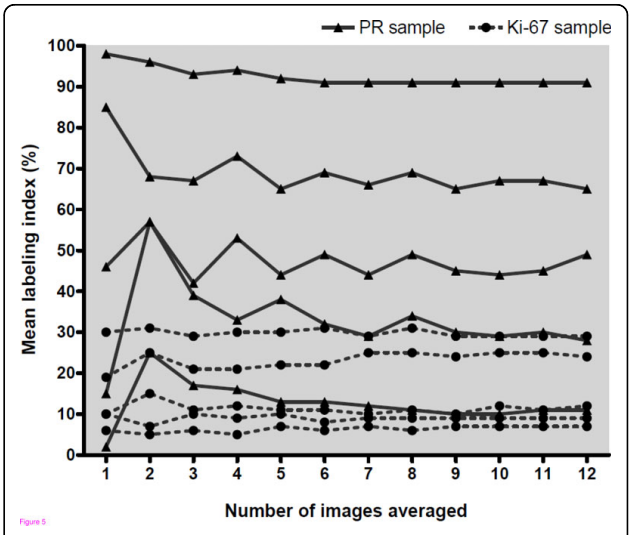

Figure 5 The mean labeling index of ImmunoRatio analysis as a function of the number of images included in the averaged result. Five samples stained for progesteron receptor (PR) and five for Ki-67 were tested.

Table 2 The compatibility of ImmunoRatio with variable staining and image acquisition settings

Immunostaining/image acquisition feature	Compatibility with ImmunoRatio	Comments
Primary antibody dilution (defined for MIB-1 Ki-67)		
too dilute (1:400)	+	too low labeling index (Figure 6a)
optimal (1:100)	+ + +	best match with visual counting (Figure 6b)
too strong (1:25)	+	cytoplasmic background causing overly high labeling indexes (Figure 6c)
Hematoxylin counterstaining		
weak	-	insufficient nuclear segmentation (Figure 6d)
optimal	+ + +	best match with visual counting (Figure 6e)
strong	+	false segmentation of cytoplasmic structures (Figure 6f)
Microscope objective magnification (using 1× phototube)		
10×	+	non-carcinomatous cells often included*
20×	+ + +	for accurate result, an average of three images per sample is recommended
40×	+ +	for accurate result, averaging several images per sample is recommended
Image brightness		
underexposed (too dim)	+	mean gray intensity of the blankfield image <200
in optimal range	+ + +	as guided by the Camera Adjustment Wizard of ImmunoRatio
overexposed (too bright)	-	mean gray intensity of the blankfield image >250
Image contrast		
too low	-	foreground mean gray intensity over 85% of the background mean gray intensity
in optimal range	+ + +	as guided by the Camera Adjustment Wizard of ImmunoRatio
too high	+	foreground mean gray intensity under 50% of the background mean gray intensity
Image compression		
uncompressed (lossless)	+ +	slow network transmission (slower overall analysis time)
JPEG, quality factor 50 to 100 (lossy)	+ + +	optimal for ImmunoRatio
JPEG, quality factor <50 (lossy)	-	visible image artifacts

+ + + = optimally compatible, + + = compatible, + = compatible with possible chance of analytical errors, - = not compatible with ImmunoRatio.
* Region of interest function can be used to exclude unwanted tissue areas.

counterstaining was found to be important. Weak counterstaining caused the nuclear segmentation to fail, whereas overly concentrated counterstaining led to false segmentation of the cytoplasmic structures. Sample images with optimal and non-optimal primary antibody and hematoxylin counterstaining are presented in Figure 6.

Owing to the Scale Finder function, the results of images acquired using 10×, 20×, and 40× objective lenses (with a 1× phototube) were highly similar (data not shown). The 20× objective was deemed to be optimal, requiring at least three images per sample to be averaged. The same results could be achieved by using the 40× objective, but more images per sample needed to be averaged. When using a 10× objective, considerably more non-carcinomatous cells were often included in the analysis. However, the ROI functionality of ImmunoRatio can be used to circumvent this problem. The differences in ImmunoRatio analysis results between the tested camera models and repeated staining batches were found to be small (data not shown).

Variation in image brightness and uneven illumination can be accurately corrected by using the blankfield image, captured using the same microscope and camera settings. However, greatly underexposed images (blankfield image mean gray intensity <200) as well as overly overexposed images (blankfield image mean gray intensity >250) may cause false labeling indexes. For accurate nuclei segmentation, the image contrast must be relatively high; the foreground mean gray intensity should be 50 to 80% of the background mean gray intensity. Users can validate their image acquisition settings by using the Camera Adjustment Wizard function of ImmunoRatio.

For the ImmunoRatio web application, it is advantageous to use lossy image file formats (e.g., JPEG) to minimize the data uploaded to the server for analysis.

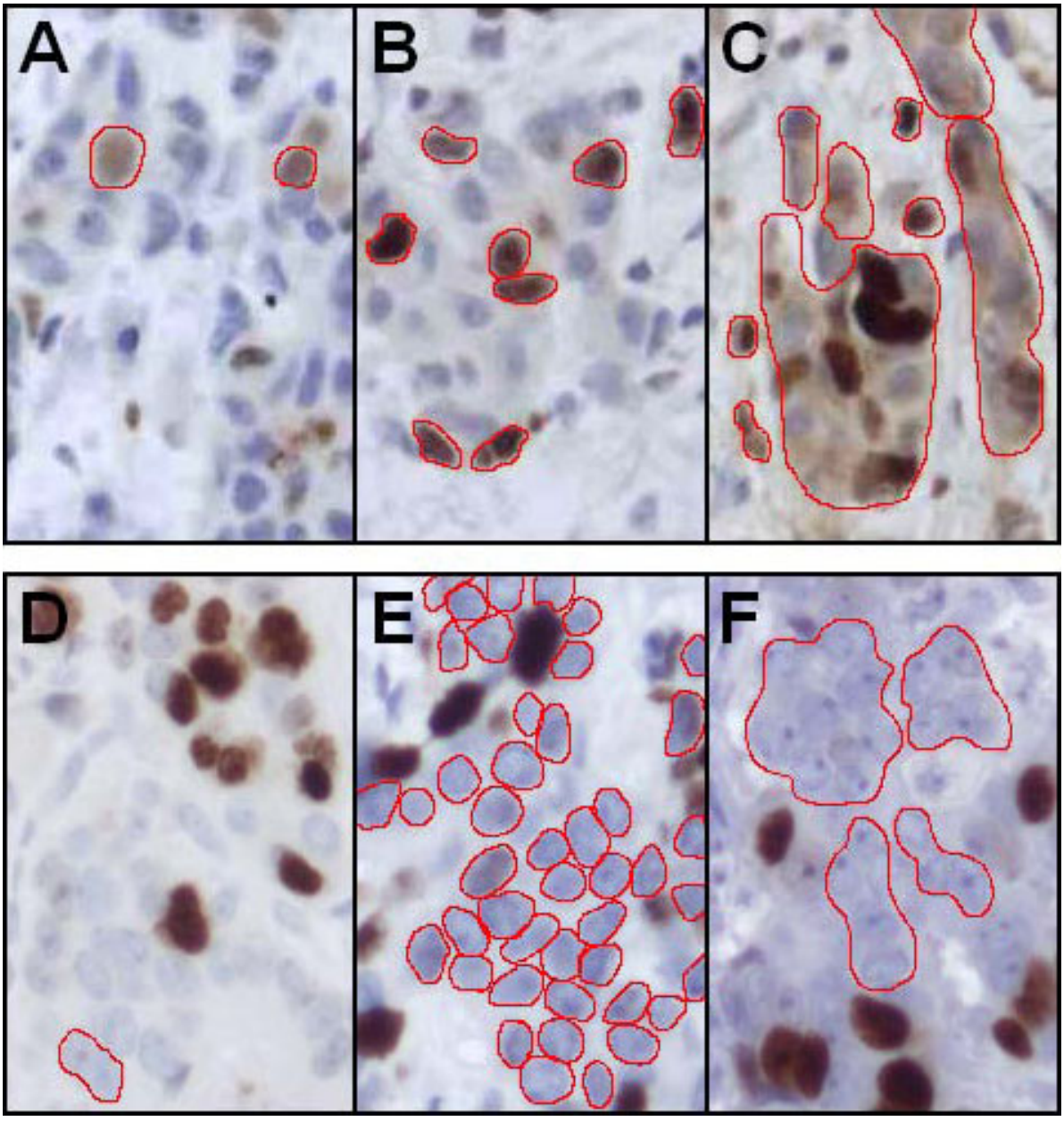

Figure 6 The importance of optimal immunostaining conditions on the accuracy of ImmunoRatio analysis. The red lines outline the nuclei and highlight the segmentation of **(a to c)** brown and **(d to f)** blue staining components. **(a)** Overly dilute primary antibody concentration (Ki-67 MIB-1, 1:400) causes inadequate brown segmentation. **(b)** Optimal antibody dilution (1:100). **(c)** Overly strong antibody concentration (1:25) results in excessive cytoplasmic staining and brown segmentation. **(d)** Overly dilute hematoxylin staining causes inadequate blue segmentation. **(e)** Optimal hematoxylin dilution. **(f)** Overly strong hematoxylin causes excessive cytoplasmic staining and blue segmentation.

We found that using lossy JPEG compression with quality factors 50 to 100 had no significant effect on the accuracy of ImmunoRatio analysis results (data not shown). This compression level allows a typical 5 megabyte uncompressed image to be compressed into 250 kilobytes (about 20:1 compression ratio), enabling rapid image transfer with almost any network bandwidth. Using very low JPEG quality factors (<50) can cause image distortion and artifacts, making the analysis unreliable.

Prognostic validation

As Ki-67 is used clinically as a prognostic parameter, we confirmed the accuracy of ImmunoRatio analysis

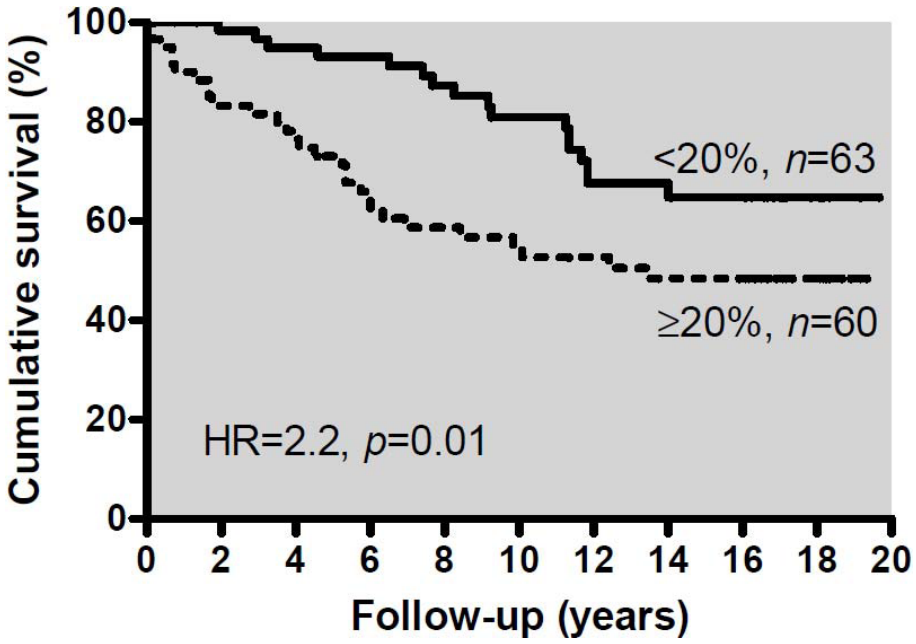

Figure 7 Breast cancer-specific survival of 123 breast cancer patients according to the Ki-67 labeling index determined with ImmunoRatio. The cut-off was set at median Ki-67 labeling index (20%). Tumors with a high labeling index were associated with poorer breast cancer-specific survival during the follow up of 20 years (hazard ratio = 2.2, P = 0.01).

by examining patient survival in a retrospective analysis of 123 breast cancer patients. As expected, based on the literature [5], a strong prognostic correlation was observed (Figure 7). Breast cancer-specific survival of patients with high Ki-67 tumors was significantly shorter than low Ki-67 during 20-year follow-up. Labeling index values of 15%, 20%, and 25% were tested as cut-off. Of those, 20% (the median in this material), gave a hazard ratio (HR) of 2.2 (P = 0.01 by log rank test). Cut-off values 15% and 25% yielded similar results (HR = 2.1 and HR = 2.4, respectively, data not shown).

Discussion

In this study, we described an image analysis application, ImmunoRatio, which is an easy-to-use tool for assessing ER, PR, and Ki-67 labeling indexes in hematoxylin-counterstained tissue sections. ImmunoRatio analysis is based on defining positively stained pixel counts, which, according to our calibration data, correlates very well with cell nuclei enumerated visually. The calibration was performed using a training set of 50 samples and validation using a separate test set of 50 samples representing ER-, PR-, and Ki-67-stained routine breast cancer specimens. The correlation between manual and automated analysis was very high and matched, or exceeded, corresponding results of other similar image analysis software [30,31]. Due to the significant inter-observer variability in visually defined labeling indexes, we recommend that the users calibrate ImmunoRatio with their own labeling index data, as demonstrated in Figure 4 for the calibration training set. Once calibrated, ImmunoRatio can be easily integrated with routine diagnostic work.

Another important aspect of calibration is to determine the optimal Ki-67 cutoff used for prognostic assessment. We tested this with a retrospective analysis of data from 123 primary breast cancer patients followed up for 20 years. The Ki-67 labeling index 20% (the median value in this material) gave a strong prognostic discrimination (HR = 2.2). Although cut-off values 15% and 25% yielded similar prognostication in this patient material, we recommend each laboratory to define their own cut-off value. We recommend using the median value of the Ki-67 labeling index as cut-off. This allows comparisons of different patient materials and provides a reproducible classification of patients according to Ki-67 labeling index.

In addition to accurate calibration, it is clear that for routine use, an image analysis system must accept variation in staining intensity, in microscope setup, and in image acquisition settings. We found up to eight-fold range in primary antibody (Ki-67) dilution to be acceptable for ImmunoRatio. However, when setting up an optimal staining protocol, the users should pay close attention to the hematoxylin counterstaining, which must be bright and clearly separate the nuclei from the

background (see example Figure 6). In terms of optical resolution, we recommend using a microscope setup that roughly corresponds to 20× objective lens magnification, 1× phototube, and a 1.5 megapixel camera. Using this setup, a representative result from a typical breast cancer tumor (diameter 1 to 2 cm) can be obtained by averaging at least three images. Variation in image brightness is well-tolerated owing to the blank-field image correction. The Camera Adjustment Wizard function is designed to help the user find the optimal image brightness and contrast settings. A collection of reference images with optimal staining and imaging settings are presented on our website [15].

ImmunoRatio analysis is based on the color deconvolution algorithm [12], which is one of the several existing alternatives for separating the staining components. In addition to color deconvolution, stain separation and nuclei segmentation have been performed using texture analysis [32], cyan-magenta-yellow-black (CMYK) color model [33], hue-saturation-intensity color model [34], CIE 1976 L*u*v (CIELUV) color model [35], pattern recognition [36], cluster analysis [37], and immunofluorescence with Automated QUantitative Analysis (AQUA) [38]. However, the software applications described in the above mentioned studies are mainly for research purposes and they have not been released for public use. Many of the methods may require considerable work if employed in a routine clinical process. The color deconvolution-based approach for separating two stains is straightforward and fast, and is readily usable for images captured with conventional microscope color cameras. If more than two staining components are used or the analysis requires accurate intensity-based quantification, the AQUA method or multispectral imaging would most likely be better alternatives [11].

ImmunoRatio was developed using ImageJ, which is a public domain (i.e., completely free and open source) image analysis software. However, a major obstacle in adopting ImageJ, or any other image analysis software, in clinical laboratories is usually the strict computer security policy. The local system and network rules usually prohibit users to download, install, and/or run external applications. To address these constraints, we released ImmunoRatio as a web application, which provides an easy-to-use web interface, requires no software downloads or installations, and can be used in highly restricted environments.

Conclusions

To the best of our knowledge, ImmunoRatio is the first ready-to-use web application for analyzing nuclear immunostains (e.g., ER, PR, and Ki-67). We want to point out that ImmunoRatio is meant to be used as a diagnostic aid by personnel trained to score immunostained breast cancer slides. Furthermore, the analysis results should always be interpreted together with the pseudo-colored images and the original sample slides. ImmunoRatio has already been used in the authors' laboratory for more than 1,000 cases and tested by several collaborators. The application is open to free public access on our research group website [15]. Complementary software for analyzing cell membrane staining (e.g., HER-2) is currently being developed.

Abbreviations

AQUA: automated quantitative analysis; CIELUV: CIE 1976 L*u*v; CMYK: cyan-magenta-yellow-black; DAB: diaminobenzidine; ER: estrogen receptor; HR: hazard ratio; PBS: phosphate-buffered saline; PR: progesterone receptor; ROI: region of interest.

Acknowledgements

This study was financially supported by the Finnish Cancer Foundation, the Sigrid Juselius Foundation, the Tampere University Hospital, and the Seinäjoki Central Hospital (governmental EVO grant). The authors wish to thank laboratory technicians Sari Toivola, Kristiina Ryömä, Ritva Kujala, Helvi Salmela, and Pirjo Pekkala for assisting in sample preparation and immunostaining.

Author details

[1]Institute of Medical Technology, University of Tampere, Biokatu 6, 33014 Tampere, Finland. [2]Department of Pathology, Seinäjoki Central Hospital, Hanneksenrinne 7, 60220 Seinäjoki, Finland.

Authors' contributions

VJT carried out the software design and implementation, prepared the manuscript, and participated in the study design. SR performed the immunohistochemistry and the software calibration. AV contributed to the software design. MJ supervised the immunohistochemistry and the calibration processes. JI was responsible for the study design and coordination, and helped to draft the manuscript. All authors read and approved the final manuscript.

Competing interests

The authors declare that they have no competing interests.

Received: 9 March 2010 Revised: 9 June 2010 Accepted: 27 July 2010
Published: 27 July 2010

References

1. Allred DC, Carlson RW, Berry DA, Burstein HJ, Edge SB, Goldstein LJ, Gown A, Hammond ME, Iglehart JD, Moench S, Pierce LJ, Ravdin P, Schnitt SJ, Wolff AC: **NCCN Task Force Report: Estrogen Receptor and Progesterone Receptor Testing in Breast Cancer by Immunohistochemistry.** *J Natl Compr Canc Netw* 2009, **7**:S1-S21, quiz S22-23.
2. **United Kingdom National External Quality Assessment Service (UK NEQAS).** [http://www.ukneqas.org.uk/].
3. **Nordic immunohistochemical Quality Control (NordiQC).** [http://www.nordiqc.org/].
4. de Azambuja E, Cardoso F, de Castro G Jr, Colozza M, Mano MS, Durbecq V, Sotiriou C, Larsimont D, Piccart-Gebhart MJ, Paesmans M: **Ki-67 as prognostic marker in early breast cancer: a meta-analysis of published studies involving 12,155 patients.** *Br J Cancer* 2007, **96**:1504-1513.
5. Stuart-Harris R, Caldas C, Pinder SE, Pharoah P: **Proliferation markers and survival in early breast cancer: a systematic review and meta-analysis of 85 studies in 32,825 patients.** *Breast* 2008, **17**:323-334.
6. Goldhirsch A, Ingle JN, Gelber RD, Coates AS, Thürlimann B, Senn HJ, Panel members: **Thresholds for therapies: highlights of the St Gallen International Expert Consensus on the primary therapy of early breast cancer 2009.** *Ann Oncol* 2009, **20**:1319-1329.

7. Harvey JM, Clark GM, Osborne CK, Allred DC: **Estrogen receptor status by immunohistochemistry is superior to the ligand-binding assay for predicting response to adjuvant endocrine therapy in breast cancer.** *J Clin Oncol* 1999, **17**:1474-1481.
8. Shousha S: **Oestrogen receptor status of breast carcinoma: Allred/H score conversion table.** *Histopathology* 2008, **53**:346-347.
9. Rüdiger T, Höfler H, Kreipe HH, Nizze H, Pfeifer U, Stein H, Dallenbach FE, Fischer HP, Mengel M, von Wasielewski R, Müller-Hermelink HK: **Quality assurance in immunohistochemistry: results of an interlaboratory trial involving 172 pathologists.** *Am J Surg Pathol* 2002, **26**:873-882.
10. Walker RA: **Quantification of immunohistochemistry - issues concerning methods, utility and semiquantitative assessment I.** *Histopathology* 2006, **49**:406-410.
11. Taylor C, Levenson R: **Quantification of immunohistochemistry - issues concerning methods, utility and semiquantitative assessment II.** *Histopathology* 2006, **49**:411-424.
12. Ruifrok AC, Johnston DA: **Quantification of histochemical staining by color deconvolution.** *Anal Quant Cytol Histol* 2001, **23**:291-299.
13. van der Loos CM: **Multiple immunoenzyme staining: methods and visualizations for the observation with spectral imaging.** *J Histochem Cytochem* 2008, **56**:313-328.
14. Rojo MG, Bueno G, Slodkowska J: **Review of imaging solutions for integrated quantitative immunohistochemistry in the Pathology daily practice.** *Folia Histochem Cytobiol* 2009, **47**:349-354.
15. **ImmunoRatio web application.** [http://jvsmicroscope.uta.fi/immunoratio/].
16. **ImageJ image analysis software.** [http://rsb.info.nih.gov/ij/].
17. **Java programming language.** [http://java.sun.com/].
18. **Calculator Plus ImageJ plugin.** [http://rsbweb.nih.gov/ij/plugins/calculator-plus.html].
19. Sternberg SR: **Biomedical Image Processing.** *IEEE Computer* 1983, **16**:22-34.
20. **Colour Deconvolution ImageJ plugin.** [http://www.dentistry.bham.ac.uk/landinig/software/cdeconv/cdeconv.html].
21. Ridler TW, Calvard S: **Picture thresholding using an iterative selection method.** *IEEE Trans Systems Man and Cybernetics* 1978, **8**:630-632.
22. Beucher S, Meyer F: **The morphological approach to segmentation: The watershed transformation.** *Mathematical Morphology in Image Processing* New York: Marcel DekkerDougherty ER , 1 1993, 433-481.
23. **Google Web Toolkit.** [http://code.google.com/webtoolkit/].
24. **Apache Commons FileUpload library.** [http://commons.apache.org/fileupload/].
25. **Apache Commons IO library.** [http://commons.apache.org/io/].
26. **The Laboratory for Optical and Computational Instrumentation (LOCI) Bio-Formats library.** [http://www.loci.wisc.edu/software/bio-formats/].
27. **Apache Tomcat Java servlet container.** [http://tomcat.apache.org/].
28. **The TWAIN standard specification.** [http://www.twain.org/].
29. **ImmunoRatio ImageJ plugin.** [http://jvsmicroscope.uta.fi/immunoratio-plugin/].
30. Mofidi R, Walsh R, Ridgway PF: **Objective measurement of breast cancer oestrogen receptor status through digital image analysis.** *Eur J Surg Oncol* 2003, **29**:20-24.
31. Faratian D, Kay C, Robson T, Campbell FM, Grant M, Rea D, Bartlett JM: **Automated image analysis for high-throughput quantitative detection of ER and PR expression levels in large-scale clinical studies: the TEAM Trial Experience.** *Histopathology* 2009, **55**:587-593.
32. Kostopoulos S, Cavouras D, Daskalakis A, Bougioukos P, Georgiadis P, Kagadis GC, Kalatzis I, Ravazoula P, Nikiforidis G: **Colour-texture based image analysis method for assessing the hormone receptors status in breast tissue sections.** *Conf Proc IEEE Eng Med Biol Soc* 2007, **2007**:4985-4988.
33. Pham NA, Morrison A, Schwock J, Aviel-Ronen S, Iakovlev V, Tsao MS, Ho J, Hedley DW: **Quantitative image analysis of immunohistochemical stains using a CMYK color model.** *Diagn Pathol* 2007, **2**:8.
34. Ruifrok AC, Katz RL, Johnston DA: **Comparison of quantification of histochemical staining by hue-saturation-intensity (HSI) transformation and color-deconvolution.** *Appl Immunohistochem Mol Morphol* 2003, **11**:85-91.
35. Rexhepaj E, Brennan DJ, Holloway P, Kay EW, McCann AH, Landberg G, Duffy MJ, Jirstrom K, Gallagher WM: **Novel image analysis approach for quantifying expression of nuclear proteins assessed by immunohistochemistry: application to measurement of oestrogen and progesterone receptor levels in breast cancer.** *Breast Cancer Res* 2008, **10**:R89.
36. Kostopoulos S, Cavouras D, Daskalakis A, Kagadis GC, Kalatzis I, Georgiadis P, Ravazoula P, Nikiforidis G: **Cascade pattern recognition structure for improving quantitative assessment of estrogen receptor status in breast tissue carcinomas.** *Anal Quant Cytol Histol* 2008, **30**:218-225.
37. Gustavson MD, Bourke-Martin B, Reilly DM, Cregger M, Williams C, Tedeschi G, Pinard R, Christiansen J: **Development of an unsupervised pixel-based clustering algorithm for compartmentalization of immunohistochemical expression using Automated QUantitative Analysis.** *Appl Immunohistochem Mol Morphol* 2009, **17**:329-337.
38. Camp RL, Chung GG, Rimm DL: **Automated subcellular localization and quantification of protein expression in tissue microarrays.** *Nat Med* 2002, **8**:1323-1327.

doi:10.1186/bcr2615
Cite this article as: Tuominen *et al.*: ImmunoRatio: a publicly available web application for quantitative image analysis of estrogen receptor (ER), progesterone receptor (PR), and Ki-67. *Breast Cancer Research* 2010 **12**:R56.

Histopathology

Histopathology 2012, **60**, 758–767. DOI: 10.1111/j.1365-2559.2011.04142.x

ImmunoMembrane: a publicly available web application for digital image analysis of HER2 immunohistochemistry

Vilppu J Tuominen,[1] Teemu T Tolonen[1,2] & Jorma Isola[1]

[1]*Institute of Biomedical Technology, University of Tampere, Tampere, Finland, and* [2]*Department of Pathology, Centre for Laboratory Medicine, Tampere University Hospital, Tampere, Finland*

Date of submission 8 July 2011
Accepted for publication 23 September 2011

Tuominen V J, Tolonen T T & Isola J
(2012) *Histopathology* **60**, 758–767

ImmunoMembrane: a publicly available web application for digital image analysis of HER2 immunohistochemistry

Aims: Assessment of the human epidermal growth factor receptor 2 (HER2) with immunohistochemistry (IHC) is routine practice in clinical pathology laboratories. Visual classification of the staining reaction (usually into 0/1+, 2+ or 3+) is subjective and prone to significant inter- and intra-observer variation. In this study, we describe ImmunoMembrane, an easy-to-use HER2 IHC analysis software, which is freely available as a web application, requiring no download or installation.

Methods and results: ImmunoMembrane uses colour deconvolution for stain separation and a customized algorithm for cell membrane segmentation. A quantitative score (IM-score, 0–20 points) is generated according to the membrane staining intensity and completeness. Specimens are classified into 0/1+, 2+ or 3+ based on IM-score cut-offs defined using a training set. The classification and membrane segmentation are presented as a pseudo-coloured overlay image. With a validation set (144 HercepTest®-stained whole tissue sections), ImmunoMembrane matched well with the pathologist's visual classification (weighted kappa $\kappa_w = 0.80$), as well as fluorescence *in-situ* hybridization (FISH) (IHC disagreement 3.5%, $n = 144$) and chromogenic *in-situ* hybridization (CISH) (IHC disagreement 2.8%, $n = 144$).

Conclusions: We anticipate that publicly available web applications, such as ImmunoMembrane, will accelerate the adoption of automated image analysis in clinical diagnostics of HER2 IHC. ImmunoMembrane is freely accessible at: http://jvsmicroscope.uta.fi/immunomembrane/.

Keywords: breast cancer, human epidermal growth factor receptor 2, immunohistochemistry, open source software, quantification

Abbreviations: CISH, chromogenic *in-situ* hybridization; DAB, diaminobenzidine; FISH, fluorescence *in-situ* hybridization; HER2, human epidermal growth factor receptor 2; IHC, immunohistochemistry

Introduction

Histopathological diagnosis of breast cancer includes assessing the human epidermal growth factor receptor 2 (HER2) oncoprotein overexpression, which is defined by immunohistochemical (IHC) staining. Positive HER2 status of a tumour (IHC score 3+ and/or positive result by an *in-situ* hybridization test) is considered necessary for patients to be eligible for trastuzumab-based chemotherapy.[1] Although the analytical quality of HER2 IHC has been debated for more than a decade, recent results of interlaboratory quality assurance studies provide evidence of reasonably high reproducibility of the laboratory staining procedure.[2,3] With the use of standardized staining reagent kits [such as HercepTest® by Dako (Copenhagen, Denmark); PATHWAY® by Ventana Medical Systems (Tucson, AZ, USA); and Oracle™ by Leica Microsystems (Wetzlar, Germany)], the interlaboratory concordance has reached up to 80–90%.[2,3]

Address for correspondence: Jorma Isola, MD, PhD, Cancer Biology, Institute of Biomedical Technology, University of Tampere, 33014 Tampere, Finland. e-mail: jorma.isola@uta.fi

Common practice in pathology laboratories is to score HER2-stained slides visually (also termed manually) using light microscopy at medium-power magnification (e.g. using ×10 or ×20 objective lenses). A tumour is scored as 0/1+ (negative), 2+ (equivocal) or 3+ (positive), as instructed in the widely accepted scoring guidelines.[1] A threshold of 30% intensively membrane stained tumour cells is used commonly as a cut-off for defining a 3+ positive HER2 status.[4] Although verbal description of the scoring principle is straightforward, in reality the microscopic evaluation of HER2 IHC is subjective and can lead to significant inter-observer variability and lack of reproducibility. To overcome this, various digital image analysis methods have been described.[5–8] The analysis algorithms are generally based on differentiating the staining components: haematoxylin counterstain (blue) and immunoreaction product (brown diaminobenzidine; DAB), followed by segmentation and quantitation of the DAB component. However, measuring the DAB component intensity is, at best, only semi-quantitative, as the optical density of the immunoreaction product does not reflect accurately the true abundance of the HER2 protein antigen.[9,10] Despite the lack of full quantitativeness, systems classifying HER2 IHC are a cornerstone in clinical breast cancer diagnostics.[1]

In a recent survey, up to one-third of laboratories reported to use quantitative image analysis in routine diagnostics of HER2.[11] Routine laboratory image analyses are usually carried out with proprietary applications [such as Aperio Digital IHC by Aperio Technologies (Vista, CA, USA), and ACIS® III by Dako (Copenhagen, Denmark)], which are tailored to work only with specific analysis instrumentation and/or are bundled with an imaging device, such as a virtual slide scanner or a microscope camera.[12] Tight hardware coupling, combined with closed software source code, make these analysis systems incompatible with existing microscope and camera setups, thereby complicating the widespread adoption of automated diagnostics. Hardware-independent and open source analysis applications would improve the situation but, to our knowledge, none of the HER2 IHC analysis software described in peer-reviewed journals have been released for public evaluation and use.

To fulfil this task, we developed ImmunoMembrane (IM), an image analysis software for HER2 IHC that is accessed and used with a web browser, without the need for any software download or installation. In order to become widely accepted and utilized, we designed the software to be compatible with existing microscope and digital camera setups. Consistent analysis results and repeatability across different staining batches and camera models is achieved by normalizing raw image intensity and contrast during image preprocessing. ImmunoMembrane is free, open source and publicly available at http://jvsmicroscope.uta.fi/immunomembrane/.

Materials and methods

IMMUNOHISTOCHEMISTRY

Formalin-fixed and paraffin-embedded tissue sections from invasive breast cancers were derived from earlier studies. The training set consisted of tissue microarrays (TMA) of 220 breast cancers[13] and the validation set of whole sections of 144 invasive breast cancers.[14] Immunohistochemical staining of HER2 was performed using the HercepTest® kit (Dako, Copenhagen, Denmark), according to the manufacturer's instructions using Lab Vision Autostainer® (Lab Vision, Fremont, CA, USA). Gene amplification status of the tumours was verified with both fluorescence *in-situ* hybridization (FISH) and chromogenic *in-situ* hybridization (CISH) (SPoT-Light® HER2 CISH kit by Life Technologies, Carlsbad, CA, USA; and PathVysion® FISH kit by Abbott Laboratories, Chicago, IL, USA).

SOFTWARE DEVELOPMENT

ImmunoMembrane was first developed as a plugin for the ImageJ image analysis software (version 1.45b; National Institutes of Health, Bethesda, MD, USA)[15] using the Java programming language.[16] In addition to built-in ImageJ functions, ImmunoMembrane uses the Calculator Plus plugin[17] for blankfield correction, the Color Deconvolution plugin[18] for DAB stain separation and the Particles4 & Particles8 plugins[19] for cell membrane segmentation. The ImmunoMembrane plugin was embedded into a Java servlet-based web application. The web application was developed using Google Web Toolkit (1.7.1),[20] Apache Commons FileUpload package (1.2.1),[21] Apache Commons IO library (1.4),[22] Laboratory for Optical and Computational Instrumentation Bio-Formats package (4.1)[23] and Apache Tomcat servlet container (6.0).[24]

ANALYSIS ALGORITHM

The main steps of the ImmunoMembrane analysis algorithm are outlined in Figure 1. A more detailed algorithm flowchart is available on our website (http://jvsmicroscope.uta.fi/immunomembrane/). Prior to the analysis, the algorithm expects the user to

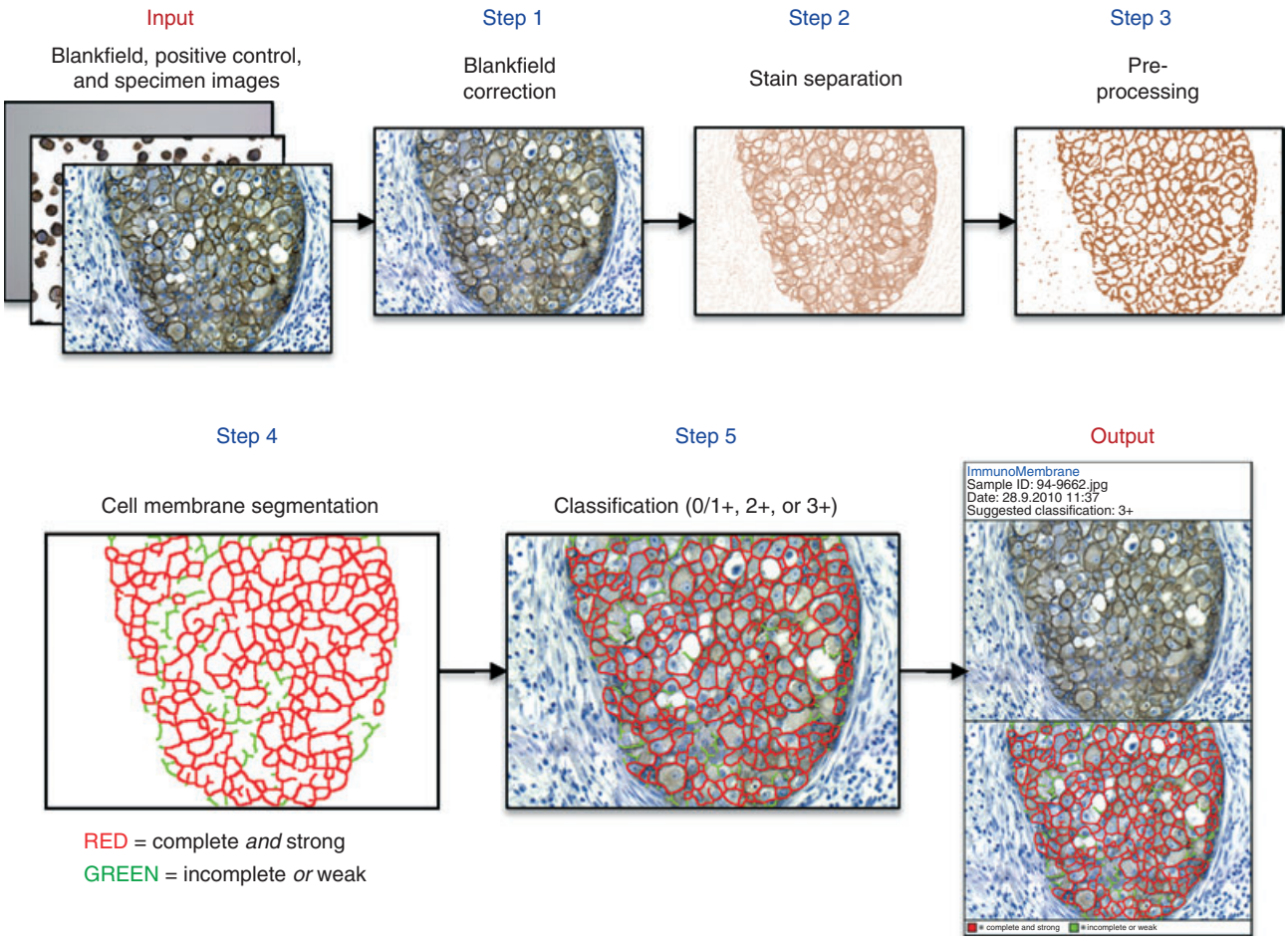

Figure 1. A flowchart outlining the ImmunoMembrane (IM) analysis algorithm. Input: the algorithm receives an RGB colour microscope image, an optional blankfield correction image, user-defined IM-score category cut-offs and reference intensity (RI) and reference contrast (RC) measured from the positive control image. Step 1: the blankfield image is used to correct uneven illumination and colour balance. Step 2: the diaminobenzidine (DAB) component is separated using colour deconvolution. Step 3: the DAB component is contrast-normalized using RC, and processed with a median filter and an unsharp mask filter, followed by binarization with a fixed threshold. Step 4: cell membrane segmentation is performed using median filtering, skeletonizing and contour- and size-based particle filtering. The segmented membrane regions are divided into two groups: membranes with complete and strong membrane staining and membranes with incomplete or weak staining. Step 5: the membrane groups are overlaid on the source image and the sample is awarded an IM-score (0–20 points) using a scheme described in Materials and methods (equation 1). Finally, the sample image is classified (0/1+, 2+ or 3+) based on the user-defined IM-score category cut-offs. Output: the resulting image consisting of image identification string, analysis date, suggested classification, the original sample image and a pseudo-coloured image showing the segmented membrane regions is created. A more detailed algorithm flowchart is available on http://jvsmicroscope.uta.fi/immunomembrane/.

provide two reference images: a blankfield image, which is captured from an empty slide background area, and a positive control image, which is captured from the positive control slide supplied with every staining kit. The blankfield image is used to correct uneven illumination and colour balance of the imaging setup, whereas the positive control image is used to normalize the intensity and contrast variations between different staining batches and image acquisition settings. More specifically, the positive control image provides reference intensity, which is the mean membrane pattern intensity, and reference contrast, which is the dynamic range width of the separated DAB component.

To quantitate the membrane pattern completeness and intensity, a point-based IM-score evaluation system was developed for the ImmunoMembrane analysis algorithm. For a given sample, the IM-score (0–20 points) is the sum of two components:

$$\text{IM-score} = C + I, \tag{1}$$

where C is the membrane completeness (0–10 points) and I is the membrane intensity (0–10 points). Com-

ponent C is divided further into two subcomponents. The first subcomponent measures the total membrane area C_1 (0–5 points):

$$C_1(M_p) = \begin{cases} 0, & M_p = 0.00 \\ 1, & 0.01 > M_p \leq 0.05 \\ 2, & 0.05 > M_p \leq 0.10 \\ 3, & 0.10 > M_p \leq 0.15 \\ 4, & 0.15 > M_p \leq 0.20 \\ 5, & M_p > 0.20, \end{cases} \quad (2)$$

where M_p is the percentage of membrane area out of total image area. The second subcomponent measures the complete membrane area C_2 (0–5 points):

$$C_2 = round\left(\frac{M_c}{M_t} * 5\right), \quad (3)$$

where M_c is the complete cell membrane area (in pixels) and M_t is the total membrane area (in pixels). The membrane intensity component I (0–10 points) is formed by normalizing component C with the reference intensity and contrast:

$$I = round(I_w * C) \quad (4)$$

$$I_w = 1 - \frac{I_{mem} - I_{ref}}{D_{ref}}, \quad (5)$$

where I_w is an intensity weight, I_{mem} is the measured membrane intensity, I_{ref} is the reference intensity and D_{ref} is the reference contrast.

ALGORITHM TRAINING

To train the algorithm to match the 0/1+, 2+ and 3+ classification by the American Society of Clinical Oncology /College of American Pathologists (ASCO / CAP), predefined category cut-offs were specified by using a training set, which consisted of 220 breast cancer on TMA slides stained with HercepTest®. The slides were scanned using Aperio ScanScope® XT (Aperio Technologies, Vista, CA, USA; ×20 objective lens, 2.0 pixels/μm). From each tissue core, one representative snapshot (1596 × 1116 pixels) was selected for analysis. The analysis was first performed visually by an expert pathologist (J.I.) and then automatically by ImmunoMembrane. Using the pathologist's visual classification as golden standard, the optimal IM-score cut-offs were defined by searching the peak weighted (equally spaced) kappa agreement κ_w.[25]

ALGORITHM VALIDATION

To validate the analysis algorithm training, first the optimal required number of image fields to be captured and averaged from a typical tumour sample (diameter 1–2 cm) was defined. From a non-negative set of 13 breast cancer samples, 10 images per sample representing central and peripheral tumour areas were imaged using Scion CFW-1612C camera (Scion Corporation, Frederick, MD, USA; 1/1.8″ sensor, ×10 objective lens, ×1 phototube, 1600 × 1200 pixels, 2.15 pixels/μm) and analysed using ImmunoMembrane. After specifying the optimal field count, a separate validation set consisting of whole sections of 144 HercepTest®-stained invasive breast cancers was analysed using ImmunoMembrane and compared against the visual assessment of an expert pathologist (J.I.). Finally, the disagreement rate of the IHC classifications was compared with the results obtained with FISH and CISH.

ALGORITHM ROBUSTNESS TESTING

Initial versions of the analysis algorithm did not include intensity and contrast normalization, which caused variable results with different imaging hardware and acquisition settings (Figure 2). After adding the normalization feature, the algorithm robustness was tested using 41 non-negative breast cancer TMA cores, which were digitized with six different camera models: (i) ColorView II by Olympus Corporation, Tokyo, Japan; (ii) Leica DFC310 FX by Leica Microsystems, Wetzlar, Germany; (iii) OptixCam OCD-3.3-ICE by The Microscope Store, VA, USA; (iv) QICAM Fast1394 by QImaging, Surrey, Canada; (v) Scion CFW-1612C by Scion Corporation, Frederick, MD, USA; and (vi) the virtual microscope scanner camera of Aperio ScanScope® XT by Aperio Technologies, Vista, CA, USA. To simulate the real-life diagnostic environment, the cameras were attached to workstations using LCD displays from various manufacturers (all set to factory default settings). Camera illumination was fixed (auto-exposure disabled) and adjusted to match with the image seen through microscope oculars. Non-linear image intensity and contrast corrections, as well as additional software image enhancements, were set as low as possible. Each camera's scale (in pixels per μm) was measured by using a stage micrometer and recorded for usage during analysis. After these initial configurations, the actual testing was split into several steps. First, to normalize camera intensity and contrast variation, a blankfield and a positive control image were captured for each camera model. Secondly, with

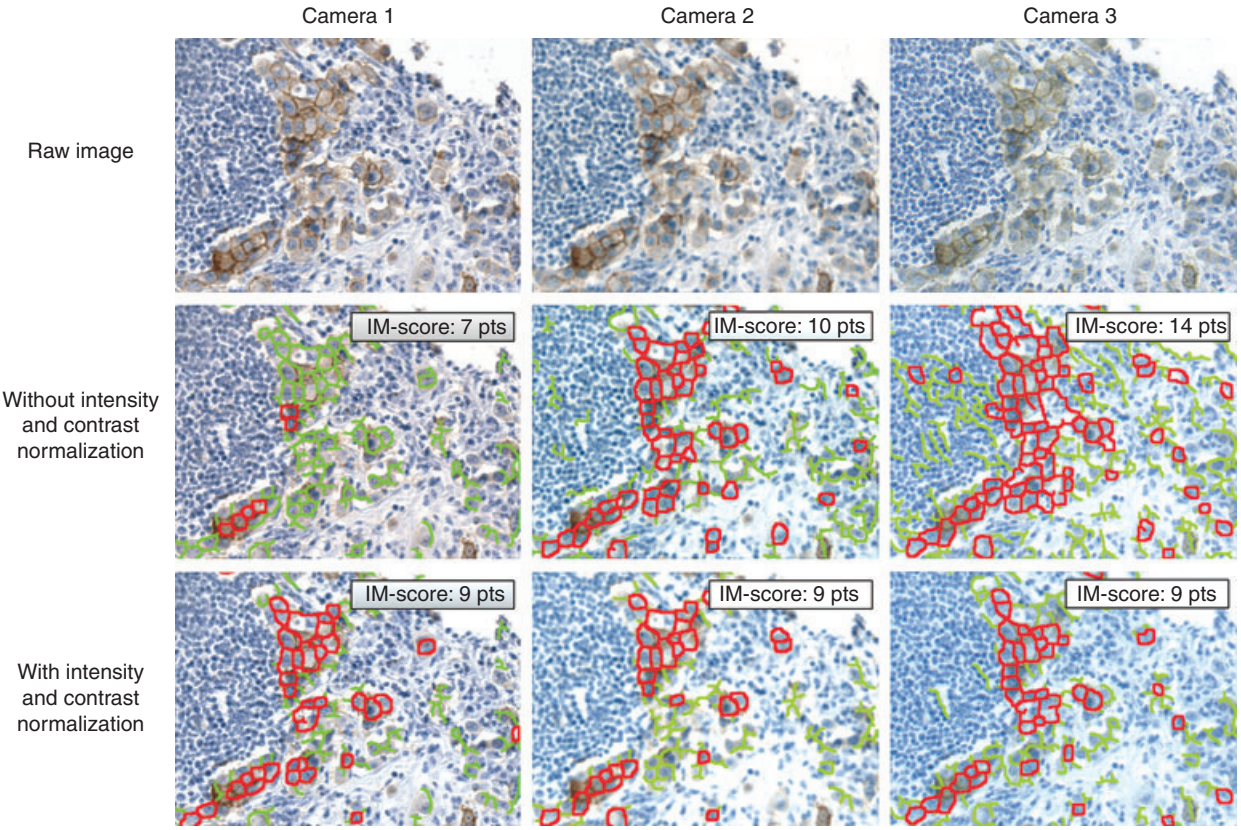

Figure 2. The effect of intensity and contrast normalization on ImmunoMembrane (IM) analysis. A predefined image field was acquired with three digital microscope cameras (using fixed exposure, camera-specific image scale and non-linear image corrections disabled) and analysed using ImmunoMembrane with and without image normalization. The normalization is performed using two reference images: a blankfield image for correcting the uneven illumination and incorrect colour balance, and a positive reference image – captured from the positive control slide – for balancing changes between staining batches and/or image acquisition settings. Without normalization, the analysis becomes inconsistent across different camera models and, for example, a failed stain separation might produce incorrectly detected membrane areas (as exemplified with camera 3).

each camera, a fixed area from each sample was imaged using a × 10 objective lens (Aperio ×20) and analysed subsequently using ImmunoMembrane. Thirdly, all result IM-scores obtained for a sample were averaged into a sample-specific reference score. For each camera–sample pair, the absolute difference of the camera-specific IM-score and the sample reference score was measured (=error value). Finally, the error values of each camera were averaged and their equivalence was compared statistically using variance analysis (Kruskal–Wallis non-parametric test, $\alpha = 0.05$).

Results

We developed the ImmunoMembrane image analysis application for semi-quantitative classification of HER2 IHC. The application segments DAB-stained cell membrane regions from a set of sample images, classifies the staining according to standard criteria (into 0/1+, 2+ or 3+) based on the membrane staining completeness and intensity. The results can be verified using a pseudo-coloured overlay result image, which matches with the detected membrane segmentation (Figure 3). ImmunoMembrane was first developed and published as an open source ImageJ plugin, which provides a graphical user interface and the possibility to integrate it with ImageJ macro language. The plugin version also enables a direct link to image capture either by using the driver plugins by the camera vendors or via the open TWAIN protocol.[26] The ImmunoMembrane plugin is available for download at http://jvsmicroscope.uta.fi/immunomembrane-plugin/.

ImmunoMembrane was precalibrated to match the visual classification of an expert pathologist. For this task, we developed the IM-score evaluation system,

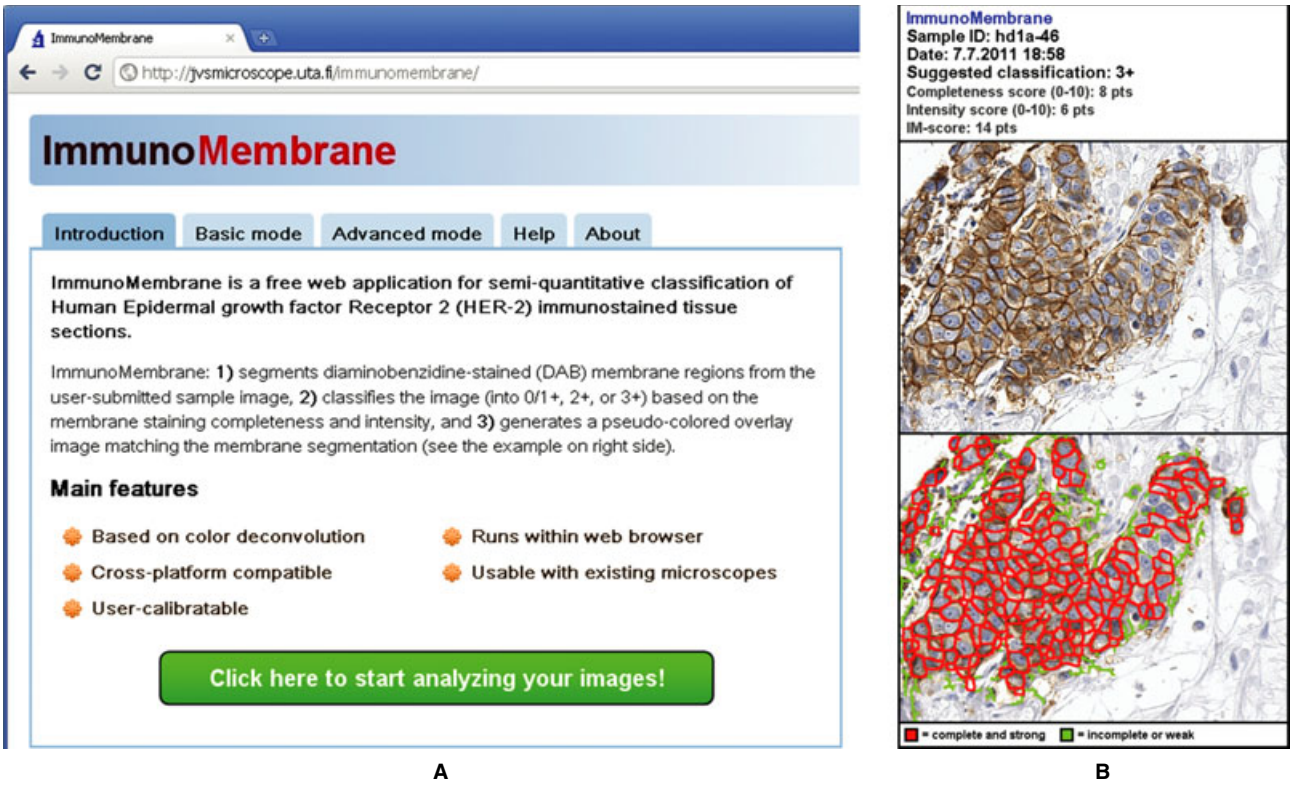

Figure 3. A screenshot of ImmunoMembrane (IM) web application and an example human epidermal growth factor receptor 2 (HER2) immunohistochemistry (IHC) classification. The analysis is performed within a web browser, which displays the analysis result in a panel window (**A**). The result (**B**) contains image identification string, analysis date, suggested classification (0/1+, 2+ or 3+) and, optionally, the IM-score (combined from the completeness and intensity score). The result also contains the original sample image (upper part) and a pseudo-coloured overlay image showing the segmented cell membrane regions (lower part). Red colour indicates complete and strong cell membrane staining, whereas green indicates incomplete or weak staining. ImmunoMembrane is publicly available for free use at http://jvsmicroscope.uta.fi/immunomembrane/.

which awards the specimen with a point score in a range from 0 to 20 points. The calibration was performed by analysing the training set and searching the optimal IM-score cut-off values. Using the visual classification of the training set as golden standard, the optimal cut-off values were found to be three and eight points (weighted kappa coefficient $\kappa_w = 0.91$, ASE = 0.08). Accordingly, the default classification of ImmunoMembrane uses the following category division: 0–2 points = negative (0/1+, 3–7 points = equivocal (2+) and 8–20 points = positive (3+). The negative category comprises both the 0 and the 1+ classification because their distinction is generally not needed in diagnostic setting. The category cut-offs are user-adjustable, allowing ImmunoMembrane to be integrated more easily with a custom diagnostic process.

Sampling of IHC-stained breast cancer tissue sections is hampered by the biological tumour heterogeneity. It is well known that a single image field is not fully representative for the tumour. Conversely, imaging an entire tumour (diameter typically 1–2 cm) is impractical. Therefore, we defined the optimal number of fields to be captured and averaged for ImmunoMembrane analysis. According to our results (using ×10 objective lens with ×1 phototube and 2 megapixel 1/1.8″ CCD camera), the sufficient number of images for a typical breast cancer sample was four to five (Figure 4). Capturing a higher number of image fields was found to have a minimal impact on the averaged IM-score and classification (0/1+, 2+ or 3+).

The validation set ($n = 144$) was analysed with ImmunoMembrane (using at least four image fields per tumour) and compared the results against the corresponding visual classifications of an expert pathologist (Table 1). The analysis of the validation set showed very good agreement with the pathologist assessment (weighted kappa coefficient $\kappa_w = 0.80$, ASE = 0.08). The FISH–IHC disagreement was 3.5% (calculated from the total number of cases), containing false IHC-positive in two cases (1.4%) and false

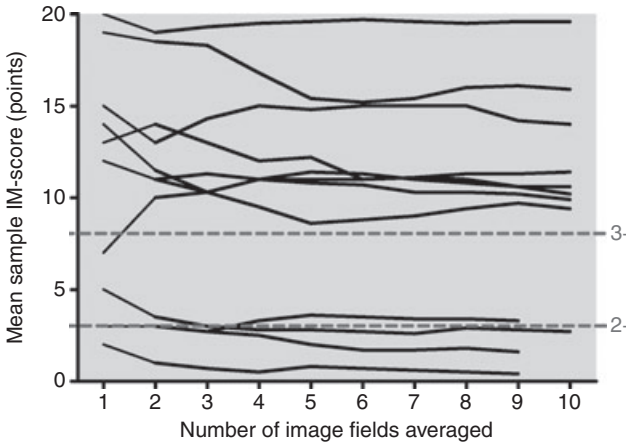

Figure 4. The mean sample ImmunoMembrane (IM)-score of IM analysis as a function of the number of image fields included in the averaged result. Thirteen non-negative human epidermal growth factor receptor 2 (HER2) breast cancer samples were tested (nine to 10 image fields per sample, imaged using a × 10 objective lens). Precalibrated IM-score category cutoffs are displayed with gray dotted line (three points for 2+ and eight points for 3+; scale 0–20 points).

IHC-negative in three cases (2.1%). Similarly, the CISH–IHC disagreement was 2.8%, containing false IHC-positive in two cases (1.4%) and false IHC-negative in two cases (1.4%).

To test the robustness of ImmunoMembrane for variations in the imaging setup, we imaged a separate test sample set using six different microscope cameras. The variation between the tested camera models was found not to be statistically significant ($P = 0.344$) and the average margin of error for each camera was within ± 1 point (IM-score scale 0–20 points).

The main features of the ImmunoMembrane web application are summarized in Table 2. The web application resides in a remote server and is accessed via the internet with a web browser, without any software downloads or installations (see screenshot in Figure 3). The software has two usage modes: an introductory Basic mode for initial test analyses and a fully-featured Advanced mode for routine analysis. The analysis can be performed using any modern web browsers (e.g. Windows Internet Explorer, Mozilla Firefox, Safari and Google Chrome) running on various operating systems (e.g. Microsoft Windows, Linux distributions and Mac OS). ImmunoMembrane adapts to various combinations of microscope objective lenses, phototubes, cameras, image resolutions and image formats. With the aid of a stage micrometer, the user can specify accurate image scale (pixels per μm) or it can be estimated empirically by using the Scale Finder function described in our earlier study.[27] The analysis can be performed either to a single image or to a series of images, in which case the analysis result is the series average. Unwanted image areas can be excluded by interactively defining regions of interest (ROIs). ImmunoMembrane is free for public use at http://jvsmicroscope.uta.fi/immunomembrane/.

Discussion

ImmunoMembrane was developed to provide an easy-to-use diagnostic tool for the classification of HER2 IHC. The application forms a comprehensive breast cancer analysis package together with our previously described ImmunoRatio software, which is meant for the digital image analysis of hormone receptors and Ki-67.[27] ImmunoMembrane shares some of the same algorithmic principles (e.g. colour deconvolution[28]), but builds a model of the cell membrane staining

Table 1. The concordance of human epidermal growth factor receptor 2 (HER2) immunohistochemistry (IHC) classification between ImmunoMembrane (IM), an expert pathologist, fluorescence *in-situ* hybridization (FISH) and chromogenic *in-situ* hybridization (CISH). All classifications followed the American Society of Clinical Oncology/College of American Pathologists (ASCO/CAP) guidelines[1]

Immuno	Pathologist				FISH*				CISH†			
Membrane	0/1+	2+	3+	Total	Non-amplified	Equivocal	Amplified	Total	Non-amplified	Equivocal	Amplified	Total
0/1+	98	2	0	100	95	2	3	100	98	0	2	100
2+	7	16	7	30	21	0	9	30	19	4	7	30
3+	0	2	12	14	2‡	0	12	14	2‡	0	12	14
Total	105	20	19	144	118	2	24	144	119	4	21	144

*FISH HER2/CEP17 ratio: <1.8 = non-amplified, 1.8–2.2 = equivocal, >2.2 = amplified.
†CISH HER2 copy number: <4 = non-amplified, 4–6 = equivocal, >6 = amplified.
‡The IM-scores of these two cases fell very close to the 2+/3+ cut-off.

Table 2. Main features of ImmunoMembrane (IM) web application for the analysis of human epidermal growth factor receptor 2 (HER2) immunohistochemistry

Feature	Description
Robust analytical principle	Utilizes the widely accepted colour deconvolution for stain separation
Consistent and repeatable classification	Uses positive control slide to normalize variation between staining batches and/or image acquisition settings
Easy to use	Runs within web browser, requiring no additional software downloads or installations
Cross-platform compatible	Supports all modern operating systems (Microsoft Windows, Linux distributions, Mac OS) and web browsers (Windows Internet Explorer, Mozilla Firefox, Safari, Google Chrome)
Readily usable with existing microscopes and cameras	Adapts to various combinations of microscope objective lenses, phototubes, cameras and resolutions and image formats
Precalibrated to match expert pathologist's visual classification	The IM-score category cut-offs (0/1+, 2+ and 3+) are adjustable to match user-specific classification

similar to the scoring principles described in the literature.[1] ImmunoMembrane is designed to be used as a diagnostic aid by a trained pathologist. The analysis results should always be interpreted together with the pseudo-coloured result images and the original histology of the slides. Although ImmunoMembrane is intended for clinical diagnostics, regulations governing the usage of automated image analysis systems vary between countries. For example, in Europe, no stringent regulations exist for software medical devices, whereas in the United States the software would require clearance from the Food and Drug Administration (FDA).

In our validation experiment, classification of HER2 IHC by ImmunoMembrane matched very well with the visual assessment made by an expert pathologist. The advantages of using automated image analysis software, such as ImmunoMembrane, include shorter overall analysis time and improved reproducibility and repeatability of the analysis. Moreover, by utilizing an image captured from the positive staining control slide as a normalization reference (as supported in ImmunoMembrane), the inter- and intra-observer variability can be decreased significantly. As with all HER2 image analysis systems, a prerequisite of valid and consistent analysis is good-quality IHC staining. Tissue morphology should be optimally preserved, and the slide should be free of non-specific staining or other well-known HER2 IHC artefacts.

Because the HER2 IHC staining itself may vary between laboratories, we recommend that the users calibrate ImmunoMembrane by defining the IM-score classification cut-offs with their own data. This is advisable especially for laboratories using staining kits other than the HercepTest®, which was used when developing ImmunoMembrane. Once calibrated, ImmunoMembrane can be integrated readily with routine diagnostic work. In terms of optical resolution, we recommend using a microscope with ×10 objective lens magnification, which is used commonly in the visual evaluation of HER2 IHC. Most of the currently used microscope cameras (typically 1.5–4 megapixels) provide sufficient image quality for the analysis. We found that capturing and averaging four to five image fields per sample provides an optimal analysis result – lower field count yielding unreliable results and higher field count having minimal impact on the sample average.

ImmunoMembrane is based on the colour deconvolution algorithm,[28] which is the most frequently applied algorithm for separating the immunostain (brown) and the counterstain (blue) components. Colour deconvolution is mathematically straightforward and fast to compute from a microscope colour image (RGB). If more than two staining components are used or the analysis requires accurate intensity based quantification, other methods (such as the AQUA[29] or multispectral imaging) would most probably be better alternatives. Although not tested in this study, ImmunoMembrane should be applicable to any immunostaining localized to cell membranes, such as truncated (p95HER2) or phosphorylated HER2, the analysis of which may become clinically important in the future.

ImmunoMembrane was developed using ImageJ, which is a public domain (i.e. completely free and open source) image analysis software. However, a

major obstacle in adopting ImageJ is the strict security policy often applied in the clinical laboratory computer systems, which often prohibit end-users to download, install and/or run any external applications. To address these constraints, we released ImmunoMembrane as a web application, which provides an easy-to-use web interface, requires no software downloads or installations, and can be used in highly restricted environments. To simplify testing and tryout of the software, first-time users can familiarize themselves with ImmunoMembrane by using the Basic mode, which contains only the bare minimum set of features needed for the analysis. In routine use, we encourage the users to switch to the Advanced mode, which contains several additional features, such as accurate image scale and intensity and contrast normalization, all of which are essential for reliable analysis.

To the best of our knowledge, ImmunoMembrane is the first free, ready-to-use web application for analysing HER2 IHC. The application is hardware-independent and robust for variations in the camera settings and laboratory-specific staining practices. We anticipate that publicly available and open source image analysis applications, such as ImmunoMembrane, will accelerate the adoption of automated analysis techniques in clinical diagnostics of HER2 IHC. ImmunoMembrane can be used anonymously and freely at http://jvsmicroscope.uta.fi/immunomembrane/.

Declarations of interest

The authors declare that they have no competing interests.

Acknowledgements

This study was supported financially by the Finnish Cancer Foundation and the Tampere University Hospital (governmental EVO grant). The authors wish to thank laboratory technicians Sari Toivola and Kristiina Salonoja for assisting in sample preparation and immunostaining.

References

1. Wolff A, Hammond M, Schwartz J *et al.* American Society of Clinical Oncology/College of American Pathologists guideline recommendations for human epidermal growth factor receptor 2 testing in breast cancer. *J. Clin. Oncol.* 2007; **25;** 118–145.
2. The United Kingdom National External Quality Assessment Service (UK NEQAS) website. Available at: http://www.ukneqas.org.uk/ (accessed 8 July 2011).
3. The Nordic immunohistochemical Quality Control (NordiQC) website. Available at: http://www.nordiqc.org/ (accessed 8 July 2011).
4. Moeder CB, Giltnane JM, Harigopal M *et al.* Quantitative justification of the change from 10% to 30% for human epidermal growth factor receptor 2 scoring in the American Society of Clinical Oncology/College of American Pathologists guidelines: tumor heterogeneity in breast cancer and its implications for tissue microarray based assessment of outcome. *J. Clin. Oncol.* 2007; **25;** 5418–5425.
5. Joshi AS, Sharangpani GM, Porter K *et al.* Semi-automated imaging system to quantitate Her-2/neu membrane receptor immunoreactivity in human breast cancer. *Cytometry A.* 2007; **71;** 273–285.
6. Hall BH, Ianosi-Irimie M, Javidian P, Chen W, Ganesan S, Foran DJ. Computer-assisted assessment of the human epidermal growth factor receptor 2 immunohistochemical assay in imaged histologic sections using a membrane isolation algorithm and quantitative analysis of positive controls. *BMC Med. Imaging* 2008; **8;** 11.
7. Masmoudi H, Hewitt SM, Petrick N, Myers KJ, Gavrielides MA. Automated quantitative assessment of HER-2/neu immunohistochemical expression in breast cancer. *IEEE Trans. Med. Imaging* 2009; **28;** 916–925.
8. Brügmann A, Eld M, Lelkaitis G *et al.* Digital image analysis of membrane connectivity is a robust measure of HER2 immunostains. *Breast Cancer Res. Treat.* 2011; [Epub ahead of print] DOI: 10.1007/s10549-011-1514-2.
9. Walker RA. Quantification of immunohistochemistry – issues concerning methods, utility and semiquantitative assessment I. *Histopathology* 2006; **49;** 406–410.
10. Taylor C, Levenson R. Quantification of immunohistochemistry – issues concerning methods, utility and semiquantitative assessment II. *Histopathology* 2006; **49;** 411–424.
11. Nakhleh RE, Grimm EE, Idowu MO, Souers RJ, Fitzgibbons PL. Laboratory compliance with the American Society of Clinical Oncology/College of American Pathologists guidelines for human epidermal growth factor receptor 2 testing: a College of American Pathologists survey of 757 laboratories. *Arch. Pathol. Lab. Med.* 2010; **134;** 728–734.
12. Slodkowska J, Filas V, Buszkiewicz E *et al.* Study on breast carcinoma Her2/neu and hormonal receptors status assessed by automated images analysis systems: ACIS III (Dako) and ScanScope (Aperio). *Folia Histochem. Cytobiol.* 2010; **48;** 19–25.
13. Tanner M, Isola J, Wiklund T *et al.* Topoisomerase IIalpha gene amplification predicts favorable treatment response to tailored and dose-escalated anthracycline-based adjuvant chemotherapy in HER-2/neu-amplified breast cancer: Scandinavian Breast Group Trial 9401. *J. Clin. Oncol.* 2006; **24;** 2428–2436.
14. Gong Y, Sweet W, Duh YJ *et al.* Chromogenic *in situ* hybridization is a reliable method for detecting HER2 gene status in breast cancer: a multicenter study using conventional scoring criteria and the new ASCO/CAP recommendations. *Am. J. Clin. Pathol.* 2009; **131;** 490–497.
15. Rasband WS. ImageJ image analysis software. Available at: http://rsb.info.nih.gov/ij/ (accessed 8 July 2011).
16. Oracle Corporation. Java programming language. Available at: http://www.java.com/ (accessed 8 July 2011).
17. Rasband WS, Landini G. Calculator Plus ImageJ plugin. Available at: http://rsb.info.nih.gov/ij/plugins/calculator-plus.html (accessed 8 July 2011).

18. Landini G. Colour Deconvolution ImageJ plugin. Available at: http://www.dentistry.bham.ac.uk/landinig/software/cdeconv/cdeconv.html (accessed 8 July 2011).
19. Landini G. Particles4 and Particles8 ImageJ plugins. Available at: http://www.dentistry.bham.ac.uk/landinig/software/software.html (accessed 8 July 2011).
20. Google Inc. Google Web Toolkit. Available at: http://code.google.com/webtoolkit (accessed 8 July 2011).
21. Apache Software Foundation. Apache Commons FileUpload library. Available at: http://commons.apache.org/fileupload/ (accessed 8 July 2011).
22. Apache Software Foundation. Apache Commons IO library. Available at: http://commons.apache.org/io/ (accessed 8 July 2011).
23. The Laboratory for Optical and Computational Instrumentation (LOCI), University of Wisonsin-Madison, USA. Bio-Formats library. Available at: http://www.loci.wisc.edu/software/bio-formats/ (accessed 8 July 2011).
24. Apache Software Foundation. Apache Tomcat Java servlet container. Available at: http://tomcat.apache.org/ (accessed 8 July 2011).
25. Cohen J. Weighted kappa: nominal scale agreement with provision for scaled disagreement or partial credit. *Psychol. Bull.* 1968; **70;** 213–220.
26. The TWAIN Working Group. TWAIN standard specification. Available at: http://www.twain.org/ (accessed 8 July 2011).
27. Tuominen VJ, Ruotoistenmäki S, Viitanen A, Jumppanen M, Isola J. ImmunoRatio: a publicly available web application for quantitative image analysis of estrogen receptor (ER), progesterone receptor (PR), and Ki-67. *Breast Cancer Res.* 2010; **12;** R56.
28. Ruifrok AC, Johnston DA. Quantification of histochemical staining by color deconvolution. *Anal. Quant. Cytol. Histol.* 2001; **23;** 291–299.
29. Camp RL, Chung GG, Rimm DL. Automated subcellular localization and quantification of protein expression in tissue microarrays. *Nat. Med.* 2002; **8;** 1323–1327.